Uremia-induced effects on cardioregulatory mechanisms in the context of the cardiorenal syndrome

Document status and date:
Published: 01/01/2023

DOI:
10.26481/dis.20230508jw

Document Version:
Publisher's PDF, also known as Version of record

Please check the document version of this publication:

• A submitted manuscript is the version of the article upon submission and before peer-review. There can be important differences between the submitted version and the official published version of record. People interested in the research are advised to contact the author for the final version of the publication, or visit the DOI to the publisher's website.
• The final author version and the galley proof are versions of the publication after peer review.
• The final published version features the final layout of the paper including the volume, issue and page numbers.

Link to publication

Download date: 27 Apr. 2024

Uremia-induced effects
on cardioregulatory mechanisms in the context
of the cardiorenal syndrome

Julia Wollenhaupt

Uremia-induced effects

on cardioregulatory mechanisms in the context

of the cardiorenal syndrome

DISSERTATION

to obtain the degree of Doctor at Maastricht University,
and Doctor rerum naturalium (Dr.rer.nat.) at the RWTH Aachen
on the authority of the Rector Magnifici,
Prof. dr. Pamela Habibović and Univ.-Prof. Dr. rer. nat. Dr. h.c. mult. Ulrich Rüdiger
in accordance with the decision of the Board of Deans,
to be defended in public

on Monday May 8th, 2023, at 13:00 hours

by

Julia Wollenhaupt

Supervisors:

Prof. Dr. Erik Biessen, Maastricht University
Prof. Dr. Joachim Jankowski, UM/ University hospital RWTH Aachen

Co-supervisor:

PD Dr. Heidi Noels, UM/ University hospital RWTH Aachen

Assessment Committee:

Prof. Dr. Leon Schurgers, Maastricht University (chair)
Prof. Dr. Alberto Ortiz, University of Madrid
Prof. Dr. Jürgen Floege, University hospital RWTH Aachen
Prof. Dr. Leon de Windt, Maastricht University
Prof. Dr. Yvonne Döring, Universitätsspital Bern

Table of Content

Chapter 1

Introduction

1. Introduction

1.1. Cardiovascular disease

Cardiovascular diseases (CVD) are the leading cause of death in the world and describe a broad range of different disorders affecting the heart, brain and blood vessels [1]. About 18 million people died through CVD in 2019, which was 31 % of all global deaths, as shown in **Figure 1** [2].
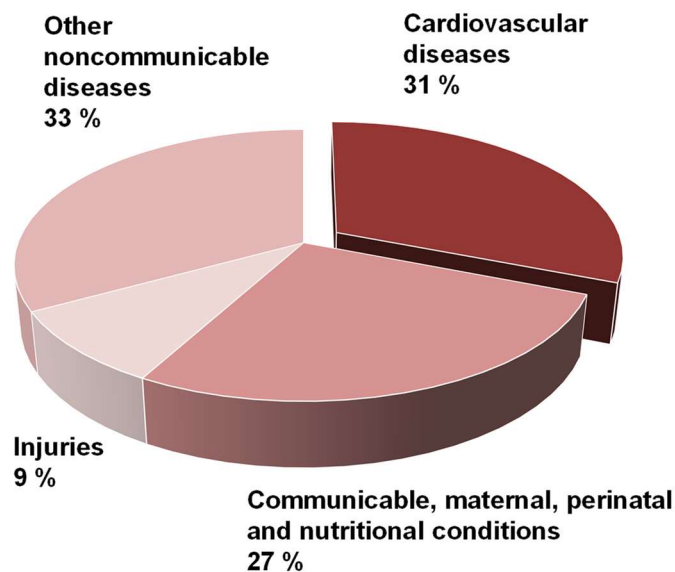
Figure 1: Distribution of major causes of death including CVD according to the World Health Organization (2019).
Except for the other noncommunicable diseases, which involve a broad range of chronic diseases that cannot be passed from person to person, cardiovascular diseases are the main cause of death. Figure adapted from *World Health Organisation on Cardiovascular Disease. Available online: https://www.who.int/en/news-room/fact-sheets/detail/cardiovascular-diseases-(cvds); accessed on March, 2022* [2].

Atherosclerosis, a chronic inflammatory process in medium and large-sized blood vessels, is the predominant inducer of CVD leading to the formation of atherosclerotic lesions in arteries [3]. The atherosclerotic process is started by dysfunctional endothelial cells which lose their integrity and cellular contacts, through which the permeability of the endothelial barrier is increased. This in turn leads to an accumulation of cholesterol, contained within low-density lipoprotein (LDL) particles, in the intima [3]. Here, LDL is oxidized and an inflammatory process is started. At this point inflammatory leukocytes, such as neutrophils and monocytes migrate into the atherosclerotic lesions, further promoting the inflammatory process and thereby the growth of atherosclerotic

lesions [3]. The latter leads to narrowing of the affected artery, which reduces the blood flow and thereby the oxygen supply to the affected organ. Once a lesion is ruptured, thrombogenic material is exposed to the blood. Platelets get activated and build a thrombus, which can reach the heart and can lead to myocardial infarction by blocking coronary arteries, which is the main cause of cardiovascular deaths [1, 4]. This type of CVD is called "coronary artery disease", also named as "ischemic heart disease" and is the most common type of CVD [5]. Of note, atherosclerosis can also lead to cerebrovascular diseases like stroke, or to peripheral vascular disease, which are diseases outside the heart and brain [5].

In contrast to atherosclerosis, cardiomyopathy is a group of CVDs that directly affect the heart muscle, more precisely the lower heart chambers, called ventricles [6]. There are two categories of cardiomyopathy, the first being ischemic cardiomyopathy caused by heart attacks or coronary artery disease, and the other being non-ischemic cardiomyopathy, which can be caused by other factors, such as diseases like diabetes or chronic kidney disease and even without any obvious reason. Cardiomyopathy can lead to stiffening, enlargement, thickening or scarring of the heart muscle depending on the type of cardiomyopathy. Upon progression of the disease, the heart is no longer able to pump the blood effectively through the body, resulting in heart failure or sudden death [7, 8].

The most behavioral risk factors for the development of CVD are smoking, physical inactivity, unhealthy diets and harmful use of alcohol. Exposure to these risk factors for a long time leads to elevated blood pressure, raised blood sugar, raised blood lipids and/or obesity, all triggering the development of CVD [9]. Other risk factors for CVD are diseases such as diabetes, chronic respiratory disease or chronic kidney disease [1].

1.2. Chronic kidney disease

Chronic kidney disease (CKD) is a progressive disorder of the kidney and is caused by a decreased excretory function of the kidney continuously worsening at least over three months [10]. The excretory function is determined by the glomerular filtration rate (GFR), being normally above 90 ml/min/1.73m^2 in healthy subjects. Increasingly losing the excretory function of the kidney contributes to an increased appearance of proteins

(albumin) in the urine, also called proteinuria or albuminuria [11]. All organs are affected by CKD through impaired regulation of the acid-base balance, water and electrolyte balance, blood pressure and bone metabolism [12]. Furthermore, in most patients a chronic, systemic state of low-grade inflammation is present [13].

CKD is classified into five stages according to the GFR (**Table 1**). The first CKD stage is described by a normal kidney function, but with signs of mild kidney damage. Patients with CKD stage 2 have a mildly reduced GFR and patients with CKD stage 3a and 3b display a mild to moderate reduction of the GFR, respectively, a moderate to severe reduction of the GFR, all of them mostly without any obvious symptoms and therefore not aware of having CKD [14]. A reduced GFR between 29-15 ml/min/1.73m^2 is classified as CKD stage 4, while a GFR below 15 ml/min/1.73m^2 means that the kidney fails completely, known as CKD stage 5 or end-stage renal disease (ESRD). In this case, the kidney is not able to remove the patient's blood from waste products being formed during metabolic processes in the body. Those patients need dialysis or even kidney transplantation to mimic the excretory function of the kidney.

Table 1: Grading of CKD stages according to glomerular filtration rate.
Table adapted from *Drawz et al, Ann Intern Med, 2015. 162(11): p. Itc1-16* [14].

CKD stage	Description	Glomerular filtration rate (ml/min/1.73m^2)
1	Normal kidney function, but signs of kidney damage	>90
2	Mild reduction	89-60
3a	Mild to moderate reduction	59-45
3b	Moderate to severe reduction	44-30
4	Severe reduction	29-15
5	Kidney failure	<15

The worldwide prevalence of CKD is rising, with an increase of patients reaching an advanced stage or end-stage of CKD [15]. The main causes for the rising prevalence of CKD are on the one hand the ageing population and on the other hand, the unhealthy lifestyle of the population in the western world resulting in an increasing prevalence of diseases such as diabetes, obesity or hypertension. These diseases are the main risk factors for CKD and therefore contribute to the prevalence of CKD in the

global world [11, 16]. For example, approximately 30% of all ESRD patients also suffer from hypertension [17, 18]. An increased blood pressure can lead to narrowing, hardening or scarring of small arteries in the kidney, resulting in a reduced blood supply and in turn in a lack of oxygen supply to the kidney, thereby reducing the filter capacity of the kidney [19]. Furthermore, it can result in progressive morphological alterations of the kidney. This includes glomerular and interstitial fibrosis, tubular injury or even tubular atrophy as the chronic condition of injured tubules [19]. Pathologies affecting the glomeruli and/or the tubules end finally in CKD [20, 21].

1.2.1. Uremia and uremic toxins

CKD is characterized by a gradual loss of the excretory kidney function. This kidney dysfunction results in an accumulation of solutes that would normally be excreted by the kidney, with for example increased levels of urea in the blood, hence the term "uremia". In patients with kidney dysfunction like CKD, these solutes are retained and can become harmful at high concentrations. Therefore, they are also referred to as "uremic toxins" [22].

Uremic toxins can be subdivided into three classes, the first one being the "water-soluble low molecular weight solutes", which can be easily removed by dialysis [22]. The second group is called "middle molecular weight solutes", which are more difficult to remove by dialysis. Even more difficult is the removal of "protein-bound solutes", which are forming the third group of uremic toxins. Some of the protein-bound solutes are only removed up to 30% with dialysis, for example indoxyl sulfate and p-cresylsulfate, which both are strongly bound to albumin due to their hydrophobic character [23, 24]. Indoxyl sulfate is derived from tryptophan, which is metabolized into indole and is then converted to indoxyl sulfate in the liver [25]. p-Cresylsulfate is metabolized from tyrosine and phenylalanine in the intestine by gut microbiota [25]. Normally both uremic toxins are excreted by the kidney, however, with impaired kidney function they accumulate in the blood. In CKD patients, increased blood levels of indoxyl sulfate and p-cresylsulfate are associated with increased aortic calcification and vascular stiffness [26, 27]. Further, p-cresylsulfate is associated with an increase in cardiovascular events and its concentration even correlates with cardiovascular mortality in CKD patients [28].

Meanwhile, around 140 uremic toxins have been reported to accumulate in the blood in case of a kidney dysfunction [22, 29]. All of them are contributing to the state of uremia in CKD patients and thereby promoting a negative impact of the kidney on the cardiovascular system [29].

1.3. The cardiorenal syndrome

The pathophysiological link between the kidney and the heart is defined as the "cardiorenal syndrome" [30]. It describes the pathophysiology in which a damaged and/or dysfunctional kidney induces functional or morphological changes in the heart or vice versa. **In this thesis, the focus has been on the impact of CKD on the heart**.

About 50% of patients with CKD stage 4-5 suffer from CVD [31]. In those patients the CVD mortality rate is about 40-50%, whereas patients with normal kidney function have a CVD mortality rate of 26% [32, 33]. CKD patients are particularly at risk for developing CVD because of their altered pathophysiology, which may include hypertension, elevated levels of triglycerides and sometimes LDL, diabetes, hyperactivation of the renin-angiotensin-aldosterone system, inflammation, reduction of GFR and albuminuria, the uremic state and increased oxidative stress [34, 35]. These altered pathophysiological processes in the blood, circulation and the heart contribute to the increased cardiovascular risk in CKD patients, since the kidney is interacting with the myocardium over the circulation (**Figure 2A**).

The processes underlying CVD in CKD patients and the involved molecular mediators differ in part from the processes underlying CVD in the general population. Increased fibrosis and neurohumoral activity, reduced collateral artery growth as well as an increased risk of coagulation and calcification contribute to the development of CVD in CKD patients [36, 37] (**Figure 2B**). Calcification of the vessel walls is especially increased in CKD patients due to an imbalance of calcification inducers vs. inhibitors and increases with progression of the disease [38]. It results in vascular stiffness and is additionally a predictor for CVD mortality in CKD patients [39]. Systemic inflammation as well as increased oxidative stress occur in both CVD and CKD (**Figure 2B**), however, in CKD is triggered by additional CKD-specific molecular processes, such as the accumulation of pro-inflammatory uremic toxins [22].
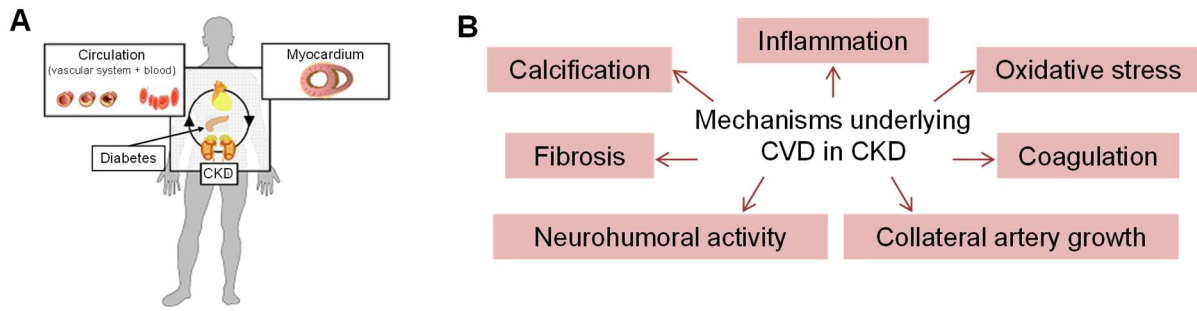
Figure 2: Complexity of the link between CKD and CVD.
A) Interaction of the kidney with the circulation and the myocardium. **B)** Mechanisms underlying elevated risk of CVD in CKD patients. Figure adapted from *Noels et al., Eur Heart J, 2018. 39(12): p. 975-977* [40].

1.3.1. Accelerated atherosclerosis in CKD

Giving an example of the detrimental interaction between the kidney, the circulation and vessels, atherosclerosis is characteristically accelerated in CKD patients [3]. In CKD patients, atherosclerotic lesions are formed in uremic vessels, in which pro-inflammatory mediators are already upregulated and suggested to support the formation of atherosclerotic lesions [41, 42]. Increased oxidative stress, which is already present in early stages of CKD, promotes oxidation of LDL resulting in increased oxLDL in CKD [43]. Additionally, increased oxidative stress markers were associated with impaired endothelial vasodilation in CKD patients [44]. These factors, together with pro-inflammatory molecules and uremic toxins, promote endothelial dysfunction as a major contributor to accelerated atherosclerosis in uremic vessels from CKD patients. Differences in atherosclerotic lesions in vessels with and without CKD are displayed in **Figure 3**.

All the mentioned factors demonstrate the complexity of the interaction between kidney, heart and circulation as well as the importance of unravelling the underlying mechanisms.
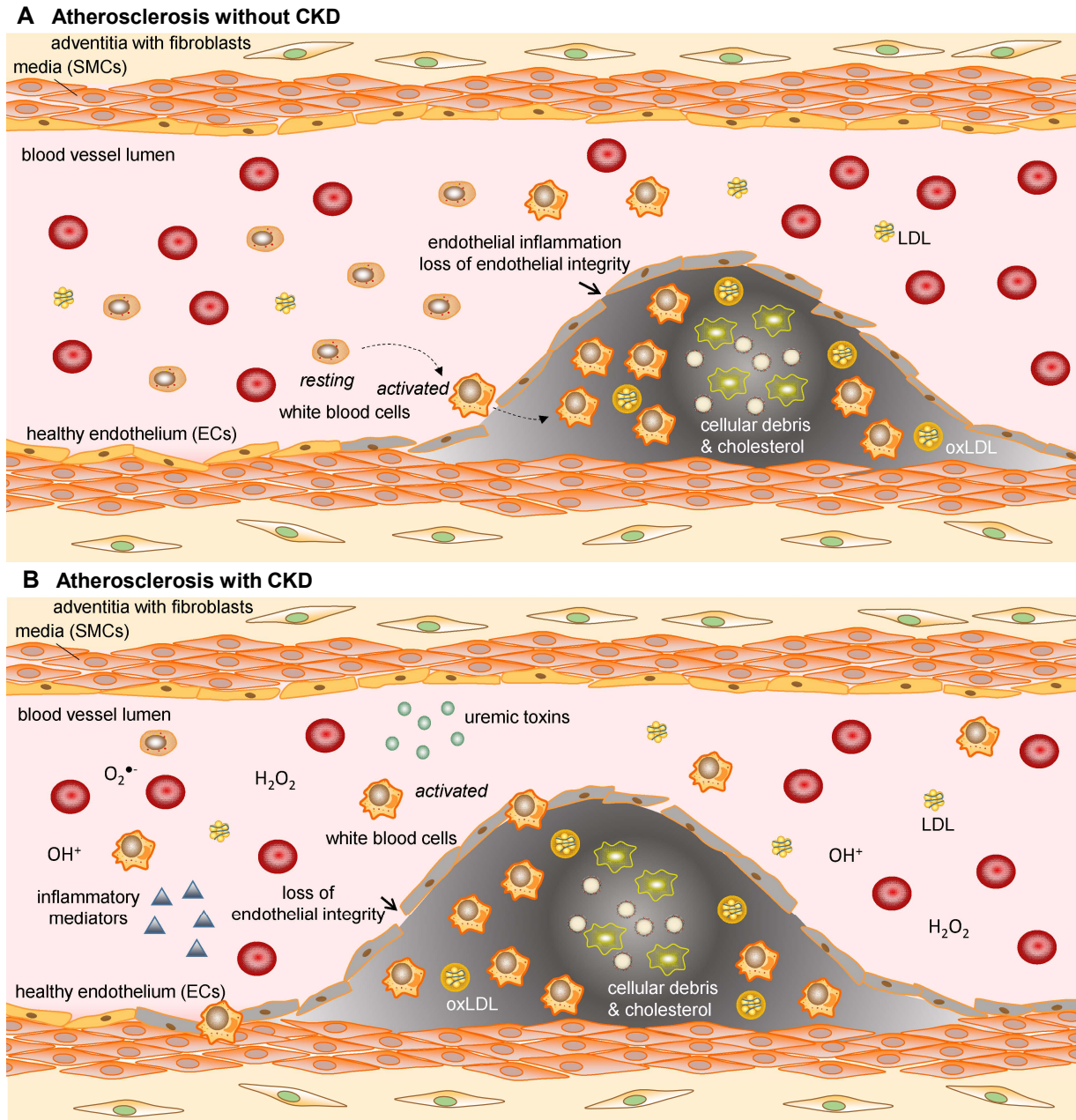
Figure 3: Atherosclerotic lesions are accelerated in vessels of CKD patients compared with patients without CKD.
A) Atherosclerotic lesion in a non-CKD vessel, characterized by lipid deposition and inflammation in the vessel. **B)** Atherosclerotic lesion in a uremic vessel, with increased levels of inflammatory mediators and oxidative stress, uremic toxins and activated white blood cells in the blood, contributing to accelerated atherosclerosis. *CKD = chronic kidney disease; EC = endothelial cell; LDL = low-density lipoprotein; oxLDL = oxidized LDL; SMC = smooth muscle cell*. Figure designed by me as published in *Harlacher et al. Int J Mol Sci, 2022. 23(1)* [42].

1.3.2. Uremic cardiomyopathy

The term "uremic cardiomyopathy" describes the pathological condition of a cardiomy-opathy induced by CKD [45]. This cardiac pathology is characterized by left ventricular hypertrophy and cardiac fibrosis, associated with the development of diastolic dysfunction [45, 46].

Left ventricular hypertrophy. Left ventricular hypertrophy (LVH) describes the thickening of the heart muscle due to the enlargement of the cardiomyocytes repre-senting the predominant cell type in the heart with about 70-80% of the total volume [47]. LVH develops in response to pressure or volume overload, for example, often occurring in case of hypertension. As compensation mechanism of the heart, the car-diomyocytes become enlarged to maintain the cardiac function, which can initially be diagnosed only by measuring the ventricular wall thickening and the LV mass via echo-cardiography [48] (**Figure 4**). LVH occurs already in early-stages of CKD in which the GFR is not yet affected. In dialysis patients LVH was seen as an independent predictor of cardiovascular mortality and occurs in even 70-80% of ESRD patients [6, 49].
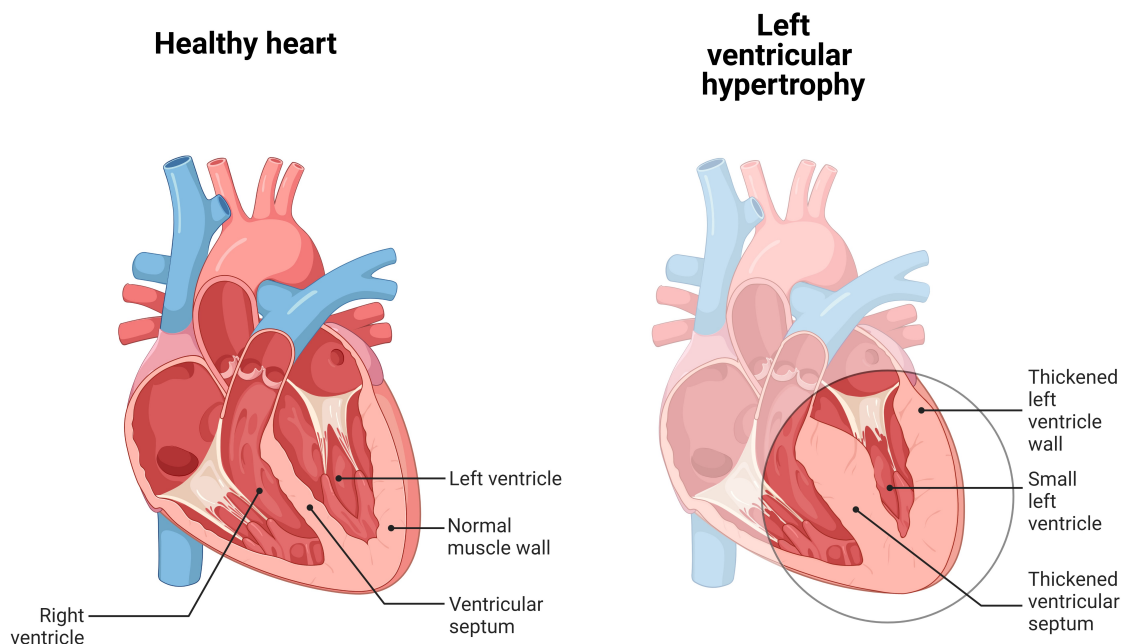
Figure 4: Cardiac hypertrophy of the left ventricle compared to a healthy heart.
Shown is the thickening of the ventricle walls and ventricular septum as well as a reduced left ventricle size in the hypertrophic heart**.**

Cardiac fibrosis. Another cardiac remodeling process is interstitial cardiac fibrosis, often found in CKD patients in combination with LVH [47]. Cardiac fibrosis is characterized by increased collagen type 1 (COL1) deposition as well as fibroblast activation with ongoing transdifferentiation into myofibroblasts. It is the wound healing process of the tissue after injury, followed by scarring of the tissue [50]. Of note, these processes are also seen in the aged heart. Activated fibroblasts excessively produce extracellular matrix (ECM) proteins, mostly collagens but also fibronectin or α-smooth muscle actin (αSMA) (**Figure 5**). Excessive ECM deposition and crosslinking lead to stiffening of the left ventricle, which complicates the diastolic filling of the heart and thus results in pressure overload [51]. Since both the relaxation and the contractility of the heart are affected, the cardiac function is restricted.

In CKD patients a chronic systemic inflammation as well as increased oxidative stress are observed, which may contribute to increased fibrosis [52]. An enhanced cytokine production as well as their decreased clearance by the failing kidney result in increased inflammatory cytokines in the circulation in CKD [53]. Also, high levels of uremic toxins in the circulation contribute to the uremic milieu in CKD patients, thereby increasing inflammation and oxidative stress, as shown in experiments with endothelial cells treated with uremic serum [54]. Decreased antioxidant enzyme levels on the one hand as well as enhanced reactive oxygen species (ROS) formation on the other hand result in redox imbalances with a shift towards increased oxidative stress [54-56]. The latter causes lipid peroxidation, oxidation of proteins, inactivation of enzymes and DNA damage. This is followed by the activation of inflammatory responses, as e.g. the expression of tumor necrosis factor α (TNF-α) or interleukin 1 (IL-1) via activation of NF-κB. This transcription factor regulates the expression of genes involved not only in inflammation, but also in apoptosis, coagulation and ECM deposition [57], thus contributing to pathological remodeling processes such as increased fibrosis in CKD patients.
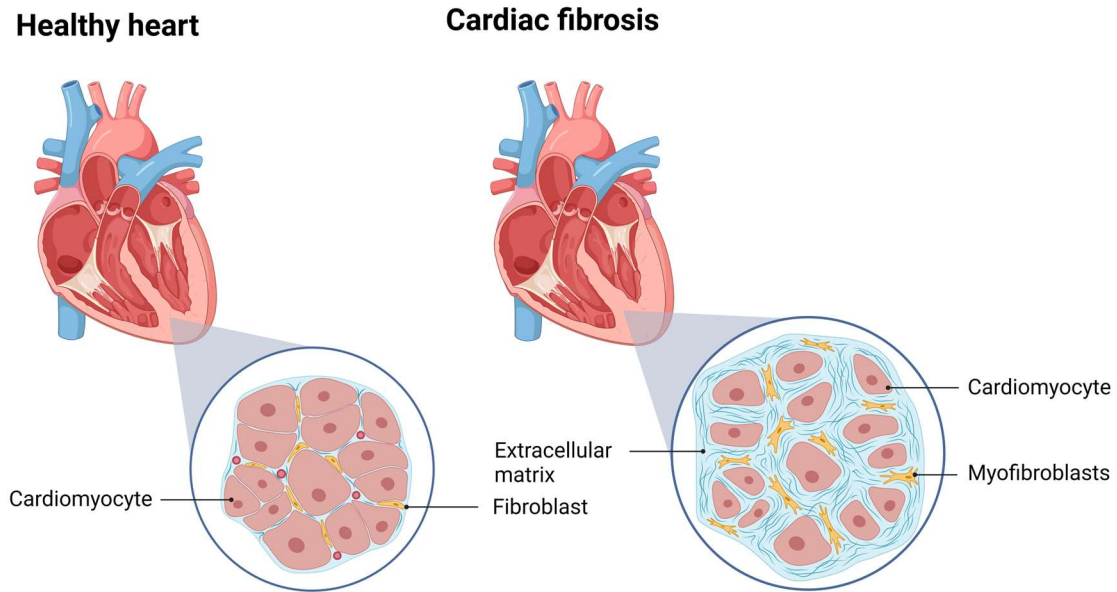
Figure 5: Cardiac fibrosis with extracellular matrix deposition and transition from fibroblasts into myofibroblasts resulting in scarring and stiffening of the heart muscle.
Adapted from *Herum et al. J Clin Med, 2017. 6(5)* [58].

Cardiac inflammation. Aside from LVH and cardiac fibrosis, the uremic milieu triggers increased expression of adhesion molecules on endothelial cells, such as vascular cell adhesion molecule 1 (VCAM-1) and E-selectin. This promotes the adhesion of monocytes and leukocytes to the vascular wall as well as the migration of both into the tissue, which in turn promotes the initiation and progression of atherosclerotic lesions [59]. After activation of NADPH oxidase in endothelial cells by e.g. the uremic toxin indoxyl sulfate, endothelial cells express increased levels of monocyte chemoattractant protein 1 (MCP-1), further triggering monocyte recruitment to the inflamed endothelium [60-62]. Also, cardiomyocytes increasingly express MCP-1 in a uremic milieu, leading to subsequent macrophage infiltration into the myocardium and thereby resulting in cardiac inflammation [63]. In CKD patients, increased MCP-1 expression in the heart as well as increased E-selectin plasma levels are associated with pathophysiological processes of cardiac remodeling, thereby suggesting a link between chronic inflammation and the development of uremic cardiomyopathy [59, 63, 64]. Additionally, circulating inflammatory cytokines, such as interleukin-6 (IL-6) and c-reactive protein (CRP), are significantly increased in CKD patients and have been associated with the development of LVH in these patients [53].

All aforementioned aspects indicate how complex the pathophysiology of uremic cardiomyopathy is and how many processes are involved, from which the underlying molecular mechanisms are not yet clearly understood.

1.4. Mouse models to study the effect of CKD on the heart

When studying cardiorenal organ crosstalk mouse models have the potential to provide insights into the pathological mechanisms underlying uremic cardiomyopathy. Additionally, mouse models in research provide the benefit of using genetically modified mouse strains for examining potential disease regulators.

Different CKD mouse models have already been investigated, however in the past with quite variable effects on the heart [65]. **One commonly used method to induce CKD is subtotal nephrectomy (5/6 Nx)** in which the poles of one kidney are resected while the other kidney is totally removed, resulting in a ~80% loss of the kidney mass. Kidney dysfunction is simply induced by the surgical reduction of the nephrons, which are responsible for the filter capacity of the kidney. Another approach for inducing CKD is **diet supplementation with adenine, resulting in tubulointerstitial nephropathy**. Adenine precipitates in the kidney where it forms 2,8-dihydroxyadenine crystals within the renal tubules, thereby blocking them [66]. This leads to injured tubules within the kidney and thus to a reduced filter capacity of the kidney.

Both methods are well established in CKD research; however with highly variable outcome on the heart, as reported in our recent systematic review with meta-analysis (*in appendix*) [65]. While some studies reported that inducing CKD in mice results in the development of cardiac hypertrophy, myocardial fibrosis or heart failure [67, 68], others described only mild alterations to even no cardiac changes [69, 70]. Different methods of CKD induction may contribute in part to this variability, but this is not a complete explanation, since different induction methods have also been reported to be able to induce effects on the heart [67-70]. Additionally, the usage of different mouse strains may contribute to the variability of the results. For example, 129/Sv mice, a mouse strain frequently used in CKD research, are more susceptible to develop hypertension as well as cardiac hypertrophy upon 5/6 Nx in comparison to C57BL/6 mice, the latter frequently applied in research since they offer a broad range for genetic modifications [65]. An additional factor that may contribute to a highly variable outcome in cardiorenal research is the lack of consistent parameter reporting in

terms of cardiac function as well as cardiac morphological changes. In fact, **most mouse studies report only on a selected parameter, which quite complicates the comparison of different mouse models from different studies as revealed by our recent systematic review with meta-analysis** (*in appendix*) [65].

Consequently, a comprehensive and comparative characterization of experimental cardiorenal mouse models to investigate cardiac effects induced by CKD is essential for future studies aimed at elucidating the molecular mechanisms underlying the pathophysiological crosstalk between kidney and heart.

Chapter 2

Aim of this thesis

2. Aim of this thesis

CKD patients have an increased risk to suffer also from CVD, with about 40-50% of patients in CKD stage 4-5 ultimately dying because of CVD instead of a failing kidney. One major cardiac pathology occurring in CKD patients is uremic cardiomyopathy. In order to design therapy opportunities more tailored to the CKD patient, the mechanisms underlying the development of uremic cardiomyopathy has to be elucidated in more detail. Since this involves an organ crosstalk of kidney and heart, an animal model is the best approach for clarifying the pathology. In literature different cardiorenal mouse models have already been presented; however, with reporting of highly varying parameters, hence a direct comparison of different animal models is not possible.

Thus, this thesis aimed at a comprehensive standardized characterization and comparison of the cardiac phenotype in different mouse models of CKD. This could bring light into the jungle of cardiorenal mouse models that were recently published with highly variable results. Also, it would enable to reflect on the suitability of a mouse model in mirroring the clinical situation of a CKD patient developing a uremic cardiomyopathy.

In detail, this thesis aimed at the **comparison of five different experimental CKD mouse models**, with subsequent characterization of:

i) the renal phenotype, aiming at kidney damage which reflects the CKD patient's situation, and

ii) the cardiac phenotype, to investigate the impact of kidney damage on the heart.

CKD was induced in **three different mouse strains** (C57BL/6J, C57BL/6J $ApoE^{-/-}$, 129/Sv) by the **two most commonly applied methods for CKD induction** (subtotal nephrectomy, adenine feeding) (**Figure 6**).

Phenotyping of kidney damage and CKD status comprised measuring serum parameters for urea and creatinine, blood pressure measurement, morphological analysis of the kidney tissue as well as examining fibrosis markers. The cardiac phenotyping included the evaluation of the heart function, investigation of cardiac tissue for fibrosis, hypertrophy and inflammation via gene expression analysis and/or histological analysis of the cardiac tissue as well as examining the oxidative stress response.
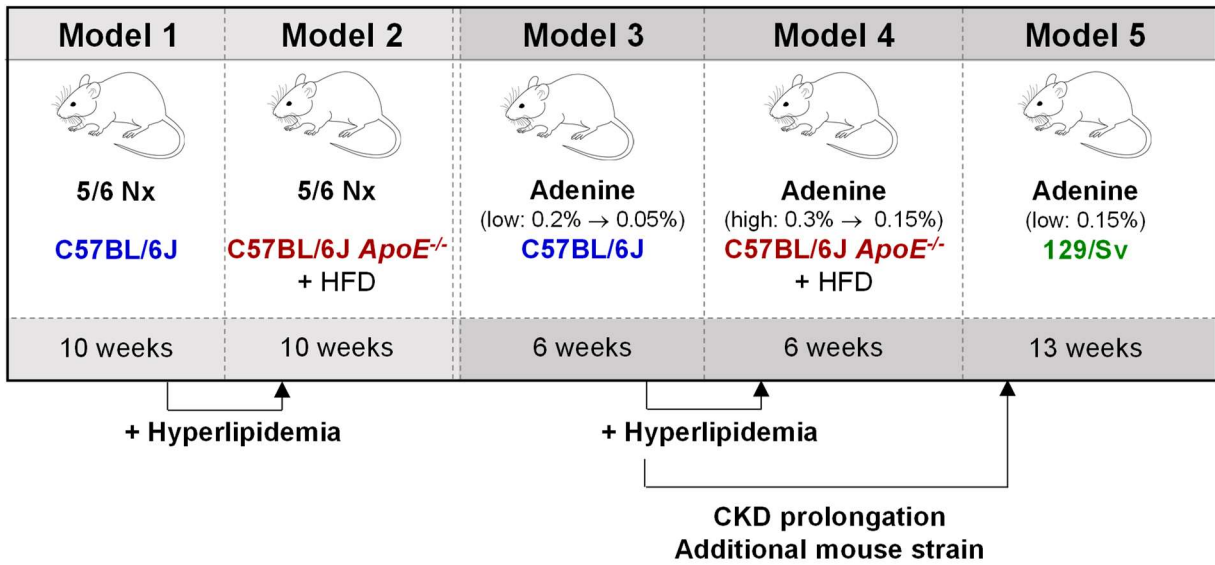
Figure 6: Overview of the five different experimental CKD mouse models which are systematically compared in this thesis.
Model 1: CKD induction by 5/6 Nx in C57BL/6J wildtype mice for 10 weeks. **Model 2:** CKD induction by 5/6 Nx in C57BL/6J *ApoE*$^{-/-}$ mice for 10 weeks, with these mice developing hyperlipidemia on high-fat diet as risk factor for CKD and CVD. **Model 3:** CKD induction by adenine diet in C57BL/6J wildtype mice for 6 weeks. **Model 4:** CKD induction by adenine diet with increased adenine concentration in hyperlipidemic C57BL/6J *ApoE*$^{-/-}$ mice for 6 weeks. **Model 5:** CKD induction by adenine diet in 129/Sv mice with a prolonged CDK duration of 13 weeks. *5/6 Nx = 5/6 nephrectomy; ApoE*$^{-/-}$ *= apolipoprotein E knockout; CKD = chronic kidney disease; CVD = cardiovascular disease; HFD = high-fat diet.*

Chapter 3

Materials and methods

3. Materials and methods

3.1. Materials

3.1.1. General laboratory equipment

Table 2: General laboratory equipment used

Equipment	Manufacturer
-20°C Freezer Economic-super	Bosch (Germany)
-20°C Freezer Premium	Liebherr (Germany)
4°C Fridge Premium frost-free	Liebherr (Germany)
-80°C Freezer Ultra Low	SANYO (The Netherlands)
Akku Trimmer (GT415)	AESCULAP (Germany)
Axio Scan.Z1	Zeiss (Germany)
C1000 Touch™ Thermal Cycler	BioRad (Germany)
Centrifuge 5417R	Eppendorf (Germany)
CODA system	Kent Scientific Corporation (USA)
GelDoc XR imaging setup	BioRad (Germany)
Heating block thermomixer comfort	Eppendorf (Germany)
Ice machine AF 100	Scotsman (Italy)
Microscope Leica DM 5500B	Leica Biosystems GmbH (Germany)
Microtome Leica RM 2250	Leica Biosystems GmbH (Germany)
Millar Mikro-Tip® Pressure Transducer Catheter	Millar Instruments (USA)
Milli-Q® Advantage A10	Merck (Germany)
NanoDrop™ One	Thermo Fisher Scientific (USA)
Paraffin embedding machine	Leica Biosystems GmbH (Germany)
pH-Meter LAB 855	SI Analytics (Germany)
Plate Reader Infinite 200M	Tecan Group Ltd (Switzerland)
QuantStudio 3	Applied Biosystems (Germany)
TissueLyzer LT	Qiagen (Germany)
Trans-Blot SD	BioRad (Germany)
VisualSonics 3100 imaging system	FUJIFILM VisualSonics, Inc. (Canada)

3.1.2. General consumables

Table 3: List of general consumables

Consumables	Manufacturer
96-well PCR plate	Applied Biosystems (Germany)
Bepanthen ®	Bayer (Germany)
Gelastyp	Sanofi (Germany)
Mersilene suture 5-0, R670H, FS-3 needle, 45 cm green	Ethicon (USA)
Needles 23G/24G/27G	BD Microlane (USA)
Nitrocellulose membrane	Thermo Fisher Scientific (Germany)
Reaction tubes (0.5 mL, 1.5 mL, 2.0 mL)	Carl Roth (Germany)
Serum tubes	Sarstedt (Germany)
Superfrost™ Plus Adhesion Microscope Slides	Epredia (Germany)
Syringe BD Plastipak (10 ml)	BD (USA)
Tabotamp Haemostyptikum	Ethicon® (Switzerland)

3.1.3. Chemicals and reagents

Table 4: List of chemicals and reagents

Chemicals / reagents	Manufacturer
10% formalin	Carl Roth (Germany)
10x lysis buffer	Cell Signaling (USA)
5x PowerUp SYBR Green Master Mix	Applied Biosystems (Germany)
Alizarin Red	Sigma Aldrich (USA)
Bovine serum albumin (BSA)	Carl Roth (Germany)
c0mplete™ mini protease inhibitor cocktail	Roche (Germany)
Clarity Western ECL Substrate	BioRad (Germany)
ddPCR™ Droplet Reader Oil	BioRad (Germany)
ddPCR™ Supermix	BioRad (Germany)
DG8TM Gaskets	BioRad (Germany)
Dithiothreitol (DTT)	Sigma-Aldrich (Germany)
Droplet Generator DG8™ Cartridge	BioRad (Germany)
Phosphate-buffered saline (PBS)	Thermo Fisher Scientific (USA)
Phospho STOP	Roche (Germany)
PowerUp™ SYBR™ Green Master Mix	Applied Biosystems (Germany)
Sirius red solution	Morphisto (Germany)
Vectashield	Vector Laboratories (UK)

3.1.4. Buffers and solutions

Table 5: List of buffers and solution used in this thesis

Buffers	Composition	Concentration
1x Tris buffered saline (TBS) (pH 7.5)	Tris Base NaCl	50 mM 150 mM
1x sodium dodecyl sulfate (SDS) running buffer	Tris Base Glycine SDS	25 mM 192 mM 0.1 %
4x SDS running gel buffer (pH 8.8)	Tris Base SDS	1.5 M 0.4 %
4x SDS stacking gel buffer (pH 6.8)	Tris Base SDS	0.5 M 0.4 %

Buffers	Composition	Concentration
Blocking solution (for immunofluorescent staining)	PBS BSA Horse serum Avidin	6 ml 1 % 3 drops 24 drops
Blocking solution (for Western blot)	Milk powder TBS-T	5 % (w/v)) 250 ml
Citrate buffer (pH 6)	H_2O Solution 1 Solution 2 Tween 20	630 ml 12.6 ml 57.4 ml 350 µl
Differentiation solution	Ethanol HCl	95 % 1.2 mM
Lysis buffer	10x Lysis buffer 10x Phospho stop 10x Protease inhibitor complex MilliQ	100 µl 100 µl 100 µl 700 µl
Methyl Carnoy's	Methanol Chloroform Acetic acid	600 ml 300 ml 100 ml
Saline	NaCl	0.9 %
SDS PAGE sample buffer	4x Laemmli sample buffer 1 M DTT	1x 100 mM
SDS running gel (10%)	4x running gel buffer (pH 8.8) 30 % Acrylamide/Bis H_2O 10 % APS TEMED	2.5 ml 3.3 ml 4.2 ml 100 µl 10 µl
SDS stacking gel (5 %)	4x stacking gel buffer (pH 6.8) 30 % Acrylamide/Bis H_2O 10 % APS TEMED	2.5 ml 1.7 ml 5.8 ml 100 µl 10 µl
Solution A	Citric acid MilliQ	21.01. g 1 L
Solution B	Natrium citrate MilliQ	29.41 g 1 L
TBS-T	1x TBS Tween 20	 0.1 %
Transfer buffer	Trans-Blot Turbo 5x buffer Ethanol H_2O	25 ml 25 ml 75 ml

3.1.5. Kits

Table 6: List of used kits

Kit	Manufacturer
DC protein assay	BioRad (Germany)
RNeasy Micro Kit	Qiagen (Germany)
RNase-free DNase Set	Qiagen (Germany)
SuperScriptTM VILO^{TM} Mastermix	ThermoFisher Scientific (Germany)

3.1.6. Antibodies

Table 7: List of antibodies used for western blot

Antibodies	Cat. number	Manufacturer
Anti-SOD1 antibody	TA321133	OriGene (USA)
Anti-SOD2 antibody	TA321189	OriGene (USA)
Anti-CAT antibody	14097	Cell Signaling (USA)
Anti-HO-1 antibody	82206	Cell Signaling (USA)
Anti-PRX2 antibody	ab50862	Abcam (UK)
Anti-PRX3 antibody	ab73349	Abcam (UK)
Anti-NOX2 antibody	ab129068	Abcam (UK)
Anti-COL1 antibody	1310-01	Southern Biotech (USA)
Anti- αSMA antibody	M0851	Dako (Denmark)
Anti-γTUB antibody	TA325961	OriGene (USA)
Anti- GAPDH antibody	21180	Cell Signaling (USA)

Table 8: List of antibodies, conjugates or dyes for immunofluoresence staining

Antibodies/ Conjugates	Cat. number	Manufacturer
Anti-8-OHdG antibody	ab62623	Abcam (UK)
DAPI staining solution, 1 µg/ml	Cat. No. 268298	Calbiochem (USA)
Fluorescein-conjugated WGA	FL-1021	Vector Laboratories (USA)

3.1.7. Software

Table 9: List of software

Software	Manufacturer
DISCUS Software	DISCUS Software Company (USA)
GraphPad Prism 9	GraphPad Software (USA)
ImageJ software	ImageJ
ImageLab 2.0	BioRad (Germany)
QuantaSoft	BioRad (Germany)
VevoLab 3.2.0.	FUJIFILM VisualSonics, Inc. (Canada)

3.2. Methods

3.2.1. Animals

The animal studies were authorized by LANUV (Landesamt für Natur, Umwelt und Verbraucherschutz Nordrhein-Westfalen, Germany, approval number 81-02.04.2017.A504) and performed according to local, national and European Union ethical guidelines. The animal experiments were performed with male C57BL/6J mice (C57BL/6JRj, Janvier, Germany: Models 1 and 3) and C57BL/6J *ApoE*$^{-/-}$ mice (bred and housed under specific pathogen-free conditions in the animal facility of the RWTH Aachen university hospital: Models 2 and 4). At experimental start, the mice were at the age of 8 to 10 weeks. During the experimental time, the mice were group housed and had free access to water and food. The general health status of the animals was checked daily and evaluated using a study-dependent score sheet according to the approval and the guidelines of the national Society of Laboratory Animal Science (GV-SOLAS).

3.2.2. Study design for animal experiments

Subtotal nephrectomy-induced CKD (Models 1-2). As the first method for CKD induction, a subtotal nephrectomy (5/6 Nx) was performed, which is a well-known method for inducing kidney damage. One kidney was removed in total and from the second kidney, 2/3 were removed, thereby reducing the nephron numbers and thus the filter capacity of the kidney. After 10 weeks the mice were sacrificed for analysis of kidney and heart. At first, C57BL/6J wildtype mice were used, which is the most commonly used mouse strain in research because of many available transgenic options (**Model 1**). The second mouse experiment was performed in apolipoprotein E deficient (*ApoE*$^{-/-}$) mice with C57BL/6J background and on high-fat diet, to include hyperlipidemia as a risk factor for CKD and CVD (**Model 2**) (experimental overview provided in **Figure 7**).
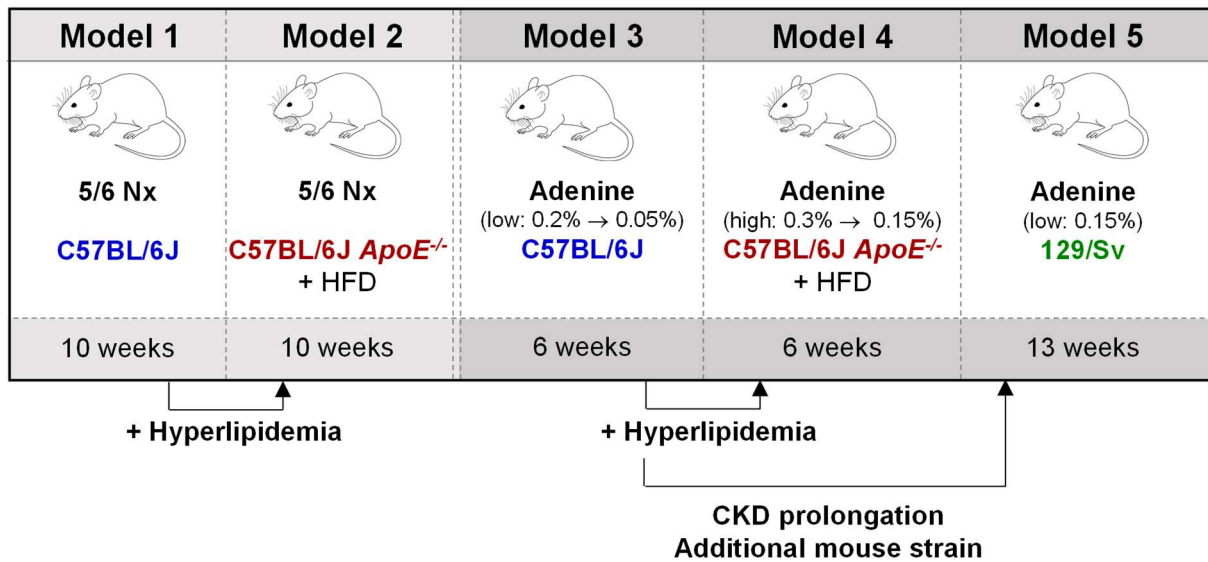
Figure 7: Exploratory overview of the studied mouse models.
Summary of the experimental CKD mouse models characterized in this thesis for cardiac phenotype, with indication of what was done by cooperation partners and by me. **Model 1:** CKD induction by 5/6 Nx in C57BL/6J wildtype mice for 10 weeks. **Model 2:** CKD induction by 5/6 Nx in C57BL/6J ApoE^{-/-} mice for 10 weeks, with these mice developing hyperlipidemia on high-fat diet as risk factor for CKD and CVD. **Model 3:** CKD induction by adenine diet in C57BL/6J wildtype mice for 6 weeks. **Model 4:** CKD induction by adenine diet with increased adenine concentration in hyperlipidemic C57BL/6J ApoE^{-/-} mice for 6 weeks. **Model 5:** CKD induction by adenine diet in 129/Sv mice with a prolonged CDK duration of 13 weeks. *5/6 Nx = 5/6 nephrectomy; ApoE^{-/-} = apolipoprotein E knockout; CKD = chronic kidney disease; CVD = cardiovascular disease; HFD = high-fat diet.*

Adenine-induced CKD (Models 3-5). A diet-induced approach was applied for the second CKD induction method, being the induction via adenine feeding. The orally consumed adenine precipitates in the kidney and forms 2,8-dihydroxyadenine crystals within the renal tubules [66]. This approach leads to tubular injury, which results in a reduced filter capacity of the kidney. As for the 5/6 Nx models, the experiment was performed in C57BL/6J wildtype mice (**Model 3**) as well as in C57BL/6J ApoE^{-/-} mice (**Model 4**) on high-fat diet, both for an experimental time of 6 weeks (experimental overview in **Figure 7**).

In cooperation with our collaborators within the SFB/TRR219 consortium, Dr. Janina Frisch and Prof. Dr. Leticia Prates Roma from the University Hospital Homburg (Universität des Saarlandes), an additional mouse model was examined. In 129/Sv mice (**Model 5**), which is a strain often used in CKD research, CKD was induced via adenine feeding (experimental overview in **Figure 7**).

3.2.3. Two-step 5/6 nephrectomy (Model 1 and 2)

Before starting the surgery, the mice received 0.05 mg/kg Buprenorphine for pain reduction. After 30 min mice were anesthetized by using inhalational isoflurane anesthesia (initial 3% isoflurane, maintenance 1.5-2% isoflurane, flowrate 0.8 l/min), mice were placed on a heating pad and eyes were treated with panthenol balm. In the first surgery, the left kidney was exposed through a flank incision and the two poles of the kidney were removed. By using absorbable surgical hemostatic (Tabotamp) and gelatin sponge (Gelastyp) the kidney bleeding was stopped, and the skin incisions were closed with a continuous suture. After one week of recovery time, the second surgery was performed. The preparation of the mice was performed according to the procedure mentioned above. After a flank incision on the right side, the kidney vessel and the ureter were ligated by a silk suture and the kidney was removed without further bleeding. The incision was closed again with a continuous suture. The procedure for sham-operated mice was analogous, without removement of kidney and kidney poles. For pain reduction, the mice received 0.05 mg/kg Buprenorphine every 8 h for the following 3 days after each surgery.

Model 1. C57BL6/J mice underwent a 5/6 nephrectomy according to the before mentioned protocol for an experimental time range of 10 weeks. The mice were fed with a chow diet.

Model 2. Before surgery, the *ApoE*$^{-/-}$ mice were fed with a western-type high-fat diet for 4 weeks. Then the 5/6 nephrectomy was performed according to the protocol, while the mice were continuously fed with the western-type high-fat diet until the end of the experiment after 10 weeks.

Details on the experiments and diets are provided in **Table 17** in appendix (page 123).

3.2.4. Adenine-induced nephropathy (Model 3-5)

The animal chow for the adenine-induced nephropathy models was purchased either from Ssniff (for C57BL/6J mice) or from Altromin (for *ApoE*$^{-/-}$ mice), both containing 20%, respectively, 19.5% casein. 129/Sv mice were fed with a chow diet from Altromin supplemented with 0.15% adenine without the addition of casein.

Model 3. The C57BL/6J mice feeding protocol was as follows: for 2 weeks mice were fed a chow diet containing 0.2% adenine, followed by a lower adenine concentration of 0.05% for further 4 weeks, resulting in a total adenine feeding time of 6 weeks. Respective sham animals received the respective control diet without addition of adenine over the whole individual experimental time range.

Model 4. The $ApoE^{-/-}$ mice were fed a western-type high-fat diet for 4 weeks before exchange to a western-type high-fat diet supplemented with 0.3% adenine for 10 days, followed by western-type high-fat diet with a reduced adenine concentration of 0.15% for further 4.5 weeks. Respective sham animals received the respective control diet without addition of adenine over the whole individual experimental time.

Model 5. The 129/Sv mice were fed a chow diet supplemented with 0.15% adenine during the whole experimental time, being 13 weeks in. After completion of the experiment, the hearts were sent to me for molecular analysis.

Details on adenine protocols and diets are provided in **Table 17** in appendix (page 123).

3.2.5. Blood sampling and processing

Blood sampling during the experiments was performed at the indicated time points by retro-orbital bleeding using a glass capillary after short inhalational isoflurane anesthesia (1.5-2% isoflurane). At the end of the experiments, mice were anesthetized by i.p. injection of ketamine (100 mg/kg bodyweight) and xylazine (10 mg/kg bodyweight) for invasive heart function measurement (please refer to corresponding section *§3.2.8; page 37* for details) and afterwards directly sacrificed by heart cannulation to collect all remaining blood of the mice in serum tubes containing coagulant (Sarstedt, Germany). After centrifugation at 3000 g for 10 min, the occurred serum was transferred into a fresh tube for analysis of creatinine (µM) and urea (mM) content in the service facility "Clinical Chemistry and Hematology" from the RWTH Aachen University Hospital. The remaining serum was kept at -80°C.

3.2.6. Blood pressure measurements

For measurements of systolic and diastolic blood pressure, the non-invasive tail-cuff method was used via the computerized CODA system (Kent Scientific Corporation, USA). Tails of the non-anesthetized mice were fixed in a specifically designed cuff that

is connected to the system and interrupted the blood flow via automated cuff air-filling. During the slow air efflux, the flow pulsation was detected by an integrated sensor. Measurements were performed at the indicated time points (please refer to *results §4*) and are displayed in mm Hg.

3.2.7. Cardiac functional measurements using non-invasive echo-cardiography

After anesthesia of the mice via inhalational isoflurane (initial 3% isoflurane, maintenance 1-2% isoflurane), mice were placed on a heating pad with continuous inhalational isoflurane via nose mask. Ultrasound imaging was performed with a high-resolution ultrasonic device (VisualSonics 3100 imaging system; scanhead: MX550D) recording the parasternal long axis (PSLAX) and the short axis (SAX), both in B- and M-mode (midventricular level, apical of the papillary muscle). Additionally, the four-chamber view was recorded to determine the mitral flow velocity. Using VevoLab 3.2.0. (VisualSonis, Canada) cardiac analysis was performed by averaging manual contouring/measuring results from all available axes and modes, assessing left ventricular end-diastolic diameter (LVEDD) and volume (LVEDV), left ventricular end-systolic diameter (LVESD) and volume (LVESV), interventricular septum thickness (IVS) and left ventricular posterior wall thickness (LVPW). Furthermore, stroke volume (SV = LVEDV - LVESV), cardiac output (CO = SV x heart rate), ejection fraction (EF = SV / LVEDV x 100), fractional shortening (FS = (LVEDD - LVESD) / LVEDD) x 100) and left ventricular mass (LVM = 1.04 x ((LVEDD + IVSd + LVPWd)^3 - LVEDD^3)) - 13.6) were averaged using automated software output and additional manual calculation by the specified mentioned equations.

3.2.8. Cardiac functional measurements using invasive Millar catheter analysis

At end of the experiment, cardiac function was determined via invasive heart function measurement using a Millar Mikro-Tip® Pressure Transducer Catheter (Millar Instruments, USA). After anesthesia by i.p. injection of ketamine (100 mg/kg bodyweight) and xylazine (10 mg/kg bodyweight), the Millar catheter was inserted into the right carotid artery and, after fixation, retrogradely advanced through the aortic valve into the left ventricle. For heart function characterization, the maximal rate (dP/dT max) and

the minimal rate (dP/dT min) of the pressure change over time was analyzed for assessing the contraction and the relaxation capacity of the heart as well as the left ventricular end-diastolic pressure (LVEDP). After completing the measurements, the catheter was removed, the occurrent bleeding was stopped by ligation of the carotid artery and mice were immediately sacrificed.

3.2.9. Organ explantation and processing

Directly after invasive heart function measurement, mice were sacrificed by heart cannulation to remove all blood for further blood processing (please refer to *blood sampling and processing in §3.2.5; page 36*). The coat was incised and after giving 0.2% lidocaine to the skin for local anesthetics, the thorax was opened. After rinsing organs and vessels with PBS to remove remaining blood, heart and kidneys were quickly removed and released from fat and remaining tissue. For RNA and protein analysis, a part of apex or ventricle of the heart as well as the longitudinal halved kidney were snap-frozen in liquid nitrogen and stored at -80°C. The remaining heart and kidney were fixed in 10% formalin, respectively, in methyl Carnoy's for histological analysis.

3.2.10. Protein isolation from tissue

Tissue homogenates from heart and kidney were generated in pre-cooled 135 µl lysis buffer (Cell signaling, USA) supplemented with protease inhibitor cocktail (Roche, Schweiz) and phosphatase inhibitors (Sigma-Aldrich, USA) using steel beads in combination with a tissue lyser (TissueLyzer LT, Qiagen, Germany). The first homogenization step was performed at 50 Hz for 7 min, followed by two further homogenization steps at 50 Hz for 5 min to ensure a consistent homogenate. Both the homogenate and the sample container were cooled at -80°C for 5 min at the start and between each homogenization step. To remove solid cell debris, the homogenate was centrifuged at 14,000 rpm for 5 min at 4°C twice, with transferring the homogenate into a fresh tube after each step. The total protein content was determined using the DC protein assay (BioRad, Germany).

3.2.11. Western blot analysis

A total of 50 µg protein from the heart lysates and 15 µg protein from the kidney lysates per lane were subjected to sodium dodecyl sulfate-polyacrylamide gel electrophoresis (SDS-PAGE), followed by transfer to a nitrocellulose membrane (Amersham Protran,

Fisher Scientific, Germany) via semi-dry blotting (Trans-Blot SD, BioRad, Germany). Blocking the membranes was performed with 5% (w/v) non-fat dry milk in TBS-T for 1 h at RT. After several washing steps with TBS-T, the membranes were incubated with primary antibody overnight at 4°C according to the manufacturer's instructions (refer to **Table 7** in *§3.1.6; page 31*). γ tubulin (γTUB) or glyceraldehyde 3-phosphate dehydrogenase (GAPDH) was used as internal loading controls. Several washing steps with TBS-T were followed by incubation with species-matched secondary antibody (HRP-conjugated, GE Healthcare, USA) for 2 h at RT. After final washing steps with TBS-T, band detection was performed by using chemoluminescent Clarity Western ECL Substrate (BioRad, Germany) and a GelDoc XR imaging setup (BioRad, Germany). Band intensities were quantified with normalization to respective loading controls (γTUB or GAPDH, as indicated) using ImageLab 2.0 (BioRad, Germany). Data are presented as a fold-increase of normalized band intensities as compared with the mean value of sham-treated animals.

3.2.12. Histological and immunofluorescent analyses

Tissue fixation and paraffin embedding. Cardiac transversal tissue was fixed in 10% formalin while the longitudinal halved kidney was fixed in methyl Carnoy's, both immediately after organ removal, for 24 to 48 h. Dehydration of the organs was performed in ascending alcohol concentrations. Then, the organs were directly embedded in paraffin. Hearts were cut in 5 µm slices and kidneys in 1 µm slices using a rotation microtome (Leica, Germany) with subsequent slide drying for ≥1 h at 60°C or slide drying at RT for a few days. For histological stainings, the paraffin slides were processed for rehydration in descending alcohol concentrations.

Histological stainings of the kidney. Fibrosis analysis in kidney sections was performed using ´**Acid Fuchsin Orange G´ (AFOG) staining**. Slides were deparaffinized and fixed a second time with Bouin's solution at 60°C for 2 h. Next, slides were hydrated for 20 min before treating with hematoxylin and iron chloride solution for 1 min, followed by washing in water for 30 s. Slides were differentiated in 0.1% hydrochloric acid for 10 s, transferred into water for 10 min and treated with 1% phosphomolybdic acid for 5 min. After an additional washing step in water, incubation with AFOG solution was performed for 10 min, followed by a final wash in ddH_2O, dehydration and covering with mounting medium.

Tubular injury was shown via ´**Periodic Acid-Schiff**´ (PAS) staining of kidney sections. Slides were deparaffinized/rehydrated/washed as mentioned before and incubated with 2% periodic acid for 30 min. After washing in ddH$_2$O, slides were stained with Schiff's reagent for 60 min and washed with running water for 5 min at 35°C. For counterstaining, slides were incubated with hematoxylin for 4 min and washed again in running water for 5 min. Next, slides were dipped in Tris buffer pH 8.3, washed again in water for 5 min, dehydrated as explained above and subsequently covered with mounting medium.

Histological stainings of the heart. Fibrosis analysis of heart sections were examined by ´**Sirius Red Staining**´. Sections were deparaffinized/rehydrated/washed and then incubated for ≥60 min in a 0.1% Sirius red solution (Morphisto, Germany). In the end, slides were dehydrated and mounted with mounting medium.

Calcification staining on heart sections was performed after deparaffinizing/rehydration/washing via incubation for 30 min in a paper-filtered solution of 2% **Alizarin Red** (Sigma Aldrich, USA) in ddH$_2$O. Slides were washed for 10 s in ddH$_2$O, followed by repeated dips in a differentiation solution (95% EtOH, 1.2 mM HCl) for a total of 15 s, a final dip in fresh xylene and mounting with mounting medium as described above.

Immunofluorescent stainings of the heart. **8-Hydroxyguanosine** (8-OHdG) immunostaining was performed on cardiac sections to analyze DNA damage induced by oxidative stress. Deparaffinized/rehydrated/washed sections were boiled in citrate buffer containing Tween 20 at pH 6.0 for 20 min, followed by blocking in a moist chamber for 30 min with blocking solution containing PBS, 1 % BSA, three drops of horse serum and 24 drops of Avidin. Then heart sections were incubated with 8-OHdG antibody for 1 h. After a PBS washing step, slides were treated with anti-mouse-biotin antibody for 30 min, washed again in PBS followed by incubation with streptavidin-FITC in the dark for 30 min. After a final washing step in PBS, heart sections were incubated with 4′,6-diamidino-2-phenylindole (DAPI) staining solution and then mounted with mounting medium

Analyzing cardiac hypertrophy was performed by ´**Wheat Germ Agglutinin**´ (WGA) staining. After deparaffinizing/dehydrating/washing, antigen retrieval was performed by boiling the tissue in the microwave in citrate buffer containing Tween 20. After cooling

down to RT and short washing in PBS, fluorescein-conjugated WGA (Vector Laboratories, FL-1021) was applied at 1:1000 in PBS and incubated for 1 h. After a PBS washing step, incubation in DAPI staining solution (Calbiochem Cat. No. 268298, 1 µg/ml) was performed for 5 min. In the end, a final washing step with ddH$_2$O was done and heart sections were mounted with mounting medium.

Microscopy and analysis of histological and immunofluorescent stainings. Histologically stained kidney sections were scanned by using an automated scanning device (Axio Scan.Z1, Zeiss, Germany) with focus control and stitching for generating full slice images. Evaluation of the kidney damage was performed by using one slide per animal derived from the middle of the longitudinal halved kidney.

From all histologically stained cardiac slides, pictures were taken with a Leica DM5500 B microscope (Leica, Germany) to generate 1.25x/10x images. Three sections per animal were stained derived from the middle to the upper part of the heart with a distance of 400 to 600 µm between each section. Quantitative analysis for cardiac fibrosis was performed on four images per slide using Fiji imaging software by detecting the percentage of positively stained area upon setting constant threshold values for individual experiments. One value per slide was calculated and values of different slides per mouse were averaged to obtain one final value per mouse.

Immunofluorescence images were generated using a Leica DM6 B microscope with an X-cite 120 PC fluorescence lamp to detect fluorescein signals generating 40x images. Three slides per animal derived from the middle to the upper part of the heart with a distance of 400 to 600 µm between each section were used to determine the mean cardiomyocyte diameter as well as the number of 8-OHdG positive nuclei both on three images per slide using Fiji image analysis software. One value per slide was calculated and values of different slides per mouse were averaged to obtain one final value per mouse.

3.2.13. Quantitative real-time PCR analysis

RNA isolation and cDNA synthesis. For gene expression analysis, approximately 5 mg of heart tissue were immediately supplemented with ice-cold RLT lysis buffer (RNeasy Micro Kit, Qiagen, Germany), and steel beads homogenizing the samples in TissueLyzer LT (Qiagen, Germany). After homogenization, RNA was isolated according to the manufacturer's instructions with an additional step for DNase treatment (RNase-

free DNase Set, Qiagen, Germany). The concentration of RNA was measured by a Nanovue Plus Spectrophotometer (Biochrom, Germany). cDNA generation was performed as follows: 200 ng RNA was transcribed into cDNA by using the SuperScriptTM VILOTM Mastermix (ThermoFisher Scientific, Germany) according to manufacturer's instructions with extension of the incubation at 42°C to 2 h to increase the cDNA yield.

Quantitative real-time PCR (qPCR) analysis. qPCR analysis for Model 1, 2 and 3 were performed by combining 1x SybrGreen master mix (PowerUp™ SYBR™ Green Master Mix, Applied Biosystems, Germany), cDNA (3 µl of 1:5) and 0.2 µM of the respective primers (**Table 10**) using QuantStudio 3 (Applied Biosystems, Germany). qPCRs with housekeeping genes were run in triplicates, while qPCRs for the gene of interest were performed in duplicate, with values averaged for further analysis. Conditions for the qPCR runs were as follows: the initial denaturation was done at 95°C for 10 min, followed by the cycles consisting of denaturation at 95°C for 15 s; annealing at 60 °C for 1 min; going back to denaturation for 39 cycles; followed by a melt curve stage starting at 60 °C with continuously rising temperature of 0.1 °C per second until 95 °C was reached. Relative quantification was performed by use of the comparative ΔΔCT method. For gene expression normalization, a combination of three housekeeping genes was used. The relative expression of the gene was first calculated for each housekeeping gene separately and afterwards calculating the geometric mean of all separate relative values to obtain the relative gene expression normalized to the combination of the housekeeping genes, as described in Vandesompele *et al.* [71].

Table 10: Primers for SybrGreen qPCR (Eurofins, Ebersberg, Germany)

Target gene	Sequence (5'-XXX-3') Forward primer	Sequence (5'-XXX-3') Reverse primer
Hprt	GCT TTC CCT GGT TAA GCA GTA CA	GAG AGG TCC TTT TCA CCA GCA A
b-actin	CAC TGT CGA GTC GCG TCC	TCA TCC ATG GCG AAC TGG TG
GusB	ATA AGA CGC ATC AGA AGC CG	ACT CCT CAC TGA ACA TGC GA
Col1a1	TCG CTT CAC CTA CAG CAC CC	TGA CTG TCT TGC CCC AAG TTC
Col3a1	TCT GAG CTG CTT CTT CCT CTC T	GAA GAA ACC AGG TTC CAC TTT G
Tgfb1	TGA CGT CAC TGG AGT TGT ACG G	GGT TCA TGT CAT GGA TGG TGC
Ccl2	GCT GTA GTT TTT GTC ACC AAG C	GAC CTT AGG GCA GAT GCA GT
Tnf	CCACCACGCTCTTCTGTCTA	AGGGTCTGGGCCATAGAACT
Icam1	GCC TTG GTA GAG GTG ACT GAG	GAC CGG AGC TGA AAA GTT GTA

Target gene	Sequence (5'-XXX-3') Forward primer	Sequence (5'-XXX-3') Reverse primer
Anp	TGG ATT TCA AGA ACC TGC TAG ACC	AGG GCA GAT CTA TCG GAG GG
Bnp	AGT CCT TCG GTC TCA AGG CA	AAC TTC AGT GCG TTA CAG CCC A

Droplet digital PCR (ddPCR) analysis. Gene expression profiling for Model 4 was performed via droplet digital PCR (ddPCR). A PCR mix with a total volume of 20 µl was prepared by adding ddPCR™ Supermix for Probes (No dUTP) (Bio-Rad, Germany), Taqman gene-specific primers and probes (ThermoFisher Scientific, Germany, **Table 11**), RNAse free water (ThermoFisher Scientific, Germany) and template cDNA, and were transferred into Droplet Generator DG8™ Cartridges (BioRad, Germany). A total of 70 µl of the Droplet Generation Oil for Probes (Bio-Rad, Germany) was added to the appropriate wells, the cartridges were covered with DG8™ Gaskets (Bio-Rad, Germany) and placed in a QX100™ Droplet Generator (Bio-Rad), generating droplets that were then transferred to a 96-well PCR plate (Eppendorf, Germany). PCR amplification was performed using a C1000 Touch™ Thermal Cycler (BioRad, Germany) with the following settings: the initial denaturation was performed at 95 °C for 10 min, followed by 40 cycles of denaturation at 94 °C for 30 s and an annealing phase at 60 °C for 60 s (ramping rate set to 2 °C/s), with a final incubation for 10 min at 98 °C, and an end temperature at 4 °C. Read out of the droplets was performed with the QX 100 Droplet reader (Bio-Rad, Germany) by use of ddPCR™ Droplet Reader Oil (Bio-Rad, Germany). Data acquisition and analysis were performed with QuantaSoft (BioRad, Germany) in which the threshold value of the fluorescence amplitude, which differentiates between positive and negative droplets, was manually set by the analyst as the midpoint between the average fluorescence amplitude of positive and negative droplets, whereas the same value was set for the whole PCR plate. The measurement provided the concentration of the transcripts indicated as copies of target per microliter (copies/µl), allowing the calculation of the total number of copies present in the original sample. The copy number of the target genes was calculated in comparison to the copy number of the housekeeping gene resulting in the ratio of target gene and housekeeping gene (*Hprt).*

Table 11: Taqman primers and probe mixes (ThermoFisher Scientific, Germany) used for ddPCR

Target gene	Taqman probe ID
Hprt	Mm03024075_m1
Col1a1	Mm00801666_g1
Col3a1	Mm00802300_m1
Tgfb1	Mm01178820_m1
Ccl2	Mm00441242_m1
Tnf	Mm00443258_m1
Icam1	Mm00516023_m1
Anp	Mm01255747_g1
Bnp	Mm01255770_g1

3.2.14. RNA Sequencing

For RNA extracted from heart tissue from Model 5, a paired-end RNA sequencing was performed. Total RNA extraction was performed using peqGOLD TriFast Kit (Peqlab) according to manufacturer's instructions. A total of 800 ng RNA per sample was analyzed at Genewiz (GENEWIZ GmbH, Germany) with the Illumina NovaSeq 6000. Quality control and adapter trimming was included. Using the NEBNext Ultra RNA Library Prep Kit for Illumina, the RNA sequencing libraries were prepared following the manufacturer's instructions. All samples passed the quality control by examination with the FastQC (v.0.11.9) software package. On average, 46,510,236 reads per sample were obtained. Sequences were aligned to the reference mouse genome GRCm38.p6 and the appropriate GTF file (vM25) from GENCODE using STAR software (v.2.7.6a), resulting in 79.10 % uniquely assigned reads [72]. By using the R package Rsubread (v.2.2.6) the gene level read counts were quantified and framed [73]. To determine the differentially expressed genes (DEGs) between the sham and adenine groups, a differential expression analysis was performed based on the matrix of read counts using the R package DESeq2 (v1.28.1) [73]. The p-values were further adjusted for multiple testing ($p_{adjusted}$) by the Benjamini-Hochberg procedure, while the parameter alpha in DESeq2, representing the acceptable probability of a Type I error, was set to 0.05.

Data were presented in a volcano plot showing $\log_2$(fold change) and $-\log_{10}(p_{adjusted})$ of genes comparing the adenine-treated group to the sham group. DEGs with $p_{adjusted}<0.05$ and $\log_2$(fold change) > 1 or < -1 were considered for further analysis. From these DEGS, further final selection of 10 DEGs per modulation (up-, downregulation) was performed using two complementary strategies:

Strategy 1: Significant DEGs were sorted by p-value, and the 10 most significant up- and down-regulated genes were reviewed based on their Gene Ontology (GO) terms relevant to cardiac (patho)physiological processes (keywords: cardiac, inflammation/inflammatory, cytokine, collagen, fibrosis/fibrotic, hypertrophy/hypertrophic, heart, reactive oxygen species, ROS, mitochondria). The resulting top 10 DEGs associated with these GO terms were further considered. Using the identical keywords as mentioned above, the DEG-associated GO lists were screened for relevant GO terms, resulting in additional genes of interest (selection from the significant DEG list). GO terms were sorted per topic (extracellular matrix (ECM), collagen/fibrosis, inflammatory response, reactive oxygen species (ROS), mitochondria, heart) and p-value.

Strategy 2: The DEG-associated GO list, which is based on significant DEGs, was screened for relevant GO terms related to (patho)physiological processes of the heart (priority #1), strong p-value (priority #2), and gene ratio (i.e. for all significantly up- or down-regulated DEGs, the fraction belonging to the respective GO term; priority #3). In the end, 10 GO terms were selected that were enriched with significantly up- and downregulated genes. In parallel, a preselected GO list of pathology-relevant GO terms was generated. Then, both GO lists were analysed for associated, significantly up- and down-regulated genes with $\log_2$(fold change) > 1 or < -1 and $p_{adjusted}<0.05$. In the final analysis, the results of the selected DEGs from the two protocols were summarized and reviewed in relation to pathological findings in the literature, and then reduced to a maximum selection of 10 genes for both up- and down-regulated genes, as shown in **Figure 44**. The selected DEGs were categorized into the most relevant and significantly regulated GO terms, which are displayed in **Figure 45** and **Figure 46** as bar graphs representing the $-\log_{10}$(p-value) for both up- and down-regulated pathways. The evaluation of significance levels from the selected GO terms in relation to significant DEGs was done using the R package clusterProfiler (v.3.16.1) [74].

RNAseq data from this study have been deposited in the Gene Expression Omnibus (GEO) and can be accessed under the accession number GSE191122.

3.2.15. Statistics

Statistics were performed by using the Student's T-test for comparing two groups with normal distribution or Mann-Whitney test for comparison of two not normally distributed groups. Two-way ANOVA or mixed-effects analysis with Sidak's post-test (95% confidence interval) was used for multiple group comparisons. All statistical analysis including analysis of normal distribution was performed with GraphPad Prism 9.0.0. software (GraphPad Software Inc., USA). A p-value of $p < 0.05$ was considered to be significant ($*p < 0.05$, $**p < 0.01$, $***p < 0.001$).

Chapter 4

Results

4. Results

In order to compare the cardiac phenotype in different mouse models of CKD, CKD induction was performed on the one hand by the frequently used 5/6 Nx method and on the other hand by adenine-feeding.

5/6 Nx describes the removal of 5/6 (~80%) of the kidney tissue. This frequently used method is a combination of unilateral nephrectomy, in which one kidney is totally removed, and pole resection of the other kidney. Due to reduction of functional nephrons and therefore of the filter capacity of the kidney, it results in the development of CKD. Whereas 5/6 Nx in Model 1 and 2 triggered kidney function decline primarily by loss of renal mass, chronic kidney damage can also be alternatively induced by adenine-feeding. Adenine is metabolized via xanthine dehydrogenase to 2,8-dihydroxyadenine, which triggers tubulointerstitial nephropathy caused by crystal deposition in the tubule lumen and interstitium [66, 75, 76]. Kidney damage occurs due to tubular occlusion and induction of inflammation and kidney fibrosis. Advantages of the adenine-feeding are on the one hand the possibility of adapting the adenine concentrations individually to the preferred degree of kidney damage and on the other hand it is diminishing the risk for mortality due to surgery. In the following section, three different CKD mouse models induced by adenine feeding are presented.

To examine strain-dependent effects, both procedures were performed in two, respectively, three different mouse strains. **C57BL6J wildtype** mice were chosen as they represent the most commonly used mouse strain because of the variety of transgenic modifications available. As a second strain **C57BL/6J** apolipoprotein E deficient **(ApoE$^{-/-}$)** mice were selected which develop hyperlipidemia and hypercholesteremia when feeding a western-type high-fat diet. Thus, they are reflecting a clinical picture often found in CKD patients and provide an additional risk factor for CKD and CVD. Additionally, **129/Sv mice** were chosen, since 129/Sv is a mouse strain often used in CKD research because of its two copies of the renin gene.

Overall, we characterized the effect of CKD on the heart upon:

- CKD-induction by _**5/6 Nx in C57BL/6J wildtype mice (Model 1) and in C57BL/6J ApoE$^{-/-}$ mice**_ on high-fat diet _**(Model 2)**_,

- CKD-induction by _**adenine diet in C57BL/6J wildtype mice (Model 3) and in C57BL/6J ApoE$^{-/-}$ mice**_ on high-fat diet _**(Model 4)**_,

> _In these models, the main focus was on the characterization of kidney function as well as of effects on heart function and the cardiac phenotype on molecular level. Additional analysis of oxidative stress was performed in Model 4._

- CKD-induction by adenine diet in _**129/Sv mice (Model 5).**_

> _In this model, analysis of effects on kidney and heart function as well as on the cardiac phenotype on molecular level were performed comparable to the analysis for Models 1-4. In addition, RNA sequencing on heart tissue as well as analysis of cardiac oxidative stress markers were performed._

A manuscript with these findings is accepted in Redox Biology

**Pro-oxidative priming but maintained cardiac function in a broad spectrum of murine models of chronic kidney disease**

Julia Wollenhaupt[*], Janina Frisch[*], Eva Harlacher, Dickson W.L. Wong, Han Jin, Corinna Schulte, Sonja Vondenhoff, Julia Moellmann, Barbara Mara Klinkhammer, Li Zhang, Adelina Baleanu-Curaj, Elisa A. Liehn, Thimoteus Speer, Andrey Kazakov, Christian Werner, Emiel P.C. van der Vorst, Simina-Ramona Selejan, Mathias Hohl, Michael Böhm, Rafael Kramann, Erik A.L. Biessen, Michael Lehrke, Nikolaus Marx, Joachim Jankowski, Christoph Maack, Peter Boor, Leticia Prates Roma, Heidi Noels

*Shared first authorship

In this thesis only those results were included, which were generated by me.

4.1. Subtotal nephrectomy in C57BL/6J wildtype mice (Model 1)

Model 1	Model 2	Model 3	Model 4	Model 5
5/6 Nx	5/6 Nx	Adenine (low: 0.2% → 0.05%)	Adenine (high: 0.3% → 0.15%)	Adenine (low: 0.15%)
C57BL/6J	C57BL/6J ApoE$^{-/-}$ + HFD	C57BL/6J	C57BL/6J ApoE$^{-/-}$ + HFD	129/Sv
10 weeks	10 weeks	6 weeks	6 weeks	13 weeks

Figure 8: Overview of experimental CKD mouse model 1.
CKD induction by 5/6 Nx in C57BL/6J wildtype mice for 10 weeks. *5/6 Nx = 5/6 nephrectomy; CKD = chronic kidney disease.*

At first, kidney damage and associated effects on the heart in C57BL/6J wildtype mice were analysed. CKD was induced by a two-step 5/6 Nx, the respective control group was sham operated (in the following referred to sham). Effects on kidney and heart were analyzed after a period of 10 weeks (**Figure 9A**). For better comparison to Model 2, the mice were housed for 4 weeks before surgery.

Both 5/6 Nx mice as well as sham mice recovered well after surgery, showing a similar weight gain over time (**Figure 9B**), with no mortality observed.
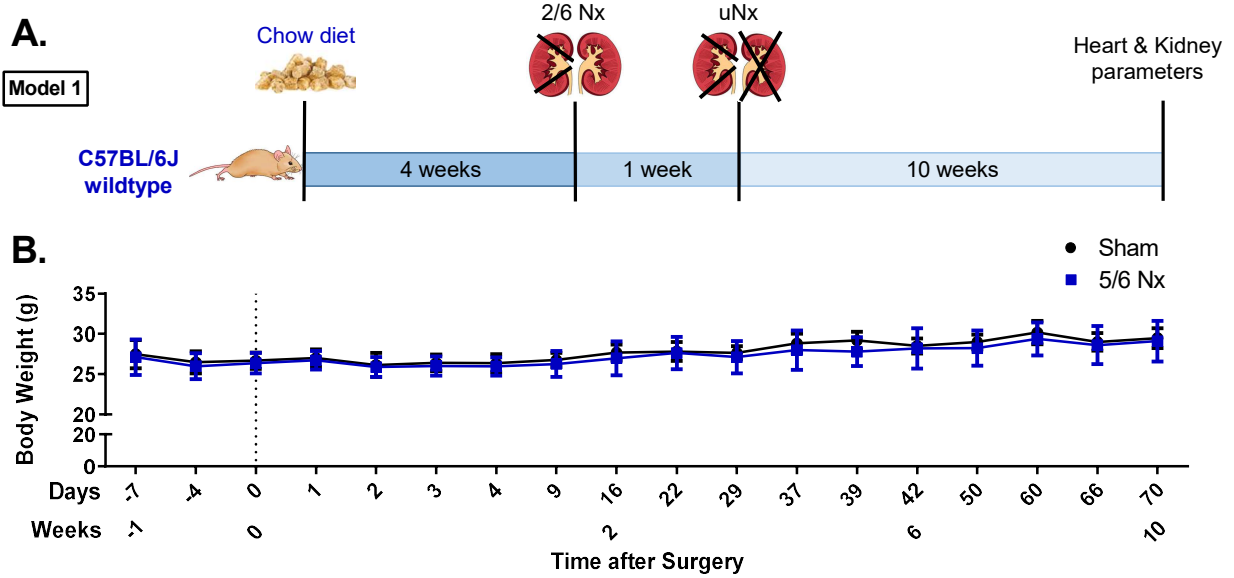
Figure 9: Model 1 - 5/6 Nx in C57BL/6J mice.
A) Experimental timeline. 2/6 Nx = 2/6 nephrectomy, pole resection; uNx = uni-nephrectomy. **B)** Body-weight curve. **A-B)** Shown are means ± SD; sham n=6; 5/6 Nx n=8. No significant changes by comparison of nephrectomy and sham animals using mixed effects analysis with matching values and Sidak's post-test. Experiments were performed by myself and are part of a submitted manuscript.

Analysis of kidney function and morphology

As typical parameters assessing the excretory function of the kidney, creatinine and urea levels in serum were analyzed at 6, 8 and 10 weeks after 5/6 Nx. Serum creatinine was significantly elevated at 8 weeks after surgery, but recovered to normal levels at the endpoint (**Figure 10A**). In contrast, serum urea levels were significantly increased 6 weeks after 5/6 Nx and remained increased ~1.7-fold compared to sham mice until the endpoint (**Figure 10B**), implying a mild kidney dysfunction after 5/6 Nx in C57BL/6J wildtype mice.
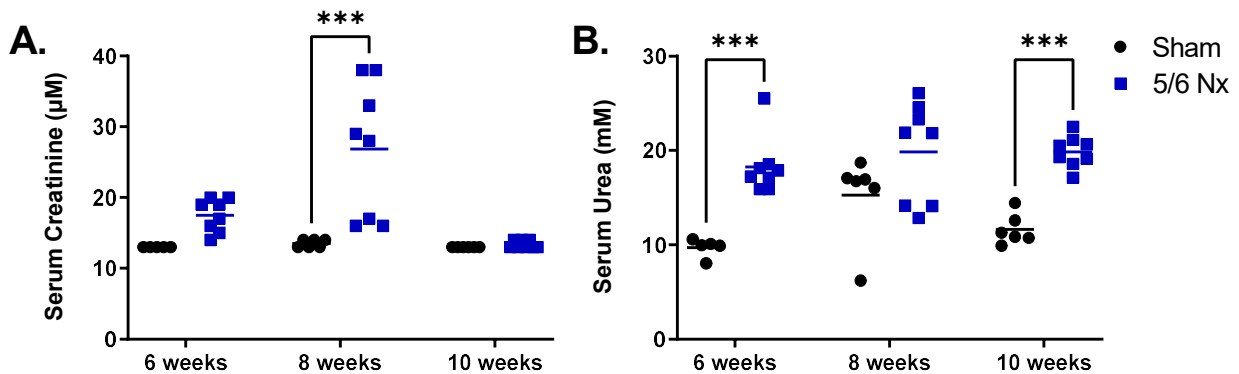
Figure 10: Serum urea levels were mildly increased after 5/6 Nx in C57BL/6J mice.
A) Serum creatinine and urea at 6, 8 and 10 weeks. **B)** Non-invasive systolic and diastolic blood pressure at 7 weeks and 9 weeks. **A-B)** Shown are dot plots with means; sham n=6; 5/6 Nx n=8. ***p<0.001 by comparison of nephrectomy and sham animals using mixed effects analysis with matching values and Sidak's post-test. Experiments were performed by myself and are part of a submitted manuscript.

Morphological changes in the kidney tissue provide further insight into the development of the CKD and are thus important in further characterization. Therefore, histological stainings on the remnant kidney were performed for analyzing kidney fibrosis (AFOG staining) and tubular injury (PAS staining), both displayed in **Figure 11A**. Histological analysis revealed only a very mild kidney damage in the remnant kidney, showing small focal fibrotic areas accompanied by less injured tubules (indicated with asterisks), without obvious signs of glomerular damage 10 weeks after surgery. Additionally, the fibrotic content of the tissue was examined by protein expression of collagen 1 (COL1) and α smooth muscle actin (αSMA). The protein level of fibrosis markers COL1 and αSMA were unchanged in the remnant kidney upon 5/6 Nx compared to sham mice (**Figure 11B**).
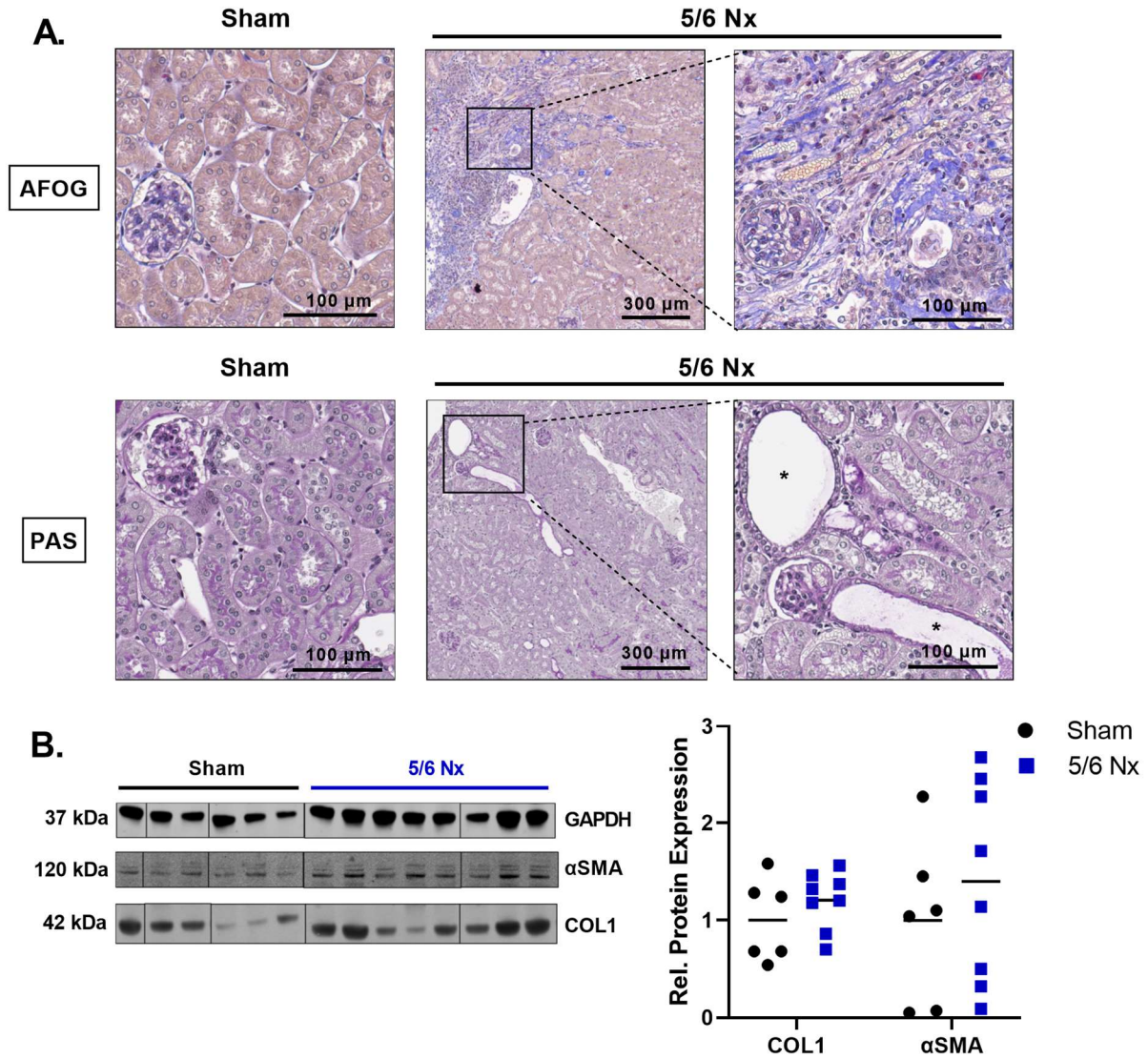
Figure 11: 5/6 Nx in C57BL/6J mice induced a mild kidney damage.
A) Representative images of AFOG and PAS staining from kidney tissue (PAS: asterisks indicate tubular injury). **B)** Images and quantification of western blot analysis for fibrosis markers (COL1, αSMA) in kidney tissue, normalized to GAPDH. Different lanes from one blot combined as indicated by the vertical lines. Shown are dot plots with means; sham n=6; 5/6 Nx n=8. Not significantly different by comparison of nephrectomy and sham animals using an unpaired two-tailed t-test. Experiments were performed by myself and are part of a submitted manuscript.

Analysis of blood pressure

Since the blood pressure can also be affected by a dysfunctional kidney and may subsequently also impact on the heart, blood pressure measurements were performed. At 7 and 9 weeks after 5/6 Nx, the blood pressure in mice was measured by using the non-invasive tail-cuff method. Neither the systolic nor the diastolic blood pressure was affected by 5/6 Nx in C57BL/6J mice and was comparable to the blood pressure of the sham mice (**Figure 12**).
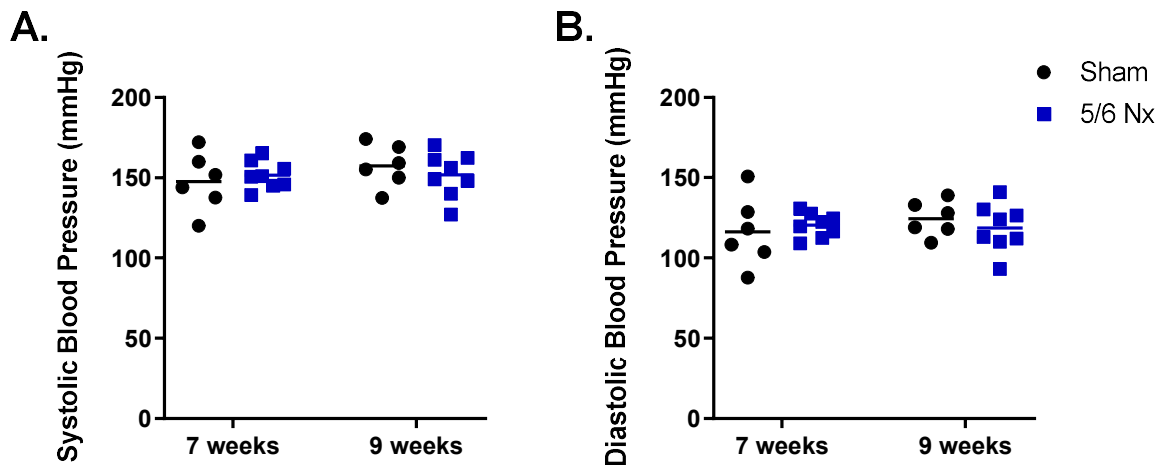
Figure 12: 5/6 Nx in C57BL/6J wildtype mice did not impact on blood pressure.
Non-invasive **A)** systolic and **B)** diastolic blood pressure measurement at 7 weeks and 9 weeks after 5/6 Nx. **A-B)** Shown are dot plots with means; sham n=6; 5/6 Nx n=8. ***p<0.001 by comparison of nephrectomy and sham animals using mixed effects analysis with matching values and Sidak's post-test. Experiments were performed by myself and are part of a submitted manuscript.

Analysis of heart function and cardiac remodeling processes

Examination of the cardiac function was performed by Millar catheter analysis, which is an invasive heart function measurement done at the endpoint of the experiment at 10 weeks after 5/6 Nx. Heart function is measured at baseline as well as under stress conditions induced by dobutamine injection. The diastolic function, also referred to as relaxation capacity and displayed as minimal rate of pressure change over time (dP/dT min) and as left ventricular end-diastolic pressure (LVEDP), were unaltered in 5/6 Nx mice, while the cardiac contractility reflecting the systolic function and displayed as maximum rate of pressure change over time (dP/dT max), was mildly reduced (14%) after dobutamine-induced stress (**Figure 13A- B;** Table 19 in appendix, page 125).
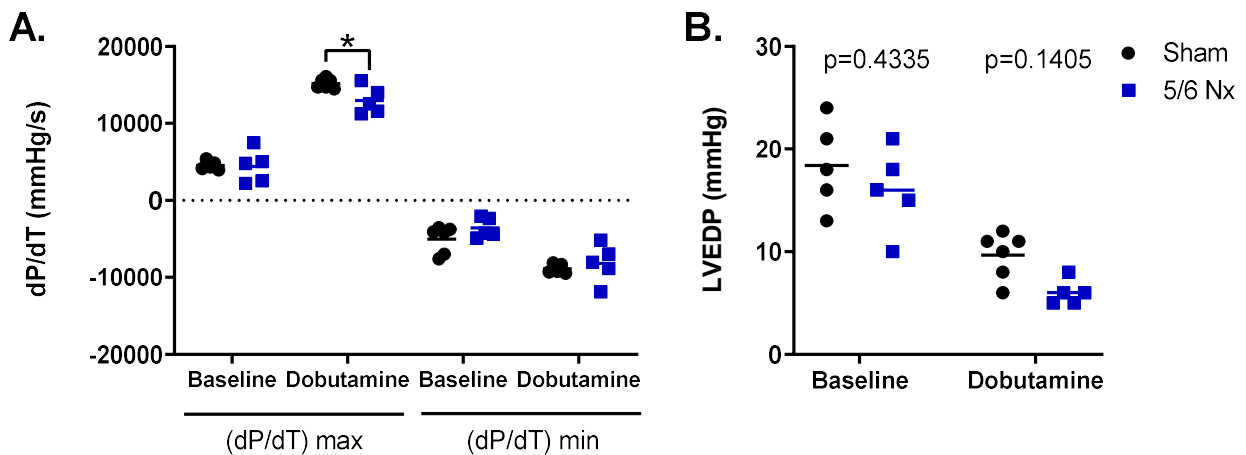
Figure 13: No changes in diastolic heart function detected, and only a mildly reduced systolic heart function in C57BL/6J mice after 5/6 Nx.
Invasive heart function analysis at endpoint by Millar catheter: **A)** (dP/dT) max and min. **B)** Left ventricular end diastolic pressure (LVEDP). **A-B)** Shown are dot plots with means; sham n=5; 5/6 Nx n=5. *p<0.05 by comparison of nephrectomy and sham animals using two-way ANOVA and Sidak's post-test. Results of all measured parameters are listed in Table 18 in appendix; page 124. Experiments were performed by myself and are part of a submitted manuscript.

Analyzing molecular changes in the heart, a gene expression analysis was performed using cardiac tissue. Genes related to hypertrophy (*Anp, Bnp*) (**Figure 14A**), fibrosis (*Col1a1, Col3a1, Tgfb1*) (**Figure 14B**) and inflammation (*Ccl2, Tnf, Icam1*) (**Figure 14C**) were analyzed. No changes could be observed on the molecular level related to fibrosis or inflammation in the cardiac tissue. The hypertrophy marker *Anp* showed an increased gene expression with a wide spreading of the individual values, but *Bnp* was not affected.
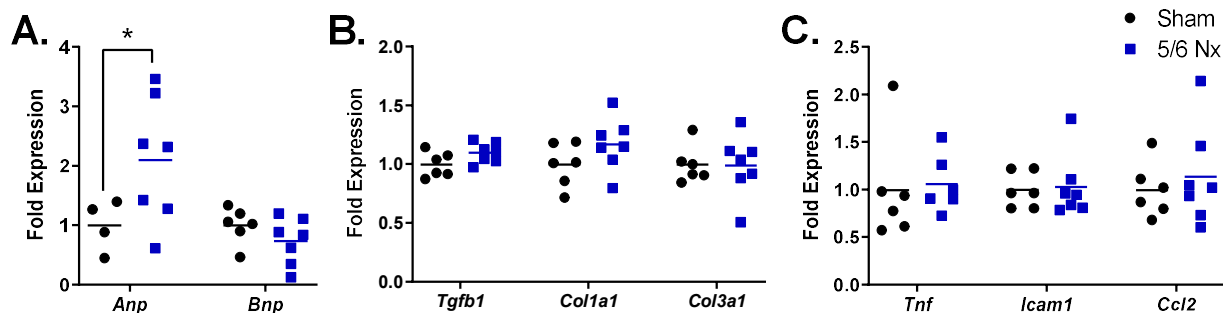
Figure 14: No molecular alterations observed in fibrosis markers nor the inflammatory profile, while the hypertrophic response is partly affected after 5/6 Nx in C57BL/6J mice.
A-C) Quantitative PCR on cardiac tissue at endpoint for markers of: **A)** hypertrophy (*Anp, Bnp),* **B)** fibrosis (*Tgfb1, Col1a1, Col3a1*), **C)** inflammation (*Tnf, Icam1, Ccl2*). **A-C)** Normalized to *Hprt1* and *GusB.* Shown are dot plots with means; sham n=5; 5/6 Nx n=6. *p<0.05 by comparison of nephrectomy and sham animals using an unpaired two-tailed t-test. Experiments were performed by myself and are part of a submitted manuscript.

> **To sum up, 5/6 Nx in C57BL/6J wildtype mice for 10 weeks led only to a mild CKD, accompanied by an only small effect on the cardiac contractility under dobutamine-induced stress. Also, the analysis on molecular level revealed no prominent cardiac effects, so that it was decided against a deeper cardiac characterization of this mouse model on cardiac morphological or molecular level (overview provided in Table 12).**

Table 12: Results summary of experimental mouse model 1. *5/6 Nx = 5/6 nephrectomy; CKD = chronic kidney disease.*

	Model	Kidney dysfunction	Heart	Oxidative stress
Model 1	5/6 Nx in C57BL/6J (10 weeks)	mild CKD	very mild decrease under stress	n.a.

4.2. Subtotal nephrectomy in C57BL/6J ApoE$^{-/-}$ mice (Model 2)

Figure 15: Overview of experimental CKD mouse model 2.
CKD induction by 5/6 Nx in C57BL/6J ApoE-/- mice for 10 weeks, with these mice developing hyper-lipidemia on high-fat diet as risk factor for CKD and CVD. *5/6 Nx = 5/6 nephrectomy; ApoE$^{-/-}$ apoliprotein E deficient; CKD = chronic kidney disease; CVD = cardiovascular disease; HFD = high-fat diet.*

Next, we examined the effects of 5/6 Nx-induced CKD in C57BL/6J *ApoE$^{-/-}$* mice. The *ApoE$^{-/-}$* mice were fed a high-fat-containing diet before surgery to induce hyper-lipidemia as risk factor for CKD and CVD. After 4 weeks of high-fat diet, the mice underwent a pole resection at one kidney, and after one week recovery the other kidney was totally removed. As control, a sham operation was performed in the control mice, referred to as "sham" in the following section. After 10 weeks of 5/6 Nx, the mice were sacrificed and heart and kidney parameters were assessed (**Figure 16A**). The postoperative mortality was 28.5% in the sham group and 25% in the 5/6 Nx group. The other mice recovered well, with no significant differences in body weight between sham and 5/6 Nx mice over time (**Figure 16B**).
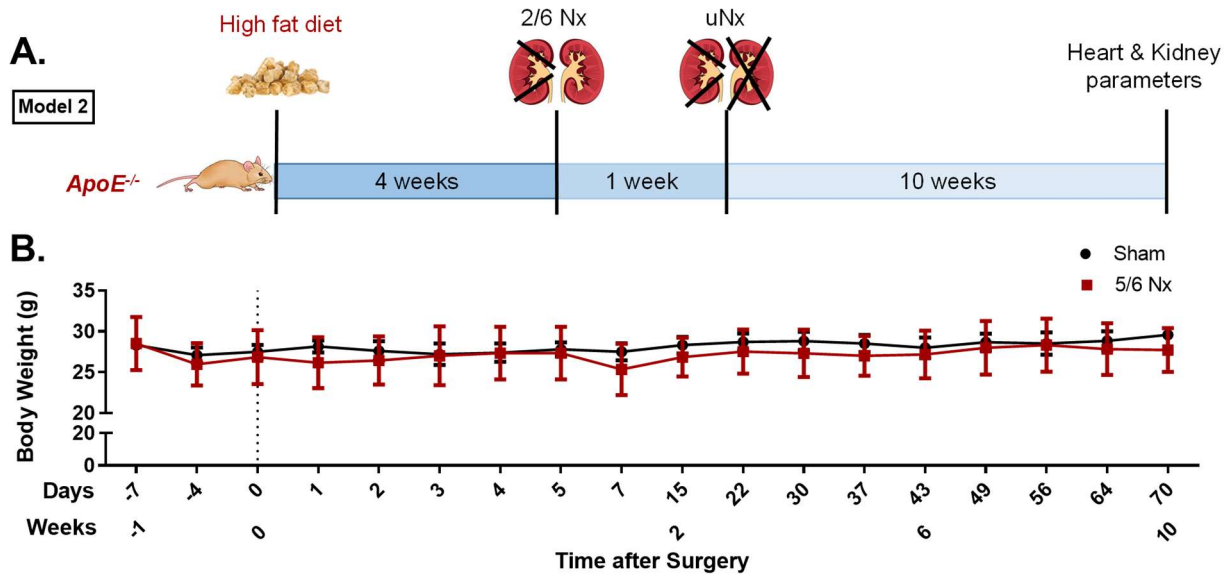
Figure 16: Model 2 - 5/6 Nx in C57BL/6J *ApoE⁻/⁻* mice.
A) Experimental timeline. HFD = high-fat diet, 2/6 Nx = 5/6 nephrectomy, pole resection; uNx = uni-nephrectomy. **B)** Bodyweight curve. Shown are means ± SD; sham n=6; 5/6 Nx n=6. No significant changes by comparison of nephrectomy and sham animals using mixed effects analysis with matching values and Sidak's post-test. Experiments were performed by myself and are part of a submitted manuscript.

Analysis of kidney function and morphology

Measuring creatinine levels in serum revealed a slightly increased trend in the 5/6 Nx group at 6 and 8 weeks after 5/6 Nx, while no significant differences were detected between sham and 5/6 Nx groups at the endpoint (10 weeks) (**Figure 17A**). However, serum urea levels were significantly increased after CKD induction and remained ~1.4-fold increased at the endpoint of the experiment (**Figure 17B**).
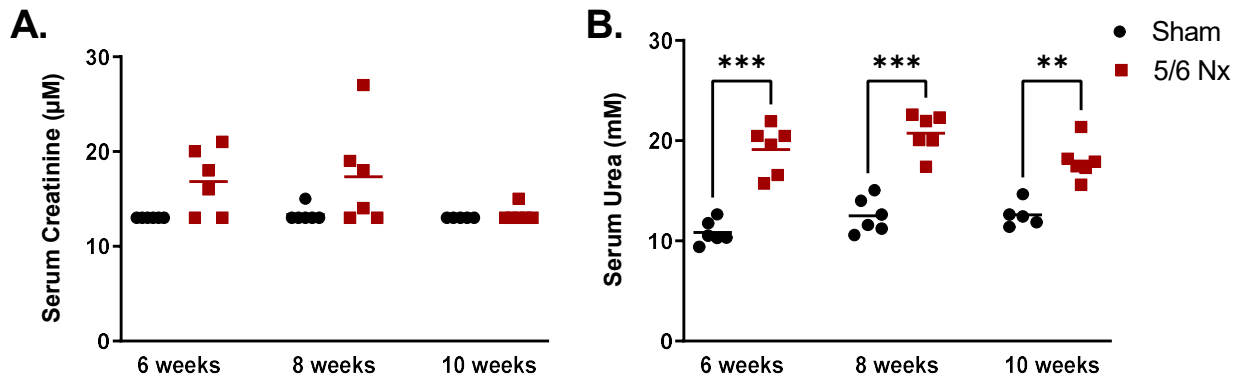
Figure 17: Serum urea levels were increased until the end of the experiment.
A) Serum creatinine and urea at 6, 8 and 10 weeks. **B)** Non-invasive systolic and diastolic blood pressure at 7 weeks and 9 weeks. **A-B)** Shown are dot plots with means; sham n=6; 5/6 Nx n=6. **p<0.01, ***p<0.001 by comparison of nephrectomy and sham animals using mixed effects analysis with matching values and Sidak's post-test. Experiments were performed by myself and are part of a submitted manuscript.

The histological analysis of the remnant kidney via AFOG and PAS staining revealed only small, focal fibrotic areas as well as inflammatory cell infiltration in the kidney of 5/6 Nx mice, in the absence of obvious signs of tubular or glomerular damage (**Figure 18A**). Consistently, the protein expression of the fibrosis markers COL1 and αSMA in the remnant kidney was also not affected by 5/6 Nx, as detected by western blot analysis (**Figure 18B**).

Figure 18: 5/6 Nx in C57BL/6J *ApoE*^{-/-} mice induced only a mild kidney damage.
A) Representative images of AFOG and PAS staining from kidney tissue (PAS: arrow indicates inflammatory cell infiltration). **B)** Quantification and images of western blot analysis for fibrosis markers (COL1, αSMA) in kidney tissue, normalized to GAPDH. Different lanes of one blot combined as indicated by the vertical lines. Shown are dot plots with means; sham n=5; 5/6 Nx n=6. Not significantly different by comparison of nephrectomy and sham animals using an unpaired two-tailed t-test. Experiments were performed by myself and are part of a submitted manuscript.

Analysis of blood pressure

The non-invasive blood pressure measurement showed no differences in 5/6 Nx mice compared to sham mice, neither at 7 weeks nor at 9 weeks after induction of 5/6 Nx (**Figure 19**).
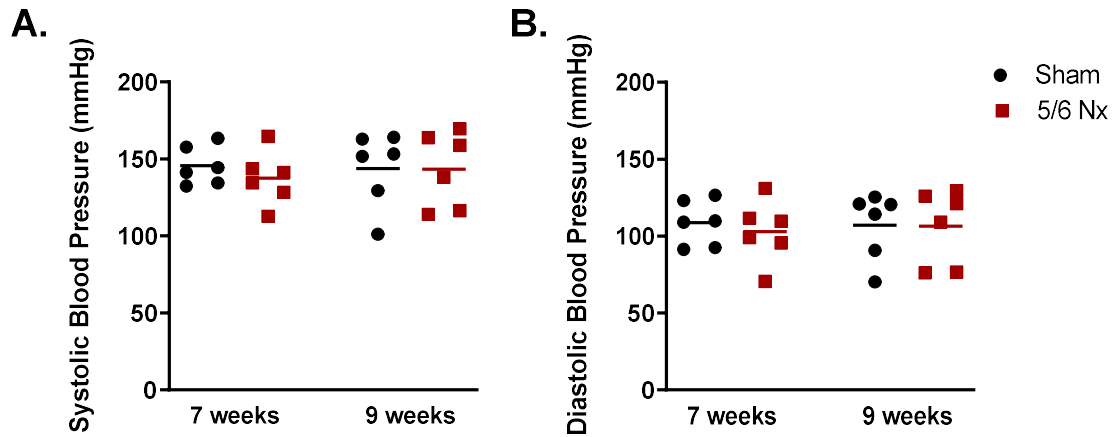
Figure 19: Blood pressure is not affected in C57BL/6J *ApoE^{-/-}* mice after 5/6 Nx.
Non-invasive **A)** systolic and **B)** diastolic blood pressure at 7 weeks and 9 weeks. **A-B)** Shown are dot plots with means; sham n=6; 5/6 Nx n=6. No significant changes by comparison of nephrectomy and sham animals using mixed effects analysis with matching values and Sidak's post-test. Experiments were performed by myself and are part of a submitted manuscript.

Analysis of heart function and cardiac remodeling processes

Heart function analysis was performed by using a Millar catheter as well as by echocardiography. Both methods revealed no significant cardiac changes at the endpoint after 10 weeks of 5/6 Nx in *ApoE*-/- mice (**Figure 20,** Table 18 in appendix page 124; Table 19 in appendix, page 125).
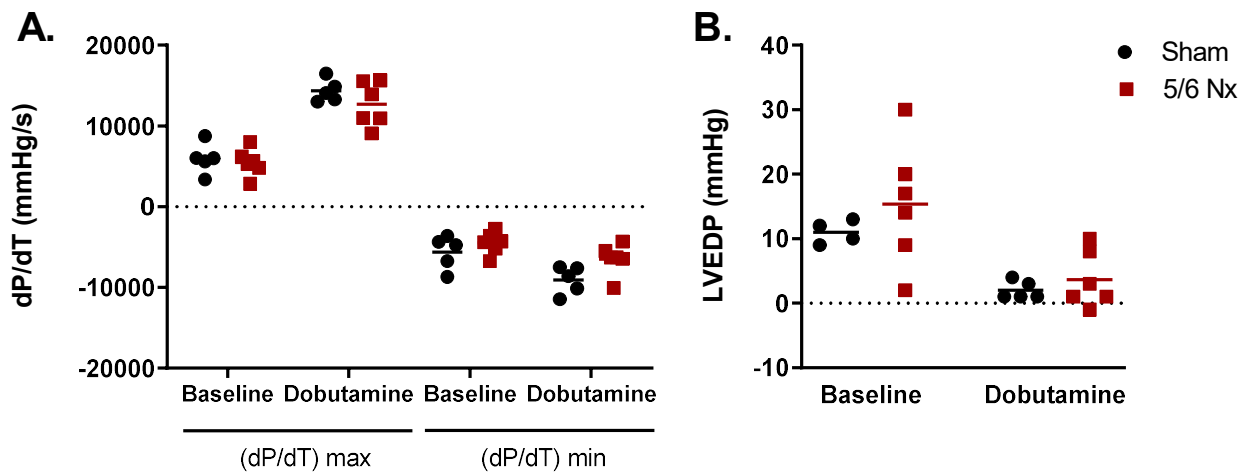
Figure 20: Heart function was not affected by 5/6 Nx in C57BL/6J *ApoE*-/- mice.
Invasive heart function analysis at endpoint by Millar catheter: **A)** (dP/dT) max and min. **B)** Left ventricular end diastolic pressure (LVEDP). **A-B)** Shown are dot plots with means; sham n=4-5; 5/6 Nx n=6. No significant changes by comparison of nephrectomy and sham animals using two-way ANOVA and Sidak's post-test. Results of all measured parameters are listed in Table 18 in appendix; page 124. Experiments were performed by myself and are part of a submitted manuscript.

Furthermore, the gene expression profile, in which characteristic markers for hypertrophy (*Anp, Bnp*), fibrosis (*Col1a1, Col3a1, Tgfb1*) or inflammation (*Ccl2, Tnf, Icam1*) were analyzed, showed no alterations in cardiac tissue in CKD mice compared to sham mice (**Figure 21**).
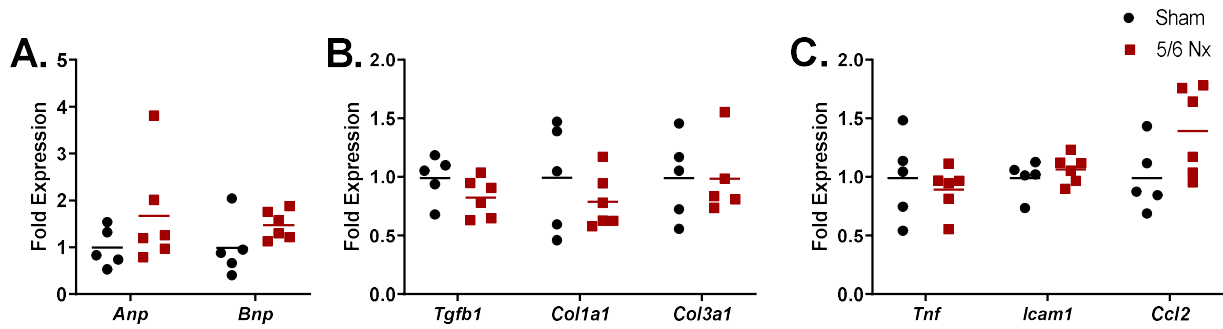
Figure 21: No molecular alterations were detected neither in hypertrophy, nor fibrosis or inflammation markers after 5/6 Nx in C57BL/6J *ApoE^-/-* mice.
A-C) Quantitative PCR on cardiac tissue at endpoint for markers of: **A)** hypertrophy (*Anp, Bnp),* **B)** fibrosis (*Tgfb1, Col1a1, Col3a1*), C) inflammation (*Tnf, Icam1, Ccl2*). **A-C)** Normalized to *Hprt1* and *GusB.* Shown are dot plots with means; sham n=5; 5/6 Nx n=6. No significant changes by comparison of nephrectomy and sham animals using an unpaired two-tailed t-test. Experiments were performed by myself and are part of a submitted manuscript.

> In summary, after 10 weeks of CKD-induction by 5/6 Nx in hyperlipidemic *ApoE^-/-* mice, only a mild impaired kidney function was observed without any effects on cardiac function nor on the molecular level in heart tissue (overview provided in Table 13).

Table 13: Results summary of experimental mouse models 1-2. *5/6 Nx = 5/6 nephrectomy; ApoE^-/- = apolipoprotein E knockout; CKD = chronic kidney disease; HFD = high-fat diet.*

	Model	Kidney dysfunction	Heart	Oxidative stress
Model 1	5/6 Nx in C57BL/6J (10 weeks)	mild CKD	very mild decrease under stress	n.a.
Model 2	**5/6 Nx in C57BL/6J *ApoE^-/-* (10 weeks)**	**mild CKD**	**no changes**	**n.a.**

4.3. Adenine-induced nephropathy in C57BL/6J wildtype mice (Model 3)

Model 1	Model 2	**Model 3**	Model 4	Model 5
5/6 Nx	5/6 Nx	**Adenine** (low: 0.2% → 0.05%)	Adenine (high: 0.3% → 0.15%)	Adenine (low: 0.15%)
C57BL/6J	C57BL/6J *ApoE⁻/⁻* + HFD	**C57BL/6J**	C57BL/6J *ApoE⁻/⁻* + HFD	129/Sv
10 weeks	10 weeks	**6 weeks**	6 weeks	13 weeks

Figure 22: Experimental CKD mouse model 3.
CKD induction by adenine diet in C57BL/6J wildtype mice for 6 weeks. *CKD = chronic kidney disease.*

At first, the adenine-induced kidney damage was induced in C57BL/6J wildtype mice. For two weeks the mice were fed with 0.2% adenine (induction phase), followed by four weeks of feeding with a reduced concentration of 0.05% adenine (maintenance phase) (**Figure 23A**). During the induction phase, a non-significant weight loss was detected in the adenine mice, while weight completely normalized during the mainte-nance phase (**Figure 23B**). No mortality was observed in either group.
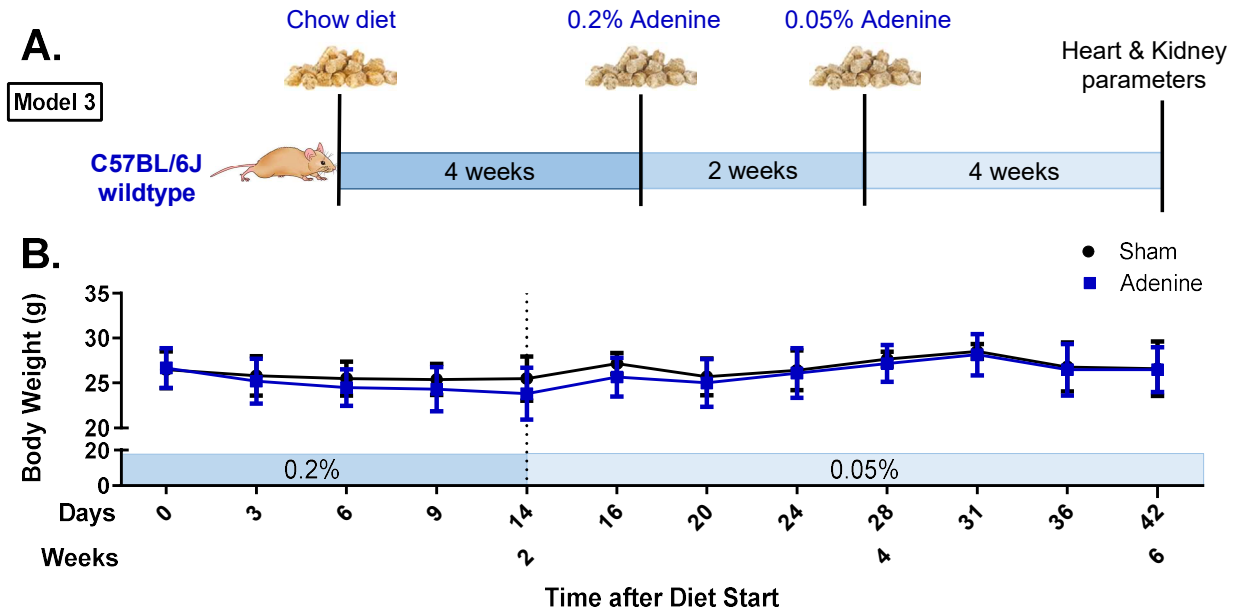
Figure 23: Model 3 - Low-dose adenine diet in C57BL/6J mice.
A) Experimental timeline. **B)** Bodyweight curve. Shown are means ± SD; sham n=10; Adenine n=10. No significant changes by comparison of adenine and sham animals using two-way ANOVA and Sidak's post-test. Experiments were performed by myself and are part of a submitted manuscript.

Analysis of kidney function and morphology

Creatinine levels measured in serum were increased after the 2-week induction phase and returned to baseline levels at the endpoint (**Figure 24A**). Similarly, urea levels were initially significantly increased after the induction phase, continued to be further increased also in the maintenance phase and declined to a non-significant ~1.2-fold increase at the end of the experiment (**Figure 24B**).
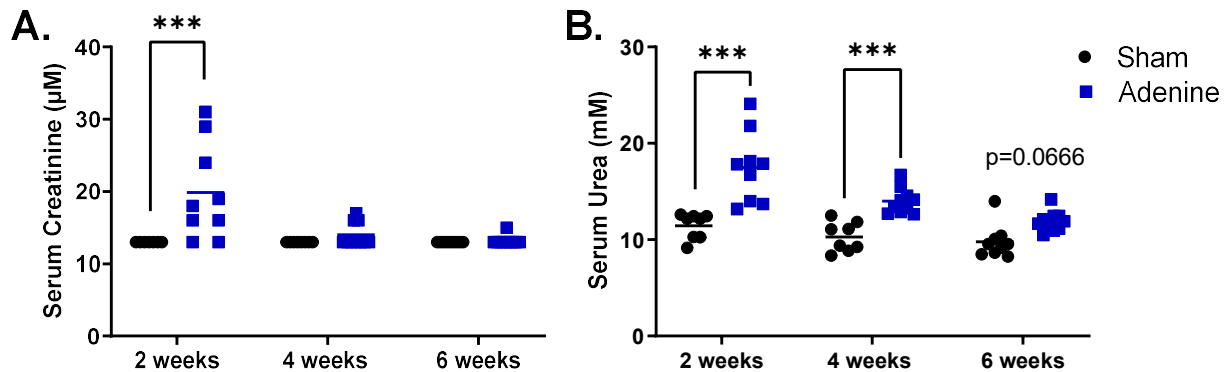
Figure 24: Adenine induced mild, but reversibly impaired kidney function in C57BL/6J mice.
A) Serum creatinine and **B)** urea at 2, 4 and 6 weeks. Shown are dot plots with means; sham n=10; Adenine n=9-10. ***p<0.001 comparing adenine to sham animals using two-way ANOVA and Sidak's post-test. Experiments were performed by myself and are part of a submitted manuscript.

Histological analysis of kidney sections was performed by AFOG and PAS staining at the endpoint, whereby a rather mild degree of diffuse or focal renal fibrosis was revealed in all adenine-fed mice (**Figure 25A**). Thickening of the basal lamina in renal tubules was observed via PAS staining in adenine-fed mice, indicating a mild tubular damage designated by the arrows in **Figure 25A**. Additionally, determining the protein expression of COL1 and αSMA by western blot analysis revealed ~2-fold increased COL1 levels in kidney tissue of adenine-fed mice, even though αSMA levels were not affected (**Figure 25B**).
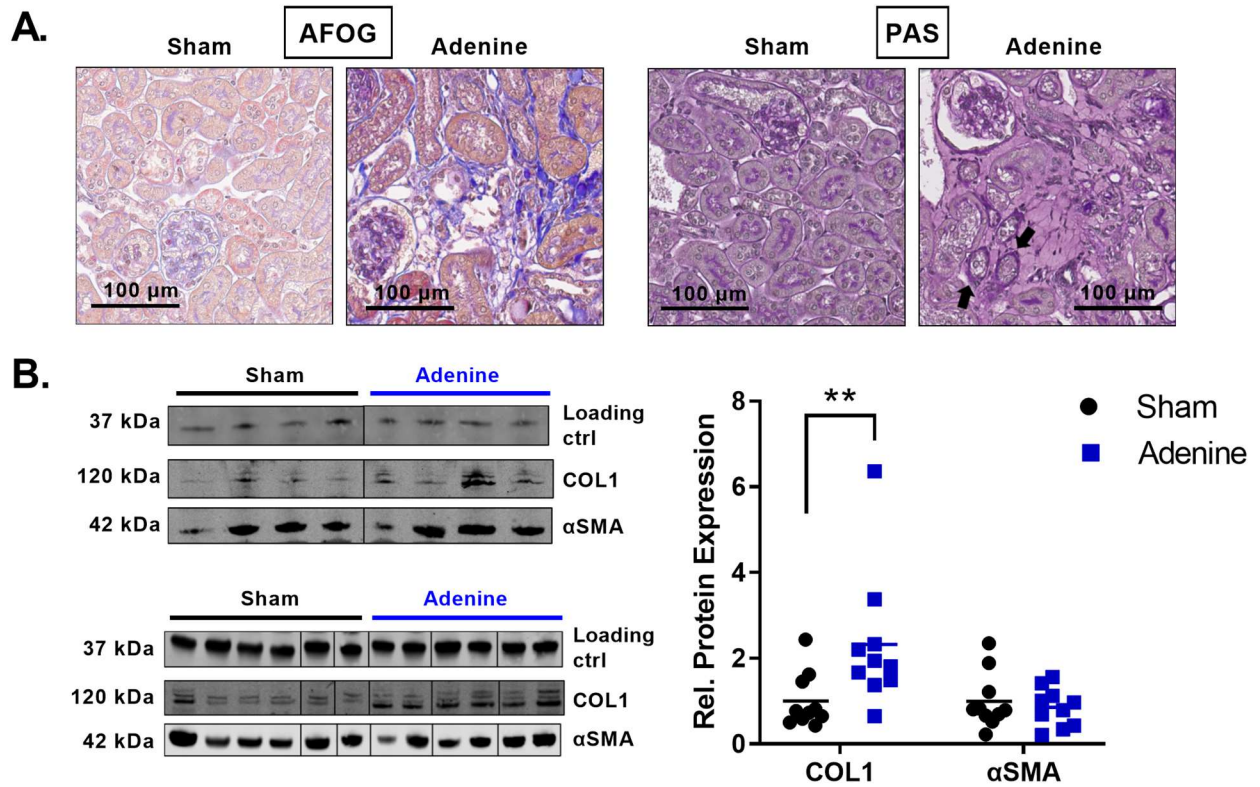
Figure 25: Mild damage in kidney tissue observed in C57BL/6J mice on adenine diet.
A) Representative images of kidney AFOG and PAS staining (PAS: arrows indicate tubular injury). **B)** Quantification and images of western blot analysis for fibrosis markers (COL1, αSMA) in kidney tissue, normalized to GAPDH. Two blots are shown, with different lanes of one blot combined as indicated by the vertical lines. The graph presents dot plots with means; sham n=10; Adenine n=9-10. **p<0.01 comparing adenine to sham animals using two-way ANOVA and Sidak's post-test. Experiments were performed by myself and are part of a submitted manuscript.

Analysis of blood pressure

Neither the systolic nor the diastolic blood pressure showed changes in adenine-fed mice compared to sham mice, as revealed by non-invasive blood pressure measurement via tail-cuff method (**Figure 26**).
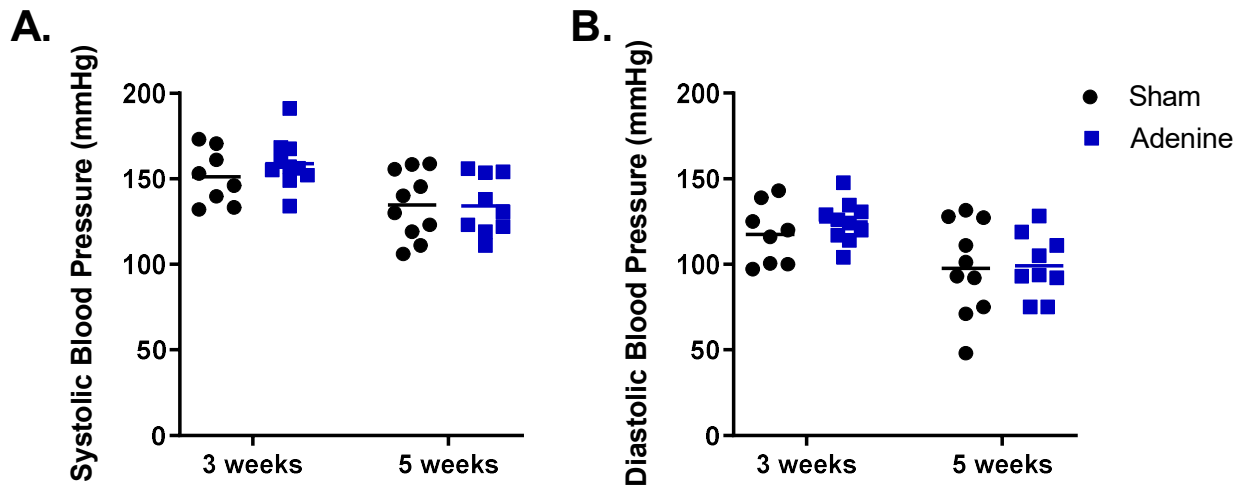
Figure 26: Blood pressure is unchanged in C57BL/6J wildtype mice fed with adenine-diet. Non-invasive **A)** systolic and **B)** diastolic blood pressure at 3 and 5 weeks. Shown are dot plots with means; sham n=10; Adenine n=9-10. No significant changes when comparing adenine to sham animals using two-way ANOVA and Sidak's post-test. Experiments were performed by myself and are part of a submitted manuscript.

Analysis of heart function and cardiac remodeling processes

Heart function analysis via Millar catheter showed no cardiac effects in adenine-treated mice compared to sham animals, neither in systolic nor in diastolic function (**Figure 27A-B;** Table 18). However, via echocardiography a ~11% relative decrease in ejection fraction was revealed at the endpoint in adenine-fed animals compared with sham animals (**Figure 27C**), while cardiac output was not affected (**Figure 27D;** Table 18 in appendix, page 124; Table 19 in appendix, page 125).
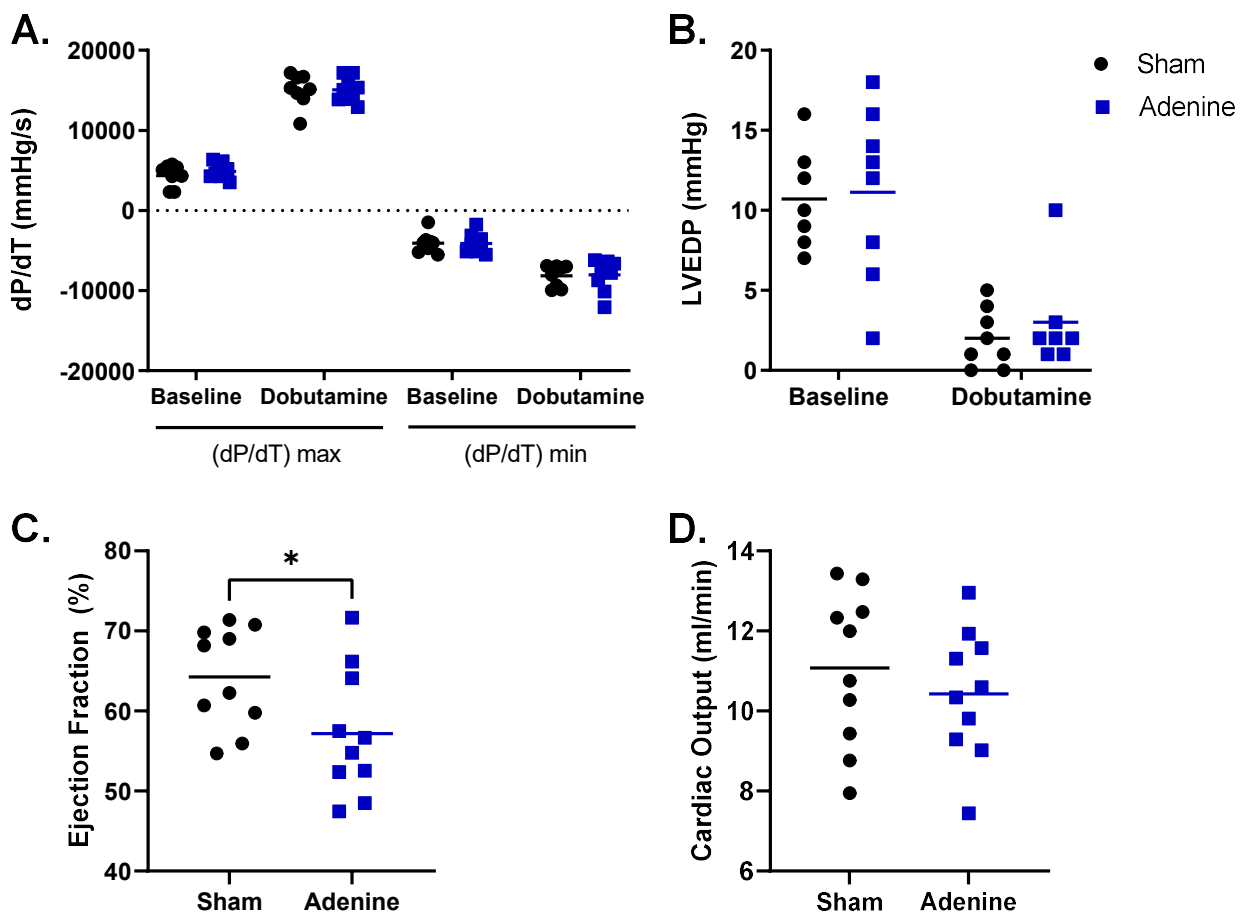
Figure 27: No effects on heart function via Millar catheter observed, while echocardiography revealed a mildly reduced ejection fraction in C57BL/6J mice on adenine diet.
A-B) Invasive heart function analysis at endpoint by Millar catheter (sham n=7-8; Adenine n=7-8): **A)** (dP/dT) max and min; **B)** Left ventricular end diastolic pressure (LVEDP). **C-D)** Non-invasive cardiac functional analysis via echocardiography (sham n=10; Adenine n=10): **C)** ejection fraction and **D)** cardiac output. Shown are dot plots with means; sham n=10; Adenine n=9-10. *p<0.05 comparing adenine to sham animals using two-way ANOVA and Sidak's post-test. Results of all measured parameters by Millar catheter are listed in Table 18 in appendix; page 124, and by echocardiography in Table 19; page 125. Experiments were performed by myself and are part of a submitted manuscript.

Analysis on molecular level via gene expression analysis in cardiac tissue exhibited no changes in either markers for hypertrophy (*Anp, Bnp*), fibrosis (*Col1a1, Col3a1,*

Tgfb1) or inflammation (*Tnf*, *Icam1*, *Ccl2*) when comparing adenine-fed mice to sham mice (**Figure 28A-C**).
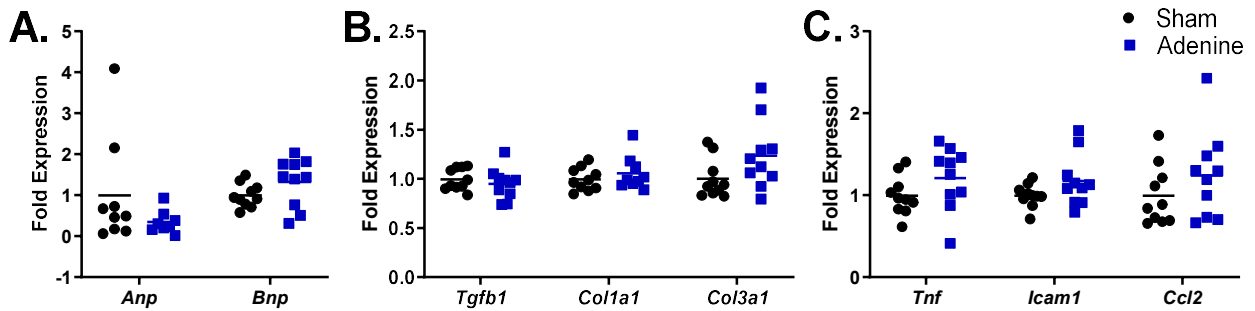
Figure 28: No hypertrophic, fibrotic or inflammatory response on molecular level observed in cardiac tissue of C57BL/6J mice on adenine diet.
A-C) Quantitative PCR on cardiac tissue at endpoint for markers of: **A)** hypertrophy (*Anp, Bnp*), **B)** fibrosis (*Tgfb1, Col1a1, Col3a1*), **C)** inflammation (*Tnf, Icam1, Ccl2*). **A-C)** Normalized to *Hprt1* and *GusB.* Shown are dot plots with means; sham n=9-10; Adenine n=10. No significant changes by comparison of adenine and sham animals using an unpaired two-tailed t-test. Experiments were performed by myself and are part of a submitted manuscript.

> Altogether, by using a low 0.2% / 0.05% adenine-supplemented diet in C57BL/6J mice, only a very mild degree of CKD could be induced. Hence, although a small reduction in ejection fraction could be observed, this mouse model was concluded to be insufficiently strong for the investigation of clinically relevant cardiac effects induced by CKD (overview provided in Table 14).

Table 14: Results summary of experimental mouse models 1-3. *5/6 Nx = 5/6 nephrectomy; ApoE⁻/⁻ = apolipoprotein E knockout; CKD = chronic kidney disease; EF = ejection fraction; HFD = high-fat diet.*

	Model	**Kidney dysfunction**	**Heart**	**Oxidative stress**
Model 1	5/6 Nx in C57BL/6J (10 weeks)	mild CKD	very mild decrease under stress	n.a.
Model 2	5/6 Nx in C57BL/6J *ApoE⁻/⁻* (10 weeks)	mild CKD	no changes	n.a.
Model 3	**Adenine diet in C57BL/6J (6 weeks)**	**very mild CKD**	**slightly decreased EF**	**n.a.**

4.4. Adenine-induced nephropathy in C57BL/6J ApoE⁻/⁻ mice (Model 4)

Figure 29: Experimental CKD mouse model 4.
CKD induction by adenine diet with increased concentration in hyperlipidemic C57BL/6J *ApoE⁻/⁻* mice for 6 weeks. *5/6 Nx = 5/6 nephrectomy; ApoE⁻/⁻ apoliprotein E deficient; CKD = chronic kidney disease; HFD = high-fat diet.*

As previously performed for the 5/6 Nx models, we next investigated the effect of the adenine protocol on kidney and cardiac phenotype in C57BL/6J *ApoE⁻/⁻* mice on high-fat diet. In a first approach, mice were fed with a high-fat diet for four weeks, followed by a high-fat diet supplemented with 0.2% adenine for a further two weeks, (induction phase). In contrast to C57BL6/J wildtype mice, the initial experiments revealed that a high-fat diet supplemented with 0.2% adenine could not induce an initial kidney damage in *ApoE⁻/⁻* mice after an initial two-week induction phase. Serum parameters creatinine and urea were not at all affected in adenine-treated mice, and the kidney tissue did not show any signs of kidney damage or inflammation (*data not shown*). Hence, in the following experiments, the adenine concentration was increased to 0.3% for 10 days during induction phase, followed by 0.15% adenine concentration in the maintenance phase, until ending the experiment after 6 weeks of adenine feeding in total (**F**igure **30A**). Although this protocol resulted in weight loss towards the end of the induction phase, the switch to 0.15% adenine stabilized weight and even resulted in weight gain again towards the end of the experiment, even though weight remained significantly lower compared to the control group. However, no mortality was observed in either group (**F**igure **30B**).
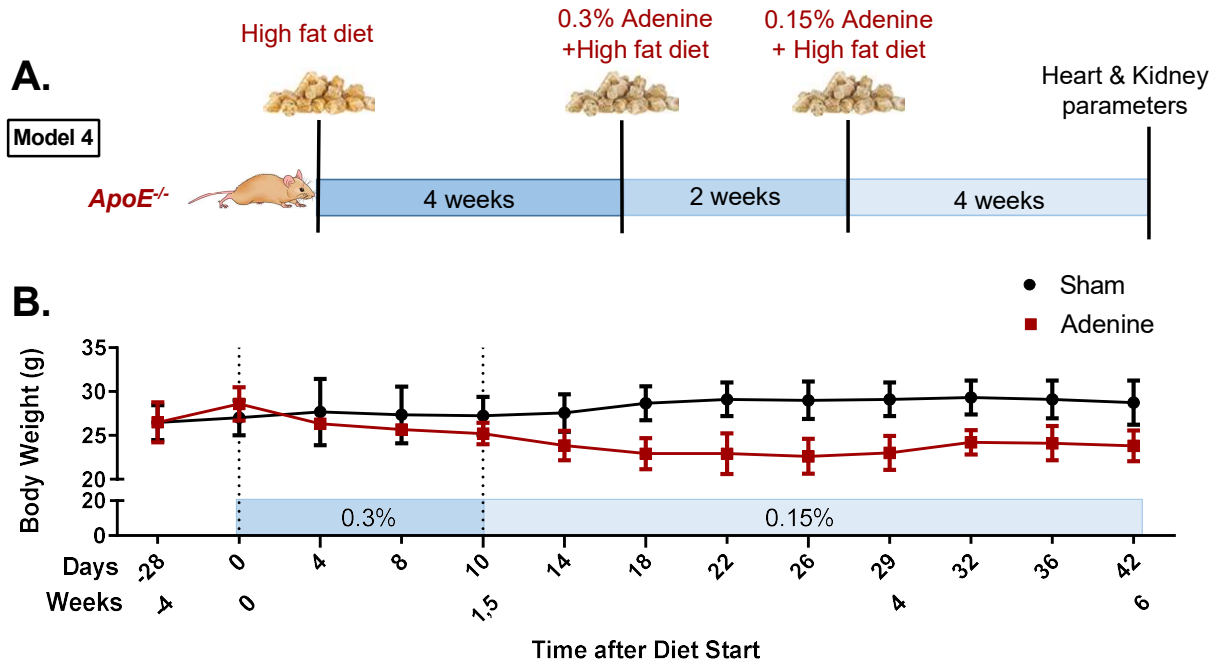
Figure 30: Model 4 – Adenine diet in C57BL/6J *ApoE^-/-* mice.
A) Experimental timeline. **B)** Bodyweight curve. Shown are means ± SD; sham n=9; Adenine n=10. Comparison of adenine and sham animals using mixed effects analysis with matching values and Sidak's post-test. Experiments were performed by myself and are part of a submitted manuscript.

Analysis of kidney function and morphology

Serum creatinine and urea levels were highly increased in the adenine-treated group compared to the sham group after the two-week induction phase. During the maintenance phase serum creatinine levels dropped, however they stayed ~1.8 fold increased at the endpoint (**Figure 31A**). Serum urea levels were significantly increased during the whole experimental time and were ~2.9-fold increased at the endpoint (**Figure 31B**).
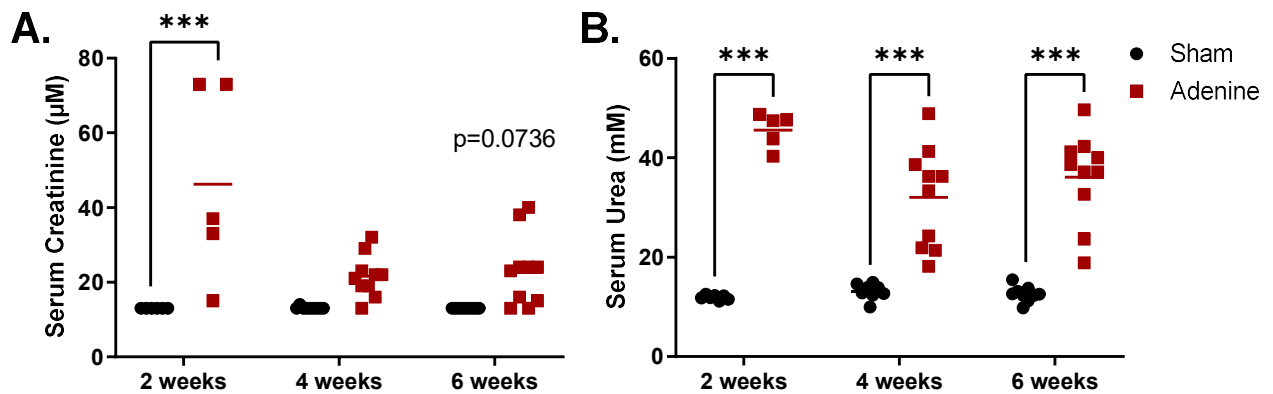
Figure 31: Adenine-treatment induced impaired kidney function in C57BL/6J *ApoE^-/-* mice.
A) Serum creatinine and **B)** urea at 2, 4 and 6 weeks. Shown are dot plots with means; sham n=6-10; Adenine n=5-10. ***p<0.001 comparing adenine to sham animals using two-way ANOVA and Sidak's post-test. Experiments were performed by myself and are part of a submitted manuscript.

Histological analysis by AFOG and PAS staining revealed a high degree of kidney fibrosis, as indicated by the blue color in kidney sections from adenine-fed mice (**Figure 32A**). Severe tubular injury as well as inflammatory cell infiltration was observed in PAS-stained kidney sections (**Figure 32A**). The protein expression of COL1 and αSMA were noted to be >5-fold increased upon adenine-feeding, thus confirming the high degree of renal fibrosis and thus nephropathy in the adenine-treated *ApoE^-/-* mice (**Figure 32B**).
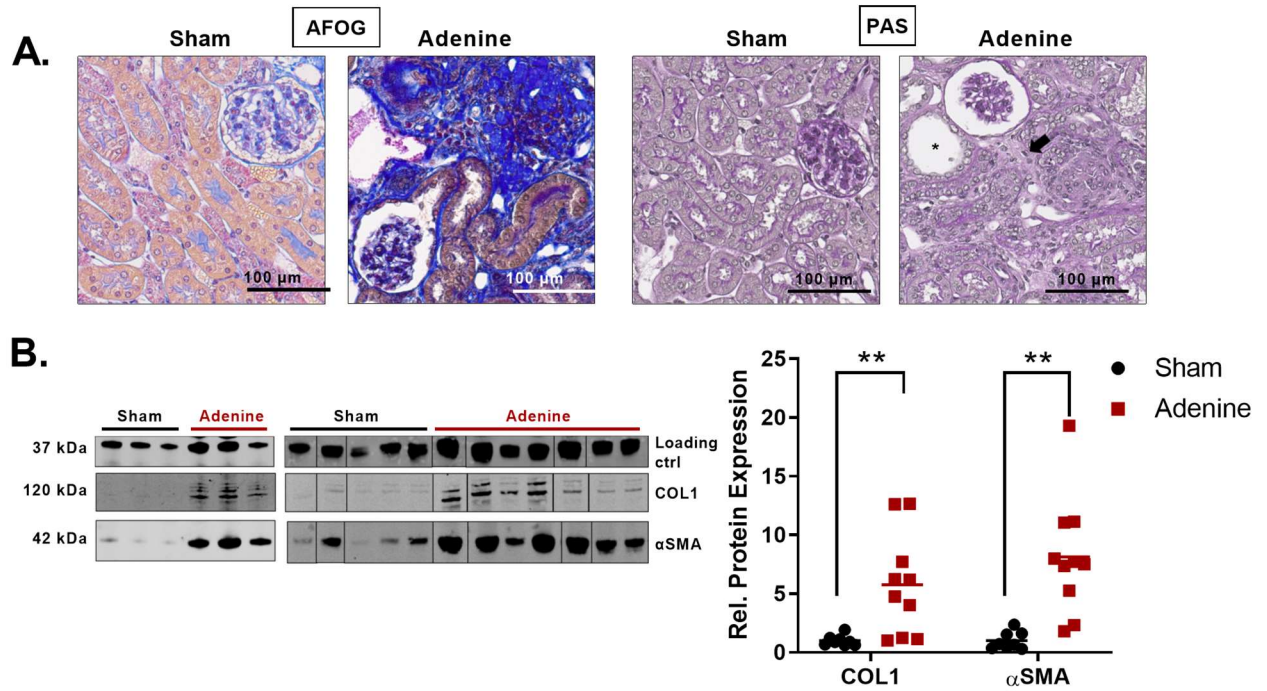
Figure 32: Increased kidney fibrosis and tubular injury in C57BL/6J *ApoE*-/- mice on adenine diet. **A)** Representative images of kidney AFOG and PAS staining (PAS: asterisk indicates tubular injury; arrow indicates inflammatory cell infiltration). **B)** Quantification and images of western blot analysis for fibrosis markers (COL1, αSMA) in kidney tissue, normalized to GAPDH. Two blots shown, with different lanes of one blot combined as indicated by the vertical lines. Shown are dot plots with means; sham n=9; Adenine n=10. **p<0.01 by comparison of adenine to sham animals using two-way ANOVA and Sidak's post-test. Experiments were performed by myself and are part of a submitted manuscript.

Analysis of blood pressure

Measurement of the blood pressure by non-invasive tail-cuff method revealed no significant differences, neither in systolic nor in diastolic blood pressure when comparing adenine-fed mice with sham mice (**Fi**gure **33**).
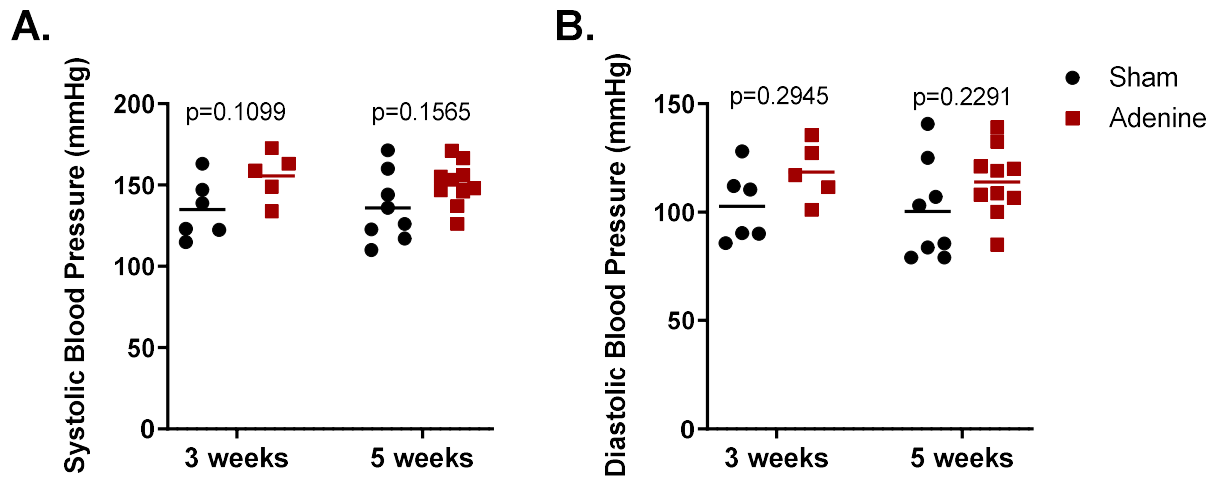
Figure 33: Blood pressure is not affected in C57BL/6J *ApoE*$^{-/-}$ mice fed with adenine diet.
Non-invasive **A)** systolic and **B)** diastolic blood pressure at 3 and 5 weeks. Shown are dot plots with means; sham n=6-10; Adenine n=5-10. No significant changes comparing adenine to sham animals using two-way ANOVA and Sidak's post-test. Experiments were performed by myself and are part of a submitted manuscript.

Analysis of heart function and cardiac remodeling processes

Despite the high degree of kidney damage observed in the *ApoE^-/-* mice, no effects on cardiac function were detected by either Millar catheter analysis or echocardiography at 2 weeks, 4 weeks, or 6 weeks after starting the adenine diet (**Figure 34**; Table 18 in appendix page 124; Table 19 in appendix, page 125).
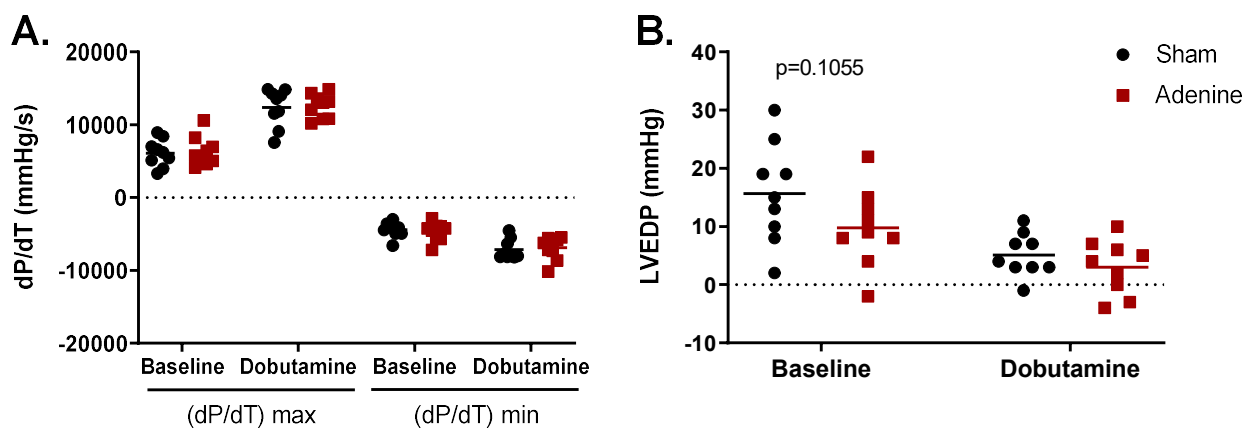
Figure 34: No cardiac functional effects detected via Millar catheter in C57BL/6J *ApoE^-/-* mice on adenine diet.
Invasive heart function analysis at endpoint by Millar catheter: **A)** (dP/dT) max and min. **B)** Left ventricular end diastolic pressure (LVEDP). **A-B)** Shown are dot plots with means; sham n=9; Adenine n=9. Not significant by comparison of adenine and sham animals using two-way ANOVA and Sidak's post-test. Results of all measured parameters by Millar catheter analysis are listed in **Table 18** in appendix; page 124. Experiments were performed by myself and are part of a submitted manuscript.

Analysis of cardiac hypertrophy was performed by WGA staining, which stains the cell membrane and allows to measure the cell diameter. Cardiomyocyte diameter was slightly reduced in adenine-fed mice (3.8% reduction vs. sham mice) (**Figure 35**). However, the hypertrophy markers *Anp* and *Bnp,* investigated on gene expression level, showed no changes in adenine-treated mice compared to sham mice (**Figure 37A**), and neither were differences observed in the heart weight normalized to tibia length (*data not shown*).
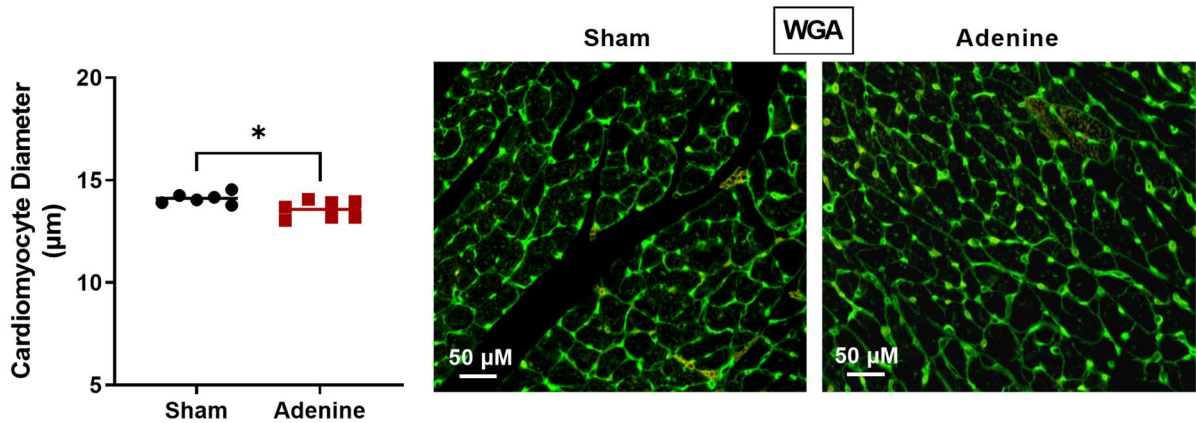
Figure 35: No cardiac hypertrophy detected in C57BL/6J *ApoE⁻/⁻* mice on adenine diet.
Quantification and representative images of WGA histological staining on heart samples. Shown are dot plots with means; sham n=6; Adenine n=7. *$p<0.05$ by comparison of adenine to sham animals using two-tailed t-test. Experiments were performed by myself and are part of a submitted manuscript.

Cardiac interstitial fibrosis was analyzed by Sirius Red staining (**Figure 36**) as well as on molecular level (**Figure 37B**). Neither the staining of cardiac tissue nor the gene expression analysis of fibrotic markers in cardiac tissue showed differences between adenine-fed and sham mice.
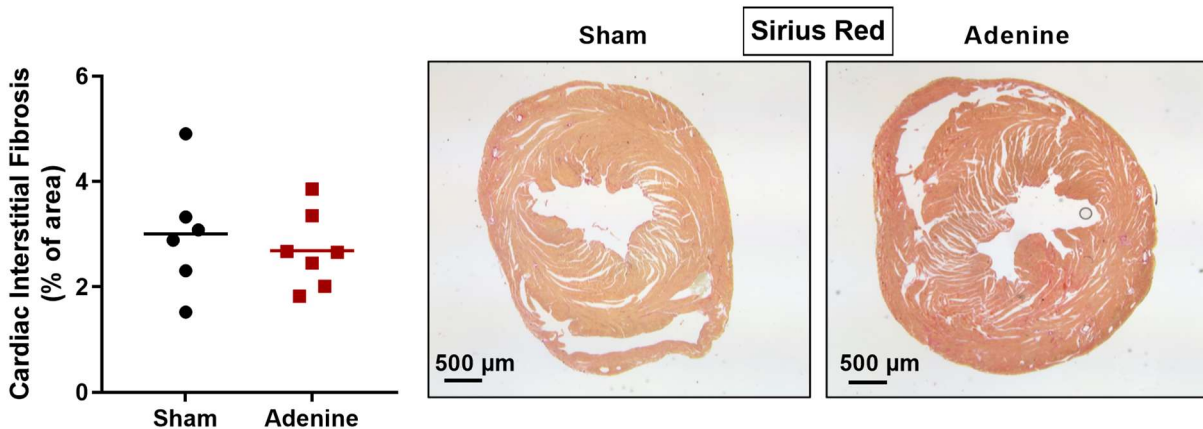
Figure 36: No cardiac interstitial fibrosis detected in C57BL/6J *ApoE⁻/⁻* mice on adenine diet.
Quantification and representative pictures of histological heart staining for fibrosis (Sirius Red). No significant changes by comparison of adenine to sham animals using two-tailed t-test. Experiments were performed by myself and are part of a submitted manuscript.

Moreover, the inflammatory response was not affected in cardiac tissue on gene expression level (**Figure 37C**). Additionally, a calcification staining (Alizarin Red) was performed in cardiac tissue, but no calcification could be detected in either mouse group (*data not shown*).
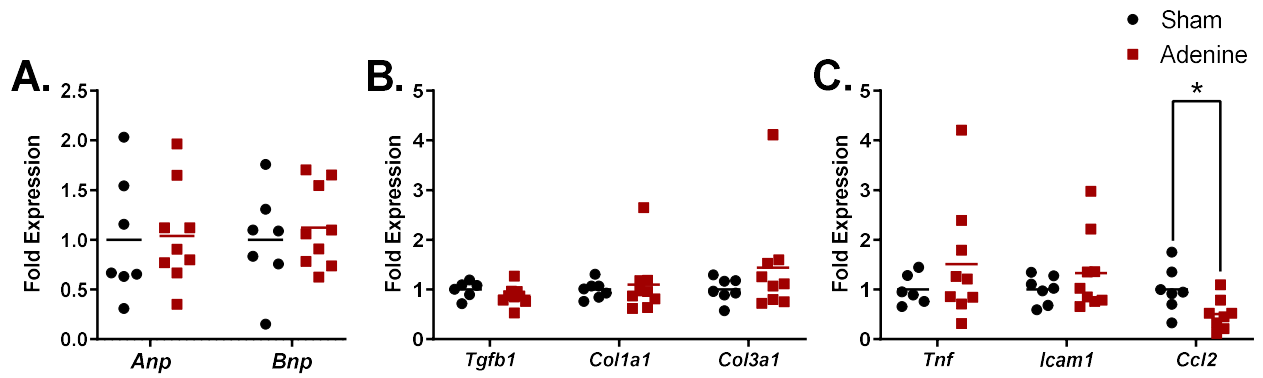
Figure 37: No hypertrophic, fibrotic or inflammatory response on molecular level observed in cardiac tissue of C57BL/6J *ApoE^-/-* mice on adenine diet.
A-C) Quantitative PCR on cardiac tissue at endpoint for markers of: **A)** hypertrophy (*Anp, Bnp),* **B)** fibrosis (*Tgfb1, Col1a1, Col3a1*), **C)** inflammation (*Tnf, Icam1, Ccl2*). **A-C)** Normalized to *Hprt1* and *GusB.* Shown are dot plots with means; sham n=7; Adenine n=9. *p<0.05 by comparison of adenine and sham animals using an unpaired two-tailed t-test. Experiments were performed by myself and are part of a submitted manuscript.

Analysis of oxidative stress

Because this was the first mouse model showing a stable and high increase in serum urea and a steady increase in serum creatinine, as well as a moderate kidney damage with high degree of kidney fibrosis and tubular injury, the oxidative stress response was additionally investigated in the heart. Expression of antioxidative enzymes super-oxide dismutase (SOD) 1, peroxiredoxin (PRX) 2 and catalase (CAT), which are acting in the cytosol, and the mitochondrial antioxidative enzymes SOD2 and PRX3 were examined by western blot. This did not show significant alterations between adenine-treated and sham mice (**Figure 38**).
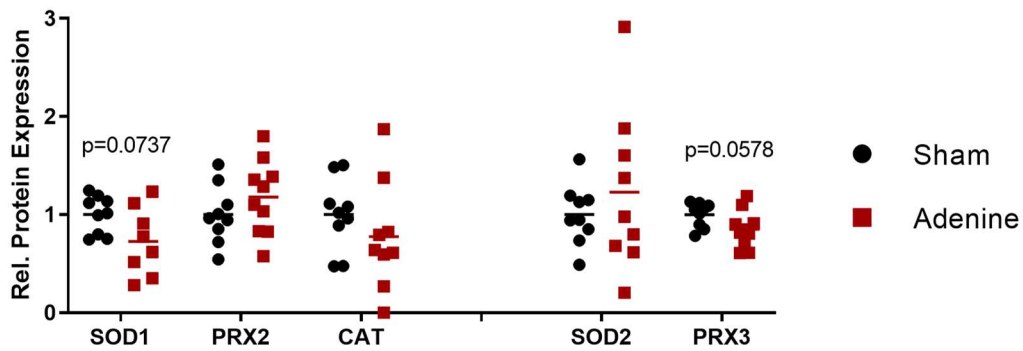
Figure 38: Antioxidative enzymes were mainly unaltered in C57BL/6J *ApoE^-/-* mice on adenine diet.
Quantitative analysis of cytosolic (SOD1, PRX2, CAT) and mitochondrial (SOD2, PRX3) antioxidative enzyme expression in heart tissue lysates via western blot, normalized to loading control (GAPDH or γTUB), and representative images. Two blots shown, with different lanes of one blot combined as indicated by the vertical lines. One outlier for SOD1 was identified in the adenine group over Grubb's test and excluded from quantification. One outlier for CAT as well as for SOD2 were excluded from quantification because of a missing band. Shown are dot plots with means; sham n=9; Adenine n=9. No significant changes by comparison of adenine and sham animals using an unpaired two-tailed t-test. Experiments were performed by myself and are part of a submitted manuscript.

As markers for oxidative stress, the expression of NADPH oxidase 2 (NOX2) and heme oxygenase 1 (HO-1) was analyzed on protein level via western blot in cardiac tissue. However, adenine-treated mice displayed no significant changes in the expression of both markers in comparison to sham mice (**Figure 39**).
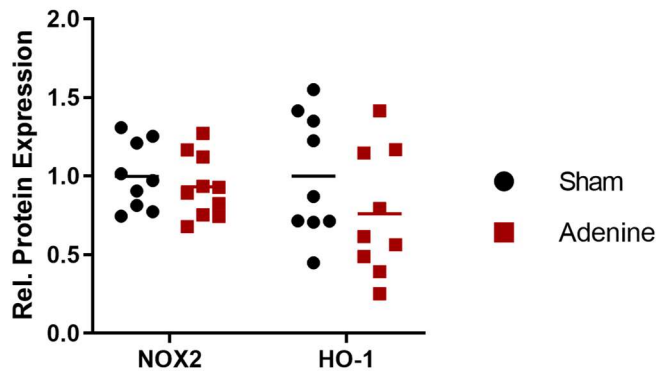
Figure 39: Protein expression of oxidative stress markers was not affected in C57BL/6J *ApoE*$^{-/-}$ mice on adenine diet.
Quantitative analysis of oxidative stress markers (NOX2, HO-1) in heart tissue lysates via western blot, normalized to loading control (GAPDH or γTUB), and representative images. Two blots shown, with different lanes of one blot combined as indicated by the vertical lines. Shown are dot plots with means; sham n=9; Adenine n=9. No significant changes by comparison of adenine and sham animals using an unpaired two-tailed t-test. Experiments were performed by myself and are part of a submitted manuscript.

Although the oxidative stress markers showed no changes on protein level, staining for 8-OHdG, a marker for oxidative stress-induced DNA damage, revealed a significant increase in hearts of adenine-treated animals (**Figure 40**).
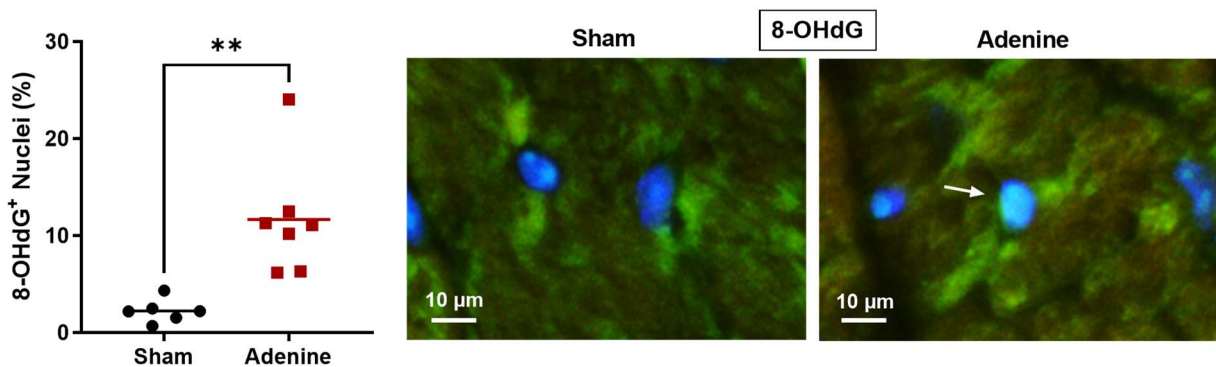
Figure 40: Increased DNA oxidation as marker for oxidative stress in adenine-treated C57BL/6J *ApoE*$^{-/-}$ mice.
Quantification and representative images of 8-OHdG positively stained nuclei as marker for oxidative stress in heart sections. Pictures are overlays of staining for 8-OHdG (green) and nuclear staining (blue). Shown are dot plots with means; sham n=6; Adenine n=7. **p<0.01 by comparison of adenine and sham animals using an unpaired two-tailed t-test. Experiments were performed by myself and are part of a submitted manuscript.

Overall, this adenine model resulted in a stable moderate CKD in C57BL6/J *ApoE$^{-/-}$* mice on high-fat diet. Although no effects on heart function, cardiac morphology or molecular changes in cardiac tissue were observed, increased cardiac oxidative stress was detected in cardiac tissue of CKD mice, as revealed by increased 8-OHdG staining in heart sections (overview provided in Table 15).

Table 15: Results summary of experimental mouse models 1-4. *5/6 Nx = 5/6 nephrectomy; ApoE$^{-/-}$ = apolipoprotein E knockout; CKD = chronic kidney disease; EF = ejection fraction; HFD = high-fat diet.*

	Model	**Kidney dys-function**	**Heart**	**Oxidative stress**
Model 1	5/6 Nx in C57BL/6J (10 weeks)	mild CKD	very mild decrease under stress	n.a.
Model 2	5/6 Nx in C57BL/6J *ApoE$^{-/-}$* (10 weeks)	mild CKD	no changes	n.a.
Model 3	Adenine diet in C57BL/6J (6 weeks)	very mild CKD	slightly decreased EF	n.a.
Model 4	**Adenine diet in C57BL/6J *ApoE$^{-/-}$* (6 weeks)**	**moderate CKD**	**no changes**	**increased oxidative stress**

4.5. Adenine-induced nephropathy in 129/Sv mice (Model 5)

Complementary to the findings in Model 4, the effect of a low dose adenine diet over a longer time period on the cardiac phenotype was investigated in an additional mouse strain. More specifically, 129/Sv mice were investigated, which is a mouse strain that harbors 2 copies of the renin gene and is often used in kidney research [77].

Model 1	Model 2	Model 3	Model 4	**Model 5**
5/6 Nx	5/6 Nx	Adenine (low: 0.2% → 0.05%)	Adenine (high: 0.3% → 0.15%)	**Adenine** (low: 0.15%)
C57BL/6J	C57BL/6J *ApoE⁻/⁻* + HFD	C57BL/6J	C57BL/6J *ApoE⁻/⁻* + HFD	**129/Sv**
10 weeks	10 weeks	6 weeks	6 weeks	13 weeks

Figure 41: Experimental CKD mouse model 5.
CKD induction by adenine diet in 129/Sv mice with a prolonged CDK duration of 13 weeks. *CKD = chronic kidney disease.*

Summary of kidney and cardiac analysis by cooperation partners as required basis for my own investigations

129/Sv mice were fed with an adenine supplemented diet containing 0.15% adenine. After 13 weeks the experiment had to be terminated because of a continuous weight reduction starting from week 6 and leading to an impaired health condition. Plasma creatinine and urea levels were ~6-7-fold increased at the endpoint. Kidney histology revealed strong kidney fibrosis identified by AFOG and Sirius Red staining, as well as increased COL1 protein expression. Additionally, tubular injury was observed in PAS-stained kidneys of all CKD-mice, confirming a dysfunctional kidney in adenine-fed 129/Sv mice.

Cardiac function was assessed by echocardiography, in which no alterations were detected except for an increased heart rate in CKD-mice. Read-outs for cardiac hyper-trophy, as Anp and Bnp gene expression level, cardiomyocyte diameter and heart weight were not altered at the endpoint in CKD-mice compared to sham-mice. Surprisingly, in all adenine-fed mice calcified deposits were observed mainly in the cardiac apex, but they were not found in sham mice. These deposits were identified visually after organ removal and were detected as calcified area by Alizarin Red staining on

the one hand and as highly fibrotic area via Sirius Red staining on the other hand. Cardiac interstitial fibrosis was detected in both CKD- and sham mice without significant differences between the groups. Cardiac protein expression of COL1 and αSMA were not increased in CKD-mice compared with sham mice, and neither was gene expression of fibrosis markers (Col1a1, Col3a1, Tgfb1). Furthermore, the gene expression profile of inflammatory genes (Tnf, Icam1, Ccl2) revealed no changes.

Expression of cytosolic antioxidative enzymes in cardiac tissue was ambivalent, with SOD1 and CAT being significantly decreased, whereas PXR2 was increased. In contrast, expression of antioxidative enzymes located in the mitochondria (SOD2, PRX3) was not affected.

Altogether, adenine feeding over 13 weeks induced a chronic, moderate to severe kidney dysfunction in 129/Sv mice. Although cardiac function was not impaired, locally calcified and severely fibrotic deposits were observed in the myocardium without an overall increase in interstitial fibrosis. This formed the basis for a further analysis of oxidative stress and molecular processes in cardiac tissue of these mice, as described in the paragraphs below.

Analysis of oxidative stress markers in cardiac tissue

Based on the results of a moderate to severe kidney damage and the altered oxidative stress response in adenine-treated 129/Sv mice, the oxidative stress markers HO-1 as well as 8-OHdG were determined in cardiac tissue.

As marker for oxidative stress the protein expression of HO-1 was analyzed via western blot, thereby revealing signs of increased HO-1 levels in the adenine-treated 129/Sv mice (**Figure 42**Figure 42: Protein expression of the oxidative stress marker HO-1 is slightly enhanced in 129/Sv mice treated with adenine-induced CKD.).
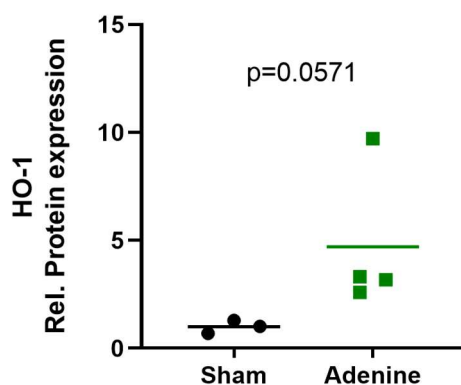
Figure 42: Protein expression of the oxidative stress marker HO-1 is slightly enhanced in 129/Sv mice treated with adenine-induced CKD.
Quantitative analysis of the oxidative stress marker HO-1 in heart tissue lysates via western blot, normalized to loading control (GAPDH), and representative images. Shown are dot plots with means; sham n=3; adenine n=4. Comparison of adenine and sham animals using a Mann-Whitney test. The mouse experiment itself was performed at the University Hospital Homburg (Universität des Saarlandes) by Dr. Janina Frisch. Shown experiments with cardiac tissue were performed by myself and are part of a submitted manuscript.

In addition, analysis of oxidative stress-induced DNA damage determined by 8-OHdG staining showed an almost significantly increased number of 8-OHdG positive cardiac nuclei in the adenine-fed mice (**Figure 43**).
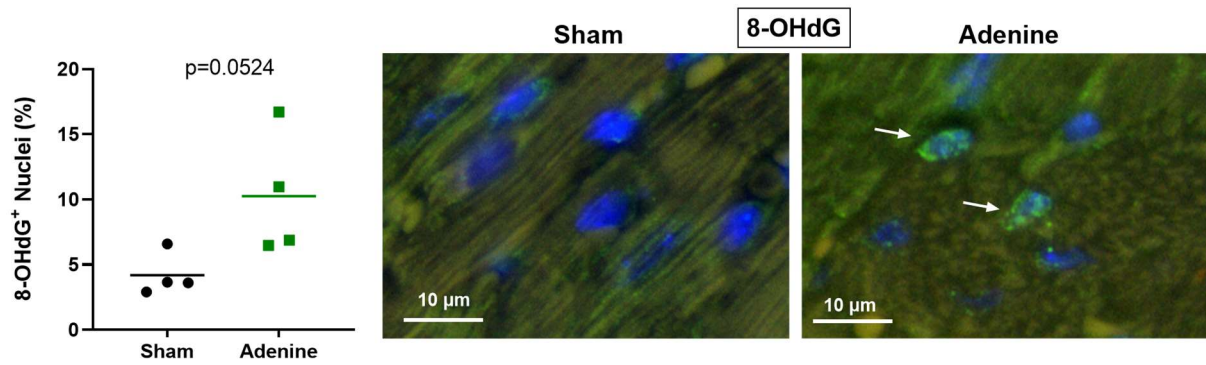
Figure 43: Oxidative stress-induced DNA damage shows signs of an increase in the hearts of 129/Sv mice fed with adenine diet.
Quantification and representative images of 8-OHdG positively stained nuclei as marker for oxidative stress in heart sections. Pictures are overlays of staining for 8-OHdG (green) and nuclear staining (blue). Shown are dot plots with means; sham n=4; adenine n=4. Comparison of adenine and sham animals using an unpaired two-tailed t-test. The mouse experiment itself was performed at the University Hospital Homburg (Universität des Saarlandes) by Dr. Janina Frisch. Shown experiments were performed by myself and are part of a submitted manuscript.

Combined, 8-OHdG staining indicating DNA oxidation and protein expression analysis of HO-1 revealed signs of increased oxidative stress responses in the hearts of adenine-treated 129/Sv mice.

Molecular insights of underlying pathways by RNA sequencing of cardiac tissue

To obtain deeper insight into CKD-induced cardiac changes on molecular level, RNA sequencing was performed on cardiac tissue of 129/Sv mice. By RNA sequencing 113 significantly up-regulated and 83 down-regulated genes were identified ($\log_2$(fold change) > 1 or < -1; adjusted p-value ($p_{adjusted}$) <0.05). Differentially expressed genes (DEGs) with $p_{adjusted}$ <0.05 were classified according to their association with enriched and pathology-relevant gene ontology (GO), with the top 10 DEG hits annotated in **Figure 44**.
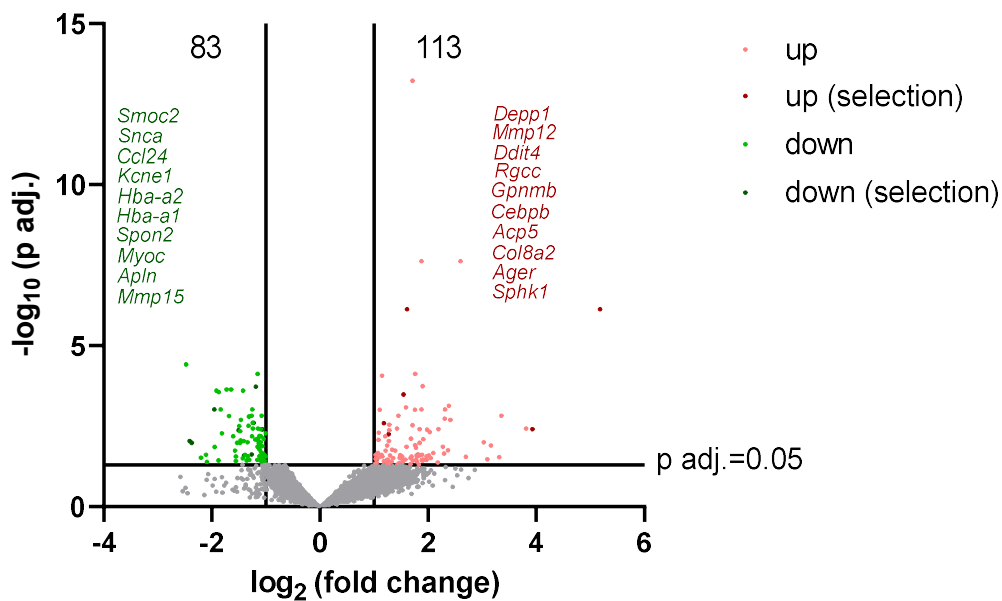
Figure 44: Pathology-relevant molecular alterations in hearts from adenine-fed 129/Sv mice, identified by RNA sequencing.
RNA sequencing was performed on cardiac tissue of 129/Sv mice comparing adenine-fed mice to sham-mice. Volcano plot showing $\log_2$(fold change) and $-\log_{10}(p_{adjusted})$ of genes, comparing the adenine-treated group to sham group. Differentially expressed genes (DEGs) with $p_{adjusted}$<0.05 and $\log_2$(fold change) > 1 or < -1 were considered as significant for further analysis and are indicated in green (down-regulated) or red (upregulated); the top ten significantly up- and downregulated genes of interest were highlighted (green: downregulated genes; red: upregulated genes). The mouse experiment itself was performed at the University Hospital Homburg (Universität des Saarlandes) by Dr. Janina Frisch. Shown experiments were performed by myself and are part of a submitted manuscript.

DEGs found to be significantly upregulated were associated with GO terms linked to reactive oxygen species (ROS) (*Depp1, Ddit4, Ager, Acp5*), inflammatory response (*Ager, Rgcc, Mmp12, Gpnmb, Cebpb*), extracellular matrix (*Mmp12, Col8a1*) and collagen/fibrosis (*Rgcc, Gpnmb, Sphk1, Ager, Col8a1*) (**Figure 45**).
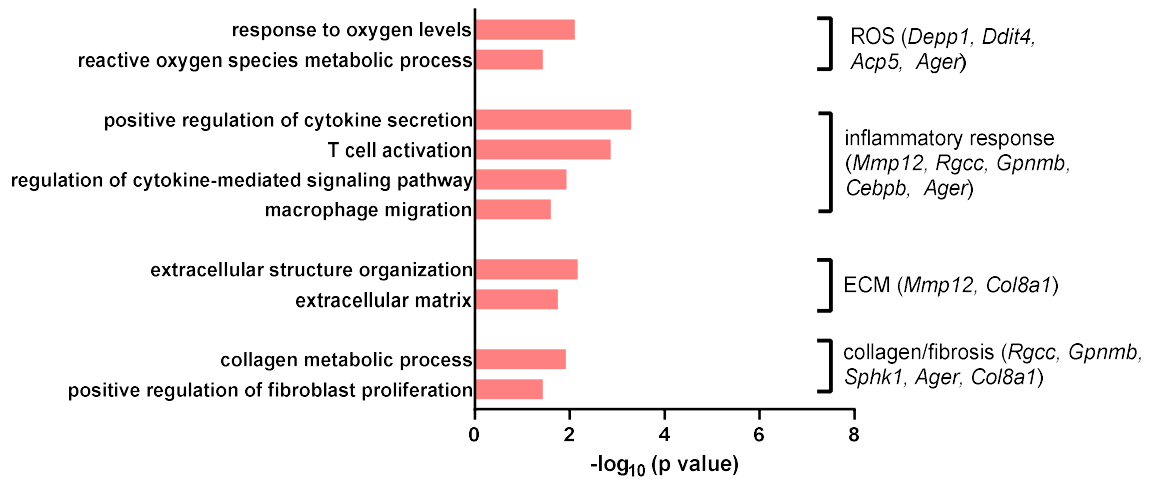
Figure 45: Upregulated enriched and pathology-relevant gene ontology (GO) terms in cardiac tissue of 129/Sv mice with CKD.
The representation of GO terms is based on the significant DEGs. Red bars indicate upregulated pathways. Selected significant DEGs associated with these GO terms are indicated. *ECM = extracellular matrix; ROS = reactive oxygen species.* The mouse experiment itself was performed at the University Hospital Homburg (Universität des Saarlandes) by Dr. Janina Frisch. Shown experiments were performed by myself and are part of a submitted manuscript.

In parallel, the downregulated DEGs were related to GO terms including ROS (*Snca, Hba-a1, Hba-a2*), inflammatory response (*Ccl24, Spon2, Snca*), mitochondria (*Myoc, Snca*), extracellular matrix (*Smoc2, Spon2, Myoc, Snca, Mmp15*), collagen/fibrosis (*Apln, Smoc2*) and heart (*Kcne1, Myoc, Apln*) (**Figure 46**).
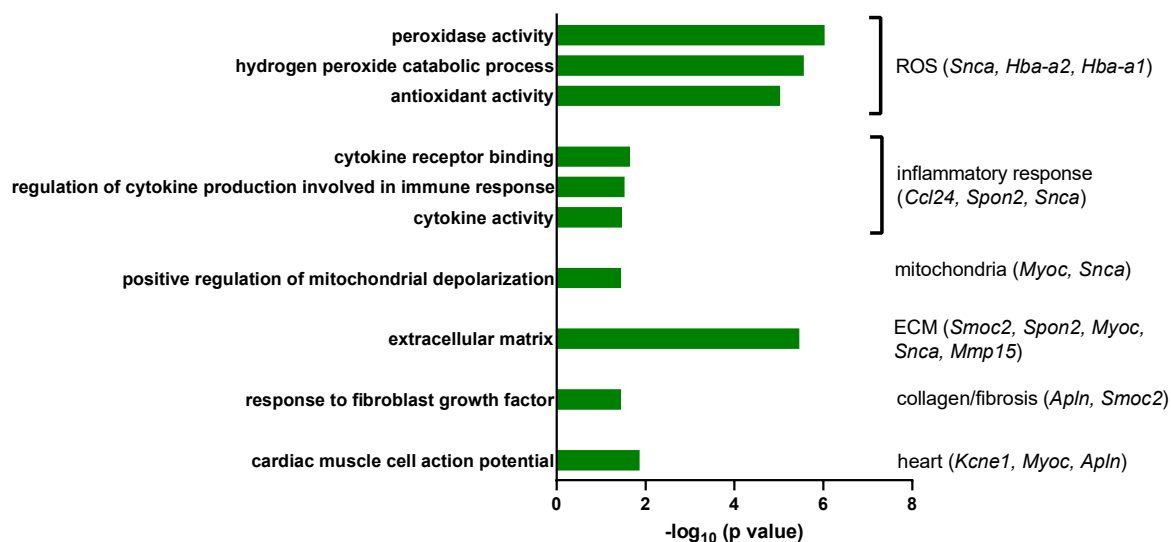
Figure 46: Downregulated enriched and pathology-relevant gene ontology (GO) terms in cardiac tissue of 129/Sv mice with CKD.
The representation of GO terms is based on the significant DEGs. Green bars indicate the downregulated pathways. Selected significant DEGs associated with these GO terms are indicated. *ECM = extracellular matrix; ROS = reactive oxygen species.* The mouse experiment itself was performed at the University Hospital Homburg (Universität des Saarlandes) by Dr. Janina Frisch. Shown experiments were performed by myself and are part of a submitted manuscript.

An increase in ROS-inducing mediators (*Depp1* [78]*, Ddit4* [79], *Ager* [80] [81]*, Sphk1* [82]) indicates increased cardiac oxidative stress in hearts of CKD-mice. On the other hand, increased levels of *Acp5* [83] and *Mmp12* [84] were detected, which are involved in protective anti-inflammatory feedback responses. Overall, an increase in ROS-inducing mediators combined with increased oxidative stress markers HO-1 and 8-OHdG in cardiac tissue revealed by immunofluorescence indicates an overall shift to a pro-oxidative milieu in CKD-hearts.

In addition, RNA sequencing revealed simultaneously an increase in pro-fibrotic mediators (Rgcc [85], Ager [86], Col8a2 [87], Mmp12 [88]) as well as a decrease in those mediators (Smoc2 [89], [90]). However, the overall imbalance was not sufficient to induce global interstitial cardiac fibrosis in the CKD-mice, as revealed by histological analysis of cardiac tissue.

Altogether, adenine feeding over 13 weeks induced a chronic, moderate to severe kidney dysfunction in 129/Sv mice. Although cardiac function was not impaired, CKD mice exhibited signs of increased cardiac oxidative stress markers, similar to previous findings in C57BL/6J *ApoE*^{-/-} mice fed with adenine diet (Model 4), as well as a shift towards a pro-oxidative milieu as revealed by RNA sequencing (overview provided in Table 16).

Table 16: Results summary of experimental mouse models 1-5. *5/6 Nx = 5/6 nephrectomy; ApoE*^{-/-} *= apolipoprotein E knockout; CKD = chronic kidney disease; EF = ejection fraction; HFD = high-fat diet.*

	Model	Kidney dys-function	Heart	Oxidative stress
Model 1	5/6 Nx in C57BL/6J (10 weeks)	mild CKD	very mild decrease under stress	n.a.
Model 2	5/6 Nx in C57BL/6J *ApoE*^{-/-} (10 weeks)	mild CKD	no changes	n.a.
Model 3	Adenine diet in C57BL/6J (6 weeks)	very mild CKD	slightly decreased EF	n.a.
Model 4	Adenine diet in C57BL/6J *ApoE*^{-/-} (6 weeks)	moderate CKD	no changes	increased oxidative stress
Model 5	**Adenine diet in 129/Sv (13 weeks)**	**moderate to severe CKD**	**no changes**	**increased oxidative stress**

Chapter 5

Discussion

5. Discussion

With CVDs being responsible for 40-50% of deaths in advanced CKD stages [32], this thesis aimed at a systematic and comprehensive study of cardiac function and pathological characteristics in different mouse models of CKD in regard to uremic cardiomyopathy. Although the CKD mice developed mild (Model 1-3), moderate (Model 4) or moderate to severe (Model 5) kidney impairment, neither the cardiac function nor the cardiac morphology was affected as observed in patients with uremic cardiomyopathy. Further **cardiac analysis on molecular level in mouse models with at least moderate CKD (Model 4-5) revealed increased oxidative stress markers in the heart of CKD-mice**. These effects were observed in hyperlipidemic C57BL/6J *ApoE*$^{-/-}$ mice as well as in 129/Sv mice with moderate, respectively, moderate to severe kidney dysfunction and thus are independent of mouse strain. Whether these findings of altered oxidative stress contribute to the enhanced cardiovascular risk in CKD patients should be addressed in future studies.

5.1. The need for a systematic characterization of cardiac effects of CKD.

Mouse models enable the characterization of functional and morphological cardiac changes in CKD as well as molecular analyses aimed at increasing insights into the pathological mechanisms underlying uremic cardiomyopathy. Over the past decade, multiple cardiac studies in CKD have been performed. Several studies reported that the mere induction of CKD triggered the development of cardiac hypertrophy and even heart failure [67, 68], whereas other studies only observed mild changes or even no clear effects on the heart in mice [69, 70]. Overall, the results are highly variable [65], which may be related to the different methods used for CKD induction, such as 5/6 nephrectomy or adenine diet. Additionally, the applied mouse strains could contribute to the high variability of the applied results, since for example 129/Sv mice were reported to be more prone to develop cardiac fibrosis or hypertrophy upon 5/6 Nx as C57BL/6J mice [91]. Clinically, uremic cardiomyopathy is resulting in cardiac fibrosis, left ventricular (LV) hypertrophy and diastolic dysfunction leading to the clinical consequences of heart failure or sudden death [92, 93]. LV hypertrophy, which occurs in 30% of CKD stage 2-4 patients and in 70-80% of patients with end-stage renal disease

(CKD stage 5D), is mainly caused by increased cardiac preload and/or afterload and by pathophysiological changes in intracellular mediators and is a characteristic contributor to cardiac remodeling and dysfunction [92]. Secretion of key fibrogenic mediators via e.g. activated myofibroblasts can lead to collagen deposition as fibrotic CKD response in the myocardium [94]. In addition, systemic inflammation and enhanced oxidative stress are both associated with CKD [93]. Most cardiorenal mouse studies focus on selected pathological processes instead of reporting all important parameters, complicating the clear comparison of different mouse models from different studies as revealed in our recent systematic review with meta-analysis (*in appendix*) [65]. Therefore, this thesis aimed to clearly compare the cardiac function and morphology in different CKD mouse models using different mouse strains as well as different methods for CKD induction with the same parameters reported.

5.2. CDK induction by adenine diet needs adaptation dependent on the mouse strain.

After performing the adenine protocol in C57BL/6J *ApoE$^{-/-}$* mice*, it was revealed that the adenine protocol needs to be adapted to obtain a sufficient CKD induction, depending on the mouse strain and/or the diet used. While supplementation of a standard diet with 0.2% adenine was able to induce initial kidney damage in C57BL/6J wildtype mice (Model 3) after two weeks, C57BL/6J *ApoE$^{-/-}$* mice that were fed a high-fat diet supplemented with 0.2% adenine showed no signs of kidney damage in the same period of time. Instead, the adenine concentration had to be increased to 0.3% in combination with high-fat diet in *ApoE$^{-/-}$* mice to induce sufficient kidney injury (Model 4).

5.3. Increased cardiac oxidative stress markers in mice with moderate to severe CKD.

Two models developed a moderate or moderate to severe kidney dysfunction, being hyperlipidemic C57BL/6J *ApoE$^{-/-}$* mice (Model 4) and 129/Sv mice (Model 5) with both CKD induced by adenine diet, with >1.5-fold serum creatinine increase, >2.5 serum urea increase and kidney fibrosis. In both models the kidney dysfunction led to an increase of oxidative stress markers in the heart, being increased 8-hydroxy-2'-deoxyguanosine (8-OHdG) positive cardiac nuclei in *ApoE$^{-/-}$* mice, and a trend to both increased 8-OHdG positive cardiac nuclei and increased protein expression of heme

oxygenase-1 (HO-1) in the heart of 129/Sv mice. Since 8-OHdG is one of the predominant forms of oxidative DNA damage caused by free radicals, it is an indicator for DNA damage induced by oxidative stress and therefore suitable as a marker for oxidative stress [95, 96]. Increased 8-OHdG positive cardiac nuclei were observed in a mouse model of cardiac pressure overload by transaortic constriction [97] and a diabetic cardiomyopathy model. Furthermore, diabetic mice with a knockout of nuclear factor erythroid 2-related factor 2 (Nrf2) displayed higher levels of 8-OHdG in cardiac tissue compared with wildtype diabetic mice, indicating that the absence of Nrf2 contributes to increased oxidative stress levels. Even in the absence of diabetes, cardiac 8-OHdG was increased in Nrf-2 knockout mice in comparison with the wildtype mice [98]. Nrf2 is a protective transcription factor that is acting as a sensor for cellular oxidative stress by inducing its downstream target heme oxygenase-1 (HO-1) in response to increased ROS formation. Although HO-1 has a cardioprotective function by degrading the pro-oxidant heme to carbon monoxide, bilirubin and iron, all of them having anti-oxidative or anti-inflammatory properties, HO-1 is used as biomarker for oxidative stress [99, 100]. For example, enhanced cardiac HO-1 levels were previously reported in 5/6 nephrectomized rats developing hyperuricemia [101] as well as in mice subjected to transaortic constriction [102].

The findings in this thesis of increased DNA damage in the CKD-heart are consistent with and extend findings in literature upon increased cardiac oxidative stress in adenine-induced CKD mice (C57BL/6 [103]; 129/Sv [104]).

Mechanisms underlying the increased oxidative stress in CKD may include accumulation of uremic toxins, which in animal models can promote inflammation or uncoupling of endothelial nitric oxide synthase and thus superoxide production [105], as we also summarized in a recent review (*in appendix*) [42].

5.4. No signs of hypertension nor of cardiac hypertrophy or fibrosis in these CKD mouse models: comparison to other studies.

To study cardiac effects induced by CKD, the induction via 5/6 Nx has been used more often than adenine-induced CKD. 129/Sv mice were more susceptible towards hypertension and cardiac hypertrophy after 5/6 Nx compared with C57BL/6 [65] and developed cardiac fibrosis even after 4 weeks of 5/6 Nx [65, 104, 106-109]. In a direct strain comparison, 129/Sv mice developed cardiac hypertrophy and fibrosis at 12 weeks after

5/6 Nx, which was not observed in C57BL/6JRj [91]. Although both strains developed hypertension in this study, 129/Sv mice had a more severe kidney damage and albuminuria when comparing to C57BL/6JRj mice [91]. Taken together, this suggests that the extent of kidney injury and the availability of hypertension contribute to the higher susceptibility of the 129/Sv strain to develop CKD-induced effects on the heart. This is in line with the observations in the mouse models used in this thesis. C57BL/6J mice subjected to 5/6 Nx developed only a mild kidney damage without hypertension nor overall cardiac remodeling processes (Model 1). Similar observations were done in hyperlipidemic C57BL/6J *ApoE*-deficient mice subjected to 5/6 Nx (Model 2). For both models it is assumed that the kidney injury was too mild for having a clear impact on the cardiac function, coming back to the statement that the extent of kidney injury, and potentially some degree of hypertension, must reach a certain degree before affecting the heart.

Also, not all experimental adenine-induced CKD mouse models in this thesis developed a sufficient kidney damage at the end of the experiment. The adenine protocol for the C57BL/6J wild-type mice (Model 3) included 2 weeks induction phase at standard diet with 0.2% adenine. Although this resulted in initial kidney damage, serum creatinine returned to basal levels and serum urea declined at 1.2-fold increase after reducing the adenine concentration to 0.05% for additional 4 weeks (maintenance phase). This suggests that the kidney function can recover after a very mild adenine-induced kidney damage. Although the ejection fraction was reduced in those very mild adenine-induced C57BL/6J wildtype mice, no other functional changes were detected neither by echocardiography nor by Millar catheter in this or any of the other adenine-induced CKD models. Additionally, no changes on molecular level could be seen. Thus, overall, it is hardly feasible to refer to cardiac dysfunction triggered by kidney damage in the animal models examined in this thesis.

In contrast, in literature, a few studies are reporting on the development of uremic cardiomyopathy in adenine-fed C57BL/6 mice. Some of these studies reported on the development of hypertension [103, 110], cardiac hypertrophy [111] and fibrosis [110] within 4-8 weeks upon adenine-mediated CKD induction in C57BL/6 mice. In 129/Sv mice, also hypertension was observed after 8 weeks of adenine-feeding [104]. Different from these findings, the mouse models in this thesis did not develop signs of cardiac hypertrophy or fibrosis, despite reaching at least a comparable extent of kidney

damage in terms of increases in serum creatinine and urea. Also, no signs of hypertension were detected in these mouse models. Of note, blood pressure of 129/Sv mice could not be measured due to restricted animal access during the recent pandemics. Whether hypertension may have enhanced the effects on the heart in adenine-induced CKD models reported in literature to date, requires further investigation.

What only a few published studies mention, is the exact designation of the applied C57BL/6 mice [65], being the distinction between C57BL/6**J** mice and C57BL/6**N** mice. Both are wildtype mice, but they are derived from a colony at the Jackson laboratories or the Taconic laboratories, respectively, thus harboring genetic differences. As one known genetic difference, C57BL/6**J** mice carry a loss-of-function mutation in the *Nnt* gene, which provides protection against pressure overload-induced oxidative stress and maladaptive cardiac remodeling [97]. In addition, some studies report on C57BL/6**J** being resistant to develop proteinuric kidney dysfunction as well as cardiac changes [112], although they do develop kidney fibrosis [113].

In contrast, some studies indicate that C57BL/6**N** mice were used, which developed sufficient kidney dysfunction after feeding adenine-supplemented diet, as shown, for example, by Klinkhammer *et al.* [66]. Since some mouse strains are more prone to develop kidney dysfunction and/or cardiac changes, as for example mentioned for the 129/Sv strain [77], than others, also the exact designation of the used C57BL/6 strain should always be reported in future studies.

5.5. RNA sequencing reveals pathological responses as well as protective (feedback) responses on molecular level in the heart of CKD mice.

With the aim to gain a further understanding of CKD-induced cardiac alterations on molecular level, RNA sequencing of cardiac tissue was performed in the mouse model with moderate to severe CKD, being adenine-induced CKD in 129/Sv mice (Model 5). ***Molecular changes were detected in inflammatory and oxidative stress responses*** (with increased *Depp1, Ddit4, Ager, Sphk1, Rgcc, Gpnmb, Cebpb, Acp5*) ***and in processes related to extracellular matrix and fibrosis*** (with increased *Ager, Rgcc, Col8a2, Mmp12, Gpnmb*; decreased *Snca, Spon2, Apln, Smoc2, Mmp15*).

Among upregulated pathological mediators, DEPP1 and DNA damage-inducible transcript 4 (DDIT4) are increased upon cellular stress and support ROS accumulation [78, 79]. Also, the advanced glycosylation end product-specific receptor (AGER) mediates ROS production [80, 81] and cardiac inflammation [114]. Sphingosine kinase 1 (SPHK1) contributes to AngII-induced cardiac remodeling [115] and triggers myocardial degeneration, cardiac fibrosis and increased levels of oxidative stress markers upon overexpression [82]. Additionally, AGER [86] and the regulator of cell cycle (RGCC) [85] contribute to ECM production and organ fibrosis. In the same line, the collagen type VIII alpha 2 chain (COL8A2) [87] and matrix metalloproteinase 12 (MMP12) [88] have been linked with profibrotic processes in the heart. Although the glycoprotein non-metastatic melanoma protein B (GPNMB) counteracted inflammation and fibrosis in for example liver [116], it contributed to pathological cardiac remodeling after myocardial infarction and dilated cardiomyopathy without effect on inflammation and fibrosis [117]. Taken together, these upregulated mediators mainly indicated a shift towards oxidative stress, fibrosis and inflammation in hearts of 129/Sv mice upon CKD.

Additionally, ***downregulated cardioprotective genes*** in hearts of CKD mice may contribute to a pathological maladaptation of the heart. For example, synuclein alpha (SNCA) counteracts organ fibrosis [118]. The extracellular matrix protein spondin 2 (SPON2) is protective against AngII- and pressure overload-induced cardiac hypertrophy, fibrosis, cardiac dysfunction and transition to heart failure [119]. In the same line, the cardioprotective peptide apelin (APLN) counteracts AngII-mediated pathological remodeling and dysfunction of the heart [120]. Finally, potassium voltage-gated channel subfamily E regulatory subunit 1 (KCNE1) is part of the slow delayed-rectifier potassium IKs channel with a key role in cardiac action potential repolarization. Significant downregulation of genes coding for certain potassium channels was previously reported in explanted human hearts of patients with end-stage heart failure [121] and potentially linked to repolarization abnormalities in human heart failure [122]. Taken together, in addition to upregulated pathological mediators, the downregulation of cardioprotective genes suggests a maladaptation of the CKD heart in 129/Sv mice.

In parallel, the molecular profile pointed to processes counteracting inflammation, fibrosis and cardiac remodeling, as for increased levels of MMP12 and ACP5. MMP12 acts as an inflammation resolution factor following myocardial infarction

[84], whereas acid phosphatase 5 (ACP5) counteracts inflammation and ROS production in macrophages [83]. In regard to the reduction in the ECM protein SPARC related modular calcium-binding protein 2 (SMOC2), SMOC2 triggers TGFβ expression [89] and drives kidney fibrosis through TGFβ-induced fibroblast to myofibroblast transition [90]. The hearts of our CKD mice furthermore revealed decreased expression of hemoglobin alpha (HBA-A1, HBA-A2) and ALAS2 (*data not shown*) as rate-limiting enzyme in heme synthesis. Excess heme production was linked to increased ROS production in the failing heart [123], so that reduced heme production could also display a protective feedback mechanism.

Taken together, the molecular profile revealed that CKD impacts the heart in an ambivalent manner. Upregulated pathological mediators as well as downregulation of cardioprotective genes point to a negative impact of CKD on the heart toward cardiac remodeling processes. In parallel, however, induced processes counteracting inflammation and fibrosis may compensate for the negative impact. Overall, this could underlie the observation of a pro-oxidative shift in the hearts of 129/Sv mice upon CKD but without signs of cardiac remodeling processes.

In summary, in this thesis, adenine-induced CKD in 129/Sv mice exhibited enhanced cardiac oxidative stress responses as evidenced by an increase in ROS-inducing mediators and a decrease in cardioprotective mediators, as well as signs of increased levels of the oxidative stress markers HO-1 and 8-OHdG. Oxidative stress can either be protective or can have detrimental effects, depending on the source, dose and duration of the oxidative stress. Detrimental effects with maladaptive consequences can lead to cardiac dysfunction and even heart failure [124], which none of the investigated mouse models in this thesis has shown. Therefore, it is unclear, whether the findings of increased oxidative stress markers predispose to the development of heart failure or rather are induced to offer protection. In addition, protective anti-inflammatory feedback responses, as well as pro- and anti-fibrotic responses on a molecular level were also observed in the RNA sequencing data, which may explain the absence of overall interstitial fibrosis observed in CKD-hearts (**Figure 47**).
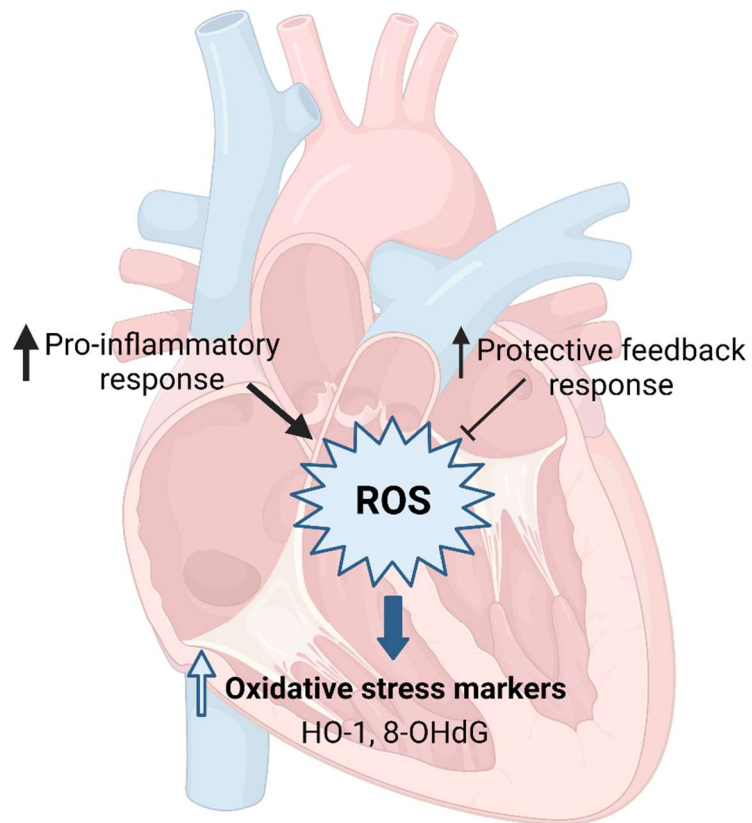
Maladaptive predisposition or protective preconditioning of the heart?

Figure 47: Cardiac analysis in 129/Sv mice developing moderate to severe CKD on adenine diet revealed increased oxidative stress markers and an increased pro-inflammatory response, but also increased protective mediators.

5.6. Does uremic cardiomyopathy require a longer CKD exposure or additional cardiovascular hits?

From the findings in this thesis, it can be concluded that developing a CKD mouse model with a clearly dysfunctional cardiac phenotype is a challenge. Given that several weeks of at least moderate CKD in different mouse strains and induced with different methods do not necessarily lead to cardiac dysfunction or cardiac remodeling, it must be critically evaluated whether extension above 13 weeks of an appropriate mouse model may induce uremic cardiomyopathy accompanied by cardiac dysfunction and remodeling, or whether additional cardiac injury "hits" are required. This is consistent with recent findings from the systematic review with meta-analysis that we recently published (*in appendix*), which revealed that on the one hand genetic factors and on the other hand additional cardiovascular risk factors may increase the cardiac susceptibility to CKD-induced damage [65]. Therefore, addition of an additional cardiac injury "hit" to the induced CKD-induced damage, such as pressure overload, diabetes or even myocardial infarction, might provide a worsened cardiac phenotype in the context of CKD.

5.7. Overall conclusion and outlook.

Altogether, the comparison of adenine-induced and 5/6 Nx-induced CKD mouse models in different mouse strains points out that induction of several weeks of at least moderate CKD does not necessarily lead to the development of uremic cardiomyopathy. **This raises concerns about the simple concept of uremic cardiomyopathy and lead to the suggestion that further stressors, such as cardiovascular injury "hits" are necessary to cause CKD-induced cardiac dysfunction and remodeling.** In the two investigated mouse models with at least moderate CKD, CKD leads to increased oxidative stress markers in the heart. Future studies will have to investigate whether this forms a cardioprotective feedback effect to prevent CKD-induced cardiac damage, or whether it in fact increases the risk of increased cardiovascular injury in the presence of additional cardiovascular risk factors and/or events.

5.8. Strength and limitations of this study.

As strength of this study, it compared five different mouse models of uremic cardiomyopathy using a standardized, detailed characterization of the kidney and the heart.

Although no clear cardiac functional or morphological phenotype in CKD could be revealed, this study was important in the light of the highly variable results found in the literature though with reporting of only a limited number and highly variable character of parameters. Furthermore, this study underlines that it is a challenge to induce a clear cardiac phenotype by mere induction of CKD in mice, and suggests that additional genetic or cardiovascular risk factors may contribute to the typical picture of uremic cardiomyopathy observed in patients. Finally, this study revealed that, despite the absence of a clear cardiac functional phenotype, CKD triggered increased cardiac oxidative stress responses in models with at least moderate CKD. Whether this oxidative stress is a maladaptive predisposition, or a protective conditioning of the heart requires further investigation in future studies. In addition, mechanisms and related mediators underlying increased cardiac oxidative stress signaling in CKD mice need to be investigated in more detail, since this was not performed in this study.

Also, additional CKD models could be further investigated in future studies. Prolongation of the adenine diet and thus long-term CKD exposure may be a possibility, considering that the 129/Sv mouse model showed a more severe kidney dysfunction after 13 weeks of CKD than the C57BL/6J *ApoE*$^{-/-}$ after only 6 weeks. Another possibility would be the induction of a cardiac injury "hit" often present in CKD patients, e.g. pressure overload, which could potentially trigger the development of uremic cardiomyopathy in CKD mice.

Chapter 6

Summary

6. Summary

Various cardiorenal mouse models have been presented in literature, although with variable outcomes and reporting of highly varying parameters, thus not allowing a direct comparison of the different models. Accordingly, this thesis aimed to perform a comprehensive and standardized characterization and comparison of different mouse models of chronic kidney disease (CKD) to examine the suitability of a mouse model to mirror the clinical situation of a CKD patient developing uremic cardiomyopathy.

CKD was induced by either 5/6 nephrectomy (Nx) or an adenine-supplemented diet in three different mouse strains (C57BL/6J mice, hyperlipidemic C57BL/6J *ApoE$^{-/-}$* mice, 129/Sv). Characterization of the mouse models was performed by analyzing kidney function and morphology, blood pressure as well as heart function, cardiac hypertrophy and fibrosis, calcification and inflammation as well as oxidative stress.

C57BL/6J mice (Model 1) as well as C57BL/6J *ApoE$^{-/-}$* mice (Model 2) developed only a mild degree of kidney damage upon 10 weeks of 5/6 Nx, without prominent effects on heart function or cardiac molecular changes. Feeding C57BL/6J mice a low adenine diet (Model 3) did not result in sufficient kidney dysfunction after 6 weeks nor in clear cardiac dysfunction, except for a slightly reduced ejection fraction.

In contrast, CKD-induction by high concentrated adenine diet in hyperlipidemic C57BL/6J *ApoE$^{-/-}$* mice resulted in a stable, moderate kidney dysfunction (Model 4). Although no effects on heart function or cardiac morphology were observed, increased oxidative stress markers were detected in cardiac tissue from CKD mice. This was also observed in 129/Sv mice with a prolonged moderate to severe kidney damage induced by adenine diet over 13 weeks (Model 5). The latter was accompanied by activation of oxidative stress signaling but also by anti-inflammatory feedback responses as revealed by additional RNA sequencing, pointing to imbalances of inflammatory and oxidative stress responses in the heart in the context of at least moderate CKD.

Overall, this thesis demonstrates that the development of a cardiorenal mouse model with a clear dysfunctional cardiac phenotype as observed in CKD patients is still challenging. Nonetheless, this study considerable advances the knowledge in cardi-

orenal research by providing a detailed, standardized comparison of different cardiorenal models, as well as by revealing that at least a moderate state of CKD results in increased oxidative stress markers in the heart.

Chapter 7

Societal Impact

7. Societal Impact

Cardiovascular diseases (CVD) are the leading cause of death worldwide. CVD accounted for about 31 % of global deaths in 2019. Moreover, the prevalence of chronic kidney disease (CKD) is rising worldwide. In the past years, there is increasing evidence that CKD is an independent risk factor for the development and progression of CVD, since about 50 % of CKD stage 4-5 patients suffer also from CVD. The CVD mortality rate in those patients is about 40-50 % compared with a 26 % CVD mortality rate in patients without CKD. The pathophysiological link between CVD and CKD is called the cardiorenal syndrome.

One major cardiac pathology occurring in CKD patients is the pathology termed as uremic cardiomyopathy. The underlying mechanisms are not completely understood yet, which complicates the precise treatment of the disease. A necessary approach to examine the underlying mechanisms of an organ crosstalk like the cardiorenal syndrome is the investigation in animal models. In literature different mouse models in the field of cardiorenal research were presented, with all reporting on highly variable parameters which highly complicates a comparison of those different mouse models.

Thus, a clear comprehensive and standardized characterization and comparison is of great importance to find a suitable cardiorenal mouse model for unravelling underlying mechanisms of uremic cardiomyopathy, and is presented in this thesis.

This study brought light into the jungle of cardiorenal mouse models. The cardiac analysis of five different mouse models revealed that at least a moderate CKD results in increased oxidative stress in hearts of CKD mice, although neither the heart function nor cardiac morphological remodeling was affected. On molecular level it was revealed that not only oxidative stress signaling is affected by CKD, but also protective feedback responses are upregulated in the heart. Future studies should address whether the increased oxidative stress is a maladaptive predisposition or a protective conditioning for subsequent cardiovascular damage. Furthermore, this study revealed that the mere induction of CKD not necessarily results in a clear cardiac functional phenotype and thus raises questions about a simple "single-hit" concept of uremic cardiomyopathy.

This leads to the suggestion that a further stressor is needed, as for example an additional cardiovascular risk factor or further cardiovascular injury, such as pressure overload, as often found in CKD patients.

The comprehensive standardized characterization and comparison of five different cardiorenal mouse models in this study enlightened unclarities about the use of mouse models in the field of cardiorenal research by using different mouse strains and different CKD induction methods. Furthermore, it raises awareness for reporting a broader set of parameters of kidney and heart function and remodeling processes in cardiorenal research instead of focusing on highly selected processes, this also to avoid unnecessarily repetition of mouse experiments which may not lead to the desired outcome.

The insights resulting from this thesis were shared with the scientific community as well as with the general public by publication in scientific journals as well as poster and oral presentations.

References

8. References

1. Mendis S, P.P., Norrving B editors, *Global Atlas on cardiovascular disease prevention and control.* World Health Organisation, 2011: p. 1-166.
2. World Health Organisation. *Cardiovascular disease (CVDs).* 2017 March, 2022]; Available from: https://www.who.int/en/news-room/fact-sheets/detail/cardiovascular-diseases-(cvds).
3. Hansson, G.K. and A. Hermansson, *The immune system in atherosclerosis.* Nat Immunol, 2011. **12**(3): p. 204-12.
4. Pagidipati, N.J. and T.A. Gaziano, *Estimating deaths from cardiovascular disease: a review of global methodologies of mortality measurement.* Circulation, 2013. **127**(6): p. 749-56.
5. Hansson, G.K., *Inflammation, atherosclerosis, and coronary artery disease.* N Engl J Med, 2005. **352**(16): p. 1685-95.
6. Alhaj, E., et al., *Uremic cardiomyopathy: an underdiagnosed disease.* Congest Heart Fail, 2013. **19**(4): p. E40-5.
7. Association, A.H. *What is Cardiomyopathy in Adults?* 2021 19.05.2022]; Available from: https://www.heart.org/en/health-topics/cardiomyopathy/what-is-cardiomyopathy-in-adults.
8. National Heart, L.a.B.I. *What Is Cardiomyopathy?* 19.05.2022]; Available from: https://www.nhlbi.nih.gov/health/cardiomyopathy.
9. Joseph, P., et al., *Reducing the Global Burden of Cardiovascular Disease, Part 1: The Epidemiology and Risk Factors.* Circ Res, 2017. **121**(6): p. 677-694.
10. Webster, A.C., et al., *Chronic Kidney Disease.* Lancet, 2017. **389**(10075): p. 1238-1252.
11. Eckardt, K.U., et al., *Evolving importance of kidney disease: from subspecialty to global health burden.* Lancet, 2013. **382**(9887): p. 158-69.
12. Meguid El Nahas, A. and A.K. Bello, *Chronic kidney disease: the global challenge.* Lancet, 2005. **365**(9456): p. 331-40.
13. Mancia, A.E.B.G., *Cardiorenal syndrome: Mechanisms, risk and treatment.* 2010.
14. Drawz, P. and M. Rahman, *Chronic kidney disease.* Ann Intern Med, 2015. **162**(11): p. Itc1-16.
15. Saran, R., et al., *US Renal Data System 2014 Annual Data Report: Epidemiology of Kidney Disease in the United States.* Am J Kidney Dis, 2015. **66**(1 Suppl 1): p. Svii, S1-305.
16. Hippisley-Cox, J. and C. Coupland, *Predicting the risk of chronic Kidney Disease in men and women in England and Wales: prospective derivation and external validation of the QKidney Scores.* BMC Fam Pract, 2010. **11**: p. 49.
17. Lea, J.P. and S.B. Nicholas, *Diabetes mellitus and hypertension: key risk factors for kidney disease.* J Natl Med Assoc, 2002. **94**(8 Suppl): p. 7s-15s.
18. Prevention, C.f.D.C.a., *Chronic Kidney Disease in the United States, 2021.* Atlanta, GA: US Department of Health and Human Services, Centers for Disease Control and Prevention, 2021.
19. Hughson, M.D., et al., *Hypertension, glomerular hypertrophy and nephrosclerosis: the effect of race.* Nephrol Dial Transplant, 2014. **29**(7): p. 1399-409.
20. Richard J. Glassock, A.D.u.A.D.R., *The Physiology and Pathophysiology of the Kidneys in Aging*, in *Brenner and Rector's The Kidney*. 2020. p. 710-730.

21. Fogo, A.B., et al., *AJKD Atlas of Renal Pathology: Kidney Transplant Interstitial Fibrosis/Tubular Atrophy.* Am J Kidney Dis, 2017. **69**(5): p. e23-e24.

22. Duranton, F., et al., *Normal and pathologic concentrations of uremic toxins.* J Am Soc Nephrol, 2012. **23**(7): p. 1258-70.

23. Itoh, Y., et al., *Protein-bound uremic toxins in hemodialysis patients measured by liquid chromatography/tandem mass spectrometry and their effects on endothelial ROS production.* Anal Bioanal Chem, 2012. **403**(7): p. 1841-50.

24. Vanholder, R., et al., *The uremic toxicity of indoxyl sulfate and p-cresyl sulfate: a systematic review.* J Am Soc Nephrol, 2014. **25**(9): p. 1897-907.

25. Curtius, H.C., M. Mettler, and L. Ettlinger, *Study of the intestinal tyrosine metabolism using stable isotopes and gas chromatography-mass spectrometry.* J Chromatogr, 1976. **126**: p. 569-80.

26. Barreto, F.C., et al., *Serum indoxyl sulfate is associated with vascular disease and mortality in chronic kidney disease patients.* Clin J Am Soc Nephrol, 2009. **4**(10): p. 1551-8.

27. Holmar, J., et al., *Uremic Toxins Affecting Cardiovascular Calcification: A Systematic Review.* Cells, 2020. **9**(11).

28. Liabeuf, S., et al., *Free p-cresylsulphate is a predictor of mortality in patients at different stages of chronic kidney disease.* Nephrol Dial Transplant, 2010. **25**(4): p. 1183-91.

29. Vanholder, R., et al., *Review on uremic toxins: classification, concentration, and interindividual variability.* Kidney Int, 2003. **63**(5): p. 1934-43.

30. Anavekar, N.S., et al., *Relation between renal dysfunction and cardiovascular outcomes after myocardial infarction.* N Engl J Med, 2004. **351**(13): p. 1285-95.

31. Stevens, P.E., et al., *Chronic kidney disease management in the United Kingdom: NEOERICA project results.* Kidney Int, 2007. **72**(1): p. 92-9.

32. Thompson, S., et al., *Cause of Death in Patients with Reduced Kidney Function.* J Am Soc Nephrol, 2015. **26**(10): p. 2504-11.

33. Drey, N., et al., *A population-based study of the incidence and outcomes of diagnosed chronic kidney disease.* Am J Kidney Dis, 2003. **42**(4): p. 677-84.

34. McCullough, P.A., *Why is chronic kidney disease the "spoiler" for cardiovascular outcomes?* J Am Coll Cardiol, 2003. **41**(5): p. 725-8.

35. Gibson, C.M., et al., *Association of glomerular filtration rate on presentation with subsequent mortality in non-ST-segment elevation acute coronary syndrome; observations in 13,307 patients in five TIMI trials.* Eur Heart J, 2004. **25**(22): p. 1998-2005.

36. Naghavi, M., et al., *From vulnerable plaque to vulnerable patient: a call for new definitions and risk assessment strategies: Part I.* Circulation, 2003. **108**(14): p. 1664-72.

37. Baaten, C., et al., *Platelet Function in CKD: A Systematic Review and Meta-Analysis.* J Am Soc Nephrol, 2021. **32**(7): p. 1583-98.

38. Briet, M., et al., *Arterial stiffness and enlargement in mild-to-moderate chronic kidney disease.* Kidney Int, 2006. **69**(2): p. 350-7.

39. Temmar, M., et al., *Pulse wave velocity and vascular calcification at different stages of chronic kidney disease.* J Hypertens, 2010. **28**(1): p. 163-9.

40. Noels, H., et al., *The new SFB/TRR219 Research Centre.* Eur Heart J, 2018. **39**(12): p. 975-977.

41. Koleganova, N., et al., *Arterial calcification in patients with chronic kidney disease.* Nephrol Dial Transplant, 2009. **24**(8): p. 2488-96.

42. Harlacher, E., et al., *Impact of Uremic Toxins on Endothelial Dysfunction in Chronic Kidney Disease: A Systematic Review.* Int J Mol Sci, 2022. **23**(1).

43. Noels, H., et al., *Lipoproteins and fatty acids in chronic kidney disease: molecular and metabolic alterations.* Nature Reviews Nephrology, 2021: p. 1-15.

44. Annuk, M., et al., *Oxidative stress and endothelial function in chronic renal failure.* J Am Soc Nephrol, 2001. **12**(12): p. 2747-2752.

45. Wang, X. and J.I. Shapiro, *Evolving concepts in the pathogenesis of uraemic cardiomyopathy.* Nat Rev Nephrol, 2019. **15**(3): p. 159-175.

46. Foley, R.N., et al., *Clinical and echocardiographic disease in patients starting end-stage renal disease therapy.* Kidney Int, 1995. **47**(1): p. 186-92.

47. Izumaru, K., et al., *Reduced Estimated GFR and Cardiac Remodeling: A Population-Based Autopsy Study.* Am J Kidney Dis, 2019. **74**(3): p. 373-381.

48. Senbonmatsu, T., et al., *Evidence for angiotensin II type 2 receptor-mediated cardiac myocyte enlargement during in vivo pressure overload.* J Clin Invest, 2000. **106**(3): p. R25-9.

49. Amann, K., et al., *Left ventricular hypertrophy in renal failure.* Kidney Int Suppl, 1998. **68**: p. S78-85.

50. Disertori, M., M. Masè, and F. Ravelli, *Myocardial fibrosis predicts ventricular tachyarrhythmias.* Trends Cardiovasc Med, 2017. **27**(5): p. 363-372.

51. Graham-Brown, M.P., et al., *Imaging of Myocardial Fibrosis in Patients with End-Stage Renal Disease: Current Limitations and Future Possibilities.* Biomed Res Int, 2017. **2017**: p. 5453606.

52. Noels, H., et al., *Lipoproteins and fatty acids in chronic kidney disease: molecular and metabolic alterations.* Nat Rev Nephrol, 2021. **17**(8): p. 528-542.

53. Gupta, J., et al., *Association between Inflammation and Cardiac Geometry in Chronic Kidney Disease: Findings from the CRIC Study.* PLoS One, 2015. **10**(4): p. e0124772.

54. García-Jérez, A., et al., *Effect of uraemia on endothelial cell damage is mediated by the integrin linked kinase pathway.* J Physiol, 2015. **593**(3): p. 601-18; discussion 618.

55. Jerotic, D., et al., *GSTM1 Modulates Expression of Endothelial Adhesion Molecules in Uremic Milieu.* Oxid Med Cell Longev, 2021. **2021**: p. 6678924.

56. Saum, K., et al., *Uremic Advanced Glycation End Products and Protein-Bound Solutes Induce Endothelial Dysfunction Through Suppression of Krüppel-Like Factor 2.* J Am Heart Assoc, 2018. **7**(1).

57. Sárközy, M., et al., *Mechanisms and Modulation of Oxidative/Nitrative Stress in Type 4 Cardio-Renal Syndrome and Renal Sarcopenia.* Front Physiol, 2018. **9**: p. 1648.

58. Herum, K.M., et al., *The Soft- and Hard-Heartedness of Cardiac Fibroblasts: Mechanotransduction Signaling Pathways in Fibrosis of the Heart.* J Clin Med, 2017. **6**(5).

59. Tsoref, O., et al., *E-selectin-targeted copolymer reduces atherosclerotic lesions, adverse cardiac remodeling, and dysfunction.* J Control Release, 2018. **288**: p. 136-147.

60. Masai, N., et al., *Indoxyl sulfate stimulates monocyte chemoattractant protein-1 expression in human umbilical vein endothelial cells by inducing oxidative stress through activation of the NADPH oxidase-nuclear factor-κB pathway.* Circ J, 2010. **74**(10): p. 2216-24.

61. Tumur, Z., et al., *Indoxyl sulfate upregulates expression of ICAM-1 and MCP-1 by oxidative stress-induced NF-kappaB activation.* Am J Nephrol, 2010. **31**(5): p. 435-41.

62. Yang, K., et al., *Amelioration of uremic toxin indoxyl sulfate-induced endothelial cell dysfunction by Klotho protein.* Toxicol Lett, 2012. **215**(2): p. 77-83.

63. Nakano, T., et al., *Involvement of chronic inflammation via monocyte chemoattractant protein-1 in uraemic cardiomyopathy: a human biopsy study.* ESC Heart Fail, 2021. **8**(4): p. 3156-3167.

64. Masiha, S., J. Sundström, and L. Lind, *Inflammatory markers are associated with left ventricular hypertrophy and diastolic dysfunction in a population-based sample of elderly men and women.* J Hum Hypertens, 2013. **27**(1): p. 13-7.

65. Soppert, J., et al., *A systematic review and meta-analysis of murine models of uremic cardiomyopathy.* Kidney Int, 2022. **101**(2): p. 256-273.

66. Klinkhammer, B.M., et al., *Cellular and Molecular Mechanisms of Kidney Injury in 2,8-Dihydroxyadenine Nephropathy.* J Am Soc Nephrol, 2020. **31**(4): p. 799-816.

67. Lin, C.Y., et al., *CB1 cannabinoid receptor antagonist attenuates left ventricular hypertrophy and Akt-mediated cardiac fibrosis in experimental uremia.* J Mol Cell Cardiol, 2015. **85**: p. 249-61.

68. Kieswich, J.E., et al., *A novel model of reno-cardiac syndrome in the C57BL/ 6 mouse strain.* BMC Nephrol, 2018. **19**(1): p. 346.

69. Thomsen, M.B., et al., *Uremia increases QRS duration after β-adrenergic stimulation in mice.* Physiol Rep, 2018. **6**(13): p. e13720.

70. Clinkenbeard, E.L., et al., *Increased FGF23 protects against detrimental cardio-renal consequences during elevated blood phosphate in CKD.* JCI Insight, 2019. **4**(4).

71. Vandesompele, J., et al., *Accurate normalization of real-time quantitative RT-PCR data by geometric averaging of multiple internal control genes.* Genome Biol, 2002. **3**(7): p. Research0034.

72. Dobin, A., et al., *STAR: ultrafast universal RNA-seq aligner.* Bioinformatics, 2013. **29**(1): p. 15-21.

73. Liao, Y., G.K. Smyth, and W. Shi, *The R package Rsubread is easier, faster, cheaper and better for alignment and quantification of RNA sequencing reads.* Nucleic Acids Res, 2019. **47**(8): p. e47.

74. Yu, G., et al., *clusterProfiler: an R package for comparing biological themes among gene clusters.* Omics, 2012. **16**(5): p. 284-7.

75. Jia, T., et al., *A novel model of adenine-induced tubulointerstitial nephropathy in mice.* BMC Nephrol, 2013. **14**: p. 116.

76. Diwan, V., L. Brown, and G.C. Gobe, *Adenine-induced chronic kidney disease in rats.* Nephrology (Carlton), 2018. **23**(1): p. 5-11.

77. Wang, Q., et al., *Blood pressure, cardiac, and renal responses to salt and deoxycorticosterone acetate in mice: role of Renin genes.* J Am Soc Nephrol, 2002. **13**(6): p. 1509-16.

78. Salcher, S., et al., *C10ORF10/DEPP-mediated ROS accumulation is a critical modulator of FOXO3-induced autophagy.* Mol Cancer, 2017. **16**(1): p. 95.

79. Qiao, S., et al., *A REDD1/TXNIP pro-oxidant complex regulates ATG4B activity to control stress-induced autophagy and sustain exercise capacity.* Nat Commun, 2015. **6**: p. 7014.

80. Coughlan, M.T., et al., *RAGE-induced cytosolic ROS promote mitochondrial superoxide generation in diabetes.* J Am Soc Nephrol, 2009. **20**(4): p. 742-52.

81. Daffu, G., et al., *Radical roles for RAGE in the pathogenesis of oxidative stress in cardiovascular diseases and beyond.* Int J Mol Sci, 2013. **14**(10): p. 19891-910.

82. Takuwa, N., et al., *S1P3-mediated cardiac fibrosis in sphingosine kinase 1 transgenic mice involves reactive oxygen species.* Cardiovasc Res, 2010. **85**(3): p. 484-93.

83. Bune, A.J., et al., *Mice lacking tartrate-resistant acid phosphatase (Acp 5) have disordered macrophage inflammatory responses and reduced clearance of the pathogen, Staphylococcus aureus.* Immunology, 2001. **102**(1): p. 103-13.

84. Mouton, A.J., et al., *Matrix metalloproteinase-12 as an endogenous resolution promoting factor following myocardial infarction.* Pharmacol Res, 2018. **137**: p. 252-258.

85. Huang, W.Y., et al., *RGC-32 mediates transforming growth factor-beta-induced epithelial-mesenchymal transition in human renal proximal tubular cells.* J Biol Chem, 2009. **284**(14): p. 9426-32.

86. Zhao, J., R. Randive, and J.A. Stewart, *Molecular mechanisms of AGE/RAGE-mediated fibrosis in the diabetic heart.* World J Diabetes, 2014. **5**(6): p. 860-7.

87. Skrbic, B., et al., *Lack of collagen VIII reduces fibrosis and promotes early mortality and cardiac dilatation in pressure overload in mice.* Cardiovasc Res, 2015. **106**(1): p. 32-42.

88. Stawski, L., et al., *MMP-12 deficiency attenuates angiotensin II-induced vascular injury, M2 macrophage accumulation, and skin and heart fibrosis.* PLoS One, 2014. **9**(10): p. e109763.

89. Yuting, Y., F. Lifeng, and H. Qiwei, *Secreted modular calcium-binding protein 2 promotes high fat diet (HFD)-induced hepatic steatosis through enhancing lipid deposition, fibrosis and inflammation via targeting TGF-β1.* Biochem Biophys Res Commun, 2019. **509**(1): p. 48-55.

90. Gerarduzzi, C., et al., *Silencing SMOC2 ameliorates kidney fibrosis by inhibiting fibroblast to myofibroblast transformation.* JCI Insight, 2017. **2**(8).

91. Hamzaoui, M., et al., *5/6 nephrectomy induces different renal, cardiac and vascular consequences in 129/Sv and C57BL/6JRj mice.* Sci Rep, 2020. **10**(1): p. 1524.

92. Jankowski, J., et al., *Cardiovascular Disease in Chronic Kidney Disease: Pathophysiological Insights and Therapeutic Options.* Circulation, 2021. **143**(11): p. 1157-1172.

93. Kaesler, N., et al., *Cardiac Remodeling in Chronic Kidney Disease.* Toxins (Basel), 2020. **12**(3).

94. Schlieper, G., et al., *The vulnerable patient with chronic kidney disease.* Nephrol Dial Transplant, 2016. **31**(3): p. 382-90.

95. Di Minno, A., et al., *8-Hydroxy-2-Deoxyguanosine Levels and Cardiovascular Disease: A Systematic Review and Meta-Analysis of the Literature.* Antioxid Redox Signal, 2016. **24**(10): p. 548-55.

96. Korkmaz, K.S., et al., *Detection of 8-OHdG as a diagnostic biomarker.* 2018, 2018. **3**.

97. Nickel, A.G., et al., *Reversal of Mitochondrial Transhydrogenase Causes Oxidative Stress in Heart Failure.* Cell Metab, 2015. **22**(3): p. 472-84.

98. He, X. and Q. Ma, *Disruption of Nrf2 Synergizes with High Glucose to Cause Heightened Myocardial Oxidative Stress and Severe Cardiomyopathy in Diabetic Mice.* J Diabetes Metab, 2012. **Suppl 7**.

99. Abraham, N.G. and A. Kappas, *Heme oxygenase and the cardiovascular-renal system.* Free Radic Biol Med, 2005. **39**(1): p. 1-25.

100. Monu, S.R., et al., *HO-1 induction improves the type-1 cardiorenal syndrome in mice with impaired angiotensin II-induced lymphocyte activation.* Hypertension, 2013. **62**(2): p. 310-6.

101. Omizo, H., et al., *Cardio-renal protective effect of the xanthine oxidase inhibitor febuxostat in the 5/6 nephrectomy model with hyperuricemia.* Sci Rep, 2020. **10**(1): p. 9326.

102. Chen, C., et al., *Systemic heme oxygenase-1 transgenic overexpression aggravates pressure overload-induced cardiac hypertrophy in mice.* Cell Physiol Biochem, 2011. **28**(1): p. 25-32.

103. Nemmar, A., et al., *Cardiac Inflammation, Oxidative Stress, Nrf2 Expression, and Coagulation Events in Mice with Experimental Chronic Kidney Disease.* Oxid Med Cell Longev, 2021. **2021**: p. 8845607.

104. Sakata, F., et al., *Sodium chloride promotes tissue inflammation via osmotic stimuli in subtotal-nephrectomized mice.* Laboratory Investigation, 2017. **97**(4): p. 432-446.

105. Daenen, K., et al., *Oxidative stress in chronic kidney disease.* Pediatr Nephrol, 2019. **34**(6): p. 975-991.

106. Elkareh, J., et al., *Marinobufagenin induces increases in procollagen expression in a process involving protein kinase C and Fli-1: implications for uremic cardiomyopathy.* American Journal of Physiology-Renal Physiology, 2009. **296**(5): p. F1219-F1226.

107. Siedlecki, A.M., X.H. Jin, and A.J. Muslin, *Uremic cardiac hypertrophy is reversed by rapamycin but not by lowering of blood pressure.* Kidney International, 2009. **75**(8): p. 800-808.

108. Xie, J., et al., *Soluble Klotho Protects against Uremic Cardiomyopathy Independently of Fibroblast Growth Factor 23 and Phosphate.* Journal of the American Society of Nephrology, 2015. **26**(5): p. 1150-1160.

109. Winterberg, P.D., et al., *Myocardial dysfunction occurs prior to changes in ventricular geometry in mice with chronic kidney disease (CKD).* Physiol Rep, 2016. **4**(5).

110. Nanto-Hara, F., et al., *The guanylate cyclase C agonist linaclotide ameliorates the gut-cardio-renal axis in an adenine-induced mouse model of chronic kidney disease.* Nephrol Dial Transplant, 2020. **35**(2): p. 250-264.

111. Huang, Y., et al., *IRF1-mediated downregulation of PGC1α contributes to cardiorenal syndrome type 4.* Nat Commun, 2020. **11**(1): p. 4664.

112. Ma, L.J. and A.B. Fogo, *Model of robust induction of glomerulosclerosis in mice: importance of genetic background.* Kidney Int, 2003. **64**(1): p. 350-5.

113. O'Sullivan, J., et al., *Refining the Mouse Subtotal Nephrectomy in Male 129S2/SV Mice for Consistent Modeling of Progressive Kidney Disease With Renal Inflammation and Cardiac Dysfunction.* Front Physiol, 2019. **10**: p. 1365.

114. Bangert, A., et al., *Critical role of RAGE and HMGB1 in inflammatory heart disease.* Proc Natl Acad Sci U S A, 2016. **113**(2): p. E155-64.

115. Józefczuk, E., et al., *Cardiovascular Effects of Pharmacological Targeting of Sphingosine Kinase 1.* Hypertension, 2020. **75**(2): p. 383-392.

116. Abe, H., et al., *Transgenic expression of osteoactivin in the liver attenuates hepatic fibrosis in rats.* Biochem Biophys Res Commun, 2007. **356**(3): p. 610-5.

117. Järve, A., et al., *Adverse left ventricular remodeling by glycoprotein nonmetastatic melanoma protein B in myocardial infarction.* Faseb j, 2017. **31**(2): p. 556-568.

118. Bozic, M., et al., *Protective role of renal proximal tubular alpha-synuclein in the pathogenesis of kidney fibrosis.* Nat Commun, 2020. **11**(1): p. 1943.

119. Bian, Z.Y., et al., *Disruption of mindin exacerbates cardiac hypertrophy and fibrosis.* J Mol Med (Berl), 2012. **90**(8): p. 895-910.

120. Sato, T., et al., *Loss of Apelin Augments Angiotensin II-Induced Cardiac Dysfunction and Pathological Remodeling.* Int J Mol Sci, 2019. **20**(2).

121. Borlak, J. and T. Thum, *Hallmarks of ion channel gene expression in end-stage heart failure.* Faseb j, 2003. **17**(12): p. 1592-608.

122. Holzem, K.M., et al., *Reduced response to IKr blockade and altered hERG1a/1b stoichiometry in human heart failure.* J Mol Cell Cardiol, 2016. **96**: p. 82-92.

123. Khechaduri, A., et al., *Heme levels are increased in human failing hearts.* J Am Coll Cardiol, 2013. **61**(18): p. 1884-93.

124. Weissman, D. and C. Maack, *Redox signaling in heart failure and therapeutic implications.* Free Radic Biol Med, 2021. **171**: p. 345-364.

Appendix

9. Appendix

9.1. Tables

Table 17: Details of experimental mouse models.
Experimental details are listed to provide full overview.

Model	Mouse Strain	CKD induction	Diet				Sex
			CKD duration	Protocol adenine diet (duration, concentration)	Basic food	Casein*	
1	C57BL/6J	5/6 Nx	10 weeks	-	Standard diet (Ssniff V1534)	/	Male
2	C57BL/6J ApoE$^{-/-}$	5/6 Nx	10 weeks	-	High-fat diet (Altromin Western-Type diet)	19.5%	Male
3	C57BL/6J	Low adenine diet (variable conc.)	6 weeks	2 weeks 0.2% + 4 weeks 0.05%	Standard diet (Ssniff S0382-E188, -E186, E185)	20%	Male
4	C57BL/6J ApoE$^{-/-}$	High adenine diet (variable conc.)	6 weeks	1.5 weeks 0.3% + 4.5 weeks 0.15%	High-fat diet (Altromin Western-Type diet)	19.5%	Male
5	129/Sv	Low adenine diet (variable conc.)	13 weeks	0.15%	Standard diet (Altromin C1000)	/	Male

*Conc. = concentration; CKD = chronic kidney disease; ApoE$^{-/-}$ = apolipoprotein knockout. *When indicated, casein was added to diet of both CKD and control groups.*

Table 18: Heart function analysis by Millar catheter at baseline and under dobutamine-induced stress.

Model	Mean ± SD	dP/dt max (mmHg/s)			dP/dt min (mmHg/s)			Heart rate (bpm)		
		Control (n)	Treatment (n)	p value	Control (n)	Treatment (n)	p value	Control (n)	Treatment (n)	p value
1	5/6 Nx in C57BL/6J (Baseline)	4544 ± 586 (5)	4427 ± 2143 (5)	>0.9999	-5015 ± 1781 (6)	-3583 ± 1284 (5)	0.3622	278 ± 89 (6)	252 ± 69 (5)	>0.9999
	5/6 Nx in C57BL/6J (Dobutamine)	15197 ± 641 (6)	12997 ± 1795 (5)	**0.0420**	-8871 ± 616 (5)	-8179 ± 2497 (5)	>0.9999	485 ± 32 (6)	427 ± 36 (5)	0.2763
2	5/6 Nx in $ApoE^{-/-}$ (Baseline)	5969 ± 1907 (5)	5473 ± 1697 (6)	>0.9999	-5615 ± 2063 (5)	-4487 ± 1376 (6)	0.6155	243 ± 31 (5)	233 ± 81 (6)	>0.9999
	5/6 Nx in $ApoE^{-/-}$ (Dobutamine)	14351 ± 1397 (5)	12691 ± 2733 (6)	0.3866	-9054 ± 1703 (5)	-6477 ± 1929 (6)	0.0551	492 ± 52 (5)	462 ± 73 (6)	0.8858
4	Adenine low/v in C57BL/6J (Baseline)	4363 ± 1359 (8)	4874 ± 934 (9)	0.9670	-4060 ± 1237 (8)	-4132 ± 1218 (9)	>0.9999	206 ± 52 (8)	233 ± 54 (9)	0.4219
	Adenine low/v in C57BL/6J (Dobutamine)	15034 ± 2026 (8)	15044 ± 1470 (9)	>0.9999	-8159 ± 1359 (8)	-8041 ± 1939 (9)	>0.9999	491 ± 27 (8)	477 ± 37 (9)	>0.9999
5	Adenine high/v in $ApoE^{-/-}$ (Baseline)	6106 ± 1876 (9)	6330 ± 2036 (9)	>0.9999	-4421 ± 1024 (9)	-4697 ± 1282 (9)	>0.9999	257 ± 73 (9)	237 ± 71 (9)	0.9900
	Adenine high/v in $ApoE^{-/-}$ (Dobutamine)	12402 ± 2621 (9)	12540 ± 1657 (9)	>0.9999	-7175 ± 1371 (9)	-6884 ± 1617 (9)	>0.9999	450 ± 56 (9)	434 ± 35 (9)	>0.9999

Model	Mean ± SD	End Diastolic Pressure (mmHg)			Maximum Pressure (mmHg)		
		Control (n)	Treatment (n)	p value	Control (n)	Treatment (n)	p value
1	5/6 Nx in C57BL/6J (Baseline)	20.8 ± 7.1 (6)	16.0 ± 4.1 (5)	0.1725	106 ± 16 (5)	90 ± 17 (4)	0.3740
	5/6 Nx in C57BL/6J (Dobutamine)	9.7 ± 2.3 (6)	6.0 ± 1.2 (5)	0.3709	133 ± 4 (5)	133 ± 25 (4)	>0.9999
2	5/6 Nx in $ApoE^{-/-}$ (Baseline)	11.0 ± 1.8 (4)	15.3 ± 9.6 (6)	0.5268	93 ± 4 (4)	92 ± 14 (5)	>0.9999
	5/6 Nx in $ApoE^{-/-}$ (Dobutamine)	2.0 ± 1.4 (5)	3.7 ± 4.4 (6)	>0.9999	121 ± 16 (4)	120 ± 29 (5)	>0.9999
4	Adenine low/v in C57BL/6J (Baseline)	10.7 ± 3.1 (7)	11.1 ± 5.4 (8)	>0.9999	99 ± 17 (8)	109 ± 17 (7)	>0.9999
	Adenine low/v in C57BL/6J (Dobutamine)	2 ± 1.8 (8)	3.0 ± 3.2 (7)	>0.9999	139 ± 37 (8)	144 ± 40 (7)	>0.9999
5	Adenine high/v in $ApoE^{-/-}$ (Baseline)	15.7 ± 8.7 (9)	9.8 ± 6.8 (9)	0.1085	101 ± 19 (9)	96 ± 14 (9)	>0.9999
	Adenine high/v in $ApoE^{-/-}$ (Dobutamine)	5.1 ± 3.7 (9)	3.0 ± 4.7 (9)	0.9579	123 ± 28 (9)	121 ± 24 (9)	>0.9999

/v refers to variable Adenine concentrations as defined in Table

dP/dt max: maximal rate of left ventricular pressure change (mmHg/s)

dP/dt min: minimal rate of left ventricular pressure change (mmHg/s)

Table 19: Heart function analysis via echocardiography.

Model	Mean ± SD	Heart rate (bpm)			Ejection Fraction (%)			Fractional Shortening (%)			Cardiac Output (ml/min)		
		Control (n)	Treatment (n)	p value	Control (n)	Treatment (n)	p value	Control (n)	Treatment (n)	p value	Control (n)	Treatment (n)	p value
1	5/6 Nx in C57BL6J (10 weeks)	n.a.	n.a.	n.a.	n.a.	n.a.	n.a.	n.a.	n.a.	n.a.	n.a.	n.a.	n.a.
2	5/6 Nx in *ApoE*$^{-/-}$ (10 weeks)	428.7 ± 22.8 (4)	449.2 ± 60.66 (3)	0.5528	64.8 ± 5.9 (4)	64.9 ± 8.2 (3)	0.9694	36.4 ± 4.34 (4)	34.9 ± 3.77 (3)	0.67	15.44 ± 3.23 (4)	19.46 ± 3.99 (3)	0.1987
3	Adenine low/v in C57BL6J (6 weeks)	319.7 ± 43.4 (10)	304.0 ± 22.6 (10)	0.3240	64.2 ± 6.3 (10)	57.1 ± 7.9 (10)	**0.0396**	32.9 ± 5.02 (10)	28.9 ± 3.49 (10)	0.05	11.07 ± 1.92 (10)	10.42 ± 1.61 (10)	0.4280
4	Adenine high/v in *ApoE*$^{-/-}$ (6 weeks)	379.2 ± 55.4 (9)	334.2 ± 48.1 (10)	0.0747	64.6 ± 10.3 (9)	65.1 ± 11.7 (10)	0.9278	34.9 ± 6.17 (9)	35.3 ± 7.29 (10)	0.91	11.07 ±1.93 (9)	10.42 ±1.61 (10)	0.4280

Model	Mean ± SD	LVEDD (mm)			LVEDV (µl)			LVPW;d (mm)		
		Control	Treatment	p value	Control	Treatment	p value	Control	Treatment	p value
1	5/6 Nx in C57BL6J (10 weeks)	n.a.	n.a.	n.a.	n.a.	n.a.	n.a.	n.a.	n.a.	n.a.
2	5/6 Nx in *ApoE*$^{-/-}$ (10 weeks)	3.52 ± 0.29 (4)	3.86 ± 0.20 (3)	0.1485	55.3 ± 9.4 (4)	66.9 ± 10.5 (3)	0.1832	0.73 ± 0.12 (4)	0.61 ± 0.05 (3)	0.4000
4	Adenine low/v in C57BL6J (6 weeks)	3.67 ± 0.23 (10)	3.72 ± 0.40 (10)	0.4813	59.5 ± 6.1 (10)	62.3 ± 7.2 (10)	0.3515	0.53 ± 0.08 (10)	0.56 ± 0.07 (10)	0.4315
5	Adenine high/v in *ApoE*$^{-/-}$ (6 weeks)	3.37 ± 0.58 (9)	3.46 ± 0.39 (10)	0.6863	54.8 ± 11.3 (9)	52.6 ± 12.5 (10)	0.6971	0.68 ± 0.12 (9)	0.75 ± 0.21 (10)	0.4285

/v refers to variable Adenine concentrations as defined in Table 4

n.a. = not analyzed; LVEDV = left ventricular end-diastolic volume; LVPW = left ventricular posterior wall thickness; d = diastolic left ventricular posterior wall thickness.

9.2. List of abbreviations

Abbreviation	Meaning
5/6 Nx	5/6 nephrectomy
8-OHdG	8-hydroxy-2'-deoxyguanosine
Acp5	Acid phosphatase 5
AFOG	Acid Fuchsin Orange G
Ager	Advanced glycosylation end product-specific receptor
ALAS2	Aminolevulinic acid synthase 2
AngII	Angiotensin II
Anp	Atrial natriuretic peptide
Apln	Apelin
ApoE	Apolipoprotein E
Bnp	Brain natriuretic peptide
BSA	Bovine serum albumine
CAT	Catalase
Ccl	CC-chemokine ligand
cDNA	Complementary deoxyribonucleic acid
Cebpb	CCAAT/enhancer binding protein (C/EBP), beta
CKD	Chronic kidney disease
cLDL	Carbamylated LDL
COL	Collagen
Ct	Cycle threshold
CVD	Cardiovascular disease
Ddit4	DNA-damage-inducible transcript 4
DEG	Differentially expressed genes
Depp1	DEPP1 autophagy regulator
DMSO	Dimethyl sulfoxide
dNTPs	Deoxynucleotides
ERK	Extracellular-signal regulated kinase
ESRD	End stage renal disease
GAPDH	Glyceraldehyde-3-phosphate dehydrogenase
GFR	Glomerular filtration rate
Gpnmb	Glycoprotein (transmembrane) nmb

GusB	Glucuronidase beta
h	Hour
Hba-a	Hemoglobin alpha, adult chain
HDL	High-density lipoprotein
HE	Hematoxylin-Eosin
HFD	Western-type high-fat diet
HO-1	Heme oxygenase 1
Hprt1	Hypoxanthine phosphoribosyltransferase 1
Icam1	Intercellular adhesion molecule 1
Kcne1	Potassium voltage-gated channel, Isk-related subfamily, member 1
L	Liter
LDL	Low-density lipoprotein
LV	Left ventricular
LVH	Left ventricular hypertrophy
M	Mole
MCP-1	Monocyte chemoattracting protein 1
min	Minute
ml	Milliliter
mM	Millimole
Mmp	Matrix metallopeptidase
Myoc	Myocilin
NCDs	Noncommunicable diseases
nM	Nanomole
NNT	Nicotinamide nucleotide transhydrogenase
NOX	NADP oxidase
NRF2	Nuclear erythrocyte-related factor 2
oxLDL	Oxidized LDL
PAS	Periodic acid-Schiff
PCR	Polymerase chain reaction
PRX	Peroxiredoxin
qPCR	Quantitative real-time polymerase chain reaction
Rgcc	Regulator of cell cycle
RNA	Ribonucleic acid
ROS	Reactive oxygen species

RT	Room temperature
SDS	Sodium dodecyl sulfate
SDS PAGE	Sodium dodecyl sulfate polyacrylamide gel electrophore-
SMA	Smooth muscle actin
Smoc2	SPARC related modular calcium binding 2
Snca	Synuclein, alpha
SOD	Superoxide dismutase
Sphk1	Sphingosine kinase 1
Spon2	Spondin 2
TAC	Transversal aortic constriction
TBS	Tris buffered saline
TBS-T	TBS-Tween
Tgfb1	Transforming growth factor beta
Tnf	Tumor necrosis factor alpha
TUB	Tubulin
VCAM-1	Vascular adhesion molecule 1
WGA	Wheat germ agglutinin

9.3. List of tables

9.4. List of figures

About the author

9.5. About the author

Julia Wollenhaupt (née Wirth) was born on December 9th 1988 in Bielefeld, Germany. After high school graduation in 2008, she started a one-year internship at the Institute of Human Genetics at the RWTH Aachen University Hospital. In 2009, she started her bachelor studies of Biotechnology at the University of Applied Science in Aachen and graduated in 2013 after a 10-months internship in the Pharmaceutical Product Development Department at the Fraunhofer Institute for Molecular Biology and Applied Ecology in Aachen. In 2017, she finished her master's degree in Molecular and Applied Biotechnology at the RWTH Aachen University with the thesis entitled "Identifying molecular mechanisms of disease and therapy in patients with increased cardiovascular risk", which was performed at the Institute for Molecular Cardiovascular Research (IMCAR) in Aachen. There, under supervision of PD Dr. Heidi Noels and Prof. Dr. Joachim Jankowski, she subsequently started her PhD study in the field of cardiorenal research, as described in this thesis. During this time, she was in involved in guiding bachelor and master students as well as in organizing practica for students of medicine and biology. As a secondment she visited the laboratory of Dr. Thimoteus Speer at the University Hospital in Homburg, as well as the lab of Prof. Dr. Boor at the Institute of Pathology of RWTH Aachen University Hospital.

Publications

9.6. Publications

Julia Wollenhaupt*, Janina Frisch*, Eva Harlacher, Dickson W.L. Wong, Han Jin, Corinna Schulte, Sonja Vondenhoff, Julia Moellmann, Barbara Mara Klinkhammer, Li Zhang, Adelina Baleanu-Curaj, Elisa A. Liehn, Thimoteus Speer, Andrey Kazakov, Christian Werner, Emiel P.C. van der Vorst, Simina-Ramona Selejan, Mathias Hohl, Michael Böhm, Rafael Kramann, Erik A.L. Biessen, Michael Lehrke, Nikolaus Marx, Joachim Jankowski, Christoph Maack, Peter Boor, Leticia Prates Roma, Heidi Noels. *"Pro-oxidative priming but maintained cardiac function in a broad spectrum of murine models of chronic kidney disease."* Accepted in Redox Biology, 2022. ***Shared first authorship.*** [IF: 10.8].

Eva Harlacher, Sonja Vondenhoff, Philippe Schmitt-Kopplin, Philippe Diederich, Corinna Schulte, Christian Hemmers, Julia Moellmann, Rogier Veltrop, **Julia Wollenhaupt**, Erik Biessen, Michael Lehrke, Christoph Kuppe, Jürgen Floege, Vera Jankowski, Nikolaus Marx, Joachim Jankowski, Heidi Noels. *"Increased levels of a mycophenolic acid metabolite in patients with kidney failure negatively affect cardiomyocyte health."* Ready for submission.

Christian Hemmers*, Corinna Schulte*, **Julia Wollenhaupt**, Dickson W.L. Wong, Eva Harlacher, Setareh Orth-Alampour, Barbara Mara Klinkhammer, Stefan H Schirmer, Michael Böhm, Nikolaus Marx, Thimoteus Speer, Peter Boor, Joachim Jankowski, Heidi Noels. *"Chemokine CCL9 Is Upregulated Early in Chronic Kidney Disease and Counteracts Kidney Inflammation and Fibrosis."* Biomedicines. 2022; 10(2): 420. **Shared first authorship.* [IF: 4.7].

Eva Harlacher, **Julia Wollenhaupt**, Constance Baaten and Heidi Noels. *"Impact of uremic toxins on endothelial dysfunction in chronic kidney disease: a systematic review."* International Journal of Molecular Science. 2022; 23(1): 531. [IF: 6.2]

Josefin Soppert*, Janina Frisch*, **Julia Wirth**, Christian Hemmers, Peter Boor, Rafael Kramann, Sonja Vondenhoff, Julia Moellmann, Michael Lehrke, Mathias Hohl, Emiel P.C. van der Vorst, Christian Werner, Thimoteus Speer, Christoph Maack, Nikolaus Marx, Joachim Jankowski, Leticia Prates Roma and Heidi Noels. *"Murine models of uremic cardiomyopathy: a systematic review and meta-analysis."* Kidney International. 2021; 101(2):256-273. **Shared first authorship.* [IF: 10.6]

Marieke Sternkopf*, Magdolna Nagy*, Constance C.F.M.J Baaten*, Marijke JE Kuijpers, **Julia Wirth**, Wendy Theelen, Tom G. Mastenbroek, Michael Lehrke, Benjamin Winnerling, Lesley Baerts, Nikolaus Marx, Judith M.E.M. Cosemans, Ingrid De Meester, Andreas Daiber, Sebastian Steven, Joachim Jankowski, Johan W.M. Heemskerk, Heidi Noels. *„Native, Intact Glucagon-Like Peptide 1 Is a Natural Suppressor of Thrombus Growth Under Physiological Flow Conditions."* Arteriosclerosis, Thrombosis and Vascular Biology. 2020;40(3): e65-e77. **Shared first authorship.* [IF: 8.3]

Conferences and Workshops

9.7. Conferences and Workshops

SFB/TRR219 Annual Meeting & summer school, Frankfurt, 08/2018
Poster and pitch presentation: "The role of angiotensin II derived peptides in cardiac hypertrophy"

International cardiorenal summer school, Frankfurt, 02/2019 (organized by SFB/TRR219 together with the European ITNs CaReSyAn & Intricare and the EU-funded consortium EURlipids)
Poster presentation: "The role of angiotensin II derived peptides in cardiomyopathy"

Aachen Conference on Cardiovascular Disease and Diabetes, Aachen, 11/2019
Poster presentation: "Inflammatory mediators linking CKD to adverse cardiac remodeling after"

International cardiorenal winter school, Frankfurt, 02/2020 (organized by SFB/TRR219 together with the European ITNs CaReSyAn & Intricare and the EU-funded consortium EURlipids)
Poster presentation: "Negative impact of CKD on cardioprotective properties?"

International cardiorenal winter school, online, 02/2021 (organized by SFB/TRR219 together with the European ITNs CaReSyAn, Intricare & Strategy-CKD and the EU-funded consortium EURlipids)
Poster meets slides: "Analyzing early effects of CKD on the heart: towards a mouse model?"

Joint meeting of 14 German SFB research consortia & graduate schools focusing on kidney, heart and vessels, Frankfurt, 05/2022
Poster presentation: "Pro-oxidative priming but maintained cardiac function in murine models of CKD"

"2. SFB/TRR219 workshop", 09/2018 organized by SFB/TRR219 in Aachen

"Redox Signaling in mammalian cells" workshop, 10/2018, organized by SFB/TRR219 in Homburg

"Statistics in Biomedicine" workshop, 06/2020, organized by SFB/TRR219 and the Marie Sklodowska-Curie ITN CaReSyAn

"Career and scientific workshop", 10/2020, KEPOS

"Graph Pad and statistics" workshop, 12/2020, STATCON

"Project Management in Science" workshop, "einszeit" management consulting & coaching, 03/2021

Acknowledgement

9.8. Acknowledgement

Attached publications

Attached publications

> **In addition to the work described in this thesis, I have contributed significantly to three publications.**

Publication 1:

Murine models of uremic cardiomyopathy:
a systematic review and meta-analysis

Josefin Soppert[*], Janina Frisch[*], **Julia Wirth**, Christian Hemmers, Peter Boor, Rafael Kramann, Sonja Vondenhoff, Julia Moellmann, Michael Lehrke, Mathias Hohl, Emiel P.C. van der Vorst, Christian Werner, Thimoteus Speer, Christoph Maack, Nikolaus Marx, Joachim Jankowski, Leticia Prates Roma and Heidi Noels

*Shared first authorship

Uremic cardiomyopathy is a prominent cardiac pathology in CKD patients characterized by cardiac hypertrophy and fibrosis as well as diastolic dysfunction. The systematic review aimed at summarizing mouse studies that investigated uremic cardiomyopathy, and compared "single hit" and "multifactorial hit" strategies. Hypertension, cardiac hypertrophy and fibrosis were found to be more prevalent in 129/Sv strains than in C57BL/6 mouse strains. Overall, the analysis revealed that genetic factors as well as additional cardiovascular risk factors promote the susceptibility to organ damage.

Publication 2:

Impact of uremic toxins on endothelial dysfunction
in chronic kidney disease: a systematic review

Eva Harlacher, **Julia Wollenhaupt**, Constance Baaten C.F.M.J.[*] and Heidi Noels[*]
*Shared last authorship

Since CKD patients have increased vascular inflammation, accelerated atherosclerosis and a high risk for thrombosis, the review provides a concise overview of literature on CKD-associated endothelial dysfunction and its underlying mechanism in a systematic approach. Uremic conditions or uremic toxin treatement of endothelial cells enhanced inflammation, oxidative stress, leucocyte migration and adhesion, cell death and a thrombotic phenotype, as shown by most studies. Targeting the underlying cellular pathways may provide new therapeutic approaches and thereby reduce the enhanced cardiovascular risk in CKD patients.

Publication 3:

Chemokine CCL9 is upregulated early in chronic kidney disease and counteracts kidney inflammation and fibrosis

Christian Hemmers[*], Corinna Schulte[*], **Julia Wollenhaupt**, Dickson W. L. Wong, Eva Harlacher, Setareh Orth-Alampour, Barbara Mara Klinkhammer, Stephan H. Schirmer, Michael Böhm, Nikolaus Marx, Thimoteus Speer, Peter Boor, Joachim Jankowski, Heidi Noels   *Shared first authorship*

CKD is accompanied by enhanced inflammation and fibrosis in the kidneys. Since chemokines coordinate leucocyte chemotaxis and tissue inflammation, we systemically profiled chemokines in early-stage CKD mice. CCL6 and CCL9 were identified as the most upregulated chemokines in the blood as well as in the kidney in two CKD mouse models. Treatment with those chemokines in a mouse model of early adenine-induced CKD almost abrogated macrophage and myeloid cell infiltration induced by CKD. Conversely, blockade of CCL9 increased the accumulation of monocytes and macrophages, increased serum urea and creatinine levels as well as collagen 1 and CCL2 levels in the kidney during CKD development. In summary, this study revealed increased CCL6 and CCL9 levels in early-stage CKD, with CCL9 blockade at the onset of CKD exacerbating kidney inflammation and fibrosis.

Publication 1:

Murine models of uremic cardiomyopathy:

a systematic review and meta-analysis

Josefin Soppert[1*], Janina Frisch[2*], Julia Wirth[1], Christian Hemmers[1], Peter Boor[3,4], Rafael Kramann[4], Sonja Vondenhoff[1], Julia Moellmann[5], Michael Lehrke[5], Mathias Hohl[6], Emiel P.C. van der Vorst[1,7,8,9,10], Christian Werner[6], Thimoteus Speer[11], Christoph Maack[12], Nikolaus Marx[5], Joachim Jankowski[1,7], Leticia Prates Roma[2] and Heidi Noels[1,13]

*Shared first authorship

[1]Institute for Molecular Cardiovascular Research (IMCAR), University Hospital RWTH Aachen, Aachen, Germany

[2]Department of Biophysics, Center for Human and Molecular Biology (ZHMB), Saarland University, Homburg, Germany

[3]Institute of Pathology, University Hospital RWTH Aachen, Aachen, Germany

[4]Department of Nephrology and Clinical Immunology, University Hospital RWTH Aachen, Aachen, Germany

[5]Department of Internal Medicine I, Cardiology, University Hospital RWTH Aachen, Germany

[6]Department of Internal Medicine III, Cardiology/Angiology, University of Homburg, Homburg/Saar, Germany

[7]Department of Pathology, Cardiovascular Research Institute Maastricht (CARIM), Maastricht University Medical Centre, Maastricht, the Netherlands

[8]Interdisciplinary Centre for Clinical Research (IZKF), RWTH Aachen University, Aachen, Germany
[9]Institute for Cardiovascular Prevention (IPEK), Ludwig-Maximilians-University Munich, Munich, Germany
[10]German Centre for Cardiovascular Research (DZHK), partner site Munich Heart Alliance, Munich, Germany
[11]Translational Cardio-Renal Medicine, Saarland University, Homburg/Saar, Germany

[12]Department of Translational Research, Comprehensive Heart Failure Center (CHFC), University Hospital Würzburg, Germany

[13]Department of Biochemistry, Cardiovascular Research Institute Maastricht (CARIM), Maastricht University, Maastricht, the Netherlands

Graphical abstract
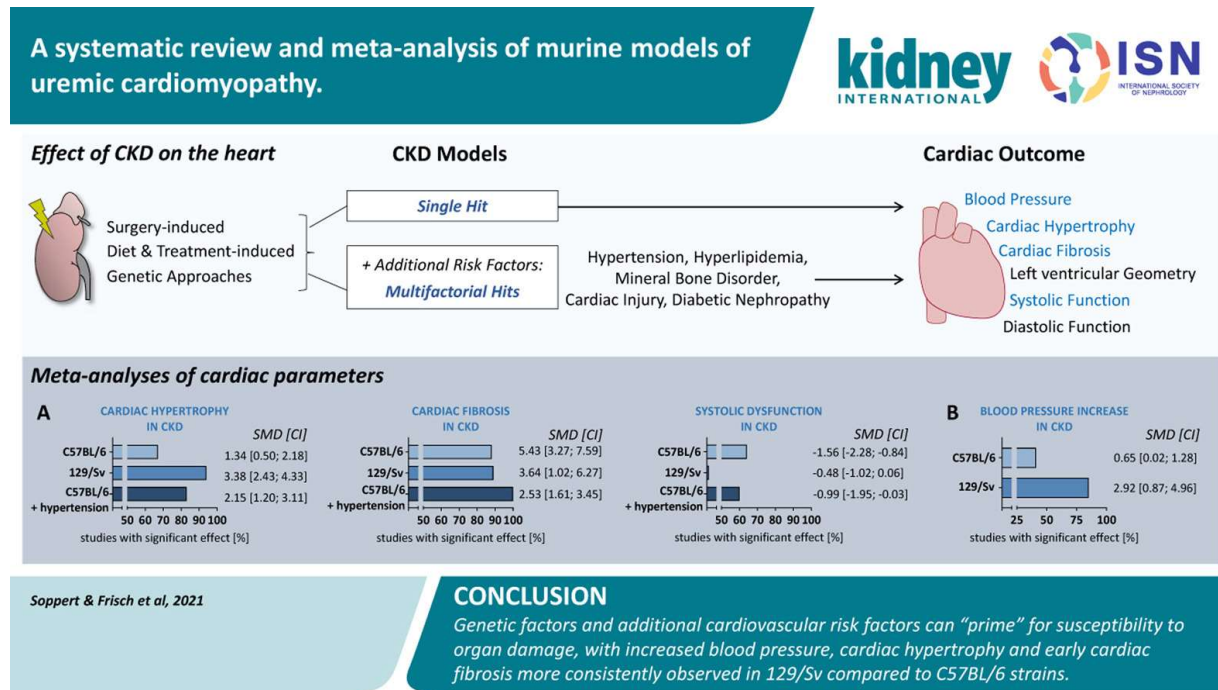
Abstract

Chronic kidney disease triggers the risk of developing uremic cardiomyopathy, e.g. characterized by cardiac hypertrophy, fibrosis and functional impairment. Animal studies are used to reveal the underlying pathological mechanism, though variable CKD models, mouse strains and readouts may reveal diverse results. Meta-analyses can support finding suitable animal models for future experimental studies on pathological kidney-heart crosstalk. This systematic review with meta-analysis summarizes mouse studies investigating uremic cardiomyopathy while comparing different mouse strains and "single hit" versus "multifactorial hit" strategies. Overall, 88 studies were included, with 52 studies being further analyzed via meta-analyses of CKD-induced cardiac hypertrophy, fibrosis and cardiac function. In C57BL/6 mice, CKD was associated with a mild increase in cardiac hypertrophy and fibrosis and a marginal systolic dysfunction. Studies revealed high variability in results, especially regarding hypertrophy and systolic function. Cardiac hypertrophy in CKD was more consistently observed in 129/Sv mice, which express two instead of one renin gene and more consistently develop increased blood pressure upon CKD induction. "Multifactorial hit" models more consistently induced cardiac hypertrophy and fibrosis compared to "single hit" kidney injury models. In summary, genetic factors and additional cardiovascular risk factors can

"prime" for susceptibility to organ damage, with increased blood pressure, cardiac hypertrophy and early cardiac fibrosis more consistently observed in 129/Sv compared to C57BL/6 strains.

Keywords: Chronic Kidney Disease, Uremic Cardiomyopathy, Cardiovascular Disease, Hypertrophy, Fibrosis, Cardiac dysfunction

Translational statement

CKD highly increases cardiovascular risk. This systematic review with meta-analyses summarizes the effect of CKD on cardiovascular remodeling and function in mice according to CKD-model, strain-dependency, CKD-duration and "single" vs. "multifactorial hits" relevant for the CKD patient. This reveals that genetic and/or multifactorial preconditioning increases susceptibility to organ damage, in line with multiple risk factors known to increase CKD and/or CVD risk in patients. Overall, this paper will support finding suitable animal models for future experimental studies on pathological kidney-heart crosstalk, which is highly needed to reveal underlying pathological mechanisms and therefore strategies for diagnosis and therapy of CKD-induced CVD.

Introduction

Chronic kidney disease (CKD) is an independent risk factor of cardiovascular disease (CVD), and almost half of the patients in CKD stage 4-5 die from cardiovascular events [1,2]. In addition to a high risk of atherosclerosis-related CVD [2], in particular patients with advanced CKD suffer from uremic cardiomyopathy [3], encompassing cardiac hypertrophy, fibrosis and inflammation [4]. This triggers, for example, reduced left ventricular function, cardiac arrhythmias and sudden cardiac death [5]. To support patient therapy, appropriate animal models are required to clarify the mechanisms underlying pathological kidney-cardiovascular crosstalk. Over the last years, an increasing number of animal studies have reported myocardial changes as a consequence of reduced kidney function [6], though using different CKD models, mouse strains and readouts.

The effect of the kidney on the heart has not only been studied in pure kidney injury models ("single hit strategies"). Patients with CKD often display additional cardiovascular risk factors such as hypertension, obesity, diabetes and dyslipidemia [4,7]. Also, especially in advanced CKD stages, patients suffer from hyperphosphatemia, a main challenge in CKD-mineral bone disorder [8,9]. Furthermore, CKD patients display reduced survival after myocardial injury [10]. Therefore, animal studies investigating CKD-

mediated effects on the heart include "multifactorial hit models" that combine models of kidney injury with models mimicking traditional cardiovascular risk factors (hypertension, hyperlipidemia, diabetes), CKD-specific cardiovascular risk factors (hyperphosphatemia) as well as myocardial infarction models.

We performed a systematic review and meta-analysis to analyze the impact of experimental animal models of CKD on the heart. Since mice are superior to rat models regarding the availability of genetic modifications to study molecular mechanisms, we focused on mouse models.

Methods

This systematic review with meta-analysis was registered in the PROSPERO database (CRD42020218123) and performed according to the PRISMA guidelines [11].

Study selection, data extraction and meta-analysis

'PubMed' and the 'Web of Science Core Collection' were searched for studies investigating parameters of cardiac function, structure and/or pathophysiology after inducing CKD in mouse models until February 14th, 2021 (**Figure 1**).
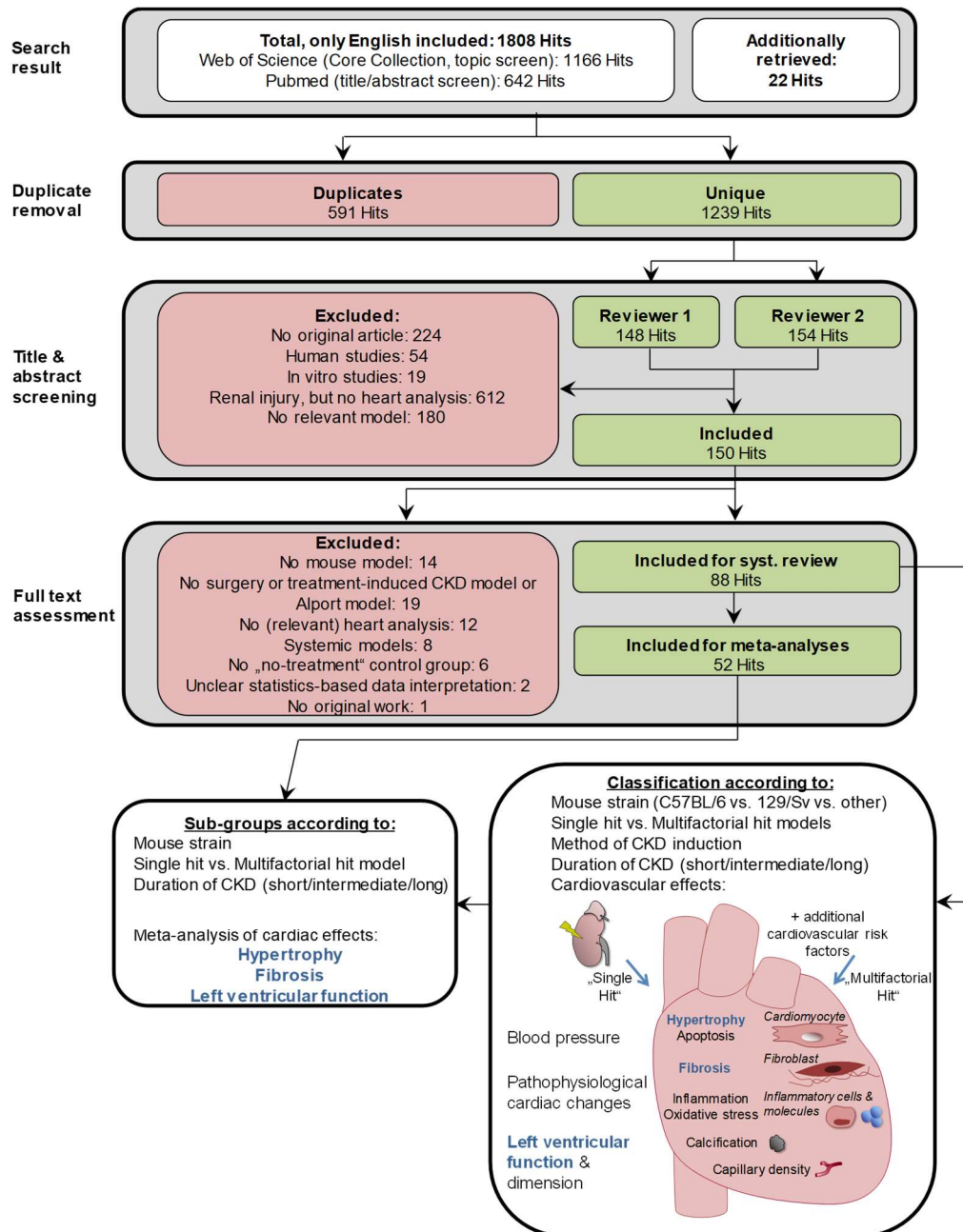
Figure 1: Flow chart of study inclusion and subsequent analyses used for systematic review and meta-analyses.

Meta-analyses were performed to analyze CKD-induced effects on cardiac hypertrophy, fibrosis and systolic function (**Suppl. Methods**). For studies included in these meta-analyses, also effects on kidney function (plasma/serum creatinine, urea or blood urea nitrogen) and blood pressure were summarized in meta-analyses and correlation analyses were performed in relation to effects on cardiac hypertrophy, fibrosis and/or systolic function, if possible. Details about the search strategy (**Table S1**), exclusion criteria (**Figure 1**), data extraction (parameter list: **Table S2;** tables summarizing effects on cardiac outcome parameters: **Tables S3-S6**) as well as quality assessment

(risk of bias: **Figure S1;** funnel plots: **Figure S2-S3)** and meta-analyses are described in **Suppl. Methods**.

Results

Study selection and data extraction

Literature screening identified 88 studies for inclusion in the systematic review (**Figure 1**). Most studies were performed in C57BL/6 mice (**Tables S3 and S5**), the mouse strain with the highest availability of genetic modifications for mechanistic analysis. 129/Sv variants were also frequently studied, whereas other strains were only scarcely analyzed (**Tables S4 and S6**).

   As depicted in **Figure 2**, all studies were categorized as (a) analyzing the direct effect of CKD on heart parameters ("single hit approach") (**Tables S3-S4**) or (b) analyzing the cardiac effect of kidney injury combined with additional cardiovascular risk factors ("multifactorial hit approach") to clarify the impact of comorbidities on the heart (**Tables S5-S6)**. Studies were classified according to the method of CKD induction as well as the duration of CKD, defined as short (0 – 4 weeks), intermediate (5 – 12 weeks) or long (≥13 weeks).
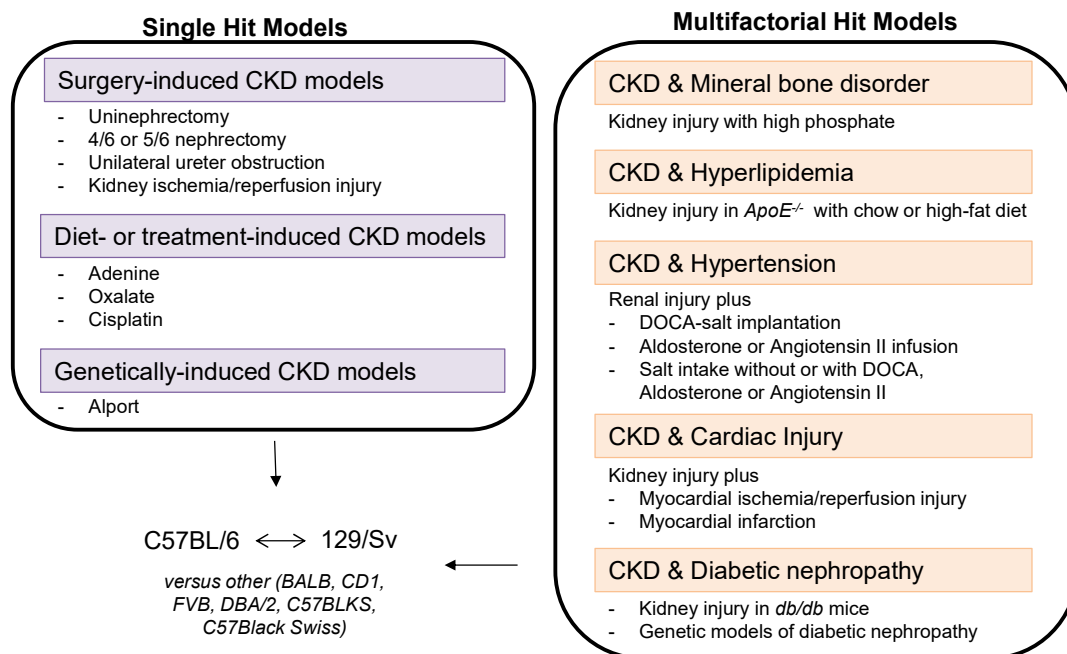
Figure 2: Overview of animal models for kidney-heart interaction analysis, with classification into single hit vs. multifactorial hit models.

Readouts for blood pressure, pathophysiological cardiac changes, left ventricular morphology and cardiac function were extracted into data tables (**Figure 1, Tables S3-S6**). Study results were described in detail for C57BL/6 and 129/Sv variants, with results from other strains available in **Suppl. Material**. Findings in the most commonly used models in C57BL/6 and 129/Sv were also summarized in **Figure 3 ("single hit approach")** and **Figure 4 ("multifactorial approach")**. Overall, 52 studies were included in a meta-analysis for CKD-induced effects on cardiac hypertrophy, fibrosis and/or systolic function. For models applying unilateral kidney surgery as a "single hit" or with a "second multifactorial hit", kidney parameters as readouts of confirmed kidney injury are summarized in **Table S7**. For "single hit" studies applying bilateral kidney surgery, a meta-analysis was performed for kidney function (serum/plasma creatinine and urea/blood urea nitrogen).

Method of CKD induction	5/6 Nephrectomy								Other surgery-induced, bilateral kidney damage			Diet- or treatment-induced CKD					Genetic approach: Alport		
	C57BL/6				129/Sv				C57BL/6		129/Sv	C57BL/6			129/Sv		C57BL/6		129/Sv
	4w	6-11w	12w	14-24w	4w	6-11w	12w	16w	Bilateral IRI 4w	Bilateral IRI 8w	Bilateral IRI 20w	Adenine 4-8w	Adenine 20w	Oxalate 3w	Adenine 8w	Cisplatin 20w	9-10w	19-21w	8-10w
Total nr of studies	6	15	9	3	5	5	2	1	1		1	3	1	1	1	1	1	3	4
Blood pressure	3/3	4/10	2/3	2/2	4/4	3/4	2/2	1/1	1		1	2/2		1/1			1/1	2/2	2/2
Pathophysiological cardiac changes																			
Hypertrophy	3/3	6/12	5/5	1/2	4/4	4/4	1/1	1/1	1/1			1/1	1/1			1/1	1/1	3/3	2/2
Fibrosis	3/4	2/3		1/1	3/3	3/4	1/1	1/1		1/1	1/1	1/1	1/1	1/1		1/1	1/1	1/2	
Inflammation/oxidative stress	3/3		7/7		1/1	1/1			1/1			1/1			1/1				
Calcification																			
Capillary density			1/1	3/3												1/1			
Apoptosis	2/2	1/1	3/3									1/1							
LV dimension																			
Systolic-Wall thickness	1/2	2/2	1/1														1/1	1/2	1/1
Systolic-LV diameter	4/4	3/3	1/1								1/1								
Diastolic-Wall thickness	3/3	1/5	1/1																1/1
Diastolic-LV diameter	3/3	2/7	6/6	1/1	1/1	2/2						1/1					1/1	1/1	1/1
LV function																			
Systolic LV volume	1/2		1/1																
Systolic function*	1/4	4/9	7/7		2/2	2/5			1/1		1/1	1/1	1/1				1/1	1/1	4/4
Diastolic LV volume		2/3		1/1								1/1							
Diastolic function*	2/2	6/7	4/4	1/1	1/1	4/4	1/1	1/1											1/1

* Other than LV volume

	Not assessed
	No significant effect
0-30% of studies	
30-70% of studies	Significant decrease
70-100% of studies	
0-30% of studies	
30-70% of studies	Significant increase
70-100% of studies	

Figure 3. Effect of chronic kidney model (CKD) models on blood pressure, pathophysiological cardiac changes, left ventricular (LV) dimension, and LV function in C57BL/6 versus 129/Sv strains. Significant effects are color-graded according to the percentage of studies reporting on the respective parameters (see legend). Refer to Supplementary Tables S3–S6 for detailed information about which study measured which cardiac parameters. When a study reported on multiple readouts for a specific parameter, the study was included as "changed" when at least 1 relevant readout was "changed." For LV function, "decreased" refers to cardiac dysfunction. Systolic dysfunction (other than altered systolic LV volume) may include decreased ejection fraction, fractional shortening, cardiac output, stroke volume, and/or dP/dt max. Diastolic dysfunction (other than altered diastolic LV volume) may include decreased E/A ratio, E/e′ ratio, E/A′ ratio, and/or dP/dt min as well as altered isovolumetric relaxation time and/or isovolumic relaxation time constant (τ). Studies examining the same mouse model at different time points were counted only once and were included as "differential effects" if these were observed at least on 1 time point. If different models were examined in 1 publication, each of these models was separately counted in this table. A, LV filling velocity, late or atrial filling (A-wave) measured by pulsed wave Doppler; A', LV filling velocity, late or atrial filling (A-wave) measured by tissue Doppler; dP/dT max, maximum rate of LV pressure change; dP/dt min, minimum rate of LV pressure change; E, LV filling velocity, early filling (E-wave) measured by pulsed wave Doppler; e', LV filling velocity, early filling (E-wave) measured by tissue Doppler; IRI, ischemia/reperfusion injury.

CKD & Hypertension — C57BL/6 and 129/Sv

Method of CKD induction	UNX + DOCA + salt		UNX + Aldo + salt		UNX/SNX + AngII ± salt		UNX/SNX + salt		UNX/SNX + salt + high protein	UNX + DOCA + salt	UNX + RAC	SNX + salt	Adenine + salt	CKD (various) + High phosphate	CKD (various) + High phosphate
(time)	2w	6w	2-4w	6w	4w	6w	8w	52w	8w	8w	9w	2-4w	8w	9-12w	16-20w
Total nr of studies	1	1	2	1	1	2	2	1	3	1	1	2	1	3	3
Blood pressure	1/1	1/1	2/2	1/1	1/1	2/2	1/1	1/1	2/2	1/1		2/2	1/1	2/2	1/1
Pathophysiological cardiac changes															
Hypertrophy	1/1	1/1	2/2	1/1	1/1	2/2	2/2	1/1	1/2	1/1			1/1	1/1	3/3
Fibrosis	1/1		2/2	1/1	2/2	2/2	1/3	1/1	3/3			1/1	1/1		3/3
Inflammation/oxidative stress	1/1	1/1		1/1			1/2					1/1	1/1		1/1
Calcification														2/2	
Capillary density															
Apoptosis									1/1						
LV dimension															
Systolic-Wall thickness							1/1		1/2						
Systolic-LV diameter							1/1		3/3						
Diastolic-Wall thickness	1/1					2/2	1/1		1/2					1/1	
Diastolic-LV diameter	1/1					2/2	1/1		1/2					1/1	
LV function															
Systolic LV volume							1/1		3/3						
Systolic function*	1/1	1/1				1/2	1/1		3/3					1/1	
Diastolic LV volume		1/1					1/1		2/2						
Diastolic function*	1/1						1/1	1/1							

* Other than LV volume

CKD & Hyperlipidemia — C57BL/6; CKD & Cardiac injury — C57BL/6

Method of CKD induction	UNX in ApoE-/-	SNX in ApoE-/-	SNX in ApoE-/-	SNX + HFD in ApoE-/-	SNX + HFD + Fructose in WT	Adenine in ApoE-/-	SNX before MIR	SNX + salt before MI
(time)	12w	6-10w	36w	11w	4w	14w	4w	8w
Total nr of studies	1	2	1	1	1	1	2	2
Blood pressure	1/1	2/2	1/1		1/1			
Pathophysiological cardiac changes								
Hypertrophy	1/1	2/2	1/1		1/1	1/1		1/2
Fibrosis	1/1		1/1		1/1			2/2
Inflammation/oxidative stress	1/1				1/1			1/1
Calcification								
Capillary density	1/1							
Apoptosis			1/1				2/2	
LV dimension								
Systolic-Wall thickness								
Systolic-LV diameter			1/1	1/1	1/1		2/2	2/2
Diastolic-Wall thickness			1/1		1/1			2/2
Diastolic-LV diameter			1/1				2/2	2/2
LV function								
Systolic LV volume								
Systolic function*	1/1		1/1	1/1	1/1		2/2	2/2
Diastolic LV volume								
Diastolic function*		2/2	1/1		1/1			1/1

* Other than LV volume

Legend

	Not assessed
	No significant effect
0-30% of studies / 30-70% of studies / 70-100% of studies	Significant decrease
0-30% of studies / 30-70% of studies / 70-100% of studies	Significant increase

Figure 4. Effect of chronic kidney disease (CKD) in combination with typical cardiovascular risk factors in CKD on blood pressure, pathophysiological cardiac changes, left ventricular (LV) dimension, and LV function in C57BL/6 versus 129/Sv strains. Significant effects are color-graded according to the percentage of studies reporting on the respective parameters (see legend). Refer to Supplementary Tables S3–S6 for detailed information about which study measured which cardiac parameters. When a study reported on multiple readouts for a specific parameter, the study was included as "changed" when at least 1 relevant readout was "changed." For LV function, "decreased" refers to cardiac dysfunction. Systolic dysfunction (other than altered systolic LV volume) may include decreased ejection fraction, fractional shortening, cardiac output, stroke volume, and/or dP/dt max. Diastolic dysfunction (other than altered diastolic LV volume) may include decreased E/A ratio, E/e′ ratio, E/A′ ratio, and/or dP/dt min as well as altered isovolumetric relaxation time and/or isovolumic relaxation time constant (τ). Studies examining the same mouse model at different time points were counted only once and were included as "differential effects" if these were observed at least on 1 time point. If different models were examined in 1 publication, each of these models was separately counted. A, LV filling velocity, late or atrial filling (A-wave) measured by pulsed wave Doppler; A', LV filling velocity, late or atrial filling (A-wave) measured by tissue Doppler; Aldo, aldosterone; AngII, angiotensin II; DOCA, deoxycorticosterone acetate; dP/dT max, maximum rate of LV pressure change; dP/dt min, minimum rate of LV pressure change; E, LV filling velocity, early filling (E-wave) measured by pulsed wave Doppler; e', LV filling velocity, early filling (E-wave) measured by tissue Doppler; HFD, high-fat diet; MI, myocardial infarction; MI/RI, myocardial ischemia/reperfusion injury; RAC, renal artery clipping; SNX, 5/6 nephrectomy; UNX, uninephrectomy; WT, wild type

I. Single Hit Strategies

Only a few studies reported on cardiac hypertrophy or fibrosis, but no cardiac dysfunction, in mice displaying signs of kidney damage in response to unilateral kidney surgery (**Tables S3-S4; Table S7**) [12-15]. In contrast, most studies analyzed cardiac effects after

160

applying bilateral kidney damage through surgery, specific food supplementation or genetic modification (**Figure 3, Tables S3-S4**).

Bilateral surgery-induced CKD

<u>C57BL/6 mice (**Figure 3, Table S3**)</u>

5/6 nephrectomy models: Four weeks after subtotal (5/6) nephrectomy (SNX), a hypertrophic, fibrotic and inflammatory response was observed in the myocardium in ≥75% of studies. Furthermore, mild diastolic cardiac dysfunction was detected, whereas systolic function or left ventricular dimensions were only rarely affected [16-21]. 6-11 weeks after nephrectomy [22-36], increased blood pressure, cardiac hypertrophy and systolic dysfunction were reported in only 40-50% of studies, while cardiac fibrosis was identified in two out of three studies. Although diastolic dysfunction was observed in 85% of studies, left ventricular diameter was only rarely affected. Analysis 12 weeks after SNX [34,37-44] revealed more consistent cardiac morphological changes in terms of hypertrophy, fibrosis, inflammation and oxidative stress. Furthermore, these studies consistently reported on increased left ventricular diameter, diastolic as well as systolic dysfunction. Only three studies performed a cardiac analysis in long experimental set-ups beyond 12 weeks [17,25,45]. Cardiac hypertrophy and diastolic dysfunction were reported 14 weeks after SNX [25], although cardiac fibrosis could not be detected 16 weeks post-surgery [17]. At 24 weeks post-surgery, systolic dysfunction was reported, though without altered left ventricular dimensions or induction of cardiac hypertrophy [45].

Further bilateral kidney surgery models: Bilateral ischemia-reperfusion injury induced cardiac hypertrophy and fibrosis after 4-8 weeks, though without effect on systolic function [46].

Meta-analyses: When using heart weight as an outcome parameter for cardiac hypertrophy, a meta-analysis for bilateral surgery-induced "single hit" approaches in C57BL/6 mice revealed a mild increase in hypertrophy (**Figure 5A**; SMD=1.34; 95% CI [0.50; 2.18], n=24 studies, $P = 0.0031$). However, study heterogeneity was very high (I^2=82%): almost half of the studies could not detect a significant induction of cardiac hypertrophy after 6-11 weeks or beyond 14 weeks of study. Subgroup analysis based on study duration did not reveal a time-dependent increase in cardiac hypertrophy (1-4 weeks: 95% CI [-1.03; 9.23]); 5-8 weeks: 95% CI [-0.01; 1.67]); 9-13 weeks: 95% CI [-0.02; 2.09] and ≥14 weeks: 95% CI [-7.89; 8.70]). No significant overall effect was observed on cardiomyocyte size among 6-12 weeks studies (**Figure S4A**; SMD=2.85;

95% CI [-2.07; 7.77]; *P*=0.1963), with low study number and high heterogeneity (n=6 studies; I² = 91%) impeding conclusions on time-dependent effects.

a Inclusion of 24 data sets derived from 19 different studies

Study	Model	Duration	Parameters	CKD – Total	Ctrl – Total	SMD	95% CI	Weight
CKD_Interval = 1 to 4 weeks								
Liu *et al.*, 2016[18]	SNX	4	LV mass/BW	21	18	1.77	[1.02; 2.52]	4.5%
Pang *et al.*, 2018[46]	bilateral IRI	4	LV mass	6	5	4.70	[1.98; 7.42]	3.2%
Sodhi *et al.*, 2020[19]	SNX	4	HW	11	8	2.83	[1.47; 4.19]	4.2%
Sodhi *et al.*, 2020[19]	SNX (4/6)	4	HW	10	8	1.30	[0.26; 2.35]	4.3%
Wang *et al.* 2017[21]	SNX	4	HW/BW	8	8	12.26	[7.27; 17.25]	1.8%
Random effects model				56	47	4.10	[−1.03; 9.23]	17.9%
Heterogeneity: I² = 83%, τ² = 15.6057, P < 0.01								
CKD_Interval = 5 to 8 weeks								
Navarro–García *et al.*, 2020[27]	SNX	6	HW	20	16	−0.41	[−1.07; 0.26]	4.5%
Gil–Fernández *et al.*, 2020 (1.Exp)[36]	SNX	6	HW	8	10	−0.98	[−1.97; 0.02]	4.4%
Gil–Fernández *et al.*, 2020 (2.Exp)[36]	SNX	6	HW	8	9	−0.84	[−1.84; 0.17]	4.4%
Maizel *et al.*, 2009[26]	SNX	6	LV mass	21	17	1.25	[0.54; 1.95]	4.5%
Maizel *et al.*, 2013[25]	SNX	6	LV mass	32	28	1.81	[1.21; 2.42]	4.5%
Verkaik *et al.*, 2018 (a)[32]	SNX	6	HW/TL	16	11	0.45	[−0.33; 1.23]	4.5%
Verkaik *et al.*, 2018 (b)[33]	SNX	6	HW/TL	6	6	0.23	[−0.90; 1.37]	4.3%
Chen *et al.*, 2017[22]	SNX	8	HW	8	5	1.46	[0.15; 2.76]	4.2%
Han *et al.*, 2015[23]	SNX	8	HW/BW	8	8	1.35	[0.23; 2.47]	4.3%
Lin *et al.*, 2015[24]	SNX	8	HW/BW	8	8	2.59	[1.17; 4.02]	4.1%
Maizel *et al.*, 2013[25]	SNX	8	LV mass	16	14	2.50	[1.51; 3.49]	4.4%
Random effects model				151	132	0.83	[−0.01; 1.67]	47.9%
Heterogeneity: I² = 85%, τ² = 1.3184, P < 0.01								
CKD_Interval = 9 to 13 weeks								
Maizel *et al.*, 2009[26]	SNX	10	LV mass	7	5	2.21	[0.64; 3.79]	4.0%
O'Sullivan *et al.*, 2019[28]	SNX	10	HW/TL	6	3	−0.34	[−1.74; 1.06]	4.1%
Hamzaoui *et al.*, 2020[35]	SNX	11	HW/TL	9	9	0.22	[−0.71; 1.14]	4.4%
Li *et al.*, 2020[41]	SNX	12	LV weight	6	6	1.30	[0.01; 2.60]	4.2%
Ogino *et al.*, 2010[44]	SNX	12	HW	8	6	2.25	[0.80; 3.69]	4.1%
Yoshida *et al.* 2019[34]	SNX	12	HW/BW	10	10	0.98	[0.04; 1.92]	4.4%
Random effects model				46	39	1.04	[−0.02; 2.09]	25.2%
Heterogeneity: I² = 56%, τ² = 0.7045, P = 0.04								
CKD_Interval = 14 weeks or more								
Maizel *et al.*, 2013[25]	SNX	14	LV mass	11	14	1.07	[0.22; 1.93]	4.4%
Ke *et al.*, 2020[45]	SNX	24	LV mass	15	11	−0.23	[−1.01; 0.55]	4.5%
Random effects model				26	25	0.41	[−7.89; 8.70]	8.9%
Heterogeneity: I² = 80%, τ² = 0.6058, P = 0.03								
Random effects model, P = 0.0031				279	243	1.34	[0.50; 2.18]	100.0%
Prediction interval							[−2.99; 5.67]	
Heterogeneity: I² = 82%, τ² = 4.1885, P < 0.01								
Residual heterogeneity: I² = 82%, P < 0.01								

Standardized mean difference. −5 0 5 10 15 20. No effect Favors hypertrophy

b Inclusion of 17 data sets derived from 7 different studies

Study	Strain	Model	Duration	Parameters	CKD – Total	Ctrl – Total	SMD	95% CI	Weight
CKD_Interval = 1 to 4 weeks									
Winterberg *et al.*, 2016[48]	129X1/SvJ mice	SNX	2	LV mass	14	11	1.83	[0.87; 2.79]	7.0%
Elkareh *et al*, 2009[50]	B6, 129SvEv		4	HW/BW	5	5	3.49	[1.16; 5.81]	5.1%
Siedlecki *et al.*, 2009[51]	129/SvJ	SNX	4	LV mass	15	12	3.98	[2.61; 5.36]	6.5%
Winterberg *et al.*, 2016[48]	129X1/SvJ mice	SNX	4	LV mass	14	11	3.93	[2.51; 5.36]	6.4%
Xie *et al.*, 2015 (1.Exp.)[49]	129/S1SvlmJ	SNX	4	HW	5	5	2.63	[0.70; 4.57]	5.6%
Xie *et al.*, 2015 (2.Exp.)[49]	129/S1SvlmJ	SNX	4	HW/BW	6	6	4.60	[2.09; 7.11]	4.8%
Xie *et al.*, 2015 (3.Exp.)[49]	129/S1SvlmJ	SNX	4	HW/BW	7	7	7.07	[3.81; 10.34]	3.8%
Random effects model					66	57	3.63	[2.25; 5.01]	39.2%
Heterogeneity: I² = 65%, τ² = 1.6400, P < 0.01									
CKD_Interval = 5 to 8 weeks									
O'Sullivan *et al.*, 2019[28]	129S2/SV	SNX	6	LV mass	10	8	0.58	[−0.37; 1.54]	7.0%
Winterberg *et al.*, 2016[48]	129X1/SvJ mice	SNX	6	LV mass	14	11	3.91	[2.49; 5.34]	6.4%
Siedlecki *et al.*, 2009[51]	129/SvJ	SNX	8	LV mass	8	7	5.67	[3.10; 8.24]	4.7%
Winterberg *et al.*, 2016[48]	129X1/SvJ mice	SNX	8	LV mass	14	11	4.53	[2.95; 6.11]	6.2%
Random effects model					46	37	3.51	[−0.01; 7.02]	24.3%
Heterogeneity: I² = 90%, τ² = 4.0691, P < 0.01									
CKD_Interval = 9 to 13 weeks									
O'Sullivan *et al.*, 2019 (1.Exp.)[28]	129S2/SV	SNX	10	LV mass	10	8	1.09	[0.08; 2.10]	7.0%
O'Sullivan *et al.*, 2019 (2.Exp.)[28]	129S2/SV	SNX	10	HW/TL	11	7	1.51	[0.41; 2.61]	6.8%
Hamzaoui *et al.*, 2020[35]	129/Sv	SNX	11	HW/TL	8	8	2.09	[0.80; 3.37]	6.6%
Winterberg *et al.*, 2016[48]	129X1/SvJ mice	SNX	12	LV mass	14	11	3.99	[2.55; 5.43]	6.4%
Random effects model					43	34	2.10	[0.11; 4.09]	26.8%
Heterogeneity: I² = 73%, τ² = 1.1991, P = 0.01									
CKD_Interval = 14 weeks or more									
Winterberg *et al.*, 2016[48]	129X1/SvJ mice	SNX	16	LV mass	14	11	7.25	[4.92; 9.58]	5.1%
Hu *et al.*, 2017[53]	129/SvJ	bilateral IRI	20	HW/BW	4	4	3.26	[0.62; 5.89]	4.6%
Random effects model					18	15	5.31	[−20.06; 30.67]	9.7%
Heterogeneity: I² = 80%, τ² = 5.6848, P = 0.03									
Random effects model, P < 0.0001					173	143	3.38	[2.43; 4.33]	100.0%
Prediction interval								[−0.30; 7.06]	
Heterogeneity: I² = 81%, τ² = 2.7792, P < 0.01									
Residual heterogeneity: I² = 80%, P < 0.01									

Standardized mean difference. −20 −10 0 10 20 30. No effect Favors hypertrophy

Figure 5. Meta-analysis for cardiac hypertrophy. A) in C57BL/6 with surgery-induced CKD. **B)** in 129/Sv with surgery-induced CKD. **C)** in C57BL/6 with CKD and hypertension-inducing strategies.

Cardiac fibrosis was significantly induced (**Figure 6A**; SMD=5.43; 95% CI [3.27; 7.59]; n=16; *P*<0.0001; I²=83%). Time-dependent subgroup analysis revealed fibrosis mainly in intermediate study setups (8 weeks: 95% CI [1.88; 5.51], n=3; 11-13 weeks: 95% CI [3.47; 10.95], n=9).

a

Inclusion of 16 data sets derived from 14 different studies

Study	Model	Duration	Parameters	CKD – Total	Ctrl – Total	Standardized mean difference	SMD	95% CI	Weight
CKD_Interval = 1 to 4 weeks									
Leelahavanichkul et al., 2010[17]	SNX	4	IHC (Masson's)	4	4		1.42	[−0.28; 3.11]	6.9%
Sodhi et al., 2020[19]	SNX	4	IHC (Sirius)	11	8		4.32	[2.53; 6.11]	6.9%
Wang et al., 2017[21]	SNX	4	WB (Col I)	11	11		7.41	[4.85; 9.96]	6.5%
Random effects model				26	23		4.27	[−3.10; 11.65]	20.3%
Heterogeneity: $I^2 = 87\%$, $\tau^2 = 7.4473$, $P < 0.01$									
CKD_Interval = 5 to 8 weeks									
Han et al., 2015[23]	SNX	8	IHC (Picro Sirius)	4	4		3.95	[0.90; 7.00]	6.3%
Lin et al., 2015[24]	SNX	8	IHC (Sirius)	8	8		4.53	[2.47; 6.58]	6.8%
Pang et al., 2018[46]	bilateral IRI	8	IHC (Sirius)	10	10		3.19	[1.78; 4.60]	7.0%
Random effects model				22	22		3.69	[1.88; 5.51]	20.1%
Heterogeneity: $I^2 = 0\%$, $\tau^2 = 0.1240$, $P = 0.56$									
CKD_Interval = 9 to 13 weeks									
Hamzaoui et al., 2020[35]	SNX	11	IHC (Sirius)	7	7		1.32	[0.13; 2.52]	7.1%
Li et al., 2020[41]	SNX	12	IHC (Masson's)	6	6		3.16	[1.25; 5.08]	6.8%
Li et al., 2007[42]	SNX	12	IHC (Masson's)	6	6		13.40	[6.76; 20.04]	4.1%
Li et al., 2009[43]	SNX	12	IHC (Masson's)	10	10		4.04	[2.39; 5.69]	6.9%
Ogino et al., 2010[44]	SNX	12	IHC (Sirius)	8	6		6.58	[3.52; 9.65]	6.3%
Yoshida et al., 2019[34]	SNX	12	IHC (Masson's)	10	10		13.97	[9.06; 18.88]	5.1%
Ding et al., 2016[39]	SNX	12	IHC (Masson's)	6	6		15.57	[7.89; 23.26]	3.6%
Yang et al., 2020 (b) (1.Exp.)[40]	SNX	13	IHC (Col I)	8	8		6.53	[3.74; 9.31]	6.4%
Yang et al., 2020 (b) (2.Exp.)[40]	SNX	13	IHC (Col I)	8	8		7.17	[4.14; 10.19]	6.3%
Random effects model				69	67		7.21	[3.47; 10.95]	52.7%
Heterogeneity: $I^2 = 87\%$, $\tau^2 = 20.5458$, $P < 0.01$									
CKD_Interval = 14 weeks or more									
Leelahavanichkul et al., 2010[17]	SNX	16	IHC (Masson's)	4	4		1.06	[−0.51; 2.62]	7.0%
Random effects model				4	4		1.06	[−0.51; 2.62]	7.0%
Heterogeneity: not applicable									
Random effects model, $P < 0.0001$				121	116		5.43	[3.27; 7.59]	100.0%
Prediction interval								[−3.19; 14.05]	
Heterogeneity: $I^2 = 83\%$, $\tau^2 = 15.1262$, $P < 0.01$									
Residual heterogeneity: $I^2 = 85\%$, $P < 0.01$									

−5 0 5 10 15 20 25
No effect   Favors fibrosis

b

Inclusion of 9 data sets derived from 8 different studies

Study	Strain	Model	Duration	Parameters	CKD – Total	Ctrl – Total	Standardized mean difference	SMD	95% CI	Weight
CKD_Interval = 1 to 4 weeks										
Elkareh et al., 2009[50]	B6, 129SvEv	SNX	4	IHC (Masson's)	8	6		4.43	[2.22; 6.63]	12.5%
Xie et al., 2015 (1.Exp.)[49]	129/S1SvlmJ	SNX	4	IHC (Masson's)	6	6		1.68	[0.28; 3.07]	13.2%
Xie et al., 2015 (2.Exp.)[49]	129/S1SvlmJ	SNX	4	IHC (Masson's)	7	7		3.06	[1.36; 4.75]	13.0%
Sakata et al., 2017[47]	129SvJJmsSlc	SNX	4	IHC (Sirius)	6	6		3.01	[1.15; 4.86]	12.8%
Random effects model					27	25		2.87	[1.11; 4.64]	51.5%
Heterogeneity: $I^2 = 36\%$, $\tau^2 = 0.6655$, $P = 0.20$										
CKD_Interval = 5 to 8 weeks										
Siedlecki et al., 2009[51]	129/SvJ	SNX	8	IHC (Masson's)	4	4		14.50	[4.43; 24.57]	4.2%
Random effects model					4	4		14.50	[4.43; 24.57]	4.2%
Heterogeneity: not applicable										
CKD_Interval = 9 to 13 weeks										
O'Sullivan et al., 2019[28]	129S2/Sv	SNX	10	IHC (Sirius)	8	7		0.49	[−0.54; 1.53]	13.5%
Hamzaoui et al., 2020[35]	129/Sv	SNX	11	IHC (Sirius)	7	7		2.02	[0.65; 3.39]	13.3%
Leelahavanichkul et al., 2010[17]	129S1/SvlmJ/Cr	SNX	12	IHC (Masson's)	4	4		4.27	[1.02; 7.52]	11.2%
Random effects model					19	18		1.85	[−2.43; 6.14]	38.0%
Heterogeneity: $I^2 = 70\%$, $\tau^2 = 2.2092$, $P = 0.04$										
CKD_Interval = 14 weeks or more										
Hu et al., 2017[53]	129/Sv	bilateral IRI	20	IHC (Masson's)	4	4		10.52	[3.15; 17.89]	6.3%
Random effects model					4	4		10.52	[3.15; 17.89]	6.3%
Heterogeneity: not applicable										
Random effects model, $P = 0.0127$					54	51		3.64	[1.02; 6.27]	100.0%
Prediction interval									[−4.87; 12.16]	
Heterogeneity: $I^2 = 72\%$, $\tau^2 = 11.6746$, $P < 0.01$										
Residual heterogeneity: $I^2 = 56\%$, $P = 0.05$										

−5 0 5 10 15 20 25
No effect   Favors fibrosis

c

Inclusion of 10 data sets derived from 9 different studies

Study	Model	Duration	Parameters	CKD – Total	Ctrl – Total	Standardized mean difference	SMD	95% CI	Weight
CKD_Interval = 1 to 4 weeks									
Araos *et al.*, 2019[69]	UNX + Aldo + Salt	2	IHC (Masson's)	5	5		1.93	[0.28; 3.58]	10.8%
Ahadzadeh *et al.*, 2018[74]	UNX + AngII + Salt	4	IHC (Masson's)	11	4		1.37	[0.09; 2.65]	12.5%
Leelahavanichkul *et al.*, 2010[17]	SNX + AngII	4	IHC (Masson's)	4	4		6.44	[1.80; 11.09]	3.2%
Tarjus *et al.*, 2015[71]	UNX + Aldo + Salt	4	IHC (Sirius)	6	6		1.68	[0.28; 3.07]	11.9%
Random effects model				26	19		2.22	[–0.65; 5.10]	38.3%
Heterogeneity: $I^2 = 30\%$, $\tau^2 = 2.9061$, $P = 0.23$									
CKD_Interval = 5 to 8 weeks									
Buonafine *et al.*, 2018[70]	UNX + Aldo + Salt	6	IHC (Sirius)	10	10		1.53	[0.51; 2.56]	13.6%
Tsukamoto *et al.*, 2013[75]	UNX + AngII	6	IHC (Sirius)	10	12		2.47	[1.30; 3.63]	13.0%
Tsukamoto *et al.*, 2013[75]	UNX + AngII + Salt	6	IHC (Sirius)	11	12		2.48	[1.34; 3.61]	13.1%
Wang *et al.*, 2020[79]	SNX + Salt	8	IHC (Masson's)	6	6		4.69	[2.13; 7.24]	7.2%
Wang *et al.*, 2019[81]	SNX + Salt + high protein	8	IHC (Masson's)	6	6		3.70	[1.57; 5.83]	8.7%
Kuma *et al.*, 2020[80]	SNX + NaCl + high protein	8	IHC (Masson's)	4	4		3.90	[0.88; 6.92]	5.9%
Random effects model				47	50		2.73	[1.59; 3.88]	61.7%
Heterogeneity: $I^2 = 39\%$, $\tau^2 = 0.7311$, $P = 0.14$									
Random effects model, $P = 0.0002$				73	69		2.53	[1.61; 3.45]	100.0%
Prediction Interval								[–0.30; 5.36]	
Heterogeneity: $I^2 = 37\%$, $\tau^2 = 1.3389$, $P = 0.11$									
Residual heterogeneity: $I^2 = 36\%$, $P = 0.13$									

−5 0 5 10
No effect Favors fibrosis

Figure 6: Meta-analysis for cardiac fibrosis. A) in C57BL/6 with surgery-induced CKD. **B)** in 129/Sv with surgery-induced CKD. **C)** in C57BL/6 with CKD and hypertension-inducing strategies.

Systolic function in terms of ejection fraction or fractional shortening was mildly decreased (**Figure 7A**; SMD=-1.56; 95% CI [-2.28; -0.84]; n=22; *P* =0.0002), although with high study heterogeneity (I²=80%) and ~30-40% of studies not detecting significant effects. Subgroup analysis revealed a stronger effect for 9-12 weeks study setups (95% CI [-4.93; -0.44]) compared to shorter time points (4 weeks: 95% CI [-1.48; -0.05]; 6-8 weeks: 95% CI [-2.08; -0.34]), with 6 of 7 studies showing significant effects, although this also with overall the highest study heterogeneity (90%). Analysis of dP/dt max revealed a reduction in systolic function after 12 weeks, though with data derived from only three studies (**Figure S5**; SMD=-6.60; 95% CI [-12.66; -0.53]). Conclusions on long-term effects remain elusive, since only one long-term study beyond 12 weeks was available.

a

Inclusion of 22 data sets derived from 18 different studies

Study	Model	Duration	Parameters	CKD – Total	Ctrl – Total	Standardized mean difference	SMD	95% CI	Weight
CKD_Interval = 1 to 4 weeks									
Liu et al., 2016[18]	SNX	4	FS	21	18		−0.07	[−0.70; 0.56]	5.1%
Pang et al., 2018[46]	bilateral IRI	4	FS	6	5		−0.79	[−2.05; 0.46]	4.5%
Song et al., 2014[20]	SNX	4	FS	6	6		−1.40	[−2.72; −0.08]	4.5%
Sodhi et al., 2020[19]	SNX	4	FS	11	8		−1.19	[−2.20; −0.19]	4.8%
Sodhi et al., 2020[19]	SNX (4/6)	4	FS	10	8		−1.04	[−2.04; −0.03]	4.8%
Random effects model				54	45		−0.76	[−1.48; −0.05]	23.8%
Heterogeneity: $I^2 = 36\%$, $\tau^2 = 0.1417$, $P = 0.18$									
CKD_Interval = 5 to 8 weeks									
Verkaik et al., 2018 (b)[33]	SNX	6	EF	7	6		−0.26	[−1.36; 0.83]	4.7%
Navarro–García et al., 2020[27]	SNX	6	EF	5	5		−1.86	[−3.48; −0.24]	4.1%
Chen et al., 2017 (1.Exp.)[22]	SNX	8	FS	23	11		−1.88	[−2.74; −1.02]	4.9%
Chen et al., 2017 (2. Exp)[22]	SNX	8	FS	7	6		−2.68	[−4.33; −1.03]	4.1%
Chen et al., 2017 (3.Exp.)[22]	SNX	8	FS	7	6		−3.17	[−5.00; −1.35]	3.9%
Han et al., 2015[23]	SNX	8	FS	6	6		−1.05	[−2.29; 0.19]	4.6%
Lin et al., 2015[24]	SNX	8	EF	6	6		0.57	[−0.60; 1.73]	4.6%
Uchida et al., 2014[31]	SNX	8	FS	10	10		−0.72	[−1.63; 0.19]	4.9%
Yoshida et al., 2019[34]	SNX	8	EF	10	10		−0.87	[−1.80; 0.06]	4.9%
Random effects model				81	66		−1.21	[−2.08; −0.34]	40.8%
Heterogeneity: $I^2 = 66\%$, $\tau^2 = 0.9771$, $P < 0.01$									
CKD_Interval = 9 to 13 weeks									
Thomsen et al., 2018[30]	SNX	9	FS	6	6		−0.05	[−1.19; 1.08]	4.7%
Hamzaoui et al., 2020[35]	SNX	11	FS	8	8		−1.13	[−2.21; −0.06]	4.7%
Ding et al., 2016[39]	SNX	12	FS	6	6		−4.65	[−7.18; −2.11]	3.1%
Jin et al., 2013[38]	SNX	12	FS	18	18		−5.51	[−7.01; −4.01]	4.3%
Li et al., 2007[42]	SNX	12	FS	12	10		−1.38	[−2.33; −0.43]	4.9%
Li et al., 2009[43]	SNX	12	FS	15	15		−5.84	[−7.58; −4.10]	4.0%
Yoshida et al., 2019[34]	SNX	12	EF	10	10		−1.01	[−1.95; −0.07]	4.9%
Random effects model				75	73		−2.68	[−4.93; −0.44]	30.5%
Heterogeneity: $I^2 = 90\%$, $\tau^2 = 5.2933$, $P < 0.01$									
CKD_Interval = 14 weeks or more									
Ke et al., 2020[45]	SNX	24	FS	15	11		−0.96	[−1.79; −0.13]	5.0%
Random effects model				15	11		−0.96	[−1.79; −0.13]	5.0%
Heterogeneity: not applicable									
Random effects model, $P = 0.0002$				**225**	**195**		**−1.56**	**[−2.28; −0.84]**	**100.0%**
Prediction interval								**[−4.83; 1.71]**	
Heterogeneity: $I^2 = 80\%$, $\tau^2 = 2.3358$, $P < 0.01$									
Residual heterogeneity: $I^2 = 81\%$, $P < 0.01$									

−10 −8 −6 −4 −2 0 2 4
Decreased function ← → Improved function

b

Inclusion of 9 data sets derived from 7 different studies

Study	Model	Duration	Parameters	CKD – Total	Ctrl – Total	Standardized mean difference	SMD	95% CI	Weight
CKD_Interval = 1 to 4 weeks									
Siedlecki et al., 2009[51]	SNX	4	FS	15	12		−0.23	[−0.99; 0.53]	15.1%
Xie et al., 2015[49]	SNX	4	EF	5	5		−0.35	[−1.61; 0.90]	9.7%
Random effects model				20	17		−0.27	[−0.95; 0.42]	24.8%
Heterogeneity: $I^2 = 0\%$, $\tau^2 = <0.0001$, $P = 0.87$									
CKD_Interval = 5 to 8 weeks									
O'Sullivan et al., 2019[28]	SNX	6	FS	10	8		−0.99	[−1.99; 0.01]	12.2%
Siedlecki et al., 2009[51]	SNX	8	FS	8	7		0.36	[−0.66; 1.39]	11.9%
Winterberg et al., 2016[48]	SNX	8	EF	9	7		−0.04	[−1.03; 0.95]	12.3%
Winterberg et al., 2019[52]	SNX	8	FS	5	5		0.38	[−0.87; 1.64]	9.6%
Random effects model				32	27		−0.10	[−1.14; 0.93]	46.1%
Heterogeneity: $I^2 = 32\%$, $\tau^2 = 0.2167$, $P = 0.22$									
CKD_Interval = 9 to 13 weeks									
O'Sullivan et al., 2019[28]	SNX	10	FS	10	8		−0.87	[−1.85; 0.11]	12.4%
Hamzaoui et al., 2020[35]	SNX	11	FS	8	8		−1.45	[−2.59; −0.31]	10.8%
Random effects model				18	16		−1.12	[−4.77; 2.52]	23.1%
Heterogeneity: $I^2 = 0\%$, $\tau^2 = 0.0370$, $P = 0.45$									
CKD_Interval = 14 weeks or more									
Hu et al., 2017[53]	bilateral IRI	20	EF	4	4		−1.70	[−3.51; 0.11]	5.9%
Random effects model				4	4		−1.70	[−3.51; 0.11]	5.9%
Heterogeneity: not applicable									
Random effects model, $P = 0.0725$				**74**	**64**		**−0.48**	**[−1.02; 0.06]**	**100.0%**
Prediction interval								**[−1.90; 0.94]**	
Heterogeneity: $I^2 = 32\%$, $\tau^2 = 0.3050$, $P = 0.16$									
Residual heterogeneity: $I^2 = 0\%$, $P = 0.41$									

−10 −8 −6 −4 −2 0 2 4
Decreased function ← → Improved function

c

Inclusion of 10 data sets derived from 8 different studies

Study	Model	Duration	Parameters	CKD – Total	Ctrl – Total	Standardized mean difference	SMD	95% CI	Weight
CKD_Interval = 1 to 4 weeks									
Silberman *et al.*, 2010[72]	UNX + DOCA + Salt	2	FS	5	6		0.80	[–0.46; 2.06]	10.2%
Random effects model				5	6		0.80	[–0.46; 2.06]	10.2%
Heterogeneity: not applicable									
CKD_Interval = 5 to 8 weeks									
Liu *et al.*, 2013[73]	UNX + DOCA + Salt	6	FS	8	8		–2.84	[–4.34; –1.34]	9.3%
Tsukamoto *et al.*, 2013[75]	UNX + AngII	6	FS	10	12		0.76	[–0.11; 1.64]	11.6%
Tsukamoto *et al.*, 2013[75]	UNX + AngII + Salt	6	FS	11	12		–1.90	[–2.92; –0.89]	11.1%
Huang *et al.*, 2018[56]	SNX + Salt	8	FS	9	10		–0.04	[–0.94; 0.86]	11.5%
Kuma *et al.*, 2020[80]	SNX + Salt + high protein	8	FS	5	5		–1.81	[–3.41; –0.20]	9.0%
Kuma *et al.*, 2020[80]	UNX + Salt + high protein	8	EF	6	5		–1.57	[–3.01; –0.13]	9.5%
Ogawa *et al.*, 2012[78]	SNX + Salt	8	EF	3	9		0.05	[–1.26; 1.36]	10.0%
Wang *et al.*, 2020[79]	SNX + Salt	8	FS	6	6		–2.04	[–3.55; –0.53]	9.3%
Wang *et al.*, 2019[81]	SNX + Salt+ high protein	8	FS	5	5		–2.19	[–3.94; –0.44]	8.4%
Random effects model				63	72		–1.18	[–2.15; –0.22]	89.8%
Heterogeneity: $I^2 = 78\%$, $\tau^2 = 1.1775$, $P < 0.01$									
Random effects model, P = 0.0442				**68**	**78**		**–0.99**	**[–1.95; –0.03]**	**100.0%**
Prediction interval								**[–3.89; 1.91]**	
Heterogeneity: $I^2 = 78\%$, $\tau^2 = 1.4032$, $P < 0.01$									
Residual heterogeneity: $I^2 = 78\%$, $P < 0.01$									

–4 –2 0 2 4
Decreased function Improved function

Figure 7: Meta-analysis for systolic function. A) in C57BL/6 with surgery-induced CKD. **B)** in 129/Sv with surgery-induced CKD. **C)** in C57BL/6 with CKD and hypertension-inducing strategies.

Of the studies included in these meta-analyses, the 4 weeks studies as well as around half of the studies of 6 weeks and beyond could not observe significant effects on blood pressure (**Figure S6A**). Serum or plasma creatinine and urea/blood urea nitrogen levels as readouts of kidney dysfunction were increased in all short and intermediate-term studies (study duration: 4-14 weeks) when reported (**Figure S7A, S8A**), and their increase correlated with an increase in cardiac hypertrophy as well as a decrease in systolic function, but not with cardiac fibrosis (**Figure S9**). In contrast, blood pressure value changes did not correlate with any cardiac outcome parameter (cardiac hypertrophy, cardiac fibrosis, systolic function; **Figure S10A**).

129/Sv mice (Figure 3, Table S4)

5/6 nephrectomy models: Increased blood pressure, cardiac hypertrophy and fibrosis were consistently observed four weeks after SNX [47-51]. Enhanced diastolic cardiac wall thickness [48,51] and diastolic dysfunction [48] were reported, though systolic function was unaffected [49,51]. After 6-11 weeks [28,35,48,51,52], SNX increased blood pressure in 75% of studies [28,35,48], consistently induced cardiac hypertrophy [28,35,48,51] and enhanced diastolic cardiac wall thickness [28,48,51,52]. Diastolic dysfunction was observed in all studies [28,35,48,52], although in one study only at 6 weeks but not 10 weeks post-surgery [28]. Cardiac fibrosis was reported in three studies 6-11 weeks after SNX [35,48,51], but could not be confirmed by others in this time frame [28]. Systolic dysfunction has been detected [28,35], but could not be confirmed by others [48,51,52]. Two studies performed cardiac analysis 12 weeks post-surgery [17,48], again detecting hypertension, cardiac hypertrophy and fibrosis [17,48], increased diastolic wall thickness [48] and diastolic dysfunction [48]. Only

one study applied SNX to 129/Sv mice with a long experimental setup (16 weeks) [48], revealing increased blood pressure, cardiac hypertrophy and fibrosis, increased diastolic wall thickness and diastolic dysfunction [48]. Altogether, applying SNX to 129/Sv variants was more consistently associated with CKD-induced hypertension and cardiac hypertrophy compared to C57BL/6 mice. Also, cardiac fibrosis and diastolic dysfunction were mostly reported, in contrast to rarely assessed but mostly unaltered systolic function and cardiac dimensions.

Further bilateral kidney surgery models: Bilateral ischemia-reperfusion injury induced cardiac hypertrophy and fibrosis, an increased diastolic cardiac wall thickness and impaired systolic function 20 weeks after surgery [53].

Meta-analyses: A hypertrophic response was more distinct in 129/Sv variants compared to C57BL/6. The meta-analysis still revealed a high study heterogeneity (I^2=81%) but indicated a higher effect size for 129/Sv (**Figure 5B**; SMD=3.38; 95% CI [2.43; 4.33]; n=17 datasets; $P < 0.0001$), with the prediction interval almost passing the no effect border ([-0.30; 7.06]). Again, no time-dependent increase was observed on hypertrophy, with also short study times (2-4 weeks) revealing consistent induction of cardiac hypertrophy (2-4 weeks: 95% CI [2.25; 5.01]; 5-8 weeks: 95% CI [-0.01; 7.02]; 9-13 weeks: 95% CI [0.11; 4.09]; ≥14 weeks: 95% CI [-20.06; 30.67]).

Cardiac fibrosis was increased (**Figure 6B**; SMD=3.64; 95% CI [1.02; 6.27]; n=9; I^2=72%; P=0.127). No significant decrease in systolic function was identified (**Figure 7B**; SMD=-0.48; 95% CI [-1.02; 0.06]; n=9; P=0.0725, I^2=32%). As for C57BL/6 mice, conclusions on long-term effects remain elusive, since only one long-term study beyond 12 weeks was available.

Of note, of the studies included in these meta-analyses and in contrast to the findings in C57BL/6, all 4 weeks studies and 6 of 8 intermediate (6-13 weeks) studies identified a significant increase in blood pressure (**Figure S6B**), though without significant correlation of blood pressure increase with changes in cardiac hypertrophy, fibrosis or systolic function (**Figure S10B**). Serum or plasma creatinine and urea/blood urea nitrogen levels as readouts of kidney dysfunction were increased in all included studies when reported (**Figure S7B, S8B**), but too few studies were available to enable correlation analyses with cardiac outcome parameters.

Diet- or treatment-induced nephropathy

Adenine, applied via food-supplementation, is metabolized via xanthine dehydrogenase to 2,8-dihydroxyadenine that precipitates in the renal tubules, leading to crystal formation and tissue damage due to tubular occlusion and induction of inflammation and kidney fibrosis [54]. Also, oxalate was used to induce kidney damage through crystal-induced tubular injury, kidney inflammation and fibrosis.

In summary, diet/treatment-induced kidney damage could induce cardiac fibrosis in C57BL/6 *(Figure 3, Table S3)* and 129/Sv *(Figure 3, Table S4)* from 4-8 weeks on, though with cardiac functional effects remaining elusive. For details, we refer to **Suppl. Results.**

Genetic approach

The Alport syndrome with progressive kidney dysfunction results from a mutation in type IV collagen (autosomal *COL4A3* or *COL4A4*, or X-linked *COL4A5*), leading to abnormalities in the collagen network of glomerular basement membranes, ultimately causing glomerulosclerosis, tubular atrophy and interstitial fibrosis [55].

The Alport syndrome impaired cardiac function in C57BL/6 *(Figure 3, Table S3)* and 129/Sv *(Figure 3, Table S4)* strains on intermediate term, but conclusions on long-term effects remained elusive. Details are described in **Suppl. Results**.

Consideration of time-dependent effects of CKD on the heart

Although only few studies examined the effect of time on cardiac hypertrophy, fibrosis and dysfunction after CKD induction in C57BL/6 and 129/Sv variants, most results may point to a faster development of cardiac dysfunction, followed by (compensatory) cardiac hypertrophy as well as cardiac fibrosis. A detailed explanation is subscribed in **Suppl. Results**.

II. Multifactorial Hit Models

CKD & Mineral and bone disorder

Since patients in an advanced CKD stage typically display increased serum phosphate levels [9], multiple studies assessed the cardiac effect of combined surgically- or diet-induced kidney damage with high phosphate amount in mouse models (**Figure 4; Tables S5-S6**).

*In C57BL/6 mice (**Figure 4, Table S5**).* Subjecting mice to SNX and high phosphate for 12 weeks induced cardiac hypertrophy, systolic impairment and increased diastolic wall thickness [56].

*In 129/Sv mice (**Figure 4, Table S6**).* Uninephrectomy (UNX) plus contralateral ischemia/reperfusion as well as cisplatin-induced CKD, both combined with high phosphate diet, induced cardiac hypertrophy and fibrosis after 16-20 weeks [53,57,58].

CKD & Hyperlipidemia

CKD patients suffer from an increased atherosclerotic burden and the development of coronary artery disease [59]. Thus, studies have analyzed the cardiac effect of UNX or SNX in C57BL/6 ApoE-deficient (*ApoE*^{-/-}) mice, which develop hypercholesterolemia and atherogenesis [60] (**Figure 4, Table S5**). UNX in *ApoE*^{-/-} mice for 12 weeks triggered cardiac fibrosis, oxidative stress, reduced capillary density and impairment of systolic function [61]. Aggravation of the model by SNX in *ApoE*^{-/-} mice induced cardiac hypertrophy and impaired diastolic function after 6-10 weeks in two studies [26,29]. However, one long-term study 36 weeks after SNX in *ApoE*^{-/-} mice could not observe any effect on cardiac hypertrophy, fibrosis, left ventricular dimension, systolic or diastolic function [62]. *ApoE*^{-/-} mice fed with 0.2% adenine diet for 14 weeks displayed a profibrotic cardiac response [63].

Feeding a Western diet to SNX *ApoE*^{-/-} mice resulted in an increase of apoptotic cells in the myocardium, increased left ventricular diameter as well as reduced systolic function after 11 weeks [64]. Feeding SNX-WT mice with a high-fat diet and fructose to mimic a combination of CKD, hyperlipidemia and oxidative stress [19], induced cardiac hypertrophy, fibrosis, inflammatory cytokine expression, left ventricular wall thickening as well as systolic and diastolic dysfunction already after four weeks [19]. In conclusion, cardiac hypertrophy and fibrosis have been observed in *ApoE*^{-/-} mice in CKD in the absence of hypertension, however with high study variability.

Meta-analyses: Low study numbers and highly variable study outcomes for both cardiac hypertrophy and fibrosis make overall conclusions elusive (**Figure S11A-B**). In contrast, three studies revealed induction of systolic impairment, although this effect was not significant in a meta-analysis (**Figure S11C**; n=4 studies, I^2=91%, SMD -1.74, 95%-CI [-4.33; 0.85]; *P*=0.1226). This urges additional analyses on time- and model-dependent effects as well as potential underlying mechanisms.

CKD & Hypertension

Multiple studies combined kidney ablation (UNX, SNX) with supplementation of (a) mineralocorticoids (Angiotensin-independent) or (b) Angiotensin II, with or without additional salt supplementation to raise blood pressure. Chronic angiotensin II infusion induces hypertension via angiotensin 1 receptor-mediated vasoconstriction as well as increased secretion of aldosterone, mediating retention of water and salt [65]. Yet, ~25% of patients suffering from primary hypertension exhibit reduced plasma renin activity and normal levels of plasma angiotensin II [66]. This is mimicked by the "deoxycorticosterone acetate (DOCA)-salt" model, which combines the implantation of a pellet of the aldosterone precursor DOCA with salt loading in mice subjected to UNX [67,68]. Alternatively, the "NAS (nephrectomy-aldosterone-salt)" model combines UNX, aldosterone infusion and salt intake [69-71]. Kidney parameters in relation to kidney damage for the included studies are in **Table S7**.

In C57BL/6 mice (**Figue 4, Table S5**).

Mineralocorticoids administration: Combining UNX and DOCA-salt induced hypertension and increased cardiac oxidative stress [72,73], with reduced systolic function and increased left ventricular volumes after 6 weeks of treatment [73]. The NAS model consistently induced hypertension, cardiac hypertrophy and fibrosis at 2-6 weeks of treatment [69-71], with cardiac inflammatory cytokine expression and oxidative stress being further reported [70].

Angiotensin II administration: Combining UNX or SNX with angiotensin II with or without salt supplementation consistently triggered hypertension, cardiac hypertrophy and fibrosis after 4-6 weeks [17,74,75]. A salt-independent increase in diastolic left ventricular wall thickness was reported after 6 weeks of AngII infusion, while impaired systolic and diastolic function were only detected when combining high salt and AngII in mice subjected to UNX [75].

Salt supplementation: Combining UNX with merely 4% salt overload for 52 weeks induced hypertension, cardiac hypertrophy and fibrosis [76]. In contrast, supplementing 0.9%-1% salt on top of UNX or SNX in the absence of angiotensin II infusion revealed variable effects on cardiac hypertrophy, fibrosis, left ventricular diameter and systolic function after 8 weeks [77-79]. Supplementation of high protein diet and 0.45%-1% salt to

mice with UNX or SNX triggered hypertension, cardiac fibrosis, decreased left ventricular volumes and reduced systolic function after 8 weeks, though with variable effects on cardiac hypertrophy and cardiac wall thickness [80,81].

Meta-analyses: Compared to "single-hit" surgery-induced CKD, adding hypertension-inducing strategies on top of kidney surgery induced a more consistent and slightly stronger induction of cardiac hypertrophy (**Figure 5C**; SMD 2.15; 95% CI [1.20; 3.11]; I^2=74%; n=12 studies, *P*=0.0004). Similar results were obtained when comparing effects on cardiomyocyte size/diameter after 6-8 weeks (**Figure S4B**; overall SMD 2.46; 95% CI [0.00; 4.93]; I^2=89%; n=5 studies; *P* = 0.0502; 1-4 weeks: 95% CI [-11.55; 13.10]; 6-8 weeks: 95% CI [-0.19; 7.37]). However, a conclusion on time-dependent effects is difficult due to low study number per study duration.

In terms of cardiac fibrosis, the effect size was smaller when adding hypertension-inducing strategies on top of kidney surgery compared to kidney surgery-induced CKD alone (**Figure 6C**; SMD 2.53; 95% CI [1.61; 3.45]; n=10; *P* = 0.0002). However, study heterogeneity was much lower (37%), with consistent effects in both short (2-4 weeks) and intermediate (6-8 weeks) study setups, and with a prediction interval almost passing the null-effect border ([-0.30; 5.36]).

Systolic function was reduced after 6-8 weeks (**Figure 7C**; SMD -1.18; 95% CI [-2.15; -0.22]; n=9; *P*<0.01). However, study variability was high (78%), with three of 9 studies not detecting significant changes.

*In 129/Sv mice (**Figure 4, Table S6**). Combination of UNX and DOCA-salt induced hypertension and cardiac hypertrophy after 8 weeks of treatment [82]. Also, challenging 129/Sv with SNX and 0.5-1% salt-intake for four weeks induced hypertension and cardiac hypertrophy, as well as cardiac inflammation and fibrosis [47,83]. Feeding a 0.25% adenine diet combined with 1% salt intake for 8 weeks triggered hypertension and cardiac inflammatory cell infiltration [47].

CKD & Cardiac injury

The effect of CKD on cardiac damage after myocardial ischemia has been investigated only in C57BL/6 mice *(**Figure 4, Table S5, Figure S12**). Details are described in **Suppl. Results**.

Discussion

Our study revealed that the impact of CKD on cardiovascular consequences is highly influenced by mouse strain, study duration as well as comorbidities. This was supported by meta-analyses of cardiac hypertrophy, fibrosis and function, with high variability of cardiac effects observed (**Figure 8**).

a

Cardiac hypertrophy in CKD

C57BL/6	1.34 (0.50 to 2.18)
129/Sv	3.38 (2.43 to 4.33)
C57BL/6 + Hypertension	2.15 (1.20 to 3.11)

Studies with significant effect (%)

Cardiac fibrosis in CKD

C57BL/6	5.43 (3.27 to 7.59)
129/Sv	3.64 (1.02 to 6.27)
C57BL/6 + Hypertension	2.53 (1.61 to 3.45)

Studies with significant effect (%)

Systolic dysfunction in CKD

C57BL/6	-1.56 (-2.28 to -0.84)
129/Sv	-0.48 (-1.02 to 0.06)
C57BL/6 + Hypertension	-0.99 (-1.95 to -0.03)

Studies with significant effect (%)

b

Creatinine increase in CKD

C57BL/6	3.94 (2.69 to 5.19)
129/Sv	2.31 (1.09 to 3.53)

Studies with significant effect (%)

Urea/bun increase in CKD

C57BL/6	3.99 (3.06 to 4.93)
129/Sv	2.98 (1.40 to 4.56)

Studies with significant effect (%)

c

Blood pressure increase in CKD

C57BL/6	0.65 (0.02 to 1.28)
129/Sv	2.92 (0.87 to 4.96)

Studies with significant effect (%)

Figure 6: Summary of meta-analyses of cardiac and kidney parameters in mice subjected to CKD. A, Cardiac hypertrophy (based on heart or LV weight), cardiac fibrosis and systolic dysfunction in mice subjected to CKD. Results obtained in C57BL/6 or 129/Sv with CKD as single hit versus C57BL/6 with combined kidney injury and hypertension-inducing treatment. **B-C,** Increase in plasma or serum creatinine or urea/blood urea nitrogen (BUN) (B) and blood pressure in C57BL/6 or 129/Sv with single hit bilateral kidney injury. **A-C,** Standardized mean differences with 95% confidence intervals, as derived from the corresponding meta-analyses, are included.

In C57BL/6 cardiac fibrosis in CKD was mainly observed in intermediate study setups (8-13 weeks after SNX). Induction of systolic dysfunction was more variable, with reduced systolic function again most consistently observed at 11-12 weeks post-SNX. A mild induction of hypertrophy was detected in C57BL/6, but without a clear time-dependent increase and with almost half of the studies not detecting a significant hypertrophic response between 6-11 or 14-24 weeks.

In the few studies that reported on systolic cardiac function in 129/Sv mice, most could not detect systolic dysfunction, although a direct comparison with C57BL/6 remains difficult due to low study numbers reporting on this parameter for 129/Sv, especially beyond 11 weeks of CKD. On the other hand, 129/Sv mice developed cardiac fibrosis already at early time points and were more prone to develop CKD-induced cardiac hypertrophy compared to C57BL/6. This was also detected by a direct comparison of SNX in both strains by Hamzaoui et al. [35]. Several factors could contribute to this strain-dependent effect, including a faster progression of CKD, higher blood pressure and higher sensitivity to blood pressure increase, altered RAAS signaling or other genetic

differences including genes involved in vascular pathophysiology, inflammation as well as fibrosis. In regard to CKD progression, a meta-analysis of studies performing bilateral kidney surgery did not reveal statistically significant differences in serum or plasma creatinine and blood urea nitrogen/urea when using C57BL/6 vs. 129/Sv mice (**Figure 8**). Nonetheless, the 129/Sv strain has been described to be more prone to develop proteinuria and kidney inflammation in response to albumin overload compared to C57BL/6 [84]; to show more severe tubular damage, kidney fibrosis and inflammation after SNX [35]; and to be more susceptible to DOCA-induced hypertension and kidney damage [85]. On a molecular level, 129/Sv mice express two instead of one renin gene [86]. Although a direct relation between renin gene number and blood pressure has been debated [85,86], both altered RAAS signaling as well as hypertension [87] may be a mechanistic trigger for an increased susceptibility of 129/Sv to glomerulosclerosis [88], which may consequently favor (earlier) cardiac pathological changes in 129/Sv. In the identified studies, C57BL/6 only showed increased blood pressure upon 5/6 nephrectomy in around half of the studies 6-12 weeks after surgery. In contrast, a blood pressure increase was observed in most studies using 129/Sv already after 4 weeks (**Figure 8**), though without significant correlation between the rise in blood pressure and changes in cardiac hypertrophy, fibrosis or systolic function. In C57BL/6, angiotensin II increased blood pressure and caused progression of SNX-induced CKD, whereas pharmacological blood pressure lowering in CD1 mice with SNX reduced both CKD progression and cardiac fibrosis [17]. Blood pressure lowering with the angiotensin-converting-enzyme inhibitor enalapril reduced kidney damage-induced cardiac hypertrophy and fibrosis in C57BL/6 [13]. However, this was not observed by antihypertensive treatment with hydralazine [13], suggesting potential direct cardioprotective effects of RAAS blockade independent of blood pressure.

Our meta-analysis demonstrates that hypertension-inducing strategies combined with CKD in C57BL/6 mice more consistently induced cardiac hypertrophy and fibrosis in intermediate study setups compared to "single hit" CKD models. Thus, in C57BL/6 mice, "multifactorial hit" models combining kidney injury and cardiovascular risk factors with high clinical relevance for CKD patients, such as hypertension [7,89], seem to remodel pathophysiological processes in the heart better than "single hit" approaches.

Genetic differences and "multifactorial hits" may impact cardiac responses to CKD also through mechanisms independent of blood pressure or RAAS. Genomic analyses

identified >8800 genes with strain-dependent molecular differences with potential pro-tein functional effects [90], including genes involved in vascular pathophysiology, inflam-mation as well as fibrosis [90]. S100/calgranulin was shown to increase the susceptibility of C57BL/6 mice to ureteral ligation-induced cardiac remodeling and dysfunction with an impact on systemic inflammation over FGF23 upregulation in fibroblasts suggested [15]. Thus, genetic differences altering strain susceptibility to inflammation and fibrosis signaling may contribute to altered sensitivity to kidney damage as well as cardiac remodeling. Within C57BL/6 mouse strains, an important aspect is the absence of a functional mitochondrial transhydrogenase (NNT) in BL/6J, but not BL/6N, which pro-tects BL/6J from mitochondrial reactive oxygen species formation, necrotic cell death, development of fibrosis and systolic dysfunction in response to pressure overload [91,92]. However, the substrains of C57BL/6 could not be considered in our systematic review since they are poorly reported. It is therefore unclear whether heterogeneity of study outcomes in C57BL/6 mice might be further related to substrain differences.

Study variability in terms of CKD-induced cardiac effects was high, also among studies with comparable setups in terms of strain, CKD-induction protocol and duration. In ad-dition to genetic differences, explanations may be methodological differences impact-ing on kidney damage degree: among studies applying 5/6 bilateral kidney surgery in C57BL/6, our analyses revealed a correlation between increases in serum or plasma creatinine and urea/blood urea nitrogen levels as readouts of kidney dysfunction with increase in cardiac hypertrophy as well as decrease in systolic function, but not with cardiac fibrosis. Other causes could be methodological differences inducing differential molecular effects (e.g. one-step vs. two-step surgery, renal mass reduction by pole infarction vs. pole resection in rats [93], adenine concentration). In addition, differences in housing conditions (e.g. temperature, group housing) or diet composition (e.g. salt, fat, protein or other) may impact on molecular and pathological processes and thereby on study results [28,94]. For example, the salt concentration could impact on blood pres-sure changes; group vs. single housing of animals may differentially impact on stress levels and thereby on the recovery of animals after operation [28]. Even differences in housing temperature can impact on metabolism, health and disease progression in animal models [11,95], as also demonstrated for e.g. inflammation and atherosclerosis [96]. Furthermore, sex has been identified as an important factor in the epidemiology of both CKD [97] and CVD [98,99]. Also in animal models, sex-dependent effects have been ob-

served, with for example male rats developing a faster decline in kidney function compared to female rats [100]. However, the factor sex could not be taken into account in the performed meta-analyses, since 71% of studies identified in our systematic review used male mice. Instead, only 8% of studies used female mice, 6% analyzed both sexes, and the remaining 15% did not report on the sex of mice studied.

Another limitation is that our meta-analyses combine different readouts per parameter, nonetheless with defined prioritization of use. Different readouts of a pathophysiological process or cardiac function may be differentially affected within one study. Lack of consistent parameter reporting also explains why no meta-analysis of diastolic function was performed, despite that a more consistent susceptibility to diastolic compared to systolic dysfunction was apparent in "single-hit" CKD models using C57BL/6 or 129/Sv variants. Compared to clinical studies, animal research is performed with much lower N-numbers and a potentially higher risk of publication bias, with assumed underreporting of studies that observed no or low cardiac remodeling in response to CKD. This consecutively will influence the outcome of our meta-analysis.

In addition to the cardiac pathophysiological changes (inflammation, hypertrophy, fibrosis) as well as findings on left ventricular morphology and function extracted in the **Tables S3-S6**, also CKD-induced alterations in cardiomyocyte cellular function may impact on cardiovascular risk, such as for intracellular calcium handling and cardiomyocyte shortening as readouts of cellular contraction. For example, cardiomyocytes from C57BL/6 mice subjected to 5/6 nephrectomy for 6-24 weeks displayed impaired systolic intracellular Ca^{2+} dynamics [27,33,36,45] and reduced cell shortening, as well as pro-arrhythmogenic diastolic Ca^{2+} leaks [27,36,45]. Increased cardiac expression of the atrial and brain natriuretic peptides (ANP, BNP) is also frequently used as biomarker of cardiac damage and/or hypertrophy. ANP and BNP expression was often reported to be increased in animal models of CKD, however did not always correlate with effects on heart weight or cardiomyocyte size as most frequently used parameters of cardiac hypertrophy (**Table S8**), with a similar finding previously observed in a systematic review of animal models of diabetic cardiomyopathy [3].

Finally, although not included in this systematic review, mouse models with genetic deficiencies or molecular treatment impacting on kidney-heart crosstalk also offer interesting animal models to study pathological kidney-heart crosstalk. For example, deficiency of Klotho as regulator of mineral metabolism induces both kidney damage as

well as cardiac functional deficits with e.g. impaired intracellular Ca^{2+} dynamics and cardiomyocyte contraction as also observed upon 5/6 nephrectomy. Conversely, treatment of 5/6 nephrectomy-subjected mice with recombinant Klotho prevented CKD-induced cardiomyocyte defects [27]. Also, bone deficiency of the phosphaturic hormone FGF-23 triggered cardiac hypertrophy in adenine-fed mice [101]. For a more in-depth discussion of the impact of the FGF-23 and Klotho axis on the heart, we refer to a recent review [102].

In conclusion, this review with meta-analyses indicates that cardiac pathophysiological changes upon CKD can be detected in mouse models, though with high variability (**Figure 8**). Genetic and/or multifactorial preconditioning was shown to increase susceptibility to organ damage (especially in terms of cardiac hypertrophy and fibrosis), which is in line with the clinical context with multiple risk factors known to increase the risk of CKD and/or CVD.

Disclosure

CM received honoraria for consulting and/or speeches from AstraZeneca, Bayer, Berlin Chemie, Boehringer Ingelheim, Novo Nordisk, Novartis, Pfizer, Servier. The other authors report that no conflict of interest exists.

Supplementary Material

Supplementary Tables; supplementary Figures

Supplementary Methods**:** *Study selection, data extraction, quality assessment and meta-analysis*

Supplementary Results**:**

> *Diet- or treatment-induced nephropathy in C57BL/6 and 129/Sv; Genetic approaches in C57BL/6 and 129/Sv*

> *Consideration of time-dependent effects of CKD on the heart in C57BL/6 and 129/Sv*

> *CKD and cardiac injury in C57BL/6*

> *CKD-induced uremic cardiomyopathy using mouse strains other than C57BL/6 and 129/Sv*

Supplementary References

Supplementary information is available on Kidney International's website.

References

1. Webster AC, Nagler EV, Morton RL, et al. Chronic Kidney Disease. *Lancet (London, England).* 2017;389(10075):1238-1252.
2. Thompson S, James M, Wiebe N, et al. Cause of Death in Patients with Reduced Kidney Function. *J Am Soc Nephrol.* 2015;26(10):2504-2511.
3. Cox EJ, Marsh SA. A systematic review of fetal genes as biomarkers of cardiac hypertrophy in rodent models of diabetes. *PLoS One.* 2014;9(3):e92903.
4. Marx N, Noels H, Jankowski J, et al. Mechanisms of cardiovascular complications in chronic kidney disease: research focus of the Transregional Research Consortium SFB TRR219 of the University Hospital Aachen (RWTH) and the Saarland University. *Clinical research in cardiology : official journal of the German Cardiac Society.* 2018;107(Suppl 2):120-126.
5. Shamseddin MK, Parfrey PS. Sudden cardiac death in chronic kidney disease: epidemiology and prevention. *Nat Rev Nephrol.* 2011;7(3):145-154.
6. Kaesler N, Babler A, Floege J, et al. Cardiac Remodeling in Chronic Kidney Disease. *Toxins.* 2020;12(3).
7. Muntner P, Anderson A, Charleston J, et al. Hypertension awareness, treatment, and control in adults with CKD: results from the Chronic Renal Insufficiency Cohort (CRIC) Study. *Am J Kidney Dis.* 2010;55(3):441-451.
8. Hruska KA, Mathew S, Lund R, et al. Hyperphosphatemia of chronic kidney disease. *Kidney Int.* 2008;74(2):148-157.
9. Viegas C, Araujo N, Marreiros C, et al. The interplay between mineral metabolism, vascular calcification and inflammation in Chronic Kidney Disease (CKD): challenging old concepts with new facts. *Aging (Albany NY).* 2019;11(12):4274-4299.
10. Nauta ST, van Domburg RT, Nuis RJ, et al. Decline in 20-year mortality after myocardial infarction in patients with chronic kidney disease: evolution from the prethrombolysis to the percutaneous coronary intervention era. *Kidney Int.* 2013;84(2):353-358.
11. Raun SH, Henriquez-Olguín C, Karavaeva I, et al. Housing temperature influences exercise training adaptations in mice. *Nat Commun.* 2020;11(1):1560.
12. Gaikwad AB, Sayyed SG, Lichtnekert J, et al. Renal failure increases cardiac histone h3 acetylation, dimethylation, and phosphorylation and the induction of cardiomyopathy-related genes in type 2 diabetes. *Am J Pathol.* 2010;176(3):1079-1083.
13. Ham O, Jin W, Lei L, et al. Pathological cardiac remodeling occurs early in CKD mice from unilateral urinary obstruction, and is attenuated by Enalapril. *Sci Rep.* 2018;8:17.
14. Lv J, Chen J, Wang M, et al. Klotho alleviates indoxyl sulfate-induced heart failure and kidney damage by promoting M2 macrophage polarization. *Aging (Albany NY).* 2020;12(10):9139-9150.
15. Yan L, Mathew L, Chellan B, et al. S100/Calgranulin-mediated inflammation accelerates left ventricular hypertrophy and aortic valve sclerosis in chronic kidney disease in a receptor for advanced glycation end products-dependent manner. *Arteriosclerosis, thrombosis, and vascular biology.* 2014;34(7):1399-1411.
16. Guo J, Zhu J, Ma L, et al. Chronic Kidney Disease Exacerbates Myocardial Ischemia Reperfusion Injury: Role of Endoplasmic Reticulum Stress-Mediated Apoptosis. *Shock (Augusta, Ga).* 2018;49(6):712-720.
17. Leelahavanichkul A, Yan Q, Hu X, et al. Angiotensin II overcomes strain-dependent resistance of rapid CKD progression in a new remnant kidney mouse model. *Kidney Int.* 2010;78(11):1136-1153.
18. Liu J, Tian J, Chaudhry M, et al. Attenuation of Na/K-ATPase Mediated Oxidant Amplification with pNaKtide Ameliorates Experimental Uremic Cardiomyopathy. *Sci Rep.* 2016;6:34592.

19. Sodhi K, Wang X, Chaudhry MA, et al. Central Role for Adipocyte Na,K-ATPase Oxidant Amplification Loop in the Pathogenesis of Experimental Uremic Cardiomyopathy. *J Am Soc Nephrol.* 2020;31(8):1746-1760.

20. Song YB, Yu QJ, Zhang JY, et al. Increased myocardial ischemia-reperfusion injury in renal failure involves cardiac adiponectin signal deficiency. *Am J Physiol-Endocrinol Metab.* 2014;306(9):E1055-E1064.

21. Wang XL, Chaudhry MA, Nie Y, et al. A Mouse 5/6th Nephrectomy Model That Induces Experimental Uremic Cardiomyopathy. *J Vis Exp.* 2017(129):6.

22. Chen J, Kieswich JE, Chiazza F, et al. IkappaB Kinase Inhibitor Attenuates Sepsis-Induced Cardiac Dysfunction in CKD. *J Am Soc Nephrol.* 2017;28(1):94-105.

23. Han H, Zhu J, Zhu Z, et al. p-Cresyl sulfate aggravates cardiac dysfunction associated with chronic kidney disease by enhancing apoptosis of cardiomyocytes. *Journal of the American Heart Association.* 2015;4(6):e001852.

24. Lin CY, Hsu YJ, Hsu SC, et al. CB1 cannabinoid receptor antagonist attenuates left ventricular hypertrophy and Akt-mediated cardiac fibrosis in experimental uremia. *J Mol Cell Cardiol.* 2015;85:249-261.

25. Maizel J, Six I, Dupont S, et al. Effects of sevelamer treatment on cardiovascular abnormalities in mice with chronic renal failure. *Kidney Int.* 2013;84(3):491-500.

26. Maizel J, Six I, Slama M, et al. Mechanisms of aortic and cardiac dysfunction in uremic mice with aortic calcification. *Circulation.* 2009;119(2):306-313.

27. Navarro-Garcia JA, Rueda A, Romero-Garcia T, et al. Enhanced Klotho availability protects against cardiac dysfunction induced by uraemic cardiomyopathy by regulating Ca(2+) handling. *Br J Pharmacol.* 2020;177(20):4701-4719.

28. O'Sullivan J, Finnie SL, Teenan O, et al. Refining the Mouse Subtotal Nephrectomy in Male 129S2/SV Mice for Consistent Modeling of Progressive Kidney Disease With Renal Inflammation and Cardiac Dysfunction. *Front Physiol.* 2019;10:17.

29. Six I, Gross P, Remond MC, et al. Deleterious vascular effects of indoxyl sulfate and reversal by oral adsorbent AST-120. *Atherosclerosis.* 2015;243(1):248-256.

30. Thomsen MB, Nielsen MS, Aarup A, et al. Uremia increases QRS duration after beta-adrenergic stimulation in mice. *Physiol Rep.* 2018;6(13):13.

31. Uchida T, Furuno Y, Tanimoto A, et al. Development of an experimentally useful model of acute myocardial infarction: 2/3 nephrectomized triple nitric oxide synthases-deficient mouse. *J Mol Cell Cardiol.* 2014;77:29-41.

32. Verkaik M, Juni RP, van Loon EPM, et al. FGF23 impairs peripheral microvascular function in renal failure. *Am J Physiol-Heart Circul Physiol.* 2018;315(5):H1414-H1424.

33. Verkaik M, Oranje M, Abdurrachim D, et al. High Fibroblast Growth Factor 23 concentrations in experimental renal failure impair calcium handling in cardiomyocytes. *Physiol Rep.* 2018;6(7):13.

34. Yoshida A, Kanamori H, Naruse G, et al. (Pro)renin Receptor Blockade Ameliorates Heart Failure Caused by Chronic Kidney Disease. *J Card Fail.* 2019;25(4):286-300.

35. Hamzaoui M, Djerada Z, Brunel V, et al. 5/6 nephrectomy induces different renal, cardiac and vascular consequences in 129/Sv and C57BL/6JRj mice. *Sci Rep.* 2020;10(1):1524.

36. Gil-Fernandez M, Navarro-Garcia JA, Val-Blasco A, et al. Genetic Deletion of NOD1 Prevents Cardiac Ca(2+) Mishandling Induced by Experimental Chronic Kidney Disease. *International journal of molecular sciences.* 2020;21(22).

37. Chin LH, Hsu YJ, Hsu SC, et al. The regulation of NLRP3 inflammasome expression during the development of cardiac contractile dysfunction in chronic kidney disease. *Oncotarget.* 2017;8(69):113303-113317.

38. Jin Q, Sun L, Li SQ, et al. Number and function impairment of resident C-Kit+ cardiac stem cells in mice with renal dysfunction caused by 5/6 nephrectomy. *Ren Fail.* 2013;35(8):1136-1141.

39. Ding W, Wang B, Zhang MM, et al. Involvement of Endoplasmic Reticulum Stress in Uremic Cardiomyopathy: Protective Effects of Tauroursodeoxycholic Acid. *Cell Physiol Biochem.* 2016;38(1):141-152.

40.   Yang Y, Ma L, Wang C, et al. Matrix metalloproteinase-7 in platelet-activated macrophages accounts for cardiac remodeling in uremic mice. *Basic Res Cardiol.* 2020;115(3):19.

41.   Li PP, Song XL, Zhang DW, et al. Resveratrol improves left ventricular remodeling in chronic kidney disease via Sirt1-mediated regulation of FoxO1 activity and MnSOD expression. *Biofactors.* 2020;46(1):168-179.

42.   Li YW, Takemura G, Okada H, et al. Molecular signaling mediated by angiotensin II type 1A receptor blockade leading to attenuation of renal dysfunction-associated heart failure. *J Card Fail.* 2007;13(2):155-162.

43.   Li YW, Wu JY, He Q, et al. Angiotensin (1-7) prevent heart dysfunction and left ventricular remodeling caused by renal dysfunction in 5/6 nephrectomy mice. *Hypertens Res.* 2009;32(5):369-374.

44.   Ogino A, Takemura G, Kawasaki M, et al. Erythropoietin Receptor Signaling Mitigates Renal Dysfunction-Associated Heart Failure by Mechanisms Unrelated to Relief of Anemia. *J Am Coll Cardiol.* 2010;56(23):1949-1958.

45.   Ke HY, Chin LH, Tsai CS, et al. Cardiac calcium dysregulation in mice with chronic kidney disease. *J Cell Mol Med.* 2020;24(6):3669-3677.

46.   Pang P, Abbott M, Abdi M, et al. Pre-clinical model of severe glutathione peroxidase-3 deficiency and chronic kidney disease results in coronary artery thrombosis and depressed left ventricular function. *Nephrol Dial Transplant.* 2018;33(6):923-934.

47.   Sakata F, Ito Y, Mizuno M, et al. Sodium chloride promotes tissue inflammation via osmotic stimuli in subtotal-nephrectomized mice. *Lab Invest.* 2017;97(4):432-446.

48.   Winterberg PD, Jiang R, Maxwell JT, et al. Myocardial dysfunction occurs prior to changes in ventricular geometry in mice with chronic kidney disease (CKD). *Physiol Rep.* 2016;4(5):11.

49.   Xie J, Yoon J, An SW, et al. Soluble Klotho Protects against Uremic Cardiomyopathy Independently of Fibroblast Growth Factor 23 and Phosphate. *J Am Soc Nephrol.* 2015;26(5):1150-1160.

50.   Elkareh J, Periyasamy SM, Shidyak A, et al. Marinobufagenin induces increases in procollagen expression in a process involving protein kinase C and Fli-1: implications for uremic cardiomyopathy. *Am J Physiol-Renal Physiol.* 2009;296(5):F1219-F1226.

51.   Siedlecki AM, Jin XH, Muslin AJ. Uremic cardiac hypertrophy is reversed by rapamycin but not by lowering of blood pressure. *Kidney Int.* 2009;75(8):800-808.

52.   Winterberg PD, Robertson JM, Kelleman MS, et al. T Cells Play a Causal Role in Diastolic Dysfunction during Uremic Cardiomyopathy. *J Am Soc Nephrol.* 2019;30(3):407-420.

53.   Hu MC, Shi MJ, Gillings N, et al. Recombinant alpha-Klotho may be prophylactic and therapeutic for acute to chronic kidney disease progression and uremic cardiomyopathy. *Kidney Int.* 2017;91(5):1104-1114.

54.   Santana AC, Degaspari S, Catanozi S, et al. Thalidomide suppresses inflammation in adenine-induced CKD with uraemia in mice. *Nephrol Dial Transplant.* 2013;28(5):1140-1149.

55.   Nozu K, Nakanishi K, Abe Y, et al. A review of clinical characteristics and genetic backgrounds in Alport syndrome. *Clinical and experimental nephrology.* 2019;23(2):158-168.

56.   Huang Y, Wang S, Zhou J, et al. IRF1-mediated downregulation of PGC1alpha contributes to cardiorenal syndrome type 4. *Nat Commun.* 2020;11(1):4664.

57.   Hu MC, Shi M, Cho HJ, et al. Klotho and phosphate are modulators of pathologic uremic cardiac remodeling. *J Am Soc Nephrol.* 2015;26(6):1290-1302.

58.   Shi MJ, McMillan KL, Wu JX, et al. Cisplatin nephrotoxicity as a model of chronic kidney disease. *Lab Invest.* 2018;98(8):1105-1121.

59.   Valdivielso JM, Rodriguez-Puyol D, Pascual J, et al. Atherosclerosis in Chronic Kidney Disease: More, Less, or Just Different? *Arteriosclerosis, thrombosis, and vascular biology.* 2019;39(10):1938-1966.

60. Zhang SH, Reddick RL, Piedrahita JA, et al. Spontaneous hypercholesterolemia and arterial lesions in mice lacking apolipoprotein E. *Science.* 1992;258(5081):468-471.

61. Piecha G, Koleganova N, Gross ML, et al. Oxidative stress after uninephrectomy alters heart morphology in the apolipoprotein E -/- mouse. *J Hypertens.* 2008;26(11):2220-2229.

62. Bro S, Bollano E, Bruel A, et al. Cardiac structure and function in a mouse model of uraemia without hypertension. *Scand J Clin Lab Invest.* 2008;68(7):660-666.

63. Zhang W, Miikeda A, Zuckerman J, et al. Inhibition of microbiota-dependent TMAO production attenuates chronic kidney disease in mice. *Sci Rep.* 2021;11(1):518.

64. Miyazaki-Anzai S, Masuda M, Demos-Davies KM, et al. Endoplasmic Reticulum Stress Effector CCAAT/Enhancer-binding Protein Homologous Protein (CHOP) Regulates Chronic Kidney Disease-Induced Vascular Calcification. *Journal of the American Heart Association.* 2014;3(3):13.

65. Szczepanska-Sadowska E, Czarzasta K, Cudnoch-Jedrzejewska A. Dysregulation of the Renin-Angiotensin System and the Vasopressinergic System Interactions in Cardiovascular Disorders. *Curr Hypertens Rep.* 2018;20(3):19.

66. Mulatero P, Verhovez A, Morello F, et al. Diagnosis and treatment of low-renin hypertension. *Clin Endocrinol (Oxf).* 2007;67(3):324-334.

67. Basting T, Lazartigues E. DOCA-Salt Hypertension: an Update. *Curr Hypertens Rep.* 2017;19(4):32.

68. Mohammed-Ali; Z, Carlisle; RE, Nademi; S, et al. Animal Models of Kidney Disease. In: *Animal Models for the Study of Human Disease.*: Elsevier Inc. ; 2017:379-417.

69. Araos P, Prado C, Lozano M, et al. Dendritic cells are crucial for cardiovascular remodeling and modulate neutrophil gelatinase-associated lipocalin expression upon mineralocorticoid receptor activation. *J Hypertens.* 2019;37(7):1482-1492.

70. Buonafine M, Martinez-Martinez E, Amador C, et al. Neutrophil Gelatinase-Associated Lipocalin from immune cells is mandatory for aldosterone-induced cardiac remodeling and inflammation. *J Mol Cell Cardiol.* 2018;115:32-38.

71. Tarjus A, Martinez-Martinez E, Amador C, et al. Neutrophil Gelatinase-Associated Lipocalin, a Novel Mineralocorticoid Biotarget, Mediates Vascular Profibrotic Effects of Mineralocorticoids. *Hypertension.* 2015;66(1):158-166.

72. Silberman GA, Fan TH, Liu H, et al. Uncoupled cardiac nitric oxide synthase mediates diastolic dysfunction. *Circulation.* 2010;121(4):519-528.

73. Liu M, Gu LZ, Sulkin MS, et al. Mitochondrial dysfunction causing cardiac sodium channel downregulation in cardiomyopathy. *J Mol Cell Cardiol.* 2013;54:25-34.

74. Ahadzadeh E, Rosendahl A, Czesla D, et al. The chemokine receptor CX3CR1 reduces renal injury in mice with angiotensin II-induced hypertension. *Am J Physiol Renal Physiol.* 2018;315(6):F1526-F1535.

75. Tsukamoto Y, Mano T, Sakata Y, et al. A novel heart failure mice model of hypertensive heart disease by angiotensin II infusion, nephrectomy, and salt loading. *Am J Physiol-Heart Circul Physiol.* 2013;305(11):H1658-H1667.

76. Yang T, Zollbrecht C, Winerdal ME, et al. Genetic Abrogation of Adenosine A(3) Receptor Prevents Uninephrectomy and High Salt-Induced Hypertension. *Journal of the American Heart Association.* 2016;5(7):24.

77. Huang D, Yan ML, Chen KK, et al. Cardiac-Specific Overexpression of Silent Information Regulator 1 Protects Against Heart and Kidney Deterioration in Cardiorenal Syndrome via Inhibition of Endoplasmic Reticulum Stress. *Cell Physiol Biochem.* 2018;46(1):9-22.

78. Ogawa M, Suzuki J, Takayama K, et al. Impaired post-infarction cardiac remodeling in chronic kidney disease is due to excessive renin release. *Lab Invest.* 2012;92(12):1766-1776.

79. Wang B, Wang ZM, Ji JL, et al. Macrophage-Derived Exosomal Mir-155 Regulating Cardiomyocyte Pyroptosis and Hypertrophy in Uremic Cardiomyopathy. *JACC Basic to translational science.* 2020;5(2):148-166.

80.   Kuma A, Wang XH, Klein JD, et al. Inhibition of urea transporter ameliorates uremic cardiomyopathy in chronic kidney disease. *FASEB J.* 2020;34(6):8296-8309.

81.   Wang B, Zhang AQ, Wang HD, et al. miR-26a Limits Muscle Wasting and Cardiac Fibrosis through Exosome-Mediated microRNA Transfer in Chronic Kidney Disease. *Theranostics.* 2019;9(7):1864-1877.

82.   Arbeeny CM, Ling H, Smith MM, et al. CXA-10, a Nitrated Fatty Acid, Is Renoprotective in Deoxycorticosterone Acetate-Salt Nephropathy. *J Pharmacol Exp Ther.* 2019;369(3):503-510.

83.   Duka I, Kintsurashvili E, Gavras I, et al. Vasoactive potential of the B-1 bradykinin receptor in normotension and hypertension. *CircRes.* 2001;88(3):275-281.

84.   Ishola DA, Jr., van der Giezen DM, Hahnel B, et al. In mice, proteinuria and renal inflammatory responses to albumin overload are strain-dependent. *Nephrol Dial Transplant.* 2006;21(3):591-597.

85.   Hartner A, Cordasic N, Klanke B, et al. Strain differences in the development of hypertension and glomerular lesions induced by deoxycorticosterone acetate salt in mice. *Nephrol Dial Transplant.* 2003;18(10):1999-2004.

86.   Ma LJ, Fogo AB. Model of robust induction of glomerulosclerosis in mice: importance of genetic background. *Kidney Int.* 2003;64(1):350-355.

87.   Lum C, Shesely EG, Potter DL, et al. Cardiovascular and renal phenotype in mice with one or two renin genes. *Hypertension.* 2004;43(1):79-86.

88.   Kagami S. Involvement of glomerular renin-angiotensin system (RAS) activation in the development and progression of glomerular injury. *Clinical and experimental nephrology.* 2012;16(2):214-220.

89.   Forouzanfar MH, Liu P, Roth GA, et al. Global Burden of Hypertension and Systolic Blood Pressure of at Least 110 to 115 mm Hg, 1990-2015. *JAMA.* 2017;317(2):165-182.

90.   Timmermans S, Van Montagu M, Libert C. Complete overview of protein-inactivating sequence variations in 36 sequenced mouse inbred strains. *Proceedings of the National Academy of Sciences of the United States of America.* 2017;114(34):9158-9163.

91.   Garcia-Menendez L, Karamanlidis G, Kolwicz S, et al. Substrain specific response to cardiac pressure overload in C57BL/6 mice. *Am J Physiol Heart Circ Physiol.* 2013;305(3):H397-402.

92.   Nickel AG, von Hardenberg A, Hohl M, et al. Reversal of Mitochondrial Transhydrogenase Causes Oxidative Stress in Heart Failure. *Cell Metab.* 2015;22(3):472-484.

93.   Griffin KA, Picken MM, Churchill M, et al. Functional and structural correlates of glomerulosclerosis after renal mass reduction in the rat. *J Am Soc Nephrol.* 2000;11(3):497-506.

94.   Pellizzon MA, Ricci MR. Choice of Laboratory Rodent Diet May Confound Data Interpretation and Reproducibility. *Current developments in nutrition.* 2020;4(4):nzaa031.

95.   Fischer AW, Cannon B, Nedergaard J. Optimal housing temperatures for mice to mimic the thermal environment of humans: An experimental study. *Molecular metabolism.* 2018;7:161-170.

96.   Giles DA, Ramkhelawon B, Donelan EM, et al. Modulation of ambient temperature promotes inflammation and initiates atherosclerosis in wild type C57BL/6 mice. *Molecular metabolism.* 2016;5(11):1121-1130.

97.   Carrero JJ, Hecking M, Chesnaye NC, et al. Sex and gender disparities in the epidemiology and outcomes of chronic kidney disease. *Nat Rev Nephrol.* 2018;14(3):151-164.

98.   Mosca L, Barrett-Connor E, Wenger NK. Sex/gender differences in cardiovascular disease prevention: what a difference a decade makes. *Circulation.* 2011;124(19):2145-2154.

99.   Colafella KMM, Denton KM. Sex-specific differences in hypertension and associated cardiovascular disease. *Nat Rev Nephrol.* 2018;14(3):185-201.

100.   Diwan V, Small D, Kauter K, et al. Gender differences in adenine-induced chronic kidney disease and cardiovascular complications in rats. *Am J Physiol Renal Physiol.* 2014;307(11):F1169-1178.

101.   Clinkenbeard EL, Noonan ML, Thomas JC, et al. Increased FGF23 protects against detrimental cardio-renal consequences during elevated blood phosphate in CKD. *JCI Insight.* 2019;4(4):13.

102.   Muñoz-Castañeda JR, Rodelo-Haad C, Pendon-Ruiz de Mier MV, et al. Klotho/FGF23 and Wnt Signaling as Important Players in the Comorbidities Associated with Chronic Kidney Disease. *Toxins.* 2020;12(3).

Acknowledgements

Publication 2:

Impact of uremic toxins on endothelial dysfunction in chronic kidney disease: a systematic review

Eva Harlacher [1], Julia Wollenhaupt [1], Constance Baaten C.F.M.J.[1, 2*] and Heidi Noels[1,2*]

Shared last authorship

[1] Institute for Molecular Cardiovascular Research, University Hospital Aachen, Rheinisch-Westfälische Technische Hochschule Aachen University, Aachen, Germany

[2] Department of Biochemistry, Cardiovascular Research Institute Maastricht, Maastricht University, Maastricht, The Netherlands

Abstract: Patients with chronic kidney disease (CKD) are at a highly increased risk of cardiovascular complications, with increased vascular inflammation, accelerated atherogenesis and enhanced throm-botic risk. Considering the central role of the endothelium in protecting from atherogenesis and throm-bosis, as well as its cardioprotective role in regulating vasorelaxation, this study aimed to systemati-cally integrate literature on CKD-associated endothelial dysfunction, including the underlying molecu-lar mechanisms, into a comprehensive overview. Therefore, we conducted a systematic review of litera-ture describing uremic serum or uremic toxin-induced vascular dysfunction with a special focus on the endothelium. This revealed 39 studies analyzing the effects of uremic serum or the uremic toxins in-doxyl sulfate, cyanate, modified LDL, the advanced glycation end products N-carboxymethyl-lysine and N-carboxyethyl-lysine, p-cresol and p-cresyl sulfate, phosphate, uric acid and asymmetric dime-thylarginine. Most studies described an increase in inflammation, oxidative stress, leukocyte migration and adhesion, cell death and a thrombotic phenotype upon uremic conditions or uremic toxin treatment of endothelial cells. Cellular signaling pathways that were frequently activated included the ROS, MAPK/NF-κB, the Aryl-Hydrocarbon-Receptor

and RAGE pathways. Overall, this review provides de-tailed insights into pathophysi-ological and molecular mechanisms underlying endothelial dysfunction in CKD. Tar-geting these pathways may provide new therapeutic strategies reducing increased the car-diovascular risk in CKD.

Keywords: chronic kidney disease, uremic toxins, vascular dysfunction, vascular pathophysiol-ogy, endothelial cells, endothelial dysfunction, cardiovascular disease

1. Introduction

As kidney function gradually declines, the risk of cardiovascular complications in-creases. This is reflected by the fact that approximately half of the patients with severe chronic kidney disease (CKD stage 4-5) die from cardiovascular disease (CVD) [1], com-pared to 26% of patients with a healthy kidney function [2, 3]. Aortic valve steno-sis, left ventricular hypertrophy, myocardial ischemia and heart failure are the leading causes of death in CKD patients [4]. As main underlying mechanism of myocardial ischemia, CKD patients are at increased risk for atherosclerosis, an inflammatory pro-cess within the in-timal layer of the vessel wall [5]. In CKD, the formation and progres-sion of such athero-sclerotic lesions is highly accelerated [6]. Also, as CKD progresses, vascular stiffness in-creases [7], with vascular stiffness as an important predictor of cardiovascular mortality in CKD patients [8].

Endothelial dysfunction underlies both atherosclerosis and vascular stiffness and is associated with an increased risk of cardiovascular death [9]. Coronary endotheli-al-dependent vasoreactivity was identified as a predictor of future cardiovascular events and disease progression [10].

Atherosclerotic lesions start out as patches of dysfunctional endothelial cells (ECs) [11]. As the endothelial barrier becomes dysfunctional and loses its integrity, permea-bility increases and low-density lipoproteins (LDL) accumulate within the vessel wall, upon which LDL becomes oxidized and an inflammation process is initiated [12]. Chemokines are secreted and adhesion molecules are expressed by inflamed ECs, triggering leukocyte recruitment, their adhesion on ECs as well as their migration into the vessel wall [11, 13]. Furthermore, increased oxidative stress and reactive oxygen species (ROS) production re-duce the bioavailability of nitric oxide (NO) [13], which in

turn causes a reduction in EC-dependent vasodilation and as such an increase in vascular stiffness. Concomitantly, dysfunctional ECs lose their antithrombotic properties and prothrombotic properties pre-vail, further increasing the risk of atherothrombosis [14]. Moreover, dysfunctional ECs show reduced survival and proliferation capacity, processes needed to restore the protec-tive endothelial barrier and counteract injury-induced stenosis after vascular injury [15, 16]. Combined, pathophysiological pro-cesses of inflammation, oxidative stress as well as impaired survival, proliferation and repair of ECs contribute to endothelial dysfunction and CVD (Figure 1A).
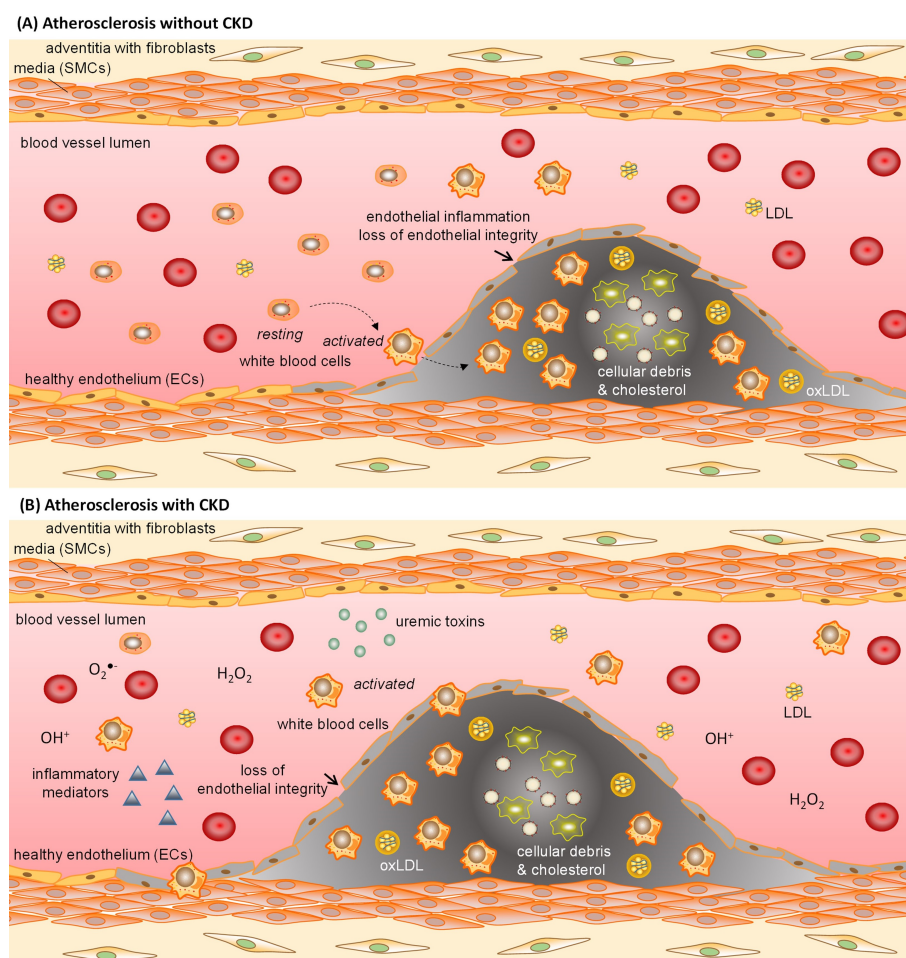
Figure 1. Endothelial inflammation and loss of endothelial integrity contribute to endothelial dysfunction and the formation of atherosclerotic lesions in the vessel wall. Atherosclerosis is characterized by en-dothelial inflammation and an increased vascular permeability. Inflamed endothelial cells secrete chem-okines that recruit white blood cells, which migrate through the dysfunctional endothelial barrier into the vessel wall. Also, LDL migrates into the vessel wall where it is oxidized to oxLDL (A). In patients with CKD, the process of atherosclerotic lesion formation is advanced because of CKD-associated factors such as systemic chronic low-grade in-flammation, increased markers of oxidative stress and lipoprotein oxidation, as well as the ac-cumulation of uremic toxins, all promoting damage to the vessel wall (B). ECs = endothelial cells; LDL = low density lipoprotein; oxLDL = oxidized LDL; SMCs = smooth muscle cells.

Several studies indicate that CKD-associated factors, like systemic chronic low-grade inflammation, increased oxidative stress and uremic toxins accelerate atherosclerosis in CKD (Figure 1B), although the underlying molecular mechanisms are not fully understood [17, 18]. CKD patients exhibit a systemic, chronic low-grade inflammation as well as increased oxidative stress even in early stages of CKD [18-20], characterized by high levels of circulating inflammatory proteins (CRP, IL6) and oxidative stress biomarkers [19]. The more CKD progresses, the more oxidative stress levels increase [20]. Further, it was shown that markers of oxidative stress (including lipid peroxidation markers and lipoprotein oxidation propensity, among others) inversely correlated with endothelial-dependent vasodilation in CKD patients, independent of classical risk factors of atherosclerosis such as gender, age, blood pressure, diabetes, lipid-lowering treatment [21]. Modification of li-pids, such as oxidation of LDL, is increased in CKD and further promotes vascular dam-age [22]. Also, high phosphate levels typical of CKD-related mineral bone disorders cause endothelial dysfunction by changing EC morphology, decreasing viability, and promoting senescence [6].

Upon kidney dysfunction, solutes accumulate in the circulation that are normally excreted by the kidneys. The accumulation of these uremic toxins causes a gradual endogenous intoxication. In literature, more than 140 uremic toxins have been described to be elevated upon kidney dysfunction [23, 24]. Uremic toxins such as indoxyl sulfate (IS) and p-cresyl sulfate (pCS) have been associated with an increased risk of cardiovascular events and cardiovascular mortality in CKD patients. Mechanistically, many of these uremic toxins have been linked to inflammation and oxidative stress [25, 26], but also to arterial stiffness and endothelial dysfunction in vitro [27]. Given the central role of the en-dothelium in preserving vascular health and counteracting atherosclerosis and cardio-vascular risk, this manuscript systematically reviewed uremic toxin-induced EC dysfunc-tion and its implications for cardiovascular disease specifically in the context of CKD.

2. Materials and Methods

This systematic review is in accordance with the guidelines provided by the PRISMA statement [28]. The completed PRISMA checklist can be found in the supplemental mate-rials (Table S2).

2.1. Search strategy

An advanced literature search was performed in PubMed and Web of Science for studies describing the mechanisms underlying vascular pathophysiology in CKD, with a special focus on CKD-induced endothelial dysfunction. Additionally, to compare pathological signaling processes within different cell types present in atherosclerotic plaques, studies on CKD-induced dysfunction of smooth muscle cells, monocytes and macro-phages were retrieved. Studies published until June 2021 were assessed. Supplemental Table S2 provides an overview of the terms and conditions that were used in the literature search.

2.2. Study selection criteria

Two reviewers (E.H. and J.W.) independently selected studies presenting original data using predefined eligibility criteria. Studies that described mechanisms responsible for CKD-induced vascular dysfunction were included for further analysis. These studies ei-ther described the effect of uremic serum or individual uremic toxins on endothelial func-tion. Reports on the effects of CKD on different cell types present within the ath-erosclerotic plaque were also taken along. In case markers of endothelial function or uremic tox-in-induced signaling pathways were measured in CKD patient populations, these patient studies were incorporated as well. Duplicates, review papers, poster ab-stracts and papers not written in the English language were excluded as well as studies that concentrated on CKD-induced vascular calcification or studies in which mechanis-tic insight was lacking. Both reviewers had to agree on inclusion. In case of disagree-ment, a third reviewer (C.B.) was consulted to achieve consensus. A graphical over-view of the number of in- and ex-cluded studies throughout the selection process is presented in Figure 2.

2.3. Data extraction

To summarize the pathophysiological effects of uremia or individual uremic toxins on endothelial cells, studies were classified based on the toxins investigated and their key effects on endothelial function. These key effects were defined as inflammation, oxi-dative stress, cell death, leukocyte adhesion and migration, cell proliferation and thrombosis. For a description of molecular mechanisms underlying uremic toxin-in-duced endothelial dysfunction, information on signaling pathways was extracted from in vivo and in vitro studies. From patient studies, information on markers for endothelial function or insights into uremic toxin-induced signaling pathways was extracted.

3. Results and discussion

3.1. Study selection

Using predefined literature search terms (Table S1), our search initially included 323 articles (105 publications identified via PubMed and 218 from Web of Science). After ex-cluding non-English publications and duplicates, 242 publications were left. Through ab-stract screening, 176 publications were excluded as being either reviews or out of scope. Of the remaining 66 papers, the full text was screened. In total, 39 publications were included in the systematic review and mechanistic data were ex-tracted. The selection procedure is shown in Figure 2.
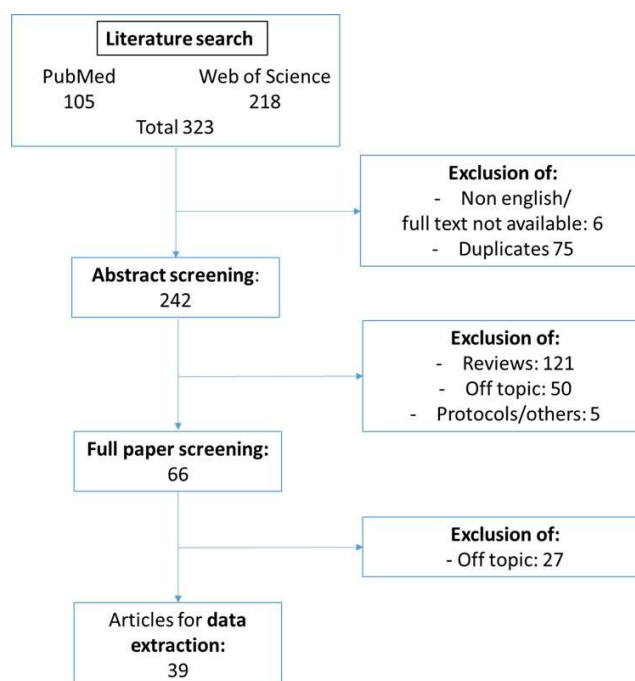
Figure 2. Flow diagram of study selection. Flow diagram of the selection of original papers il-lustrating the number of in- and excluded studies throughout the selection process.

3.2. Pathophysiological effect of uremic toxins on endothelial cells

To provide insights into how a reduced kidney function may impact endothelial func-tion, our literature search retrieved studies in which endothelial cells were treated with uremic serum or with individual uremic toxins.

Uremic serum triggered processes of oxidative stress, cell adhesion as well as in-flam-mation. Decreased antioxidant enzyme activity as well as elevated lipid peroxidation indicated redox imbalances in endothelial cells treated with uremic serum [29]. Further, in endothelial cells, oxidative stress was induced by uremic serum as reflected by an

increase in the formation of reactive oxygen species (ROS) [30, 31] via a RAGE-NF-κB dependent pathway [30]. RAGE-NF-κB signaling as well as glutathione S-transferase μ1 (GSTM-1), which is a downstream gene in the Aryl-Hydrocarbon-Receptor (AhR) signaling pathway, were also responsible for a uremic serum-mediated increase in endothelial expression of adhesion molecules [29, 30]. Among inflammatory mediators dysregulated in CKD [29], increased levels of VCAM-1 and the pro-inflammatory cytokine MCP-1 in uremic endo-thelial cells led to increased monocyte adhesion and thus increased inflammation [30, 32].

Among the uremic toxins studied for direct effects on endothelial cells, our literature search identified studies investigating indoxyl sulfate, cyanate, the advanced glycation end products (AGEs) N-carboxymethyl-lysine (CML) and N-carboxyethyl-lysine (CEL), p-cresol and p-cresyl sulfate, uric acid and asymmetric dimethylarginine (ADMA) [33, 34]. Also, phosphate and post-translationally modified LDL, both with increased levels in advanced CKD [22, 35, 36], were studied for direct effects on endothelial cells. Table 1 summarizes the effect of these molecules on endothelial cells, classified in effects on in-flammation, oxidative stress, leukocyte adhesion and migration, proliferation, cell death and thrombosis.

Table 1. Effects of uremic toxins on key mechanisms in endothelial cells.

Toxin	Inflamma-tion	Oxidative stress	Cell death	Migration/ Adhesion	Prolifera-tion	Throm-bosis
Indoxyl sulfate	+ [37-40]	+ [31, 37-39, 41, 42]	+ [31, 40, 42, 43]	+ [37, 39, 40]	- [31	
Cyanate	+ [44, 45]			+ [44]		+ [45]
cLDL	+ [46, 47]		+ [47, 48]	+ [46]		
AGE	+ [49]	+[30, 49, 50]	+ [30]	+ [30, 51]	- [51]	
p-Cresol/ p-cresyl sul-fate	+ [52]	+[30, 31, 52, 53]	+ [30, 31, 54]	+ [30, 52]	- [31]	
Phosphate		+[55]	+ [55, 56]			+ [57]
ADMA			+ [58]			
Uric acid		+ [59-61]	+ [60, 61]			

(+) increased; (-) decreased effect

ADMA = asymmetric dimethylarginine; AGE = advanced glycation end products; cLDL = carbamylated LDL; LDL = low density lipoproteins

3.3. Identification of molecular mechanisms underlying uremic toxin-induced endothelial dysfunction

3.3.1. Tryptophan-derived toxins trigger inflammation and oxidative stress in endothelial cells

Tryptophan-derived indoxyl sulfate (IS), a protein-bound uremic toxin which highly accumulates in CKD patients, and which can only to a minor extent amount be removed through dialysis, has been frequently investigated in the context of CKD-induced endothe-lial dysfunction. Of the 11 papers identified through our literature search that report on IS-induced signaling and cellular effects, eight describe the effects of IS on endothelial function. Three studies reported on different cell types, one of which examined the cross-talk between the effects of IS on macrophages and endothelial dysfunction. Oxidative stress, inflammation, cell death as well as reduced proliferation are central to IS-induced endothelial dysfunction (Table 1) [31, 37-43]. The main mechanisms and the contributing signaling pathways are summarized in Figure 3.
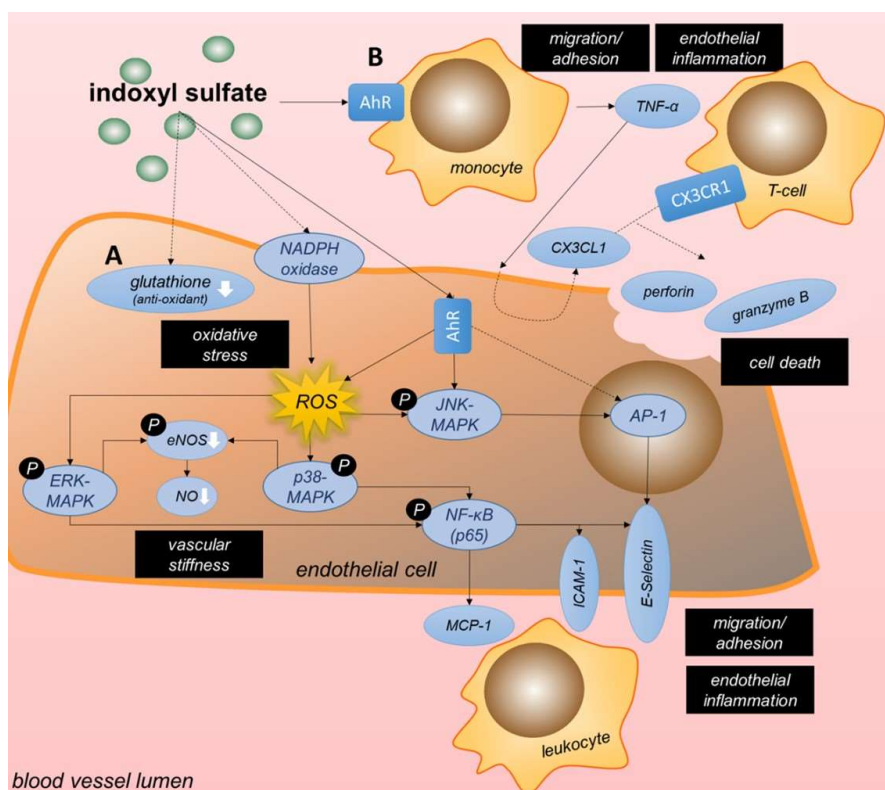
Figure 3. Mechanisms underlying indoxyl sulfate-induced endothelial dysfunction. The uremic toxin indoxyl sulfate (IS), which highly accumulates in CKD patients, leads to endothelial dys-function by enhancing oxidative stress, endothelial inflammation, recruitment and adhesion of inflammatory cells, cell death as well as by reducing endothelial proliferation. Also, it reduces endothelial nitric oxide production, contributing to enhanced vascular stiffness. As underlying mechanisms, IS induces the production of reactive oxygen species (ROS) and binds to the Aryl Hydrocarbon Receptor (AhR), thereby enhancing

intracellular signaling through MAP Kinases (ERK, p38, JNK) and NF-κB (p65), triggering pro-inflamma-tory and apoptotic responses in en-dothelial cells (A). In addition, IS-AhR pro-inflammatory activation of monocytes contributes to endothelial dysfunction (B).

With the focus on the cell signaling pathways, the figure does not take into account a differentiation between basal and apical side of the cell. AhR = Aryl Hydrocarbon Receptor, AP-1 = activator protein-1; eNOS = en-dothelial nitric oxide synthase; MAPK = mitogen activated protein kinase; NF-κB = nuclear factor kappa B; NO = nitric oxide; p-eNOS = phosphorylated, active eNOS; ROS = reactive oxygen species; TNF = tumor necrosis factor.

Six out of eight studies detected an increase in ROS levels and thus oxidative stress upon IS treatment of endothelial cells [31, 37-39, 41, 42]. Here, oxidative stress was in-duced by activating NADPH oxidase [38, 41], reducing levels of the antioxidant glu-tathi-one [41] or by triggering the AhR pathway [37] (Figure 3A). Subsequently, these high levels of IS-induced ROS resulted in an upregulated expression of MCP-1 and ICAM-1, promi-nent mediators of inflammatory cell recruitment and adhesion, by ROS-dependent ERK/MAPK-induced activation of NF-κB signaling [38, 39, 42]. But not only IS is linked to inflammation in CKD patients, also tryptophan-derived 3-hydroxyan-thranilic acid has been associated with levels of the pro-inflammatory chemokines MCP-1 as well as mac-rophage inflammatory protein-1β (CCL4) in CKD patients [62]. Contributing to IS-induced oxidative stress, IS also decreased NO production and eNOS phosphorylation in endothe-lial cells via the ROS-ERK/MAPK pathway [42], alt-hough without effects on mRNA ex-pression of eNOS [41]. Additionally, high ROS lev-els upon IS were shown to enhance TNF-α-induced E-selectin expression by increas-ing NF-κB activation and AP-1 over JNK phosphorylation [37]. The antioxidants vitamin C, N-acetylcysteine and vitamin E could reduce IS-induced oxidative stress by pre-venting the activation of NADPH in a dose-dependent fashion [41]. Klotho protein was identified as another negative regulator of IS-induced ROS formation, and could also abrogate the reduction in eNOS phosphory-lation and NO production observed in en-dothelial cells upon IS-induced p38/MAPK-NF-κB signaling [42]. Furthermore, the ki-nases integrin linked kinase (ILK) and AKT, whose activity was upregulated by IS, counteracted IS-induced ROS production and apoptosis of endothelial cells as nega-tive feedback mechanism [31], although the un-derlying mechanisms were not investi-gated.

As introduced above, IS exposure also activates the AhR pathway. AhR is a lig-and-activated transcription factor expressed in macrophages, monocytes [40, 63] and en-dothelial cells [64] - amongst other cells - and its activation can trigger an inflammatory response. For example, stimulation with AhR agonists has been shown to increase

cho-lesterol levels in macrophages and to trigger the release of various inflammatory markers like IL-8 and MCP-1 [65, 66]. Further, activation of the AhR pathway worsens atheroscle-rosis in mice [67]. Amongst other ligands, AhR signaling is triggered by IS, as shown in endothelial cells [37], monocytes [40] and macrophages [68, 69] in vitro. As underlying mechanism of pro-atherogenic effects of AhR signaling in endothelial cells, IS increased leukocyte-endothelium interactions in TNF-α-treated mice through endothelial AhR sig-naling. In vitro, IS-AhR signaling upregulated endothelial E-selec-tin expression through activator protein-1 (AP-1) transcriptional activity [37]. Of note, also other trypto-phan-derived uremic toxins have been shown to interact with AhR, like indole acetic acid (IAA), which triggers endothelial inflammation and oxidative stress via AhR-dependent signaling [70]. AhR expression on peripheral blood mono-nuclear cells (PBMCs) from CKD patients positively correlated with plasma levels of IAA [71].

Besides its inflammatory effects, increased IS levels have been shown to cause apop-tosis of endothelial cells via the COX-2/PGE2 axis, which was upregulated by a decreased expression of miR-214. Subsequently, PGE2 increased the expression of caspase-3 and BAX and caused an increase in the levels of cleaved caspase-3 in mouse aortic endothelial cells [43]. However, studies in human umbilical vein endothe-lial cells contradicted this effect on caspase-3 protein expression and apoptosis in re-sponse to similar amounts of IS [42]. Another study revealed an indirect effect of IS on endothelial apoptosis through pro-inflammatory responses in monocytes and subse-quent T-cells. Also, in monocytes and macrophages, IS can activate the AhR pathway, which mediated the secretion of high concentrations of TNF-α [40, 69] via crosstalk between the NF-κB and AhR pathways. These increased levels of TNF-α subsequently initiated CX3CL1 production in endothelial cells [40]. This triggered the recruitment and activation of CX3CR1-expressing T-cells with subsequent secretion of cytotoxic gran-ules containing perforin and granzyme B, ultimate-ly causing apoptosis of endothelial cells [40] (Figure 3B). In patients with kidney failure, increased plasma CX3CL1 levels have been detected [40] with higher CX3CL1 levels asso-ciated with an increased overall mortality as well as a higher prevalence of CVD in a CKD cohort [72]. In mac-rophages, IS also increased pro-IL-1β mRNA expression through NF-κB/p65 signaling, however, without effect on mature IL-1β protein levels due to IS-mediated reduction in NLRP3 expression [68]. Finally, in contrast to the pro-apoptotic effect of IS on endo-thelial cells discussed above, it was reported that vascular smooth muscle cells (SMCs)

stimulated with IS were more proliferative, with the pro-proliferative cyclin D1 and p21, and the anti-apoptotic p53 upregulated in a glucose transporter-1 (GLUT1) dependent fashion. IS reduced the phosphorylation of AKT and TSC2, thereby increasing mTOR/S6K signaling to drive GLUT1 expression [73].

3.3.2. Cyanate triggers inflammatory signaling and protein carbamylation

In CKD patients, cyanate levels can rise to three times the normal levels resulting from the conversion of the uremic toxin urea, which levels are also highly increased in CKD [74-76]. Another endogenous source of cyanate is the oxidation of thiocyanate by the phagocyte protein myeloperoxidase (MPO) [77, 78]. High local MPO concentrations have been found in the subendothelial matrix of inflamed vascular tissue, which suggests that vascular endothelial cells are particularly exposed to high cyanate levels [44, 79]. Six pub-lications identified by our literature search examined the relevance of cyanate in context of CKD-induced endothelial dysfunction (Table 1). The mechanisms are summarized in Figure 4.
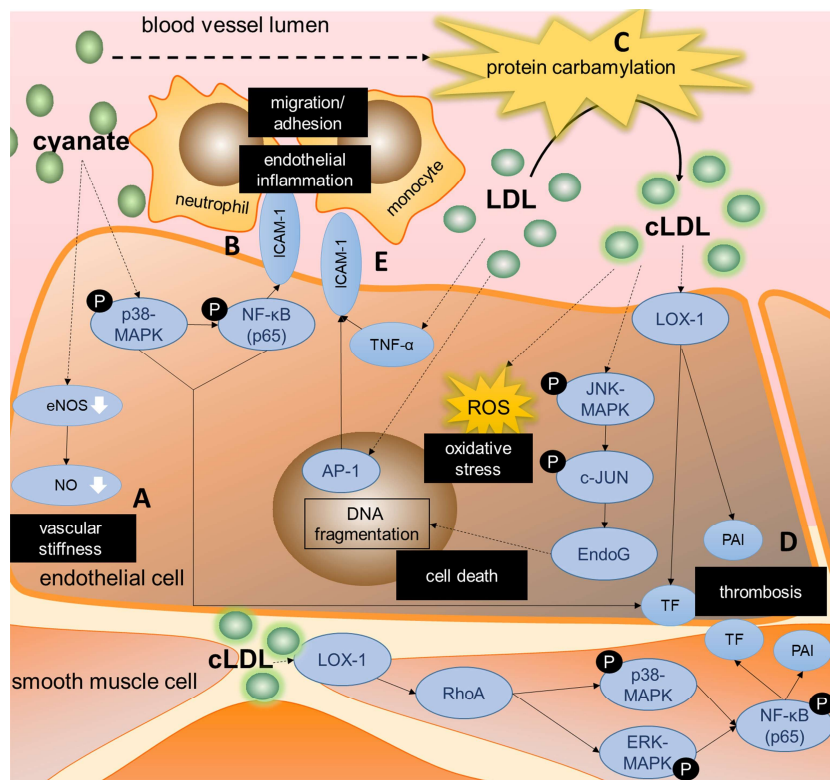
Figure 4. Mechanisms underlying cyanate or (modified) LDL-induced endothelial dysfunction. Increased cyanate levels as in CKD patients induce cellular signaling triggering endothelial dysfunction as displayed in increased vascular stiffness (A) as well as enhanced endothelial in-flammation, triggering the recruitment and adhesion of inflammatory cells (B). Furthermore, cyanate-induced protein carbamylation leads to carbamylated low-density lipoprotein (cLDL), which can trigger oxidative stress and cell death (C) and can increase thrombotic risk through increases in tissue factor and PAI (D). Also, LDL

was shown to contribute to endothelial inflam-mation by upregulating pro-inflammatory cytokines and adhesion molecules, triggering in-flammatory cell recruitment and adhesion (E).

AP-1 = activator protein-1; cLDL = carbamylated LDL; EndoG = endonuclease G; eNOS = endothelial nitric oxide synthase; ICAM = intracellular adhesion molecule; LDL = low density lipoprotein; LOX-1 = Lec-tin-like oxidized low density lipoprotein receptor-1; MAPK = mitogen activated protein kinase; NF-kB = nu-clear factor kappa B; NO = nitric oxide; PAI = plasminogen activator inhibitor; TF = tissue factor; TNF = tumor necrosis factor.

The important role of cyanate in the development of endothelial dysfunction and vas-cular inflammation in CKD patients was shown in two publications by El Gamal et al. [44, 45]. They showed that cyanate-treated mice produced lower nitrite levels and dis-played decreased acetylcholine-induced vasorelaxation [45]. Mechanistically, cyanate re-duced eNOS protein levels and its phosphorylation in mouse aortas, contributing to a de-creased NO production [45] (Figure 4A). Further, in vitro as well as in vivo, cya-nate in-duced the expression of ICAM-1 in endothelial cells by activating the p38-MAPK and NF-κB pathways. This triggered enhanced neutrophil adhesion, thereby contributing to vascular inflammation [44] (Figure 4B). In patients with kidney failure, ICAM-1 plasma levels correlated with the carbamyllysine level as marker of cyanate formation [44].

Furthermore, urea-derived cyanate is known to mediate post-translational 'car-bam-ylation' of proteins [80], as for example demonstrated for low-density lipoproteins (LDL) [44]. Carbamylated LDL (cLDL) is associated with endothelial injury and athero-scle-rosis in mice [35, 81-86]. Aposotlov et al. showed that in vitro, elevated cLDL-levels led to endothelial mitotic cell death by DNA fragmentation [48]. They described caspa-se-independent signaling via JNK/c-JUN, resulting in DNA fragmentation by endonucle-ase G [48] (Figure 4C). Their data suggested that other DNA-destroying mechanisms are also involved, with a role of Mitogen-activated protein kinase (MEK) and ERK1/2 kinases, but precise details are unknown at present [48].

In regard to atherothrombosis, in vitro cyanate was shown to upregulate the expres-sion of tissue factor and plasminogen activator inhibitor-1 (PAI-1) in endothelial cells, key mediators in mediating coagulation and inhibiting fibrinolysis [45] (Figure 4D). Also, both mRNA expression and activity of tissue factor and PAI-1 were upregulated in ar-terial tissue and plasma of mice treated with cLDL as well as in vitro in aortic SMCs and endo-thelial cells [47]. In aortic SMCs, the increase in tissue factor and PAI-1 was mediated by binding of cLDL to the oxidated LDL-receptor LOX-1 and the subsequent activation of the RhoA/ERK/p38/NF-κB pathway (Figure 4D). In whole blood of cLDL-

treated mice, the upregulation of tissue factor led to increased thrombin generation. In addition to effects of cLDL on the coagulation cascade, cLDL also enhanced agonist-induced platelet aggrega-tion by phosphorylating p38 and translocating LOX-1 to the platelet surface [47].

Also unmodified LDL was shown to cause endothelial inflammation by, among oth-ers, increasing monocyte adhesion [46]. LDL increased the nuclear binding activity of AP-1 in endothelial cells, which in turn upregulated TNF-α and ICAM-1 expression me-diating monocyte adhesion [46] (Figure 4E). LDL can be divided into two subclasses based on size, CKD patients have increased levels of small dense LDL compared to healthy con-trols [22, 87]. Ambrosch et al. differentiated between these LDL subtypes and showed that the smaller LDL particles (diameter <25.5nm) caused a stronger in-crease in AP-1 binding activity in HUVECs and subsequent TNF-α and ICAM1 expres-sion compared to the larger LDL particles (diameter >25.5nm), resulting in more mon-ocyte adhesion [46].

Besides carbamylation, also other post-translational modifications of lipoproteins have been studied in the context of CKD and CVD [12, 22]. Our search revealed a study by Tao et al., who investigated the mechanisms behind acetylated LDL (AcLDL)-induced apoptosis in macrophages [88]. Endoplasmic reticulum stress - indicated by increased CHOP and decreased B-cell lymphoma-2 (BCL-2) expression - was sug-gested to be a key mediator of AcLDL-induced macrophage apoptosis [88].

3.3.3. AGEs are an important group of uremic toxins inducing endothelial dysfunction

Advanced glycation end (AGE) products belong to the protein-bound uremic toxins and are highly increased in CKD [89]. AGEs are proteins or protein degradation prod-ucts that become post-translationally modified upon exposure to sugars. The trans-membrane receptor for advanced glycation end products (RAGE) is a cell surface marker involved in cell migration, adhesion, and oxidative stress [30, 49-51]. Ten pa-pers from our search dis-cussed the AGE-RAGE signaling pathway in the context of uremic toxin-induced endo-thelial dysfunction. RAGE as well as its binding partners were shown to have a pro-inflammatory and pro-oxidative effect in CKD and as such to promote endothelial dysfunction. Mechanisms are summarized in Figure 5A.

It was demonstrated by three groups that AGEs (including protein bound N-carbox-ymethyl-lysine (CML) and methyl-glyoxal (MG)) induced RAGE-signaling and en-hanced RAGE expression in endothelial cells [30, 49, 50]. In CKD patients stage 1-5,

glomerular filtration rate as measure of kidney function was inversely correlated with RAGE mRNA levels in PBMCs as well as total CML levels in serum [50]. RAGE-mediated ROS formation is reported in response to AGEs in endothelial cells [30]. CML-mediated RAGE signaling in endothelial cells decreased endothelial expression of transcription factor Krüppel like factor 2 (KLF2) via NF-κB and subsequently increased ROS production. These effects of CML were enhanced with exposure of endothelial cells to shear stress [30]. Further, it was shown that AGEs inhibit eNOS expression [50] as well as eNOS phos-phorylation via RAGE in endothelial cells [49]. As underlying mechanism, RAGE activa-tion by AGEs decreased SIRT3 expression, which in turn led to mitochondrial oxidative stress. Consequently, NOX-2 activity was upregulated, increasing cytosolic oxidative stress and thereby reducing eNOS phosphorylation [49]. The reduction in KLF2 expres-sion also resulted in an increased VCAM1 surface expression and as such supported monocyte adhesion [30]. However, in hemodialysis patients, plasma levels of the AGEs CML and MG did not correlate with increased circulating levels of VCAM-1 [90] and nei-ther with soluble ICAM levels [44].

Also non-RAGE related cellular effects of AGEs toxins, such as CML and N-carbox-yethyl-lysine (CEL), were identified in our literature search. Zhu et al. identified CML and CEL to induce endothelial inflammation and oxidative stress independently of RAGE signaling, and also revealed these AGEs to negatively influence endothelial pro-genitor cell (EPC) adhesion and proliferation [51], thus further contributing to a dys-func-tional endothelium.
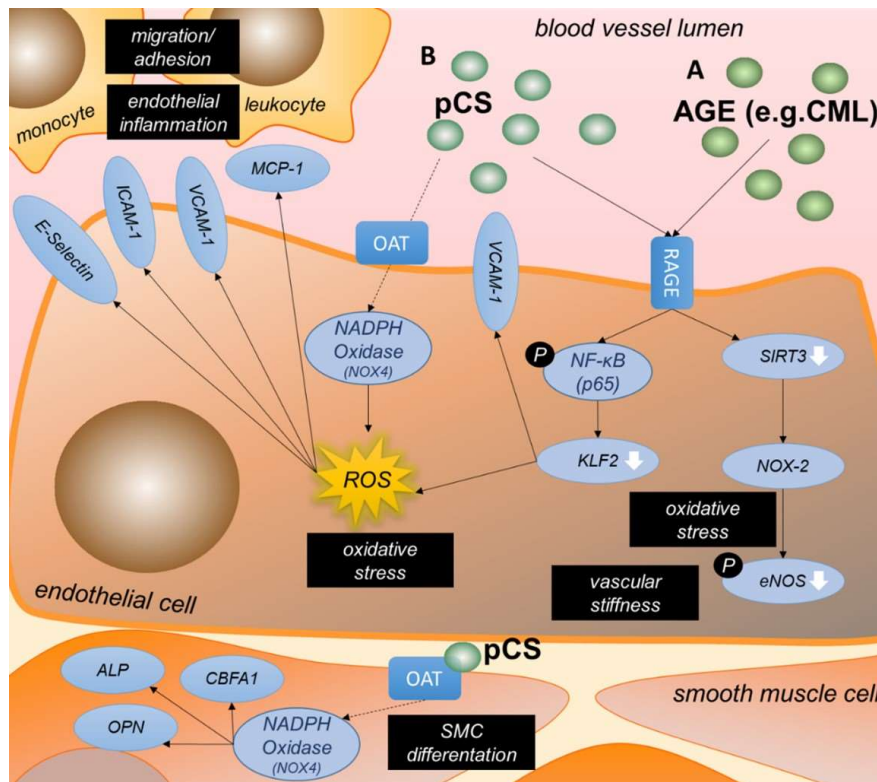
Figure 5. Mechanisms underlying p-cresyl sulfate or AGE-induced endothelial dysfunction. By activating RAGE, AGEs mediate oxidative stress and reduce vasoreactivity by decreasing eNOS activation in endothelial cells. Further, AGEs as well as p-cresyl sulfate increase ROS generation via KLF2. ROS increase endothelial inflammation by enhancing surface expression of chemo-kines (e.g. MCP-1) and surface adhesion proteins (e.g. VCAM-1, ICAM-1, E-Selectin), triggering leukocyte recruitment and binding (A). Cellular uptake of p-cresyl sulfate by endothelial cells as well as SMCs takes place via organic anion transporters. This results in the activation of NADPH oxidase NOX-4, leading to the differentiation of SMCs and ROS generation in endothelial cells (B).
ALP = alkaline phosphatase; CBFA = core-binding factor alpha; eNOS = endothelial nitric oxide synthase; ICAM = intracellular adhesion molecule; KLF = krüppel like factor; MCP = monocyte chemoattractant pro-tein; NADPH = nicotinamide adenine dinucleotide phosphate; NF-κB = nuclear factor kappa B, OAT = or-ganic anion transporters; OPN = osteopontin; ROS = reactive oxygen species; SIRT = sirtuin; NOX = NADPH oxidase; SMC = smooth muscle cell; VCAM = vascular cell adhesion molecule.

3.3.4. p-cresyl sulfate contributes to oxidative stress and inflammation in endothelial cells

P-cresol occurs mainly in its sulfate conjugated form (>95%), called p-cresyl sulfate (pCS) [91]. It is this protein-bound uremic toxin that is identified to be associated with CVD in hemodialysis patients [92]. Five papers from our literature search discussed the effects of p-cresol or pCS on endothelial function.

Three studies showed a connection between pCS, oxidative stress and endothelial dysfunction (Figure 5B). Not only AGEs, as discussed above, but also pCS binds to RAGE, thereby activating NF-κB signaling in endothelial cells and as such decreasing KLF2 ex-pression [30]. pCS stimulation of endothelial cells also resulted in NADPH

oxi-dase-mediated ROS formation, independent of RAGE, and mainly mediated by free pCS rather than protein-bound pCS. Especially in human aortic SMCs the effect appeared to be induced by free pCS, as the addition of albumin reduced the effect by 90% [53]. pCS accu-mulates in the kidney via the organic anion transporters (OAT) receptor [93]. pCS was also shown to be absorbed by vascular endothelial and smooth muscle cells via OAT and sub-sequently enhanced expression of NOX-4, a component of NADPH oxidase. This triggered endothelial MCP-1 expression in vascular SMCs, as well as upregulated the expression of alkaline phosphatase (ALP) as early pheno-typic marker of osteoblast differentiation [53]. Furthermore, an increase in intracellular pCS via OAT is directly associated to osteogenic SMC differentiation, as shown by high expression of other osteoblast-specific proteins os-teopontin (OPN) and core-binding factor alpha 1 (CBFA1) as well as activation of ALP. In pCS-treated 5/6-ne-phrectomized rats this connection of MCP-1 levels in serum, vascular OPN expression, and vascular ALP activity accompanied by the induction of NOX-4 ex-pression could be confirmed [53]. Also, Jing et al. confirmed the pCS-induced increase of NOX-4 via ROS in endothelial and smooth muscle cells in vivo and in vitro and in addi-tion showed an increase in NOX-1 and p22phox, proteins involved in ROS production [52].

pCS also affected leukocyte adhesion and migration. Increases in NOX-1, NOX-4 and p22phox by pCS led to higher levels of MCP-1, TNF-α, ICAM, VCAM as well as E-Selectin in endothelial cells in vitro, with increased expression of these pro-inflam-matory chemo-kines and adhesion molecules also confirmed in aortic tissue of ApoE-/- mice with CKD and pCS treatment [52]. In hemodialysis patients, pCS was shown to be an independent risk factor for the presence of carotid atherosclerotic plaque [52]. Furthermore, in hemodi-alysis patients, the increase in free and total p-cresol was re-ported to correlate with the number of endothelial microparticles (EMPs) and shed EMPs. In vitro, the Rho kinase pathway was shown to be mediating this increase in shed EMPs and EMP numbers in response to both p-cresol and pCS as well as uremic serum [54].

Finally, Garcia-Jerez et al. showed that in addition to uremic serum and IS, also p-cresol induced ROS-mediated apoptosis of endothelial cells. However, similarly as shown for IS, p-cresol also triggered a protective feedback mechanism by activating integ-rin-linked kinase (ILK) via an unknown pathway [31], thereby upregulating AKT

phos-phorylation at Ser471 and as such counteracting p-cresol-induced ROS and apoptosis [31].

3.3.5. Phosphate reduces NO production and triggers inflammation in vascular cells

In CKD patients serum phosphate levels are increased and associated with increased cardiovascular risk and mortality [94, 95]. Hyperphosphatemia (>3 mM) is associated with inflammation and oxidative stress and contributes to endothelial dysfunction as well as to calcium deposition in SMCs [55, 57, 96, 97].

The effect of high phosphate levels in the context of CKD and CVD was addressed in four publications within our systematic literature search [55-57, 97]. In addition to hyper-phosphatemia, one of these papers also examined the endothelial effects of low phosphate in comparison.

Phosphate levels that deviated upwards or downwards from the physiological value of 1 mM led to reduced NO production in endothelial cells [55]. Exposure of endothelial cells to increased extracellular phosphate resulted in increased intracellular phosphate concentrations mediated by sodium-dependent Pi transporters (PiT1/PiT2) [57]. Hyper-phosphatemia reduced intracellular calcium and increased PKCβ2 signaling, leading to decreased eNOS abundance and reduced NO production in endothelial cells [55]. Also, hypophosphatemia reduced NO production [55]. On signaling level, hyper-phosphatemia triggered a downregulation of PI3K/AKT/NF-κB and MAPK/NF-κB pathways in endothe-lial cells, whereas in hypophosphatemia these pathways were increased [55].

Additionally, hyperphosphatemia as well as hypophosphatemia negatively affected cell viability of endothelial cells [55]. High phosphate levels were associated with a decreased BCL-XL/BAX ratio, and although low phosphate levels increased this ratio, also hypophosphatemia increased the number of apoptotic endothelial cells [55]. Hsu et al. described an inhibition of AKT/mTOR phosphorylation caused by increased phosphate in endothelial cells, with a subsequent increase in autophagic activity [56]. Increased au-tophagic activity was confirmed in CKD rats along with increased cleaved caspase 3 as apoptotic marker in endothelial cells [56], with inhibition of autophagy further increasing the amount of apoptotic cells [56].

Also, in endothelial cells, elevated phosphate levels increased membrane blebbing and enhanced the release of procoagulant endothelial microparticles. Microparticles

from phosphate-treated cells were comparable in terms of total protein amount when compared to microparticles released from healthy cells, but given the increase in phosphatidyl serine exposure, phosphate-induced microparticles were more supportive of thrombin genera-tion [57]. Apoptosis and oxidative stress were excluded as the major cause of microparti-cle release. Protein phosphorylation differed in phosphate-treated ECs, based on which metabolic stress was suggested as a potential cause of membrane blebbing. Abbasian et al. hypothesized that hyperphosphatemia led to hyper-phosphorylation of phosphatases like PTPase and PSPase, decreasing their activity indicated by a decreased phosphorylation of Tropomyosin-3 (TM-3) [57].

Finally, in vascular SMCs, hyperphosphatemia led to an increased ROS formation, which in turn led to enhanced formation of inflammatory proteins like TNF-α, ICAM-1, IL-6, IL-1ß and IL-8, contributing to increased vascular inflammation [97].

3.3.6. High ADMA levels as in CKD lead to increased endothelial cell death

High levels of asymmetric dimethylarginine (ADMA) have been associated with an in-creased cardiovascular risk [58, 98, 99]. Our systematic literature search revealed one study that examined ADMA in the context of endothelial dysfunction (Table 1), showing that in vitro treatment of endothelial cells with ADMA induced apoptosis [58]. Endoplas-mic reticulum (ER) stress increased as cytosolic Ca2+ levels rose and ER Ca2+ levels de-clined due to the inhibition of the sarco/endoplasmic reticulum calcium-ATPase [58]. Further, increased phosphorylation of protein kinase RNA-like ER kinase (PERK) and in-ositol requiring enzyme-1 (IRE1) was observed, both known to be associated with cell death [100, 101]. Additionally, ADMA treatment of endothelial cells enhanced levels of the ER chaperone 78-kDa glucose-regulated protein (GRP78/BiP), indicating defective protein folding and degradation. Together with decreased levels of apoptosis inhibitor BCL-2 and increased cleavage of caspase-3, a critical executioner of apopto-sis, ADMA was shown to be an inducer of apoptosis in endothelial cells [58].

3.3.7. Uric acid increases oxidative and ER stress as well as endothelial cell apoptosis

Uric acid, a water-soluble uremic toxin that is the end product of purine metabolism, was discussed in three publications identified in our systematic literature search. Uric ac-id levels are highly increased in patients suffering from CKD stage 4-5 even after hemodi-alysis [102]. Hyperuricemia contributes to the genesis and progression of CVD and CKD [103, 104], with as underlying mechanisms increased oxidative stress and

endothelial dysfunction [103]. Besides many other proteins whose expression is influenced by high uric acid levels, enhanced alanine dehydrogenases (ALDR) was identified to mediate in-creased uric acid-induced ROS production in endothelial cells [59]. Komori et al. described that hyperuremic conditions increased ROS production in endothelial cells in vitro and thereby decreased PI3K/AKT signaling [61]. This subsequently reduced plasma membrane localization of breast cancer resistance protein (BCRP), a transporter protein that mediates the efflux of uric acid, thus further resulting in the intracellular accumulation of uric acid [61]. High intracellular levels of uric acid with subsequent ROS formation was also shown to increase ER stress and apoptosis indicated by increased levels of caspase-12 [60]. De-creased viability of endothelial cells in response to uric acid treatment was confirmed by Komori et al. [61]. Further, Li et al. reported that uric acid induced increased phosphoryla-tion of eNOS at Thr495 mediated via PKC activation in response to ROS and ER stress. In addition, they showed a reduced binding of calmodulin (CaM) to eNOS upon uric acid treatment. Altogether, this resulted in a decreased eNOS activity and reduced NO produc-tion [60].

3.4. Discussion

CKD patients are at higher risk of developing CVD [105] and as kidney function declines, the risk of cardiovascular events increases and endothelial function decreases [50, 106]. Given that endothelial dysfunction is key in the initiation and progression of athero-sclerosis and contributes to decreased vascular reactivity, we investigated uremic tox-in-induced endothelial dysfunction and its underlying mechanisms by means of a sys-tematic review. Overall, cellular processes that were affected by uremic conditions or ure-mic toxins were inflammation, leukocyte migration and adhesion, oxidative stress, cell death, proliferation and thrombosis. Moreover, uremic toxins appeared to share common signaling pathways in endothelial cells, including pathways linked to MAPK, AhR, the RAGE receptor or pro-inflammatory transcription factors like NF-κB. Also, ROS as pro-inflammatory signal transducer was shared by multiple uremic toxins.

p38-MAPK is a well-known mediator of pro-inflammatory cytokine expression and regulator of NF-κB activation. Uremic toxins like IS signal via p38-MAPK/NF-κB to induce ICAM-1 or MCP-1 expression and thereby contribute to inflammatory responses of endo-thelial cells [38, 42, 44]. The role of NF-κB in uremic toxin-induced cytokine

release was confirmed in macrophages by an IS-induced NF-κB and AhR dependent expression of TNF-α [40].

IS increases intracellular AhR expression in different cell types contributing to CVD progression [37, 40, 68, 69]. Further, IS but also other uremic toxins derived from trypto-phan metabolism are ligands of AhR [107]. Activation of AhR signaling in endothelial cells was shown to enhance an inflammatory response as demonstrated by e.g. increased levels of E-Selectin expression [37]. In CKD patients, serum E-Selectin was shown to be a predictor of cardiovascular events, with high levels of E-Selectin associated with a worse outcome [108]. Moreover, AhR as a contributor to CVD independent of CKD is described in several studies [109, 110]. Furthermore, RAGE expression in endothelial cells was in-creased in response to uremic serum [30], AGEs like CML [30, 49, 50] and pCS [30], in-ducing endothelial dysfunction and inflammation. In CKD patients, increased CML levels correlated with RAGE mRNA and VCAM-1 protein levels and inversely with endothelial reactivity [50]. In non-CKD patients, the association between increased RAGE expression and CVD is controversial [111], nonetheless, in vitro studies linked RAGE signaling to cardiovascular pathological processes also in the absence of CKD [112, 113]. Combined, this suggests an amplification of both the AhR and RAGE pathways due to accumulation of uremic toxins in CKD and as such a larger contribution to inflammatory processes and the development of atherosclerosis.

Different uremic toxins like IS, phosphate, cyanate, AGEs and uric acid led to a de-creased eNOS expression and/or activity, resulting in a reduced production of NO and a decreased vasorelaxation [42, 45, 49, 50, 55, 60]. With NO also being a thrombocyte inhib-itor, decreased NO levels in combination with increased endothelial tissue factor and PAI expression in response to increased cyanate or carbamylated proteins like cLDL, create a pro-thrombotic environment [45, 47], which could contribute to the highly increased risk of thrombotic events in patients with CKD [114] [115].

Furthermore, beyond the uremic toxins identified through our systematic literature search, also the phosphaturic hormone fibroblast growth factor 23 (FGF23) is highly in-creased in CKD and known to impair endothelial-dependent vasorelaxation. Under-lying mechanisms include increased ROS production and reduced NO bioavailability, most likely independently of the FGF23 cofactor Klotho [116, 117]. Instead, Klotho is reduced in CKD patients and mainly serves a protective role in endothelial cells by supporting NO production and vasorelaxation, as shown in both animal models of

Klotho-deficiency and overexpression as well as in vitro experiments [117-121]. Furthermore, Klotho is capable of reducing endothelial inflammation, also when induced by IS, [40, 122, 123] and has been shown to reduce endothelial permeability and apoptosis [124]. Of note, uremic toxins can reduce Klotho levels, as for example shown for AGEs in mouse podocytes [125] and for IS in SMCs [126] .

A clear example of how post-translational modifications can contribute to atherosclerosis development and progression, is provided by the detrimental effects of oxidized LDL on the vascular wall, triggering endothelial dysfunction [12]. However, also other post-translational modifications are important in mediating CVD, with specific modifica-tions catalyzed by uremic toxins [127]. Thus, the contribution of these post-translational modifications to CVD is expected to be of even greater relevance in CKD. In addition to af-fecting endothelial cell function, CKD-induced post-translational modifications also nega-tively affect other cell types important in CVD. For example, increased acetylation of LDL in CKD led to increased ER-stress induced apoptosis of macrophages [88]. Altogether, this shows that additional insights into CKD-induced post-translational modifications and their pathological effects regarding CVD are required to enable development of strategies to reduce CKD-induced post-translational modifications.

What is apparent from our literature search, is that most studies investigated the effect of individual uremic toxins on single endothelial cellular functions or signaling pathways. Here, a proteomics and/or metabolomics approach would provide a broad overview of cellular functioning and could aid in the discovery of novel mediators and signaling pathways involved. Further, while it is important to study the individual uremic toxin to elucidate the underlying signaling mechanisms, the vasculature of CKD patients is continuously exposed to a multitude of uremic toxins, which then combined contribute to endothelial dysfunction. Thus, crosstalk between different toxins and their signaling pathways should also be investigated by combining toxins or using uremic serum or he-mofiltrate obtained after dialysis of CKD patients, to study a broader spectrum of cellular effects induced by CKD-induced uremia. Of the identified studies, two studies investigated uremic serum as well as single toxins. Saum et al. showed that 10% uremic serum as well as CML-BSA equally decreased KLF2 expression, however, the effect of CML-BSA on ROS formation and monocyte adhesion was stronger than that of uremic serum [30]. This might be explained by the dilution of uremic serum in

in vitro cell studies, resulting in lower concentrations of uremic toxins compared to patients with severe kidney failure. Furthermore, the composition of both serum and hemofiltrate differ drastically from plasma, due to coagulation in the case of serum preparation and, for hemofiltrate, due to the absence of larger uremic metabolites that are retained in the blood during dialysis as well as the low dialysis efficiency towards protein-bound uremic toxins. Overall, whether studying individual uremic toxins, toxin pools, uremic serum or hemofiltrate, there is no perfect solution to mimic CKD conditions in vitro; each approach has its benefits and drawbacks, and these should be considered based on the specific study aim when de-signing the experiment.

This review underlines the importance of improving current dialysis treatments and developing novel, more efficient strategies to remove uremic toxins from the bloodstream and as such halt further uremic toxin-induced endothelial damage. Especially, pro-tein-bound uremic toxins like IS are notoriously difficult to dialyze and their accumula-tion has major consequences for endothelial health, as summarized in this review. As there is currently no universal technique that optimally removes all types of (pro-tein-bound) uremic toxins [128], more research is needed to improve uremic toxin removal and thereby improve the cardiovascular health of CKD patients. In the past decade, there has been a focus on improved removal of protein-bound uremic toxins through adsorp-tion techniques, as discussed in more detail elsewhere [128]. This review highlights the signaling pathways frequently used by uremic toxins to exert detrimental cellular effects, as a potential complementary approach to reduce the cardiovascular burden of these uremic toxins in CKD.

4. Conclusion

In summary, this review connects current knowledge on pathophysiological and molecular mechanisms underlying increased cardiovascular risk in CKD, contributing to a deeper understanding of uremic toxin-induced signaling and providing indications on factors that should be considered in further analysis of uremic toxin-induced pathological effects. Overall, the accumulation of uremic toxins in CKD triggers endothelial dys-func-tion and contributes to inflammation, oxidative stress, thrombosis as well as cell death, thereby accelerating the development and progression of CVD. Uremic toxins frequently trigger ROS, MAPK/NF-κB, RAGE and/or AhR dependent pathways. Alt-hough these are already known in connection with the development of CVD also in the

absence of CKD, this review clearly summarizes how uremic toxins accelerate or amplify these pathologi-cal mechanisms. Targeting these pathways or interfering with uremic toxin accumulation or uremic toxins-induced post-translational modifications, may open therapeutic strate-gies to reduce the highly increased cardiovascular risk in CKD patients.

Supplementary Materials: The following are available online at www.mdpi.com/xxx/s1, Table S1: Overview of search terms and conditions; Table S2: PRISMA checklist

References

1. Stevens, P.E., et al., Chronic kidney disease management in the United Kingdom: NEOERICA project results. Kidney Int, 2007. 72(1): p. 92-9.
2. Drey, N., et al., A population-based study of the incidence and outcomes of diagnosed chronic kidney disease. Am J Kidney Dis, 2003. 42(4): p. 677-84.
3. Thompson, S., et al., Cause of Death in Patients with Reduced Kidney Function. J Am Soc Nephrol, 2015. 26(10): p. 2504-11.
4. Masuda, C., et al., Impact of chronic kidney disease on the presence and severity of aortic stenosis in patients at high risk for coronary artery disease. Cardiovasc Ultrasound, 2011. 9: p. 31.
5. Hansson, G.K. and A. Hermansson, The immune system in atherosclerosis. Nat Immunol, 2011. 12(3): p. 204-12.
6. Valdivielso, J.M., et al., Atherosclerosis in Chronic Kidney Disease: More, Less, or Just Different? Arterioscler Thromb Vasc Biol, 2019. 39(10): p. 1938-1966.
7. Briet, M., et al., Arterial stiffness and enlargement in mild-to-moderate chronic kidney disease. Kidney Int, 2006. 69(2): p. 350-7.

8.   Temmar, M., et al., Pulse wave velocity and vascular calcification at different stages of chronic kidney disease. J Hypertens, 2010. 28(1): p. 163-9.
9.   Katz, S.D., et al., Vascular endothelial dysfunction and mortality risk in patients with chronic heart failure. Circulation, 2005. 111(3): p. 310-4.
10.   Schächinger, V., M.B. Britten, and A.M. Zeiher, Prognostic impact of coronary vasodilator dysfunction on adverse long-term outcome of coronary heart disease. Circulation, 2000. 101(16): p. 1899-906.
11.   Weber, C. and H. Noels, Atherosclerosis: current pathogenesis and therapeutic options. Nat Med, 2011. 17(11): p. 1410-22.
12.   Soppert, J., et al., Lipoproteins and lipids in cardiovascular disease: from mechanistic insights to therapeutic targeting. Adv Drug Deliv Rev, 2020. 159: p. 4-33.
13.   Cai, H. and D.G. Harrison, Endothelial dysfunction in cardiovascular diseases: the role of oxidant stress. Circ Res, 2000. 87(10): p. 840-4.
14.   Yau, J.W., H. Teoh, and S. Verma, Endothelial cell control of thrombosis. BMC cardiovascular disorders, 2015. 15: p. 130-130.
15.   Hutter, R., et al., Vascular endothelial growth factor regulates reendothelialization and neointima formation in a mouse model of arterial injury. Circulation, 2004. 110(16): p. 2430-5.
16.   Noels, H., et al., Deficiency of endothelial CXCR4 reduces reendothelialization and enhances neointimal hyperplasia after vascular injury in atherosclerosis-prone mice. Arterioscler Thromb Vasc Biol, 2014. 34(6): p. 1209-20.
17.   Vanholder, R., et al., Uremic toxicity: present state of the art. Int J Artif Organs, 2001. 24(10): p. 695-725.
18.   Nowak, K.L., et al., Vascular Dysfunction, Oxidative Stress, and Inflammation in Chronic Kidney Disease. Kidney360, 2020. 1(6): p. 501-509.
19.   Oberg, B.P., et al., Increased prevalence of oxidant stress and inflammation in patients with moderate to severe chronic kidney disease. Kidney Int, 2004. 65(3): p. 1009-16.
20.   Cachofeiro, V., et al., Oxidative stress and inflammation, a link between chronic kidney disease and cardiovascular disease. Kidney Int Suppl, 2008(111): p. S4-9.
21.   Annuk, M., et al., Oxidative stress and endothelial function in chronic renal failure. J Am Soc Nephrol, 2001. 12(12): p. 2747-2752.
22.   Noels, H., et al., Lipoproteins and fatty acids in chronic kidney disease: molecular and metabolic alterations. Nature Reviews Nephrology, 2021: p. 1-15.
23.   Vanholder, R., et al., Review on uremic toxins: classification, concentration, and interindividual variability. Kidney Int, 2003. 63(5): p. 1934-43.
24.   Duranton, F., et al., Normal and pathologic concentrations of uremic toxins. J Am Soc Nephrol, 2012. 23(7): p. 1258-70.
25.   Watanabe, H., et al., p-Cresyl sulfate causes renal tubular cell damage by inducing oxidative stress by activation of NADPH oxidase. Kidney Int, 2013. 83(4): p. 582-92.
26.   Holmar, J., et al., Uremic Toxins Affecting Cardiovascular Calcification: A Systematic Review. Cells, 2020. 9(11).
27.   Dou, L., et al., The uremic solutes p-cresol and indoxyl sulfate inhibit endothelial proliferation and wound repair. Kidney Int, 2004. 65(2): p. 442-51.
28.   Moher, D., et al., Preferred reporting items for systematic reviews and meta-analyses: the PRISMA statement. PLoS Med, 2009. 6(7): p. e1000097.
29.   Jerotic, D., et al., GSTM1 Modulates Expression of Endothelial Adhesion Molecules in Uremic Milieu. Oxidative medicine and cellular longevity, 2021. 2021.
30.   Saum, K., et al., Uremic Advanced Glycation End Products and Protein-Bound Solutes Induce Endothelial Dysfunction Through Suppression of Krüppel-Like Factor 2. J Am Heart Assoc, 2018. 7(1).
31.   Garcia-Jerez, A., et al., Effect of uraemia on endothelial cell damage is mediated by the integrin linked kinase pathway. Journal of Physiology-London, 2015. 593(3): p. 601-618.

32.   Eloueyk, A., et al., Uremic Serum Induces Inflammation in Cultured Human Endothelial Cells and Triggers Vascular Repair Mechanisms. Inflammation, 2019. 42(6): p. 2003-2010.

33.   Nilsson, L., et al., Plasma cyanate concentrations in chronic renal failure. Clinical Chemistry, 1996. 42(3): p. 482-483.

34.   The European Uremic Toxins (EUTox) Database. Available online at www.uremic-toxins.org, 2021.

35.   Speer, T., et al., Carbamylated low-density lipoprotein induces endothelial dysfunction. Eur Heart J, 2014. 35(43): p. 3021-32.

36.   Moore, L.W., et al., Association of dietary phosphate and serum phosphorus concentration by levels of kidney function. The American Journal of Clinical Nutrition, 2015. 102(2): p. 444-453.

37.   Ito, S., et al., Crucial Role of the Aryl Hydrocarbon Receptor (AhR) in Indoxyl Sulfate-Induced Vascular Inflammation. J Atheroscler Thromb, 2016. 23(8): p. 960-75.

38.   Masai, N., et al., Indoxyl sulfate stimulates monocyte chemoattractant protein-1 expression in human umbilical vein endothelial cells by inducing oxidative stress through activation of the NADPH oxidase-nuclear factor-κB pathway. Circ J, 2010. 74(10): p. 2216-24.

39.   Tumur, Z., et al., Indoxyl Sulfate Upregulates Expression of ICAM-1 and MCP-1 by Oxidative Stress-Induced NF-kappa B Activation. American Journal of Nephrology, 2010. 31(5): p. 435-441.

40.   Kim, H.Y., et al., Indoxyl sulfate (IS)-mediated immune dysfunction provokes endothelial damage in patients with end-stage renal disease (ESRD). Scientific Reports, 2017. 7.

41.   Dou, L., et al., The uremic solute indoxyl sulfate induces oxidative stress in endothelial cells. Journal of Thrombosis and Haemostasis, 2007. 5(6): p. 1302-1308.

42.   Yang, K., et al., Amelioration of uremic toxin indoxyl sulfate-induced endothelial cell dysfunction by Klotho protein. Toxicology Letters, 2012. 215(2): p. 77-83.

43.   Li, S., et al., MicroRNA-214 targets COX-2 to antagonize indoxyl sulfate (IS)-induced endothelial cell apoptosis. Apoptosis, 2020. 25(1-2): p. 92-104.

44.   El-Gamal, D., et al., Cyanate Is a Novel Inducer of Endothelial ICAM-1 Expression. Antioxidants & Redox Signaling, 2012. 16(2): p. 129-137.

45.   El-Gamal, D., et al., The urea decomposition product cyanate promotes endothelial dysfunction. Kidney International, 2014. 86(5): p. 923-931.

46.   Ambrosch, A., et al., Small-sized low-density lipoproteins of subclass B from patients with end-stage renal disease effectively augment tumor necrosis factor-alpha-induced adhesive properties in human endothelial cells. American Journal of Kidney Diseases, 2002. 39(5): p. 972-984.

47.   Holy, E.W., et al., Carbamylated Low-Density Lipoproteins Induce a Prothrombotic State Via LOX-1 Impact on Arterial Thrombus Formation In Vivo. Journal of the American College of Cardiology, 2016. 68(15): p. 1664-1676.

48.   Apostolov, E.O., et al., Endonuclease G mediates endothelial cell death induced by carbamylated LDL. Am J Physiol Heart Circ Physiol, 2011. 300(6): p. H1997-2004.

49.   Wang, C.C., et al., Spironolactone ameliorates endothelial dysfunction through inhibition of the AGE/RAGE axis in a chronic renal failure rat model. Bmc Nephrology, 2019. 20(1).

50.   Linden, E., et al., Endothelial dysfunction in patients with chronic kidney disease results from advanced glycation end products (AGE)-mediated inhibition of endothelial nitric oxide synthase through RAGE activation. Clin J Am Soc Nephrol, 2008. 3(3): p. 691-8.

51.   Zhu, J., et al., The effects of low-dose nepsilon-(carboxymethyl)lysine (CML) and nepsilon-(carboxyethyl)lysine (CEL), two main glycation free adducts considered as potential uremic toxins, on endothelial progenitor cell function. Cardiovasc Diabetol, 2012. 11: p. 90.

52. Jing, Y.J., et al., p-Cresyl sulfate is associated with carotid arteriosclerosis in hemodialysis patients and promotes atherogenesis in apoE-/- mice. Kidney Int, 2016. 89(2): p. 439-49.

53. Watanabe, H., et al., p-Cresyl sulfate, a uremic toxin, causes vascular endothelial and smooth muscle cell damages by inducing oxidative stress. Pharmacol Res Perspect, 2015. 3(1): p. e00092.

54. Meijers, B.K.I., et al., The Uremic Retention Solute p-Cresyl Sulfate and Markers of Endothelial Damage. American Journal of Kidney Diseases, 2009. 54(5): p. 891-901.

55. Peng, A., et al., Adverse effects of simulated hyper- and hypo-phosphatemia on endothelial cell function and viability. PLoS One, 2011. 6(8): p. e23268.

56. Hsu, Y.J., et al., Hyperphosphatemia induces protective autophagy in endothelial cells through the inhibition of Akt/mTOR signaling. Journal of Vascular Surgery, 2015. 62(1): p. 210-U384.

57. Abbasian, N., et al., Hyperphosphatemia, Phosphoprotein Phosphatases, and Microparticle Release in Vascular Endothelial Cells. J Am Soc Nephrol, 2015. 26(9): p. 2152-62.

58. Guo, W., Z. Diao, and W. Liu, Asymmetric dimethylarginine downregulates sarco/endoplasmic reticulum calcium-ATPase 3 and induces endoplasmic reticulum stress in human umbilical vein endothelial cells. Mol Med Rep, 2017. 16(5): p. 7541-7547.

59. Zhang, Y., et al., ALDR Enhanced Endothelial Injury in Hyperuricemia Screened using SILAC. Cellular Physiology and Biochemistry, 2014. 33(2): p. 479-490.

60. Li, P., et al., Uric acid enhances PKC-dependent eNOS phosphorylation and mediates cellular ER stress: A mechanism for uric acid-induced endothelial dysfunction. International Journal of Molecular Medicine, 2016. 37(4): p. 989-997.

61. Komori, H., K. Yamada, and I. Tamai, Hyperuricemia enhances intracellular urate accumulation via down-regulation of cell-surface BCRP/ABCG2 expression in vascular endothelial cells. Biochimica Et Biophysica Acta-Biomembranes, 2018. 1860(5): p. 973-980.

62. Pawlak, K., et al., 3-hydroxyanthranilic acid is independently associated with monocyte chemoattractant protein-1 (CCL2) and macrophage inflammatory protein-1 beta (CCL4) in patients with chronic kidney disease. Clinical Biochemistry, 2010. 43(13-14): p. 1101-1106.

63. Frericks, M., M. Meissner, and C. Esser, Microarray analysis of the AHR system: tissue-specific flexibility in signal and target genes. Toxicol Appl Pharmacol, 2007. 220(3): p. 320-32.

64. Stockinger, B., et al., The aryl hydrocarbon receptor: multitasking in the immune system. Annu Rev Immunol, 2014. 32: p. 403-32.

65. Vogel, C.F., E. Sciullo, and F. Matsumura, Activation of inflammatory mediators and potential role of ah-receptor ligands in foam cell formation. Cardiovasc Toxicol, 2004. 4(4): p. 363-73.

66. Vogel, C.F., et al., Induction of proinflammatory cytokines and C-reactive protein in human macrophage cell line U937 exposed to air pollution particulates. Environ Health Perspect, 2005. 113(11): p. 1536-41.

67. Wu, D., et al., Activation of aryl hydrocarbon receptor induces vascular inflammation and promotes atherosclerosis in apolipoprotein E-/- mice. Arterioscler Thromb Vasc Biol, 2011. 31(6): p. 1260-7.

68. Wakamatsu, T., et al., Indoxyl Sulfate Promotes Macrophage IL-1β Production by Activating Aryl Hydrocarbon Receptor/NF-κ/MAPK Cascades, but the NLRP3 inflammasome Was Not Activated. Toxins (Basel), 2018. 10(3).

69. Kim, H.Y., et al., Indoxyl sulfate-induced TNF-alpha is regulated by crosstalk between the aryl hydrocarbon receptor, NF-kappa B, and SOCS2 in human macrophages. Faseb Journal, 2019. 33(10): p. 10844-10858.

70. Dou, L., et al., The cardiovascular effect of the uremic solute indole-3 acetic acid. J Am Soc Nephrol, 2015. 26(4): p. 876-87.

71. de Brito, J.S., et al., Aryl Hydrocarbon Receptor and Uremic Toxins from the Gut Microbiota in Chronic Kidney Disease Patients: Is There a Relationship between Them? Biochemistry, 2019. 58(15): p. 2054-2060.

72. Shah, S.V., et al., Recent advances in understanding the pathogenesis of atherosclerosis in CKD patients. J Ren Nutr, 2015. 25(2): p. 205-8.

73. Lin, C.Y., et al., Enhanced expression of glucose transporter-1 in vascular smooth muscle cells via the Akt/tuberous sclerosis complex subunit 2 (TSC2)/mammalian target of rapamycin (mTOR)/ribosomal S6 protein kinase (S6K) pathway in experimental renal failure. Journal of Vascular Surgery, 2013. 57(2): p. 475-485.

74. Bell, J.D., et al., Nuclear magnetic resonance studies of blood plasma and urine from subjects with chronic renal failure: identification of trimethylamine-N-oxide. Biochim Biophys Acta, 1991. 1096(2): p. 101-7.

75. Blackmore, D.J., W.J. Elder, and C.H. Bowden, Urea distribution in renal failure. J Clin Pathol, 1963. 16(3): p. 235-43.

76. Nilsson, L., et al., Plasma cyanate concentrations in chronic renal failure. Clin Chem, 1996. 42(3): p. 482-3.

77. Wang, Z., et al., Protein carbamylation links inflammation, smoking, uremia and atherogenesis. Nat Med, 2007. 13(10): p. 1176-84.

78. Arlandson, M., et al., Eosinophil peroxidase oxidation of thiocyanate. Characterization of major reaction products and a potential sulfhydryl-targeted cytotoxicity system. J Biol Chem, 2001. 276(1): p. 215-24.

79. Baldus, S., et al., Endothelial transcytosis of myeloperoxidase confers specificity to vascular ECM proteins as targets of tyrosine nitration. J Clin Invest, 2001. 108(12): p. 1759-70.

80. Kalim, S., et al., Protein carbamylation in kidney disease: pathogenesis and clinical implications. American journal of kidney diseases : the official journal of the National Kidney Foundation, 2014. 64(5): p. 793-803.

81. Apostolov, E.O., et al., Chronic uremia stimulates LDL carbamylation and atherosclerosis. J Am Soc Nephrol, 2010. 21(11): p. 1852-7.

82. Apostolov, E.O., et al., Scavenger receptors of endothelial cells mediate the uptake and cellular proatherogenic effects of carbamylated LDL. Arterioscler Thromb Vasc Biol, 2009. 29(10): p. 1622-30.

83. Basnakian, A.G., et al., Carbamylated LDL. Adv Clin Chem, 2010. 51: p. 25-52.

84. Gonen, B., et al., Abnormal cell-interactive properties of low-density lipoproteins isolated from patients with chronic renal failure. Metabolism, 1985. 34(1): p. 10-4.

85. Hörkkö, S., et al., Decreased clearance of uraemic and mildly carbamylated low-density lipoprotein. Eur J Clin Invest, 1994. 24(2): p. 105-13.

86. Ok, E., et al., Carbamylated low-density lipoprotein induces death of endothelial cells: a link to atherosclerosis in patients with kidney disease. Kidney Int, 2005. 68(1): p. 173-8.

87. Chu, M., et al., Serum small-dense LDL abnormalities in chronic renal disease patients. British journal of biomedical science, 2012. 69(3): p. 99-102.

88. Tao, J.L., et al., Endoplasmic reticulum stress is involved in acetylated low-density lipoprotein induced apoptosis in THP-1 differentiated macrophages. Chin Med J (Engl), 2009. 122(15): p. 1794-9.

89. Miyata, T., et al., Alterations in nonenzymatic biochemistry in uremia: origin and significance of "carbonyl stress" in long-term uremic complications. Kidney Int, 1999. 55(2): p. 389-99.

90. Peppa, M., et al., Glycoxidation and inflammation in renal failure patients. American Journal of Kidney Diseases, 2004. 43(4): p. 690-695.

91. Martinez, A.W., et al., Removal of P-cresol sulfate by hemodialysis. J Am Soc Nephrol, 2005. 16(11): p. 3430-6.

92. Meijers, B.K., et al., Free p-cresol is associated with cardiovascular disease in hemodialysis patients. Kidney Int, 2008. 73(10): p. 1174-80.

93.   Watanabe, H., et al., Human organic anion transporters function as a high-capacity transporter for p-cresyl sulfate, a uremic toxin. Clin Exp Nephrol, 2014. 18(5): p. 814-20.

94.   Giachelli, C.M., et al., Regulation of vascular calcification: roles of phosphate and os-teopontin. Circ Res, 2005. 96(7): p. 717-22.

95.   Mizobuchi, M., D. Towler, and E. Slatopolsky, Vascular calcification: the killer of pa-tients with chronic kidney disease. J Am Soc Nephrol, 2009. 20(7): p. 1453-64.

96.   Martínez-Moreno, J.M., et al., In vascular smooth muscle cells paricalcitol prevents phosphate-induced Wnt/β-catenin activation. American Journal of Physiology-Renal Physiology, 2012. 303(8): p. F1136-F1144.

97.   Martínez-Moreno, J.M., et al., High phosphate induces a pro-inflammatory response by vascular smooth muscle cells and modulation by vitamin D derivatives. Clin Sci (Lond), 2017. 131(13): p. 1449-1463.

98.   Konya, H., et al., Asymmetric dimethylarginine, a biomarker of cardiovascular compli-cations in diabetes mellitus. World J Exp Med, 2015. 5(2): p. 110-9.

99.   Böger, R.H., et al., Asymmetric dimethylarginine (ADMA) as a prospective marker of cardiovascular disease and mortality--an update on patient populations with a wide range of cardiovascular risk. Pharmacol Res, 2009. 60(6): p. 481-7.

100.   Woehlbier, U. and C. Hetz, Modulating stress responses by the UPRosome: a matter of life and death. Trends Biochem Sci, 2011. 36(6): p. 329-37.

101.   Walter, P. and D. Ron, The unfolded protein response: from stress pathway to homeo-static regulation. Science, 2011. 334(6059): p. 1081-6.

102.   Snauwaert, E., et al., Uremic Toxin Concentrations are Related to Residual Kidney Function in the Pediatric Hemodialysis Population. Toxins (Basel), 2019. 11(4).

103.   Kanbay, M., et al., The role of uric acid in the pathogenesis of human cardiovascular disease. Heart, 2013. 99(11): p. 759-66.

104.   Ryu, E.S., et al., Uric acid-induced phenotypic transition of renal tubular cells as a novel mechanism of chronic kidney disease. Am J Physiol Renal Physiol, 2013. 304(5): p. F471-80.

105.   Sarnak, M.J., et al., Kidney disease as a risk factor for development of cardiovascular disease. Circulation, 2003. 108(17): p. 2154-2169.

106.   Ortiz, A., et al., Epidemiology, contributors to, and clinical trials of mortality risk in chronic kidney failure. The lancet, 2014. 383(9931): p. 1831-1843.

107.   Sallée, M., et al., The aryl hydrocarbon receptor-activating effect of uremic toxins from tryptophan metabolism: a new concept to understand cardiovascular complications of chronic kidney disease. Toxins, 2014. 6(3): p. 934-949.

108.   Malatino, L., et al., Circulating E-selectin as a risk marker in patients with end-stage renal disease. Journal of internal medicine, 2007. 262(4): p. 479-487.

109.   Yi, T., et al., Aryl hydrocarbon receptor: a new player of pathogenesis and therapy in cardiovascular diseases. BioMed research international, 2018. 2018.

110.   Zhu, K., et al., Aryl hydrocarbon receptor pathway: Role, regulation and intervention in atherosclerosis therapy (Review). Molecular medicine reports, 2019. 20(6): p. 4763-4773.

111.   Reichert, S., et al., Soluble form of receptor for advanced glycation end products and incidence of new cardiovascular events among patients with cardiovascular disease. Atherosclerosis, 2017. 266: p. 234-239.

112.   Uekita, H., et al., Integral role of receptor for advanced glycation end products (RAGE) in nondiabetic atherosclerosis. Fukushima journal of medical science, 2019. 65(3): p. 109-121.

113.   Jandeleit-Dahm, K. and M.E. Cooper, The role of AGEs in cardiovascular disease. Cur-rent pharmaceutical design, 2008. 14(10): p. 979-986.

114.   Baaten, C., et al., Platelet Function in CKD: A Systematic Review and Meta-Analysis. J Am Soc Nephrol, 2021. 32(7): p. 1583-98.

115.   Baaten, C.C.F.M.J., et al., Platelet abnormalities in CKD and their implications for an-tiplatelet therapy. Clin J Am Soc Nephrol, 2021.

116. Silswal, N., et al., FGF23 directly impairs endothelium-dependent vasorelaxation by increasing superoxide levels and reducing nitric oxide bioavailability. American Journal of Physiology-Endocrinology and Metabolism, 2014. 307(5): p. E426-E436.

117. Six, I., et al., Direct, acute effects of Klotho and FGF23 on vascular smooth muscle and endothelium. PLoS One, 2014. 9(4): p. e93423.

118. Saito, Y., et al., Klotho protein protects against endothelial dysfunction. Biochem Biophys Res Commun, 1998. 248(2): p. 324-9.

119. Nagai, R., et al., Endothelial dysfunction in the klotho mouse and downregulation of klotho gene expression in various animal models of vascular and metabolic diseases. Cell Mol Life Sci, 2000. 57(5): p. 738-46.

120. Shimada, T., et al., Angiogenesis and vasculogenesis are impaired in the precocious-aging klotho mouse. Circulation, 2004. 110(9): p. 1148-55.

121. Saito, Y., et al., In vivo klotho gene delivery protects against endothelial dysfunction in multiple risk factor syndrome. Biochem Biophys Res Commun, 2000. 276(2): p. 767-72.

122. Maekawa, Y., et al., Klotho suppresses TNF-alpha-induced expression of adhesion molecules in the endothelium and attenuates NF-kappaB activation. Endocrine, 2009. 35(3): p. 341-6.

123. Chen, C., et al., The role of AMP-activated protein kinase α1-mediated endoplasmic reticulum stress in alleviating the toxic effect of uremic toxin indoxyl sulfate on vascular endothelial cells by Klotho. J Appl Toxicol, 2021. 41(9): p. 1446-1455.

124. Kusaba, T., et al., Klotho is associated with VEGF receptor-2 and the transient receptor potential canonical-1 Ca2+ channel to maintain endothelial integrity. Proc Natl Acad Sci U S A, 2010. 107(45): p. 19308-13.

125. Suk Kang, J., et al., Protective effects of klotho on palmitate-induced podocyte injury in diabetic nephropathy. PLoS One, 2021. 16(4): p. e0250666.

126. Chen, J., et al., Indoxyl Sulfate Enhance the Hypermethylation of Klotho and Promote the Process of Vascular Calcification in Chronic Kidney Disease. Int J Biol Sci, 2016. 12(10): p. 1236-1246.

127. Gajjala, P.R., et al., Emerging role of post-translational modifications in chronic kidney disease and cardiovascular disease. Nephrol Dial Transplant, 2015. 30(11): p. 1814-24.

128. Saar-Kovrov, V., et al., Reduction of protein-bound uraemic toxins in plasma of chronic renal failure patients: A systematic review. J Intern Med, 2021. 290(3): p. 499-526.

Publication 3:

Chemokine CCL9 is upregulated early in chronic kidney disease and counteracts kidney inflammation and fibrosis

Christian Hemmers[1*], Corinna Schulte[1*], **Julia Wollenhaupt[1]**, Dickson W. L. Wong[2], Eva Harlacher[1], Setareh Orth-Alampour[1], Barbara Mara Klinkhammer[2], Stephan H. Schirmer[3], Michael Böhm[3], Nikolaus Marx[4], Thimoteus Speer[5], Peter Boor[2,6], Joachim Jankowski[1,7], Heidi Noels[1,8]

*Shared first authorship

[1]Institute for Molecular Cardiovascular Research (IMCAR), University Hospital RWTH Aachen, Aachen, Germany;

[2]Institute of Pathology, University Hospital RWTH Aachen, Aachen, Germany;

[3]Saarland University, Homburg/Saar, Germany;

[4]Department of Internal Medicine I, Cardiology, University Hospital RWTH Aachen, Aachen, Germany;

[5]Translational Cardio-Renal Medicine, Saarland University, Homburg/Saar, Germany;

[6]Department of Nephrology and Clinical Immunology, University Hospital RWTH Aachen, Aachen, Germany

[7]Department of Pathology, Cardiovascular Research Institute Maastricht (CARIM), Maastricht University, Maastricht, the Netherlands;

[8]Department of Biochemistry, Cardiovascular Research Institute Maastricht (CARIM), Maastricht University, Maastricht, the Netherlands.

Graphical abstract
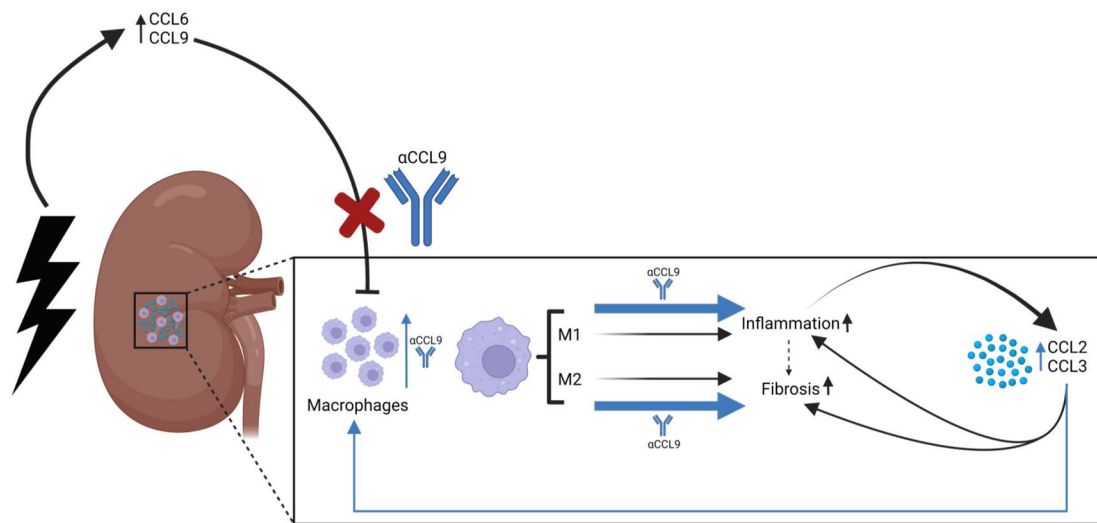
Abstract: Inflammation and fibrosis play an important pathophysiological role in chronic kidney disease (CKD), with pro-inflammatory mediators and leukocytes promoting organ damage with subsequent fibrosis. Since chemokines are the main regulators of leukocyte chemotaxis and tissue inflammation, we performed systemic chemokine profiling in early CKD in mice. This revealed CCL6 and CCL9 as most upregulated chemokines, with significantly higher levels of both chemokines in blood (CCL6: 3-4 fold; CCL9: 3-5 fold) as well as kidney as confirmed by ELISA in two additional CKD models. Chemokine treatment in a mouse model of early adenine-induced CKD almost completely abolished the CKD-induced infiltration of macrophages and myeloid cells in the kidney without impact on circulating leukocyte numbers. The other way around, especially CCL9-blockade aggravated monocyte and macrophage accumulation in kidney during CKD development, without impact on the ratio of M1-to-M2 macrophages. In parallel, CCL9-blockade raised serum creatinine and urea levels as readouts of kidney dysfunction. Also, it exacerbated CKD-induced expression of collagen (3.2-fold) and the pro-inflammatory chemokines CCL2 (1.8-fold) and CCL3 (2.1-fold) in kidney. Altogether, this study reveals for the first time that chemokines CCL6 and CCL9 are upregulated early in experimental CKD, with CCL9-blockade during CKD initiation enhancing kidney inflammation and fibrosis.

Keywords: chronic kidney disease; chemokine; inflammation; macrophage; CCL6; CCL9; MIP-1γ; fibrosis; collagen

1. Introduction

Chronic kidney disease (CKD), with an estimated global prevalence of more than 10% [1], is defined by a decrease in kidney filtration function and/or the presence of kidney damage markers for over 90 days [2]. Based on the estimated glomerular filtration rate (eGFR) and albuminuria together as a measure of filtration capacity, CKD is classified in five stages [1]. In addition to CKD burden, patients with CKD also suffer from increased risk of cardiovascular disease, with CKD identified as an independent risk factor of car-diovascular morbidity and mortality [3,4]. In both diseases, organ inflammation and fi-brosis play important pathophysiological roles.

Initial kidney injury triggers the expression of pro-inflammatory mediators as well as the recruitment and accumulation of inflammatory leukocytes, including neutrophils, monocytes and macrophages, in the kidney. These contribute to further organ damage and also produce pro-fibrotic mediators triggering fibrotic phenotypes [5-7]. Fibrosis fol-lowing tissue injury is due to the excessive formation of extracellular matrix proteins, e.g. collagen, and further promotes organ dysfunction [8]. Patients with CKD often exhibit kidney fibrosis, detectable as glomerulosclerosis, arterio- and arteriolosclerosis and/or tu-bulointerstitial fibrosis, which is associated with an impairment of kidney function [8,9].

Key players of the fibrosis-driving inflammatory response are chemokines and their receptors. They play an important role in leukocyte chemotaxis and associated in-flamma-tion, as shown in the context of both cardiovascular disease [10] and CKD [5]. For exam-ple, C-C chemokine receptors type 1 and 2 (CCR1, CCR2) expressed by neutrophils and monocytes mediate their infiltration in the injured kidney [11-13]. In addition to various chemokine receptors, up to 50 chemokines have been identified, which often can bind multiple receptors [14]. Despite a number of studies, many of them currently remain un-investigated in CKD. Thus, we initiated our study with chem-okine profiling to identify chemokines upregulated in an early stage of experimental CKD. This revealed an upregulation of mouse chemokine (C-C motif) ligands 6 and 9 (CCL6, CCL9) in different CKD mouse models, with CCL6 and CCL9 the only two mouse chemokines belonging to the NC6 subfamily of CC-chemokines, a subclass not yet studied in CKD. With the human closest related chemokine CCL15 also upregu-lated in CKD patients [15], the upregulation of CCL6 and CCL9 detected in early stage of CKD and the fact that both chemokines have been described as ligands of the pro-

inflammatory and pro-fibrotic CCR1 [16], we here in-vestigated a potential role of these chemokines in kidney inflammation and fibrosis in early experimental CKD.

2. Materials and Methods

2.1. Animal experiments

All animal experiments were approved by local regulatory authorities and performed according to local and national ethical guidelines. Mice were 8-12 weeks at experiment start and had free access to food and water. Chemokine screening was performed in 129/Sv mice (mixed gender, purchased from Charles River) subjected to one-step 5/6 ne-phrectomy, with sham-operated animals as controls. Chemokines were also quan-tified in male C57BL/6N mice (purchased from Charles River) and C57BL/6J apolipo-protein E defi-cient mice (ApoE-/-, own breeding) with adenine-induced CKD. C57BL/6N mice were fed with a 0.2% adenine-rich diet (Altromin) for 3 weeks. C57BL/6J mice received a high-fat diet (HFD: Altromin Western Type diet) for 4 weeks, followed by HFD mixed with 0.3% adenine / 19.5 % casein for 10 days and HFD with 0.15% adenine / 19.5 % casein for fur-ther 4 days. Control mice received over the last 14 days the same HFD with 19.5% casein but without adenine.

The role of mouse chemokines CCL6 (Entrez Gene ID 20305; also called C10) and CCL9 (Entrez Gene ID 20308; also called MIP-1γ) was studied in two sets of experi-ments. In the first set of experiments, female C57BL/6J mice (purchased from Janvier) were im-planted with a mini-osmotic pump (Alzet, Model 2002) for continuous delivery of endo-toxin-free mouse CCL6 (amino acids 42-116) or mouse CCL9 (amino acids 50-122) (both from R&D systems; 1 µg/day; 0.5 µl/h), or with 0.9% NaCl as vehicle control. Pumps were implanted subcutaneously (s.c.) under 1.5-2% isoflurane anes-thetics, preceded by 0.1 mg/kg s.c. Buprenorphine treatment. On the day of pump im-plantation, CKD was induced by feeding a 0.2% adenine diet (Ssniff) for 2 weeks. C57BL/6J mice treated with a vehicle through pump implantation and on standard diet (Ssniff) served as non-CKD controls. In the second set of experiments, female mice received a high-fat diet (HFD; Altromin West-ern Type diet) for 4 weeks, followed by HFD mixed with 0.3% adenine for 10 days to in-duce CKD. On days 3, 5, 7 and 9 after CKD induction, mice were intraperitoneally injected with a blocking antibody against mouse CCL6 (R&D systems, AF487) or CCL9 (R&D sys-tems, MAB463), in total 10 µg in 0.9% NaCl per injection. 'Isotype CKD controls' were on the same diet but re-ceived the isotype-matched antibody (R&D systems, MAB005). Hyper-lipidemic Apoe-

/- mice without adenine but with isotype-matched antibody treatment served as non-CKD controls ('isotype controls').

2.2. Blood sampling and organ isolation

Upon sacrifice, blood was collected by heart cannulation under anesthetics with ketamine (100 mg/kg) and xylazine (10 mg/kg). Serum was prepared and stored at -80°C. Serum creatinine and urea were quantified by clinical laboratory routine (Vitros 350, Or-tho Clinical Diagnostics, Institut für Versuchstierkunde, Aachen, Germany). After gentle in vivo rinsing with PBS, kidneys were harvested for flow cytometric analysis, histological tissue analysis or snap-frozen in liquid nitrogen and stored at -80°C for protein extraction.

2.3. Leukocyte profiling and flow cytometry

Leukocyte counts in blood were determined using a Celltac MEK-6550 (Nihon Kohden, Tokyo, Japan), with differential blood counts obtained through Wright's stain. Half of a kidney was mechanically minced using a scalpel and digested with 0.25 mg/ml Liberase (Merck) in RPMI-1640 medium at 37°C for 1 h. The resulting solution was sieved through over a 70 µm cell strainer (Greiner Bio-One) and the enzymatic reaction stopped via diluting the solution in RPMI-1640 with 10% fetal calf serum (medium and supple-ment from Thermo Fisher Scientific). Subsequently, cells were pelleted by centrifugation, washed in HANKS Complete buffer (1x HBSS with 0.3 mM EDTA and 0.1% bovine serum albumin) and stained with antibody mixtures directed against CD115 (Invitrogen), CD11b, CD45 (BD Pharmingen), Ly-6G (Gr1), F4/80 (eBioscience) and CD206 (BioLegend). CountBrightTM Absolute Counting Beads (Invitrogen) were added for absolute cell count-ing. Stained cells were analyzed by flow cytometry using a FACSCanto II and FACSDiva software (BD Biosciences) with appropriate fluorescence compensation. Using FlowJo software, cell populations were gated and analyzed as following: leukocytes (CD45+), neutrophils (CD45+ CD11b+ CD115- Ly-6G+), monocytes (CD45+ CD11b+ CD115+) with Ly-6G -high and Ly-6G -low subsets, tissue macrophages (CD45+ CD11b+ F4/80+) with subsets M1 (CD206-) or M2 (CD206+).

2.4. Histological tissue analysis: Acid Fuchsin Orange G (AFOG) staining

Longitudinally cut kidneys were fixed for 24-48h in methyl carnoy's solution directly after organ isolation. Fixed samples were dehydrated in ascending alcohol concentrations, paraffin embedded and cut into 1 µm sections using a rotation microtome. For

histological analyses, the slides were deparaffinized and fixed in Bouin's solution for 2 h at 60°C, re-hydrated and sequentially treated with hematoxylin and iron chloride solution (1 min), 0.1% hydrochloric acid (10 sec), 1% phosphomolybdic acid (5 min) and AFOG solution (10 min), each separated by a washing step in water. Finally, slides were dehydrated and covered with Histokitt for microscopic analysis.

2.5. Tissue protein isolation, Western Blot analysis and ELISA

Approximately 5-10 mg of kidney tissue, snap-frozen in liquid nitrogen, was lysed in 150 µl of an ice-cold, non-denaturing lysis buffer (consisting of Cell Lysis Buffer (Cell Sig-naling), c0mpleteTM Mini Protease Inhibitor Cocktail (Roche) and PhosSTOP (Sigma)), us-ing steel beads for homogenization with a Qiagen tissue lyser. After centrifugation, su-pernatant was collected, protein concentration measured using a NanoDrop One and stored at -80°C for further analysis.

For Western Blot analysis, 15 µg total protein was mixed with 4x Laemmli protein sample buffer (BioRad) and heated to 95°C for 5 min before analysis over SDS-PAGE and standard western blot detection protocols. Primary antibodies were used against collagen 1 (1310-01, SouthernBiotech) and β-actin (4967, Cell Signaling), with secondary antibodies HRP-conjugated (Santa Cruz Biotechnology or Cell Signaling) for chemiluminescent de-tection (Super SignalTM West Pico PLUS Chemiluminescent Substrate, ThermoFisher Sci-entific) with a GelDoc XR (BioRad). Image Lab 2.0 (BioRad) was used for quantitative analysis by normalizing the band intensities to β-actin as loading control.

CCL6 and CCL9 levels in serum and kidney lysates were quantified by using a commercially available ELISA (DuoSet, R&D Systems) according to the manufacturer's instructions.

2.6. Chemokine profiling and LUNARIS assay

Chemokine profiling in serum of CKD mice was performed using a Proteome Profiler™ Array 'Mouse Chemokine Array Kit' (R&D Systems), according to the manufacturer's instructions. Levels of the chemokines CCL2 (MCP1), CCL3, CCL4, CCL5 (RANTES), CCL11, CCL19, CCL20, CCL22, CXCL10 (IP10), CXCL11 and CX3CL1 (Fractalkine) in kidney lysates were quantified using a LUNARIS Custom Kit 20103S assay (CUST-20103S, Ayoxxa) according to the manufacturer's instructions. Analysis of data was done using LUNARIS Analysis Suite Software.

2.7. Statistics

Data are shown as individual values and mean ± SD. All statistical analyses were performed by using Graphpad (Version 9 or higher). After testing for normality, P-values were calculated using student's t-test (unpaired, two-tailed) for two-group comparisons with parametric data, Mann-Whitney test (unpaired, two-tailed) for two-group comparisons with non-parametric data, Kruskal-Wallis test with Dunn's post-test (non-parametric) or one-way ANOVA (parametric) or two-way ANOVA with Dunnett's multiple comparisons tests for multiple group comparisons, as appropriate. Outliers were identified with the Grubbs' test. P-value <0.05 was considered to be statistically significant (*P<0.05, **P<0.01, ***P<0.001, ****P<0.0001).

3. Results

3.1. Chemokines CCL6 and CCL9 are increased in CKD

To identify the effect of CKD on systemic chemokine levels in an early stage, a chemokine profiling was performed in the blood of 129/Sv mice, three weeks after 5/6 ne-phrec-tomy (5/6 Nx). This revealed a significant increase in CCL6, with CCL9 being the chemo-kine with the second highest upregulation (Figure 1a). CCL6 (also known as C10 or MRP-1) and CCL9 (also known as MIP-1γ or MRP-2) are the only two mouse chemokines belonging to the NC6 subfamily of CC-chemokines, based on a separately encoded N-terminal extension upstream of the chemokine body compared to other CC-chemokines [16-18]. We thus further examined the expression of these chemokines in CKD, and re-vealed that both CCL6 and CCL9 were also upregulated in early stage of adenine-induced CKD in C57BL/6N mice, in serum as well as kidney lysates (Figure 1b). Similar observa-tions were made in hyperlipidemic C57BL/6J ApoE-/- mice on a high-fat, adenine-rich diet (Figure 1c), with the latter CKD mouse model chosen based on the high clinical relevance of hyperlipidemia as risk factor for both CKD [19] and CVD [20].
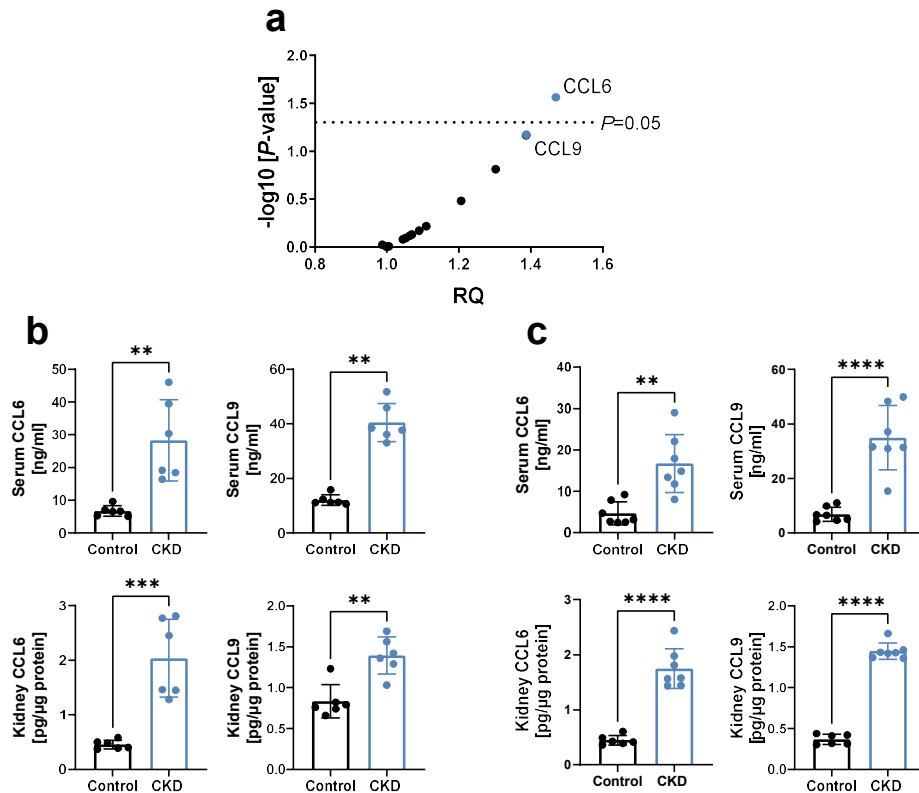
Figure 1. Chemokines CCL6 and CCL9 are increased in experimental CKD. **(a)** Chemokine profiling using a 'Mouse Chemokine Array Kit' in serum of 129/Sv mice three weeks after 5/6 Nx, relative to sham-operated controls (n=5-7). RQ = relative quantity, with each dot representing the mean RQ of an analyzed chemokine; CCL6 and CCL9 are highlighted in blue. *P* via unpaired t-tests with single pooled variance. **(b-c)** Concentration of CCL6 and CCL9 in serum and kidney lysates of **(b)** C57BL/6N mice after three weeks of 0.2% adenine or control diet (n=6); and **(c)** hyperlipidemic C57BL6/J *ApoE*$^{-/-}$ mice fed for four weeks a HFD, followed by two weeks of a 0.3%/0.15% adenine-HFD compared to HFD diet without adenine (n=6-7). *HFD = high-fat diet.* **(b-c)** Data represent means ± SD. Unpaired two-tailed t-test or Mann-Whitney test, comparing CKD animals vs. controls. **P<0.01; ***P<0.001; ****P<0.0001.

3.2. Blocking CCL9 increases kidney fibrosis during CKD induction

We hypothesized that in vivo treatment with CCL6 or CCL9 during CKD induction would enhance kidney inflammation. However, continuous delivery of CCL6 or CCL9 to C57BL/6J mice during the two weeks of feeding with 0.2% adenine-diet almost completely abolished the adenine-induced infiltration of macrophages and overall CD11b+ cells in the kidney (* for CCL9; P=0.0772 for CCL6) (suppl. Figure S1a-b). This was not accompanied by a significant effect on leukocyte, neutrophil, monocyte counts or lymphocytes in pe-ripheral blood (suppl. Figure S1c). Our CKD protocol was insufficient to induce kidney dysfunction in terms of serum creatinine or urea changes, and the additional treatment with CCL6 or CCL9 did not impact on these markers either in this early stage of CKD in-duction (data not shown).

In a proof of concept experiment, we next examined the effects of blocking the two chemokines during CKD induction in hyperlipidemic C57BL6/J ApoE-/- mice. More specif-ically, during 10 days of CKD induction by supplementing a high-fat diet with 0.3% ade-nine, mice received four i.p. injections with neutralizing antibodies directed against mouse CCL6 or CCL9 (Figure 2a). As controls, mice on the same diet were treated with isotype control antibodies ('isotype CKD'). ApoE-/- mice on high-fat diet without adenine but with isotype-matched antibody treatment served as non-CKD iso-type controls (Figure 2a). During this early stage of CKD induction, no significant in-crease in serum creatinine or urea was observed when comparing isotype CKD con-trols with non-CKD mice. How-ever, serum creatinine significantly increased when blocking CCL9 during CKD induction (Figure 2b). Histology confirmed early kidney damage with initial kidney fibrosis upon adenine feeding (Figure 2c). Furthermore, kid-ney fibrosis significantly increased in αCCL9-treated CKD mice compared to isotype-treated CKD controls, as revealed by quan-tification of collagen 1 in kidney protein lysates (Figure 2d). Blocking CCL6 or CCL9 did not significantly alter the absolute numbers of monocytes, neutrophils or lymphocytes in the blood (Figure 2e). Overall, and in contrast to our initial hypothesis, these findings un-expectedly revealed that CCL9 blockade increases CKD-induced kidney fibrosis without effect on systemic in-flammatory cells.
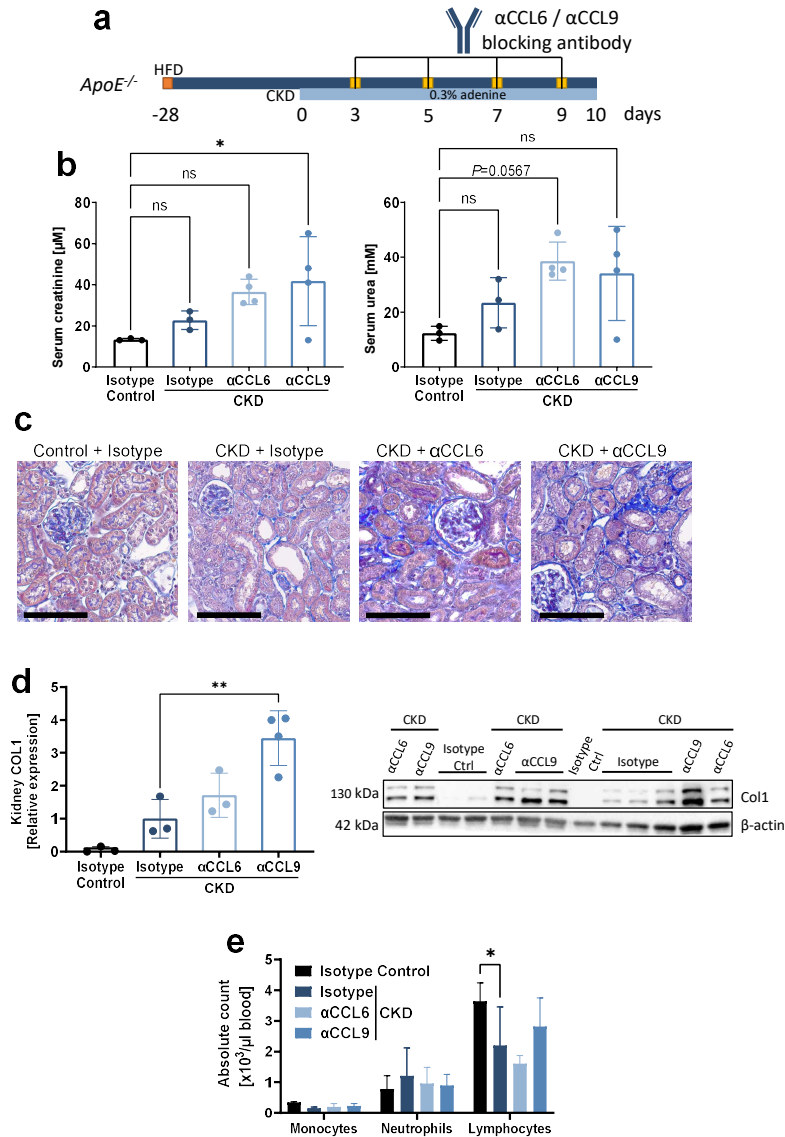
Figure 2. Systemic antibody-mediated blocking of CCL9 increases CKD-induced kidney fibrosis without effect on systemic inflammatory cells. Hyperlipidemic *ApoE^-/-* mice on adenine-induced CKD were treated with blocking antibodies against CCL6 (αCCL6 CKD) or CCL9 (αCCL9 CKD), or with isotype-matched antibody controls (Isotype CKD), as indicated (n=3-4). Hyperlipidemic *ApoE^-/-* mice without adenine but with isotype-matched antibody treatment served as non-CKD controls (Isotype Control). **(a)** Experimental timeline. *CKD = chronic kidney disease; HFD = high-fat diet.* **(b)** Serum creatinine and urea at the end point. **(c)** Representative images of AFOG staining of kidney sections revealing kidney damage in all CKD conditions. Scale bar = 100 μm. **(d)** Quantification of collagen 1 (COL1) in kidney lysates by western blot, normalized to β-actin and displayed relative to non-CKD controls. *One value for 'αCCL6 CKD' excluded due to incomplete blotting (full western blot images available online).* **(e)** Leuko-cyte cell counts in peripheral blood. **(b,d,e)** Data represent means ± SD. Kruskal-Wallis test with Dunn's post-test, one-way ANOVA with Dunnett's post-test, or two-way ANOVA with Dunnett's post-test for multiple comparisons, as appropriate. **P<0.05; **P<0.01; ***P<0.001; ns = not significant.*

3.3. Blocking CCL9 enhances kidney inflammation during CKD induction

Since inflammation and fibrosis are highly interlinked in the damaged kidney [19], we next analyzed the effect of chemokine blockade on inflammatory processes in the kid-

ney during CKD development. Flow cytometric analysis revealed that monocytes and macrophages increasingly accumulated in the kidney during CKD induction, and this was further aggravated by blocking CCL9 as compared to isotype CKD controls (Figure 3a, suppl. Figure S2a-b). Of note, although CKD induction favored the accumulation of M2 over M1 macrophages and increased the ratio of Ly-6Ghigh over Ly-6Glow mono-cytes com-pared to non-CKD controls, these ratios were not significantly altered by blocking of either CCL6 or CCL9 (Figure 3b-c). Finally, CKD induction created a pro-inflammatory milieu in the kidney with enhanced levels of the pro-inflammatory chem-okines CCL2, CX3CL1 and CXCL10, as revealed by a chemokine LUNARIS assay. CCL9 blockade further increased kidney levels of CCL2 as well as of the pro-inflam-matory chemokine CCL3. No impact on CKD-induced upregulation of CX3CL1, CXCL10 and CCL20 was found (Figure 3d, suppl. Figure S3). CCL22 was not induced by CKD, whereas levels of CCL5, CCL11, CCL19 and CXCL1 were outside of the quantitative range (data not shown). Taken together, these data indicate that CCL9 blockade enhances kidney inflammation during CKD induction.
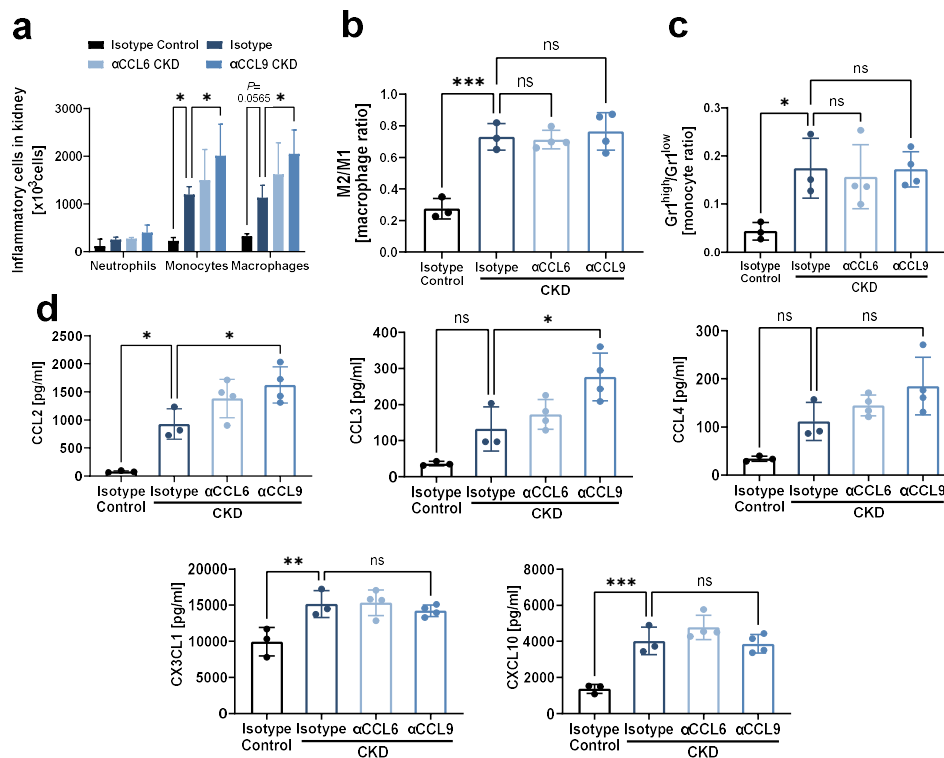
Figure 3. Systemic antibody-mediated blocking of CCL9 increases kidney inflammation. As in Figure 2a, hyperlipidemic *ApoE*-/- mice on adenine-induced CKD were treated with blocking antibodies against CCL6 (αCCL6 CKD) or CCL9 (αCCL9 CKD), or with isotype-matched antibody controls (Isotype CKD) (n=3-4). Hyperlipidemic *ApoE*-/- mice without adenine but with isotype-matched antibody treatment served as non-CKD controls (Isotype Control). **(a)** Flow cytometric analysis of neutrophils, monocytes and macrophages in kidney. **(b-c)** The ratio of (b) M2 vs. M1 macrophages and (c) Ly-6Ghigh vs. Ly-

$6G^{low}$ monocytes in kidney by flow cytometric analysis. **(d)** Chemokine concentration in kidney analyzed using a LUNARIS assay. **(a-d)** Two-way ANOVA (a) or one-way ANOVA (b-d) with Dunnett's post-test for multiple comparisons. *$P<0.05$, **$P<0.01$, ***$P<0.001$.

4. Discussion

Early infiltration of pro-inflammatory leukocytes in the damaged kidney contributes to kidney fibrosis and CKD progression [7]. In this study, we identified an early upregulation of the chemokines CCL6 and CCL9 in experimental CKD, with CCL9 blockade during CKD initiation unexpectedly enhancing kidney inflammation and fibrosis.

Initial kidney injury triggers the expression of pro-inflammatory mediators, includ-ing cytokines and chemokines that upregulate inflammatory processes and mediate the recruitment of inflammatory leukocytes. These contribute to further organ damage and also produce pro-fibrotic mediators triggering fibrotic phenotypes [5,6]. For example, the chemokine CCL2 was upregulated already three hours after induction of glomeru-lone-phritis by an anti-thymocyte antibody in rats and anti-CCL2 antiserum reduced neutro-phil and monocyte/macrophage accumulation in the injured kidney [21,22]. In patients with CKD, interstitial macrophage numbers in kidney biopsies are closely cor-related with kidney damage, with urinary CCL2 levels and interstitial macrophage num-bers interde-pendent parameters in multivariate analysis [23]. The chemokine ligands CCL3 and CCL5, both agonists of the CCR1 receptor, are significantly upregulated in the progres-sively injured kidney, as revealed after six weeks of adriamycin-induced nephropathy [24]. Subsequent studies showed that the CCR1 receptor contributes to kidney fibrosis through the recruitment and accumulation of macrophages in two mod-els of kidney dis-eases [11,24].

We initiated our study with a chemokine profiling in blood three weeks after 5/6 ne-phrectomy (5/6 Nx) to identify chemokine dysregulation in early stages of CKD, i.e. being potentially the initial steps in the disease pathogenesis. CCL6 and CCL9 were the highest upregulated mediators and also increased in two other mouse models of adenine-induced nephropathy. Both chemokines are mostly related to human CCL15 and CCL23 [16], with CCL15 recently identified to be upregulated in CKD patients [14]. As for human CCL15 and CCL23, mouse CCL6 and CCL9 have been described as agonists of the chemokine re-ceptor CCR1 [16,25,26].

Given that no data were available on the role of both upregulated chemokines in CKD, we examined the effect of chemokine treatment and blockade. Unexpectedly, mac-

rophage and monocyte accumulation was reduced by chemokine treatment, whereas it was aggravated by blockade of CCL9, although without significant impact on the ratio of M2 to M1 macrophages. Monocytes and pro-inflammatory M1 macrophages are well-known to contribute to ongoing kidney inflammation and damage [27]. And although M2 macrophages can mediate anti-inflammatory effects upon acute kidney injury, they contribute to CKD by promoting kidney fibrosis and increasingly accumulate in the injured kidney during CKD development [27-31]. In line with the increased accumulation of both M1 and M2 macrophages in kidney upon CCL9 blockade during CKD onset, these animals displayed a higher pro-inflammatory milieu (with increased levels of CCL2 and CCL3) as well as increased kidney fibrosis upon CKD induction. CCL2, CCL3 and CCL5 (the latter remaining outside of the quantitative range of our assay) are agonists of the chemokine receptors CCR2 (for CCL2) and CCR1 (for CCL3, CCL5), which are expressed on macrophages. CCL2 [21,22,32] and its receptor CCR2 [13] as well as CCL5 [32] and its receptor CCR1 [11,33] play an important role in macrophage infiltration in the damaged kidney, as evident from multiple experimental studies. Upregulation of CCL2 and CCL5, and to a lesser extent CCL3, was also shown to mediate the accumulation of macrophages in kidney in a mouse model of the hemolytic-uremic syndrome [34]. These findings jointly reveal especially CCL2, but also CCL5 and CCL3, as important drivers of inflammatory macrophage accumulation in the injured kidney. Both tubular epithelial cells and infil-trating leukocytes contribute to the production of CCL2, CCL3 and CCL5 in injured kid-neys [12,13,35-37], and mice lacking CCR1 also show reduced upregulation of the CCR1 ligands CCL3 and CCL5 in kidney along with reduced neutrophil and macrophage infil-tration upon kidney injury [12]. Combined, this suggests a positive feedback loop between increased pro-inflammatory leukocyte infiltration and enhanced production of pro-inflammatory CCL2 and CCL3, as also observed in our CKD study with CCL9 block-ade.

Furthermore, this positive feedback loop with increased CCL2 and CCL3 production upon CCL9 blockade may also further promote kidney fibrosis, as shown for both CCL2 and CCL3. Indeed, antibody-mediated neutralization of CCL2 was previously shown to reduce the development of kidney fibrosis in nephrotoxic serum-induced glomerulone-phritis [32]. Furthermore, deficiency of the CCL2 receptor CCR2, and to a lesser extent de-ficiency of CCL3, reduced kidney fibrosis after unilateral ureter obstruction (UUO) [13]. Thus, with CCL2, CCL3 as well as M2 macrophages known to be crucial drivers

of kidney fibrosis, the increased accumulation of these chemokines and M2 macrophages in kidney upon CCL9 blockade during CKD onset could further explain the observed parallel in-crease in kidney fibrosis in our study.

The initial trigger that links CCL9 antibody-mediated neutralization to either macrophage accumulation or increased CCL2/CCL3 production currently remains unclear. Since CCL9 has been described as a ligand of CCR1 [16], CCL9 neutralization in vivo might favor CCR1 binding to its ligands CCL3 and CCL5, and in this way trigger increased kidney inflammation and subsequently fibrosis [5,11]. Also, interference with CCL9 may alleviate the constraining effect of CCL9 on the pro-inflammatory and pro-fibrotic effect of CCL2/CCR2 signaling, as was also revealed for Ccl5-knockout. Indeed, in a model of hypertensive kidney injury, *Ccl5*-knockout surprisingly enhanced macro-phage infiltration, levels of CCL2 (but not CCL3) and the pro-inflammatory cytokines IL1β and TNF, as well as fibrosis in the kidney, with comparable observations upon UUO [38]. Since Ccl5-knockout did not induce any significant effects on UUO-induced kidney fibro-sis or inflammation in the presence of CCL2 blockade, upregulated CCL2 levels seemed to underlie increased kidney damage upon Ccl5-deficiency [38]. As another potential mech-anism, CCL9 might be competing for glycosaminogly-can (GAG) binding with pro-inflammatory and/or pro-fibrotic chemokines or other factors. Chemokine binding to GAGs on the endothelium as well as tissue extracellular matrix is important for leukocyte extravasation and thereby tissue accumulation [39]. In accordance, interference with chemokine-GAG interactions, for example by using peptides with high GAG affinity, has been suggested as a potential strategy to target chemokines and their roles in leukocyte re-cruitment and inflammation [39]. Recently, in a contact sensitivity model, a GAG-binding C-terminal fragment of the CXCL9 chem-okine was shown to prevent locally produced chemokines to recruit leukocytes by competing for GAG binding [40]. Also, chemokine CXCL10 has been shown to act anti-fibrotic in the lung through interaction with syndecan-4, a proteoglycan with covalently attached GAG chains. This anti-fibrotic effect occurred independently of its receptor CXCR3, most likely by competition with pro-fibrotic factors for GAG binding [41]. Whether similar mechanisms underlie pro-inflammatory and pro-fibrotic effects of CCL9 neutralization, with CCL9 competing for either chemokine receptor or GAG binding with pro-inflammatory/pro-fibrotic chemokines or other factors, remains currently unclear. Of note, opposite to increased macrophage accumulation in kidney upon CCL9 neutralization, CCL9 peptide treatment significantly counteracted macrophage

accumulation upon CKD induction, thus confirming a role for CCL9 in blocking kidney inflammation in CKD.

Finally, also CCL6 peptide treatment during CKD induction highly reduced inflam-matory cell infiltration in kidney. Nonetheless, compared to CCL9 neutralization, block-ade of CCL6 did not increase the overall kidney collagen content in CKD mice and also had less impact on inflammatory cell infiltration and chemokine production in the kid-neys of these mice. Whether this is caused by a compensatory role of CCL9 (or other up-regulated chemokines) and whether CCL6 blockade could still provide an additive effect on kidney inflammation and fibrosis in CKD in the absence or neutralization of CCL9, remains currently unclear.

5. Conclusions

In summary, in this study, we provide first insights into the role of CCL9 in CKD, with CCL9 upregulated early in CKD and counteracting kidney inflammation and fibro-sis. Whether the human homologue CCL15 could exert comparable effects or would be a useful biomarker of kidney inflammation and fibrosis, remains to be investigated in fu-ture studies.

Supplementary Materials: The following are available online at www.mdpi.com/xxx/s1, Figure S1: CCL9 treatment reduces kidney inflammation in CKD, Figure S2: Flow cytometry gating of leukocyte subsets in kidney, Figure S3: Sys-temic antibody-mediated blocking of CCL9 or CCL6 does not affect kidney CCL20 ex-pression in CKD. Also, complete western blot images are avail-able as Online Supple-mental Information.

References

1. Hill, N.R.; Fatoba, S.T.; Oke, J.L.; Hirst, J.A.; O'Callaghan, C.A.; Lasserson, D.S.; Hobbs, F.D. Global Prevalence of Chronic Kidney Disease - A Systematic Review and Meta-Analysis. PLoS One 2016, 11, e0158765, doi:10.1371/journal.pone.0158765.
2. Lameire, N.H.; Levin, A.; Kellum, J.A.; Cheung, M.; Jadoul, M.; Winkelmayer, W.C.; Stevens, P.E. Harmonizing acute and chronic kidney disease definition and classification: report of a Kidney Disease: Improving Global Outcomes (KDIGO) Consensus Conference. Kidney international 2021, 100, 516-526, doi:10.1016/j.kint.2021.06.028.
3. Marx, N.; Noels, H.; Jankowski, J.; Floege, J.; Fliser, D.; Böhm, M. Mechanisms of cardiovascular complications in chronic kidney disease: research focus of the Transregional Research Consortium SFB TRR219 of the University Hospital Aachen (RWTH) and the Saarland University. Clinical research in cardiology : official journal of the German Cardiac Society 2018, 107, 120-126, doi:10.1007/s00392-018-1260-0.
4. Jankowski, J.; Floege, J.; Fliser, D.; Böhm, M.; Marx, N. Cardiovascular Disease in Chronic Kidney Disease: Pathophysiological Insights and Therapeutic Options. Circulation 2021, 143, 1157-1172, doi:10.1161/circulationaha.120.050686.
5. Anders, H.J.; Vielhauer, V.; Schlöndorff, D. Chemokines and chemokine receptors are involved in the resolution or progression of renal disease. Kidney international 2003, 63, 401-415, doi:10.1046/j.1523-1755.2003.00750.x.
6. Wynn, T.A.; Ramalingam, T.R. Mechanisms of fibrosis: therapeutic translation for fibrotic disease. Nature medicine 2012, 18, 1028-1040, doi:10.1038/nm.2807.
7. Meng, X.M. Inflammatory Mediators and Renal Fibrosis. Advances in experimental medicine and biology 2019, 1165, 381-406, doi:10.1007/978-981-13-8871-2_18.
8. Liu, Y. Renal fibrosis: new insights into the pathogenesis and therapeutics. Kidney Int 2006, 69, 213-217, doi:10.1038/sj.ki.5000054.
9. Hewitson, T.D. Renal tubulointerstitial fibrosis: common but never simple. Am J Physiol Renal Physiol 2009, 296, F1239-1244, doi:10.1152/ajprenal.90521.2008.
10. Noels, H.; Weber, C.; Koenen, R.R. Chemokines as Therapeutic Targets in Cardiovascular Disease. Arteriosclerosis, thrombosis, and vascular biology 2019, 39, 583-592, doi:10.1161/atvbaha.118.312037.
11. Anders, H.J.; Vielhauer, V.; Frink, M.; Linde, Y.; Cohen, C.D.; Blattner, S.M.; Kretzler, M.; Strutz, F.; Mack, M.; Grone, H.J.; et al. A chemokine receptor CCR-1 antagonist reduces renal fibrosis after unilateral ureter ligation. J Clin Invest 2002, 109, 251-259, doi:10.1172/JCI14040.

12. Furuichi, K.; Gao, J.L.; Horuk, R.; Wada, T.; Kaneko, S.; Murphy, P.M. Chemokine receptor CCR1 regulates inflammatory cell infiltration after renal ischemia-reperfusion injury. J Immunol 2008, 181, 8670-8676, doi:10.4049/jimmunol.181.12.8670.

13. Braga, T.T.; Correa-Costa, M.; Silva, R.C.; Cruz, M.C.; Hiyane, M.I.; da Silva, J.S.; Perez, K.R.; Cuccovia, I.M.; Camara, N.O.S. CCR2 contributes to the recruitment of monocytes and leads to kidney inflammation and fibrosis development. Inflammopharmacology 2018, 26, 403-411, doi:10.1007/s10787-017-0317-4.

14. Charo, I.F.; Ransohoff, R.M. The many roles of chemokines and chemokine receptors in inflammation. The New England journal of medicine 2006, 354, 610-621, doi:10.1056/NEJMra052723.

15. Richter, R.; Forssmann, U.; Henschler, R.; Escher, S.; Frimpong-Boateng, A.; Forssmann, W.G. Increase of expression and activation of chemokine CCL15 in chronic renal failure. Biochem Biophys Res Commun 2006, 345, 1504-1512, doi:10.1016/j.bbrc.2006.05.057.

16. Berahovich, R.D.; Miao, Z.; Wang, Y.; Premack, B.; Howard, M.C.; Schall, T.J. Proteolytic activation of alternative CCR1 ligands in inflammation. J Immunol 2005, 174, 7341-7351, doi:10.4049/jimmunol.174.11.7341.

17. Berger, M.S.; Kozak, C.A.; Gabriel, A.; Prystowsky, M.B. The gene for C10, a member of the beta-chemokine family, is located on mouse chromosome 11 and contains a novel second exon not found in other chemokines. DNA and cell biology 1993, 12, 839-847, doi:10.1089/dna.1993.12.839.

18. Hara, T.; Bacon, K.B.; Cho, L.C.; Yoshimura, A.; Morikawa, Y.; Copeland, N.G.; Gilbert, D.J.; Jenkins, N.A.; Schall, T.J.; Miyajima, A. Molecular cloning and functional characterization of a novel member of the C-C chemokine family. Journal of immunology (Baltimore, Md. : 1950) 1995, 155, 5352-5358.

19. Noels, H.; Lehrke, M.; Vanholder, R.; Jankowski, J. Lipoproteins and fatty acids in chronic kidney disease: molecular and metabolic alterations. Nat Rev Nephrol 2021, 17, 528-542, doi:10.1038/s41581-021-00423-5.

20. Soppert, J.; Lehrke, M.; Marx, N.; Jankowski, J.; Noels, H. Lipoproteins and lipids in cardiovascular disease: from mechanistic insights to therapeutic targeting. Advanced drug delivery reviews 2020, 159, 4-33, doi:10.1016/j.addr.2020.07.019.

21. Wenzel, U.; Schneider, A.; Valente, A.J.; Abboud, H.E.; Thaiss, F.; Helmchen, U.M.; Stahl, R.A. Monocyte chemoattractant protein-1 mediates monocyte/macrophage influx in anti-thymocyte antibody-induced glomerulonephritis. Kidney international 1997, 51, 770-776, doi:10.1038/ki.1997.108.

22. Haller, H.; Bertram, A.; Nadrowitz, F.; Menne, J. Monocyte chemoattractant protein-1 and the kidney. Curr Opin Nephrol Hypertens 2016, 25, 42-49, doi:10.1097/MNH.0000000000000186.

23. Eardley, K.S.; Zehnder, D.; Quinkler, M.; Lepenies, J.; Bates, R.L.; Savage, C.O.; Howie, A.J.; Adu, D.; Cockwell, P. The relationship between albuminuria, MCP-1/CCL2, and interstitial macrophages in chronic kidney disease. Kidney Int 2006, 69, 1189-1197, doi:10.1038/sj.ki.5000212.

24. Vielhauer, V.; Berning, E.; Eis, V.; Kretzler, M.; Segerer, S.; Strutz, F.; Horuk, R.; Grone, H.J.; Schlondorff, D.; Anders, H.J. CCR1 blockade reduces interstitial inflammation and fibrosis in mice with glomerulosclerosis and nephrotic syndrome. Kidney Int 2004, 66, 2264-2278, doi:10.1111/j.1523-1755.2004.66038.x.

25. Du, X.; Li, F.; Zhang, C.; Li, N.; Huang, H.; Shao, Z.; Zhang, M.; Zhan, X.; He, Y.; Ju, Z.; et al. Eosinophil-derived chemokine (hCCL15/23, mCCL6) interacts with CCR1 to promote eosinophilic airway inflammation. Signal Transduct Target Ther 2021, 6, 91, doi:10.1038/s41392-021-00482-x.

26. Kitamura, T.; Kometani, K.; Hashida, H.; Matsunaga, A.; Miyoshi, H.; Hosogi, H.; Aoki, M.; Oshima, M.; Hattori, M.; Takabayashi, A.; et al. SMAD4-deficient intestinal tumors recruit CCR1+ myeloid cells that promote invasion. Nature genetics 2007, 39, 467-475, doi:10.1038/ng1997.

27. Wang, X.; Chen, J.; Xu, J.; Xie, J.; Harris, D.C.H.; Zheng, G. The Role of Macrophages in Kidney Fibrosis. Frontiers in physiology 2021, 12, 705838, doi:10.3389/fphys.2021.705838.

28. Shen, B.; Liu, X.; Fan, Y.; Qiu, J. Macrophages regulate renal fibrosis through modulating TGFβ superfamily signaling. Inflammation 2014, 37, 2076-2084, doi:10.1007/s10753-014-9941-y.

29. Han, Y.; Ma, F.Y.; Tesch, G.H.; Manthey, C.L.; Nikolic-Paterson, D.J. Role of macrophages in the fibrotic phase of rat crescentic glomerulonephritis. American journal of physiology. Renal physiology 2013, 304, F1043-1053, doi:10.1152/ajprenal.00389.2012.

30. Kim, M.G.; Kim, S.C.; Ko, Y.S.; Lee, H.Y.; Jo, S.K.; Cho, W. The Role of M2 Macrophages in the Progression of Chronic Kidney Disease following Acute Kidney Injury. PloS one 2015, 10, e0143961, doi:10.1371/journal.pone.0143961.

31. Yang, Q.; Wang, Y.; Pei, G.; Deng, X.; Jiang, H.; Wu, J.; Zhou, C.; Guo, Y.; Yao, Y.; Zeng, R.; et al. Bone marrow-derived Ly6C(-) macrophages promote ischemia-induced chronic kidney disease. Cell death & disease 2019, 10, 291, doi:10.1038/s41419-019-1531-3.

32. Lloyd, C.M.; Minto, A.W.; Dorf, M.E.; Proudfoot, A.; Wells, T.N.; Salant, D.J.; Gutierrez-Ramos, J.C. RANTES and monocyte chemoattractant protein-1 (MCP-1) play an important role in the inflammatory phase of crescentic nephritis, but only MCP-1 is involved in crescent formation and interstitial fibrosis. The Journal of experimental medicine 1997, 185, 1371-1380, doi:10.1084/jem.185.7.1371.

33. Eis, V.; Luckow, B.; Vielhauer, V.; Siveke, J.T.; Linde, Y.; Segerer, S.; Perez De Lema, G.; Cohen, C.D.; Kretzler, M.; Mack, M.; et al. Chemokine receptor CCR1 but not CCR5 mediates leukocyte recruitment and subsequent renal fibrosis after unilateral ureteral obstruction. J Am Soc Nephrol 2004, 15, 337-347, doi:10.1097/01.asn.0000111246.87175.32.

34. Keepers, T.R.; Gross, L.K.; Obrig, T.G. Monocyte chemoattractant protein 1, macrophage inflammatory protein 1 alpha, and RANTES recruit macrophages to the kidney in a mouse model of hemolytic-uremic syndrome. Infection and immunity 2007, 75, 1229-1236, doi:10.1128/iai.01663-06.

35. Vielhauer, V.; Anders, H.J.; Mack, M.; Cihak, J.; Strutz, F.; Stangassinger, M.; Luckow, B.; Gröne, H.J.; Schlöndorff, D. Obstructive nephropathy in the mouse: progressive fibrosis correlates with tubulointerstitial chemokine expression and accumulation of CC chemokine receptor 2- and 5-positive leukocytes. Journal of the American Society of Nephrology : JASN 2001, 12, 1173-1187, doi:10.1681/asn.V1261173.

36. Segerer, S.; Nelson, P.J.; Schlöndorff, D. Chemokines, chemokine receptors, and renal disease: from basic science to pathophysiologic and therapeutic studies. Journal of the American Society of Nephrology : JASN 2000, 11, 152-176, doi:10.1681/asn.V111152.

37. Wada, T.; Furuichi, K.; Segawa-Takaeda, C.; Shimizu, M.; Sakai, N.; Takeda, S.I.; Takasawa, K.; Kida, H.; Kobayashi, K.I.; Mukaida, N.; et al. MIP-1alpha and MCP-1 contribute to crescents and interstitial lesions in human crescentic glomerulonephritis. Kidney international 1999, 56, 995-1003, doi:10.1046/j.1523-1755.1999.00646.x.

38. Rudemiller, N.P.; Patel, M.B.; Zhang, J.D.; Jeffs, A.D.; Karlovich, N.S.; Griffiths, R.; Kan, M.J.; Buckley, A.F.; Gunn, M.D.; Crowley, S.D. C-C Motif Chemokine 5 Attenuates Angiotensin II-Dependent Kidney Injury by Limiting Renal Macrophage Infiltration. Am J Pathol 2016, 186, 2846-2856, doi:10.1016/j.ajpath.2016.07.015.

39. Crijns, H.; Vanheule, V.; Proost, P. Targeting Chemokine-Glycosaminoglycan Interactions to Inhibit Inflammation. Frontiers in immunology 2020, 11, 483, doi:10.3389/fimmu.2020.00483.

40. Vanheule, V.; Crijns, H.; Poosti, F.; Ruytinx, P.; Berghmans, N.; Gerlza, T.; Ronsse, I.; Pörtner, N.; Matthys, P.; Kungl, A.J.; et al. Anti-inflammatory effects of the GAG-binding CXCL9(74-103) peptide in dinitrofluorobenzene-induced contact hypersensitivity in mice. Clinical and experimental allergy : journal of the British Society for Allergy and Clinical Immunology 2018, 48, 1333-1344, doi:10.1111/cea.13227.

41.   Jiang, D.; Liang, J.; Campanella, G.S.; Guo, R.; Yu, S.; Xie, T.; Liu, N.; Jung, Y.; Homer, R.; Meltzer, E.B.; et al. Inhibition of pulmonary fibrosis in mice by CXCL10 requires glycosaminoglycan binding and syndecan-4. The Journal of clinical investigation 2010, 120, 2049-2057, doi:10.1172/jci38644.